

**Development of concepts to assess, monitor and
evaluate increased CO₂ concentrations arising
from potential leakages of CCS sites**

Dissertation

zur Erlangung des Doktorgrades

der Mathematisch-Naturwissenschaftlichen Fakultät

der Christian-Albrechts-Universität

zu Kiel

vorgelegt von

Diplom-Geologin Alexandra Schulz

Geb. 11.06.1983 in Halle/ Saale

Kiel, 2013

Erster Gutachter: Prof. Dr. Andreas Dahmke

Zweiter Gutachter: Dr. habil. Hans-Hermann Richnow

Tag der mündlichen Prüfung: 17.04.2013

Zum Druck genehmigt: 17.04.2013

Table of Contents

Index of tables	V
Index of figures	VII
Acronyms	XIII
Zusammenfassung	XV
Summary	XVII
1. Introduction	1
1.1 Technologies for capturing and transportation of CO ₂	6
1.2 Storage of CO ₂ in deep geological formations	7
1.3 Trapping mechanisms for injected CO ₂	10
1.4 Potentials for CO ₂ leakage from storage sites and monitoring concepts	11
1.5 CO ₂ in soil and groundwater	14
1.6 Stable carbon isotopes	15
1.7 The importance of CO ₂ for microorganisms	19
1.8 Objectives of the work and cooperation	20
2. Investigation of the geochemical impact of CO₂ on shallow groundwater: Design and implementation of a CO₂ injection test in Northeast Germany	24
2.1 Kurzfassung	24
2.2 Abstract	24
2.3 Introduction	25
2.4 Test site	27
2.4.1 <i>Geology</i>	27
2.4.2 <i>Hydrogeology</i>	30
2.4.3 <i>Monitoring network</i>	31
2.5 Injection test design and operation	32
2.6 Monitoring of CO ₂ and geochemically altered groundwater	35
2.6.1 <i>Groundwater sampling and analysis</i>	35
2.6.2 <i>Geophysical monitoring</i>	38
2.6.3 <i>Isotope monitoring</i>	39
2.6.4 <i>Multiparameter Probes</i>	41
2.6.5 <i>Passive samplers</i>	43
2.7 Discussion	44
2.8 Summary	46

2.9	Acknowledgements	47
3.	Monitoring of a simulated CO₂ leakage in a shallow aquifer using stable carbon isotopes	48
3.1	Kurzfassung	48
3.2	Abstract	48
3.3	Introduction	49
3.4	Injection test and sampling methods	52
3.4.1	<i>Field Site</i>	52
3.4.2	<i>Injection test</i>	53
3.4.3	<i>Soil gas sampling in the unsaturated zone</i>	53
3.4.4	<i>Groundwater sampling</i>	54
3.4.5	<i>Measurement settings for stable carbon isotope analyses of CO₂</i>	54
3.5	Results	55
3.5.1	<i>Stable carbon isotope ratios of the soil gas</i>	55
3.5.2	<i>Stable carbon isotope ratios of the groundwater</i>	57
3.6	Discussion	60
3.7	Acknowledgement	64
3.8	Supporting information	64
4.	Feasibility of geoelectrical monitoring and multiphase modelling for process understanding of gaseous CO₂ injection into a shallow aquifer	65
4.1	Kurzfassung	65
4.2	Abstract	66
4.3	Introduction	66
4.4	Geoelectrical monitoring of subsurface processes	68
4.4.1	<i>An overview of physical parameters affecting electrical conductivity</i>	68
4.4.2	<i>An overview of geoelectrical time-lapse monitoring of subsurface processes</i>	72
4.5	CO ₂ injection scenario: test site and test setup	73
4.5.1	<i>Geoelectrical monitoring of the performed CO₂ injection scenario</i>	75
4.6	Multiphase modeling with TOUGH2	79
4.6.1	<i>Mathematical and numerical basis</i>	79
4.6.2	<i>Creating heterogeneous parameter fields</i>	82
4.6.3	<i>CO₂ injection scenario: distribution of gaseous CO₂ and dissolved CO₂</i>	84
4.6.4	<i>CO₂ injection scenario: simulating breakthrough curves</i>	85
4.7	Summary and concluding remarks	91
4.8	Acknowledgement	92

5. Effects of high CO₂ concentrations on typical aquifer microorganisms	93
5.1 Kurzfassung	93
5.2 Abstract	93
5.3 Introduction	94
5.4 Material and methods	95
5.4.1 <i>Microorganisms and culture media</i>	95
5.4.2 <i>Growth experiments under different CO₂ concentrations at ambient pressure</i>	96
5.4.3 <i>Viability experiments under CO₂ stress at high pressure</i>	97
5.5 Results	99
5.5.1 <i>Influence of pH on growth and viability</i>	99
5.5.2 <i>Cell growth and viability under different CO₂ concentrations at ambient pressure</i>	101
5.5.3 <i>Cell viability under CO₂ stress at high pressure</i>	103
5.6 Discussion	104
5.7 Acknowledgement	108
5.8 Supporting information	108
6. Changes in the proteome of soil bacteria induced by elevated CO₂ concentrations	109
6.1 Kurzfassung	109
6.2 Abstract	109
6.3 Introduction	110
6.4 Material and methods	111
6.4.1 <i>Microorganisms and culture media</i>	111
6.4.2 <i>Growth experiments under different CO₂ concentrations at ambient pressure</i>	112
6.4.3 <i>Sample preparation for protein analysis</i>	113
6.4.4 <i>Differential Proteomics</i>	113
6.5 Results	114
6.5.1 <i>Growth curves of the different strains under different CO₂ concentrations</i>	114
6.5.2 <i>Protein data</i>	115
6.6 Discussion	118
6.7 Acknowledgement	120
7. Final discussion and outlook	121
7.1 Evaluation of the monitoring approach	121
7.2 Implementation of the isotope monitoring approach to other field site scenarios	124

Table of contents

7.3 Further steps in the investigation of microorganisms concerning elevated CO ₂ concentrations	125
8. References	126
9. Acknowledgements	138
10. List of publications	139
10.1 Articles and manuscripts	139
10.2 Conference posters	139
10.3 Talks	140
11. Curriculum vitae	142

Eidesstattliche Erklärung

Appendix (CD)

- A Investigation of the geochemical impact of CO₂ on shallow groundwater: design and implementation of a CO₂ injection test in Northeast Germany.** *Environmental Earth Sciences*, 2012, 67 (2), pp 335-349.
- B Monitoring of a simulated CO₂ leakage in a shallow aquifer using stable carbon isotopes.** *Environmental Science and Technology*, 2012, 46 (20); pp 11243-11250.
- Supporting Information
- C Feasibility of geoelectrical monitoring and multiphase modeling for process understanding of gaseous CO₂ injection into a shallow aquifer.** *Environmental Earth Sciences*, 2012, 67, pp 447-462
- D Effects of high CO₂ concentrations on ecophysiologicaly different microorganisms.** *Environmental Pollution*, 2012, 169, pp 27-34.
- Supporting Information

Index of tables

Table 1.1	Changes in concentrations of greenhouse gases and their global warming potential (GWP) for a 100 years' time horizon.	2
Table 1.2	Estimated storage capacities for some geological storage options.	4
Table 1.3	Four model strains used for growth experiments with high CO ₂ concentrations and elevated pressure. Growth condition, growth temperature, pH, and growth substrates are listed.	21
Table 2.1	Schematic geological profile at the test site.	28
Table 2.2	Hydraulic parameters of geological layers in aquifer 2.	32
Table 2.3	Statistics of background concentrations of groundwater samples from three sampling campaigns before the injection test: mean, standard deviation, minimum and maximum values and number of samples (n). RP-redox potential; EC – electrical conductivity	35
Table 2.4	$\delta^{13}\text{C}$ values of CO ₂ in the groundwater and pH at monitoring well ML 2C-3.	39
Table 4.1	Hydraulic parameters of different geological layers at the test site (see also Peter et al. 2012).	82
Table 5.1	The relative inhibitory effect (RI) of CO ₂ and the growth rate μ for CO ₂ concentrations from 0 – 100 % for the investigated microorganisms.	99
Table 6.1	¹⁶ N (% average) incorporation for selected proteins at different headspace carbon dioxide concentrations for <i>P. putida</i> .	115
Table 6.2	Labeling ratios for selected proteins at different headspace carbon dioxide concentrations for <i>P. putida</i> F1. The significant decrease of the labeling ratio from 0.987 at 0 % CO ₂ down to 0.351 for 80 % CO ₂ for acetyl-CoA synthetase shows that this protein is only weakly new synthesized.	116

Index of tables

Table 7.1	Comparison of different monitoring approaches used in the presented field experiment.	123
-----------	---	-----

Index of figures

Figure 1.1	The map shows the location of three onshore (including one CCS pilot site in Ketzin, Germany) and two offshore (blue boxes) CCS projects, which are in operation. The year of injection begin, the storage formation, the injection rate, and the separation technology for capturing the CO ₂ is given.	3
Figure 1.2	Scheme about potential geological CO ₂ storage sites (modified after http://www.beardall-parry.com/menus/main.asp?PageName=CCS).	4
Figure 1.3	CO ₂ trapping mechanisms in geological formations divided into physical trapping and geochemical trapping (images provided by the CO ₂ CRC Online Image Library, Cooperative Research Center for Greenhouse Gas Technologies).	10
Figure 1.4	Potential leakage pathways for injected CO ₂ . I. Injected CO ₂ can leak through “gaps” in the cap rock into a higher aquifer. II. The injected CO ₂ can migrate up dip and can escape along faults and fractures. III. The injection pressure exceeds the capillary pressure and migrates through the overlaying formation. IV. The injected CO ₂ can leak along old and not tightly plugged abandoned wells (modified after (IPCC, 2005)).	11
Figure 1.5	Overview of possible monitoring methods of a CO ₂ leakage in different depth levels. Most of the methods are indirect measurements (pH, TIC, EC) of the injected CO ₂ .	13
Figure 1.6	Ranges of $\delta^{13}\text{C}$ values for different natural compounds involved in the global carbon cycle (modified after Clark and Fritz (1997)). The more positive the $\delta^{13}\text{C}$ value, the more enriched is the compound in heavy isotopes.	15
Figure 1.7	¹³ C discrimination during CO ₂ uptake and fixation in plant cells. CO ₂ fixation takes place in the stoma of the chloroplasts via the Calvin cycle. The enzyme RuBisCO catalyses the first major step of carbon fixation.	16

Values in green boxes indicate that ^{13}C is discriminated in the product compared to atmospheric CO_2 . Data for isotope fractionation are taken from O'Leary (1988).

- Figure 1.8 Schematic illustration of a GC-IRMS system for analyzing stable carbon isotopes. The standard is a CO_2 gas with a known isotopic signature normed according to the international V-PDB standard (after Fischer (2006)). 17
- Figure 2.1 Map of test site for CO_2 injection with injection lances, groundwater monitoring wells and intersection line for geological cross section (s. Fig. 2.3). 26
- Figure 2.2 EC-log, geological profile and HPT-log located 2 m east of injection well Inj1. 27
- Figure 2.3 Geological profile from A to A' (see Fig. 2.1) with position of injection lance 1. Layer numbers refer to Tab. 2.1. 27
- Figure 2.4 Normalized equipotential lines of salt tracer injection at different times. Left: before saline water injection; middle: after 36 hours saline water injection; right: after 84 hours saline water injection. 30
- Figure 2.5 (a) Geological structure model showing the model boundaries of the simulated aquifer 2, the locations of the borehole profiles and injection lances (green). (b) 3D simulated gas distribution (blue isolines correspond to 0.5 % gas saturation), accumulating beneath the glacial loam 10 days after stopping the gas injection. Viewing direction is from northeast. 33
- Figure 2.6 Concentration time series at GWM 2D, which is approximately 5m downstream of injection lance Inj2, for total inorganic carbon (TIC) and (a) pH, electrical conductivity and tracer SF_6 , (b) sulfate, nitrate and chloride, (c) calcium, sodium, potassium, magnesium and (d) aluminium, silica, iron and manganese. The grey bar indicates the duration of the injection period. 36

Index of figures

- Figure 2.7 Piper diagram for groundwater samples from three monitoring wells (GWM 1D, 2D, 3D) for two sampling campaign, prior to and after the injection test. 37
- Figure 2.8 Comparison of (a) TIC and (b) pH values measured by multiparameter probes (MPP) and obtained from groundwater sampling. TIC from MPP is calculated from sensor measuring dissolved CO₂. 42
- Figure 3.1 Map of Germany with the field site in the north-east (left), and detailed plan for the monitoring field of the CO₂ injection test site. The plan is showing the installed monitoring wells and the three CO₂ injection lances (red) (modified after (Peter et al., 2012)). The control levels (B-F) are explained in more detail in the text. 49
- Figure 3.2 Contour maps showing the distribution of $\delta^{13}\text{C}$ values of CO₂ [‰] in soil gas before, during, and after (from left to the right) the injection of isotopically light CO₂ in March/ April 2011. Relatively homogeneously distributed values were observed before and after the injection of CO₂. During the injection, a slight leakage occurred at the northern injection lance *Inj2*, which was detected immediately in the soil gas samples taken in the close vicinity of the leak. 55
- Figure 3.3 Distribution of $\delta^{13}\text{C}$ values of CO₂ [‰] in groundwater from the start of the CO₂ injection until the final sampling campaign at day 204. The numbers in boxes indicate the number of days after the beginning of the injection test. The red spots show the location of the CO₂-injection lances. 56
- Figure 3.4 Various parameters for the shallowest sampling level (13 meters) of the multilevel well ML 2C in the northern part of the monitoring field. In addition to the parameters that were measured in the field (pH, electrical conductivity), the total inorganic carbon content, the concentration of the tracer SF₆ and the isotopic ratios are given for all sampling campaigns. 58

- Figure 3.5 The variation of the isotope ratio (circles) of five specific wells along a cross-section in correlation with the variation of the pH (squares). Well ML 1C-3 is the closest well to the injection lance; well ML 1G-3 is about 25 meters away (see Fig. 3.1). At first, the two closest wells showed indication of the injected CO₂ while no change either in pH or isotope ratio was measured at the monitoring well farthest away from the injection well. 59
- Figure 4.1 Relative variation of electrical fluid resistivity due to temperature variation. Approximation according to Arps (1953) and Schön (1996), reference temperature: 10 °C. 70
- Figure 4.2 *a)* Test site Wittstock. Regional groundwater flow is directed from GWM 1A to GWM 1I, roughly from east to west. *b)* Schematic geological profile and schematic illustration of a well equipped with electrodes. 73
- Figure 4.3 Temporal variation of apparent conductivity (σ_a) relative to baseline measurements at well ML 1C (1.1" diameter well) during Monitoring Campaign 1; electrode configuration: Wenner (AMNB). Depths (meter below ground level) of potential electrodes M–N are given in the legend. The bottom of glacial loam layer is located 12.0 m bgl. 75
- Figure 4.4 Temporal variation of apparent conductivity (σ_a) relative to baseline measurements at well GWM 1D (2" diameter well) during Monitoring Campaign 1; electrode configuration: Wenner (AMNB). Depths (meter below ground level) of potential electrodes M–N are given in the legend. The bottom of glacial loam layer is located approx. 11 m bgl. 76
- Figure 4.5 Field parameters of groundwater samples (symbols) and temporal variation of apparent conductivity (σ_a) relative to baseline measurements (solid lines) at well ML 1E (1.1" diameter well); electrode configuration: Wenner (AMNB). Depths (meter below ground level) of potential electrodes M–N are given in the legend. The bottom of glacial loam layer is located 12.1 m bgl. 78

Index of figures

- Figure 4.6 a) Heterogeneous permeability for the test site: values of the color scale are given in 10^{-10} m^2 , b) Simulated capillary pressure distribution: values of color scale are given in kPa. 83
- Figure 4.7 Upper row saturation gaseous CO_2 (%); lower row dissolved CO_2 as mol-fraction X_{CO_2} (mol/mol), both at $t = 5, 10, \text{ and } 20$ days after CO_2 injection started; red square in S_g (10 days)-image indicates the CO_2 injection point (18 m bgl), black squares indicate positions of installed electrodes at wells ML 1C and GWM 1D from left to right. 85
- Figure 4.8 Relative conductivity (σ_{ps}) for monitoring wells GWM 1D (black and red curves) and ML 1C (blue curves) at different depths. For monitoring well GWM 1D the experimental curve (σ_{a}) is shown for depth of approx. 11.75 m (black curve with squares). 88
- Figure 4.9 Comparison of experimental (σ_{a}) and theoretical conductivity (σ_{ps}) relative to baseline measurements at well GWM 1D for two different depths: 11 m (black curves) and 13 m (green curves). 89
- Figure 5.1 Experimental set up for growth experiments with CO_2 at high pressure. The two stainless steel pressure vessels were placed in a water bath and connected to a thermostat. The pressure was applied by using CO_2 cylinders and a pressure-reducing valve permitting pressure up to 7500 kPa. 97
- Figure 5.2 Comparison of growth at different pH values for *P. putida* and *B. subtilis* (left) and for *D. vulgaris* and *T. aromatica* (right). The pH in the medium was reduced by the addition of HCl (0.5 M). 98
- Figure 5.3 Growth (OD 660nm) at different CO_2 concentrations between 0 and 80 % (for aerobic strains *P. putida* – (A), *B. subtilis* – (B)) and 100 % (for anaerobic strains *D. vulgaris* – (C) and *T. aromatica* – (D)). The time is plotted against the optical density, measured at a wavelength of 660 nm. For *P. putida*, growth with acetate (5 mM) or glucose (5 mM) at different CO_2 concentrations is plotted (E). 101

- Figure 5.4 MPNs of the tested strains after incubation at high pressure and elevated CO₂ concentrations. To examine a negative effect of the pressure itself on the viability of the cells, control experiments were performed with pure nitrogen and no CO₂ amendments. For the anaerobic strains *T. aromatica* and *D. vulgaris*, all cells were killed at a pressure of 5000 kPa (no growth corresponds to the value one for the log scale) and elevated CO₂ concentrations. A significant number of *P. putida* and *B. subtilis* cells still survived at 5000 kPa pressure. 102
- Figure 6.1 Growth curves of *Pseudomonas putida* F1 for 0, 50 and 80% CO₂ with unlabeled Brunner medium (left graph) and with ¹⁵N-labeled Brunner medium (right graph). 113
- Figure 6.2 Growth curves of *Thauera aromatica* for 0, 50 and 80 % CO₂ with unlabeled Brunner medium (left graph) and with ¹⁵N-labeled Brunner medium (right graph). 114
- Figure 6.3 Protein changes in *Pseudomonas putida* (left) and *Thauera aromatica* (right) in the presence of different headspace concentrations of carbon dioxide (0, 50, and 80 %). Data points above or below the central diagonal line show differences between CO₂ levels. Histograms along the diagonal show the distribution of log₂-transformed LFQ intensities for replicates. 115

Acronyms

Acronyms

A	mixing ratio of the background isotope ratio
bgl	below ground level
BMBF	Bundesministerium für Bildung und Forschung
BTEX	benzene-toluol-ethylbenzene-xylene
^{12}C	stable carbon with the atomic mass 12
^{13}C	stable carbon with the atomic mass 13
$^{13}\text{C}/^{12}\text{C}$	isotope ratio of ^{13}C to ^{12}C
CAU	Christian-Albrechts University
CCS	carbon capture and storage
DCE	dichlorethene
DIN	Deutsches Institut für Normung
DOC	dissolved organic carbon
DP	direct push
DVWK	Deutscher Verband für Wasserwirtschaft und Kulturbau
EC	electrical conductivity
EOR	enhanced oil recovery
Eq	equation
Fig	figure
GC-IRMS	gas-chromatography isotope ratio mass spectrometer
GUK	Geländeunterkante
GWM	Grundwassermessstelle
GWP	global warming potential
HPLC	high-performance liquid chromatography
HPT	hydraulic profiling tool
Inj	injection lance
IPC-MS	inductively-coupled-plasma mass-spectrometry

Acronyms

MPP	multi-parameter probes
MPN	Most Probable Number Method
OD ₆₀₀	optical density at a wave length of 600 nm
PCE	polycarboxylate ether
RI	inhibitory effect
scCO ₂	supercritical CO ₂
Tab.	table
TCE	trichlorethane
TIC	total inorganic carbon
TOC	total organic carbon
VC	volatile compounds
V-PDB	Vienna-PeeDee-Belemnite-Standard
ZERT	Zero Emission Research and Technology
¹³ δ _(B)	isotope signature of the background
¹³ δ _(I)	isotope signature of the injected CO ₂
¹³ δ _(M)	isotope signature after the injection
μ	growth rate

Zusammenfassung

Die vorliegende Arbeit wurde im Rahmen des BMBF Verbundprojektes „CO₂-Leckage“ *CO₂-Leckageversuch in einem oberflächennahen Grundwasserleiter zur Erprobung von Monitoringkonzepten und –methoden* erstellt (Projekt-Nr. 03G0670C).

Die steigende atmosphärische CO₂-Konzentration ist Anlass für die Suche nach Möglichkeiten die anthropogene CO₂ Emission zu reduzieren. Eine Strategie ist der Auf- und Ausbau der Nutzung von erneuerbaren Energien. Eine andere Möglichkeit ist die Speicherung von CO₂, das bei der Verbrennung fossiler Rohstoffe entsteht. Dabei wird CO₂ vom Rauchgas abgetrennt und in tiefe geologische Formationen eingespeist. Diese Technologie wird als *Carbon Capture and Storage*, kurz CCS, bezeichnet. Zur Speicherung werden tief liegende Aquifere, erschöpfte Erdgaslagerstätten und tiefe nicht-abbaubare Kohleflöze in Betracht gezogen. Auch wenn die Wahrscheinlichkeit einer potentiellen CO₂ Leckage aus dem tiefen Untergrund in oberflächennahe Schichten als sehr gering einzuschätzen ist, kann eine absolute Dichtigkeit nicht angenommen werden. Somit muss das Restrisiko einer Leckage bewertet werden. Um eine umfassende Risikobewertung der CCS Technologie durchzuführen, wurde ein mögliches Leckageszenario untersucht. CO₂, das aus der Speicherformation austritt, könnte nach oben migrieren und beispielsweise in Grundwasserleiter gelangen, welche für die Trinkwasserversorgung genutzt werden. Im Rahmen dieser Arbeit wurde ein Monitoringkonzept für die frühzeitige Detektion einer solchen Leckage entwickelt und erprobt. Es basiert auf der Nutzung stabiler Kohlenstoffisotopen und deren Analyse. Eine detaillierte Studie über die geochemischen und mikrobiologischen Einflüsse erhöhter CO₂ Konzentrationen wurde mit Hilfe einer simulierten Leckage in einen oberflächennahen Grundwasserleiter (18 m Tiefe) durchgeführt. Durch das Einbringen von ca. 800 kg gasförmigen CO₂ mit bekannter Isotopensignatur ($\delta^{13}\text{C} -30.5 \pm 0.4 \text{ ‰}$) kam es als direkte Folge zu einer deutlichen Absenkung des pH-Wertes und zu einer Zunahme der TIC-Gehalte des Grundwassers. Weiterhin wurde die Freisetzung von Kationen und Spurenelementen beobachtet. Verschiedene geochemische und geophysikalische Methoden wurden getestet, um die Ausbreitung der injizierten CO₂-Fahne zu verfolgen. Darüber hinaus wurden die Isotopensignaturen des CO₂ für die Quellenidentifizierung genutzt. Die unterschiedlichen Isotopensignaturen des injizierten CO₂ und des natürlichen Hintergrundes ($\delta^{13}\text{C} -21.9 \pm 1.4 \text{ ‰}$) ermöglichten eine detaillierte Kartierung der künstlich erzeugten CO₂-Fahne im Grundwasser.

Neben der Überwachung des Grundwassers wurden Bodengaslanzen zur Überwachung des obersten Bodenhorizontes getestet, welche sich ebenfalls für die frühzeitige Detektion einer Leckage eignen. Der Vorteil des Monitorings mittels Überwachung der Isotopensignaturen des CO₂ liegt dabei in der Identifizierung der CO₂-Quelle, was mit anderen Monitoringmethoden nicht möglich ist.

Im Falle einer CO₂ Leckage, wäre das Ökosystem im oberen Bodenhorizont erhöhten CO₂-Konzentrationen ausgesetzt. Daher wurde im zweiten Teil dieser Arbeit der Einfluss erhöhter CO₂ Konzentrationen auf Mikroorganismen aus oberflächennahen Bodenhorizonten untersucht. Es wurden Wachstumsversuche mit vier Modellorganismen durchgeführt. Zwei aerobe Stämme (*Pseudomonas putida* F1/ *Bacillus subtilis* sbsp. *subtilis* strain 168) wurden unter einer Atmosphäre, bestehend aus 0-80 % CO₂, kultiviert, wohingegen die CO₂ Konzentration für die beiden anaeroben Stämme (*Desulfovibrio vulgaris* Hildenborough/ *Thauera aromatica* K172) auf 100 % erhöht wurde. Erhöhte CO₂ Konzentrationen führten zu einer Verlängerung der lag-Phase und zu einer Reduzierung der Wachstumsraten und Zellzahlen bei allen vier Stämmen. Die Intensität der Auswirkungen verhielt sich dabei proportional zu den CO₂ Konzentrationen. Anschließend wurden die Effekte erhöhter CO₂-Konzentrationen in Kombination mit erhöhtem Druck (1-5000 kPa) untersucht, um Aussagen über tiefer liegende Aquifere mit hohen CO₂ Partialdrücken zu treffen. Bereits nach 24 Stunden kam es bei Drücken ≥ 1000 kPa zu einer signifikanten Reduzierung der Lebendzellzahlen, die sich mit zunehmendem Druck weiter ausprägte. Um Hinweise auf die Ursachen des reduzierten Wachstums bei erhöhten CO₂-Konzentrationen zu bekommen, wurden proteomische Untersuchungen an zwei Stämmen (*Pseudomonas putida* F1/ *Thauera aromatica* K172) durchgeführt. Anhand der Unterdrückung einzelner Proteinen, die eine zentrale Rolle im Energiemetabolismus spielen, konnten Zusammenhänge des verringerten Wachstums erklärt werden.

Summary

The presented work was performed in the context of the BMBF funded project „*CO₂ leakage test into a shallow aquifer for testing monitoring concepts and methods*” (grant: 03G0670C).

Increasing CO₂ concentrations in the atmosphere are the reason for numerous studies about possibilities to reduce CO₂ emission. Besides developing and supporting the supply of energy from renewable sources, one idea is to separate CO₂ that is produced by burning fossil fuels, from the flue gas and to store it in deep geological formations. This technology is called *Carbon Capture and Storage* (CCS). Deep saline aquifers, depleted oil and gas fields and deep non-mineable coal seams are considered as potential storage formations. Even if the probability of a CO₂ leakage from a storage sites is rather small, this scenario has to be taken into account to conduct a proper risk assessment and to evaluate CCS technologies. CO₂ that leaks from a storage site could migrate upward and could reach shallow aquifers that are used for drinking water supply. For answering questions about microbiological and geochemical influences of elevated CO₂ concentrations on the environment, an artificially created leakage scenario in a shallow aquifer was performed. After injecting about 800 kg of gaseous CO₂ with a known isotopic signature ($\delta^{13}\text{C} -30.5 \pm 0.4 \text{ ‰}$), groundwater pH decreased significantly, whereas TIC values increased. Furthermore, some major cations (Ca, K, Mg) and trace elements (Al, Mn, Si) have been released. In addition to geochemical and geophysical monitoring methods, a monitoring strategy based on stable carbon isotopes was tested. Different isotope signatures of injected CO₂ and of the natural background ($\delta^{13}\text{C} -21.9 \pm 1.4 \text{ ‰}$) allowed a detailed mapping of the artificially created CO₂ plume in the shallow aquifer. The application of soil gas probes for monitoring the shallowest soil horizon showed a very high sensitivity of this monitoring approach. In contrast to the other monitoring concepts, stable carbon isotopes are the only possibility for source identification of CO₂ in the underground. To assess the influence of increasing CO₂ concentrations on microorganisms living in the shallow surface, growth experiments were conducted with four different model strains. Two aerobic strains (*Pseudomonas putida* F1/ *Bacillus subtilis* sbsp. *subtilis* strain 168) were cultivated under an atmosphere containing 0-80 % CO₂, whereas the CO₂ concentration was increased up to 100 % for two anaerobic strains (*Desulfovibrio vulgaris* Hildenborough/ *Thauera aromatica* K172).

Summary

Elevated CO₂ concentrations caused prolonged lag-phases and a reduction of growth rates and cell yields for all four strains. The extent of the effect was proportional to the CO₂ concentration. Further, the effect of increased CO₂ concentration in combination with elevated pressure (0-5000 kPa) was studied, to make additional conclusions about deep aquifers. Already after 24 hours a significant reduction of cell numbers was observed at pressures ≥ 1000 kPa. With increasing pressure the reduction of cell numbers increased as well. To get information about the reasons for reduced growth under elevated CO₂ concentrations proteomic studies have been performed with two strains (*Pseudomonas putida* F1/ *Thauera aromatica* K172). The assumption that certain proteins are induced or repressed due to high CO₂ concentrations could be verified by performing analysis of the proteome. In summary, it was possible to apply and verify a new approach for monitoring leakages in the shallow surface at CCS sites. Furthermore, it was shown that increasing levels of CO₂ affect microorganisms of the shallow subsurface but serious toxicity, which would lead to sterilization, was never achieved.

1. Introduction

One of the first scientists, who correlated increasing CO₂ concentration in the atmosphere with increasing temperature was Arrhenius (1896). He considered CO₂ as the main absorbent for radiation in the atmosphere and calculated temperature increases resulting from increasing CO₂ concentrations. Although, many studies have been done since then, there is still a lack of detailed understanding of the processes influencing atmospheric CO₂ concentration and disagreement about the most significant controls of pCO₂ over long time periods (Pearson and Palmer, 2000). Nevertheless, it is stated that increasing CO₂ concentrations might thus have significant effects on the Earth's climate (Hansen et al., 1981). Besides the often discussed anthropogenic emission of CO₂, atmospheric CO₂ derives from a variety of geological processes, such as volcanic and hydrothermal outgassing, metamorphic decarbonation reactions, weathering of silicate minerals, and limestone formation (Pearson and Palmer, 2000). It is a fact that the change of CO₂ concentration over the Holocene (last 12 000 years) was two orders of magnitude smaller compared to the increase of anthropogenic CO₂ emission since the beginning of industrialization (Indermuhle et al., 1999). Only since 1959, the atmospheric CO₂ concentration has risen from approximately 315 ppm to 385 ppm (Keeling and Piper, 2009). By the end of the year 2011, the global atmospheric CO₂ concentration had reached 391.38 ± 0.13 ppm (Le Quéré et al., 2012). The IPCC report of 2007 even forecasted an increase to as much as 500 – 1000 ppm by the year 2100, due to expanding use of fossil fuels and land-use changes. Latest analyses reported an increase of global CO₂ emission by 3 % in 2011, which equals a total emission of 34 Gt CO₂ compared to about 23 Gt CO₂ in 1990 (Olivier et al., 2012).

Actually about 10.1 ± 0.7 Gt of carbon are emitted as CO₂ to the atmosphere by anthropogenic activities like fossil fuel burning (Sarmiento and Gruber, 2002). By some researchers it is stated that the airborne fraction (the amount of CO₂ emission, which remains in the atmosphere) increased since 1959 from 40 to 45 %. This results from a combination of increasing CO₂ emission and decreasing ability of oceans or terrestrial ecosystems to sequester CO₂ (Le Quere et al., 2009). These statements are discussed controversially by other researchers (Knorr, 2009). This only shows that not enough precise and long-term measurements exist to make specific predictions about the future development of the carbon cycle (Levin, 2012).

1. Introduction

The carbon cycle is actually a well-balanced natural regulated system of the CO₂ concentration in the atmosphere. Numerous natural sinks can store huge amounts of CO₂. Most of the global carbon is stored in rocks in form of minerals. The rest of the carbon is stored in the atmosphere, the oceans, soils, plants, and fossil fuels (<http://earthobservatory.nasa.gov/Features/CarbonCycle/>). According to Canadell et al. (2007), natural terrestrial key carbon sink processes are the CO₂ fertilization of photosynthesis, woody vegetation thickening and encroachment, forest regrowth in abandoned cropland and afforestation and reforestation respectively. In contrast, natural key carbon emission sources are soil respiration, permafrost thawing and subsequent decomposition of organic matter, deforestation, fires and peatland drainage. Furthermore, Canadell et al. stated that the long-term carbon balance of the major carbon pools is controlled by different processes, such as changes in atmospheric composition, climate change or land-use change. The estimation about specific amounts of anthropogenic emitted CO₂ that is stored by natural processes is very uncertain and it is often based on computer simulations rather than on empirical data. In average (from the year 2001 to 2011) about 2.6 ± 1.0 GtC/year are stored by terrestrial sinks. Ocean sinks sequester about 2.4 ± 0.5 GtC/years and the atmosphere 5 ± 0.2 GtC/year (Le Quere et al., 2009). Resulting effects of increasing CO₂ concentrations in the atmosphere can be an enhanced uptake of CO₂ by plants or a northward forest migration. A rather serious consequence that has to be considered is the thawing of permafrost and resulting microbial decomposition of carbon that was previously frozen (Schuur et al., 2008). Permafrost is a sink for about 1672 Gt organic carbon (Tarnocai et al., 2009) and it is predicted that till the end of 2100 about 100 GtC could be released to the atmosphere (Gruber et al., 2004). As all the models predict disequilibrium of the global carbon cycle, solutions to reduce the CO₂ emission to the atmosphere have to be found.

As CO₂ is a radiatively active greenhouse gas, such as methane (CH₄), water vapor, nitrous oxide (N₂O) or ozone, it affects the global climate. Besides these natural occurring, but also extensively anthropogenic produced greenhouse gases, synthetic greenhouse gases like hydrofluorocarbons (HFCs), perfluorocarbons (PFCs), and sulfur hexafluoride (SF₆) exist, (see Tab. 1.1). The concentrations and the global warming potential (GWP) of these greenhouse gases vary in a wide range. The global warming potential is a time-integrated global mean of the radiative force of the emission of one kg of a certain gas relative to one kg CO₂ (IPCC, 2007).

1. Introduction

The radiative force is “the rate of energy change per unit area of the globe as measured at the top of the atmosphere” (Rockstrom et al., 2009). Greenhouse gases absorb and emit radiation in different amounts within the thermal infrared range (750 nm – 1mm). By trapping the heat, released from the earth surface, they contribute to an increase of the surface temperature of the Earth, which is called global warming (Khalil, 1999). Resulting effects could be changes in average air temperature, alteration in drought intensity and frequency, changes in precipitation and storm patterns, and/or melting of glaciers accompanied by increasing sea levels (IPCC, 2007). In turn, this could lead to increasing land degradation and negative effects on aquatic and terrestrial ecosystems, agricultural production, and drinking water supply (Alexandratos, 1988; Watson et al., 1996; Dixon, 1997).

Table 1.1 Changes in concentrations of greenhouse gases and their global warming potential (GWP) for a 100 years’ time horizon.

	CO ₂	CH ₄	N ₂ O	O ₃	HFC	SF ₆
Concentration from pre-1750 [ppm]	280 ⁽¹⁾	0.700 ⁽²⁾	0.270 ⁽³⁾	0.025 ⁽³⁾	zero	zero
Recent concentration [ppm]	391.5 ⁽⁴⁾	1.871 ^{*(5)}	0.323 ^{*(6)}	0.034 ^{*(3)}	6.4x10 ⁻⁵ ⁽⁷⁾	7.4x10 ⁻⁶ ^{*(8)}
Increased radiative force [W/m ²] ⁽³⁾	1.79	0.50	0.18	0.35	0.0055	0.0029
GWP ⁽³⁾	1	25	298	n.d.	1430	22 800

*(1) IPCC (2001), (2) Khalil et al. (1996) (3)IPCC, (2007), (4) Tans (2012), (5) Cunnold et al. (2002), (6) Prinn et al. (1990), (7) Miller et al. (1998), (8) Sturges et al. (2000), *values represent a mid-latitude Northern-Hemisphere site, n.d. no data available.*

The aim to slow down global warming and to limit global temperature increase to below 2 °C is stated in the Kyoto protocol. This protocol, which is part of the United Nations Framework Convention on Climate Change (UNFCCC), was signed by 191 states and the European Union. The objective is a reduction of greenhouse gases emission, mainly CO₂, of about five percent compared to 1990 for industrial countries (article 3, paragraph 1) (KyotoProtocol, 1998).

1. Introduction

Different strategies are considered for an emission reduction, such as using alternative energy sources (e.g. wind power, solar power, and water power), or by increasing carbon sequestration within the soil (Batjes, 1999). Another discussed strategy is the capture of CO₂ from large point sources, like power plants and subsequent storage in deep geological formations. This technology, known as *Carbon Capture and Storage* (CCS), was initiated in 1989 by the Carbon Capture and Sequestration Technologies Program at the Massachusetts Institute of Technology (MIT), USA. The first off-shore and on-shore storage facilities are running since 1996 at Sleipner, Norway and since 2000 at Weyburn, Canada, respectively. Since then, several CCS operating sites as well as pilot sites have been built worldwide. According to the MIT – Carbon Capture and Sequestration Project Database about 27 new projects are planned within the next ten years (<http://sequestration.mit.edu/>, access date 13/11/2012). Fig. 1.1 shows the location and characteristics of the main CCS running projects and the sole German pilot site.

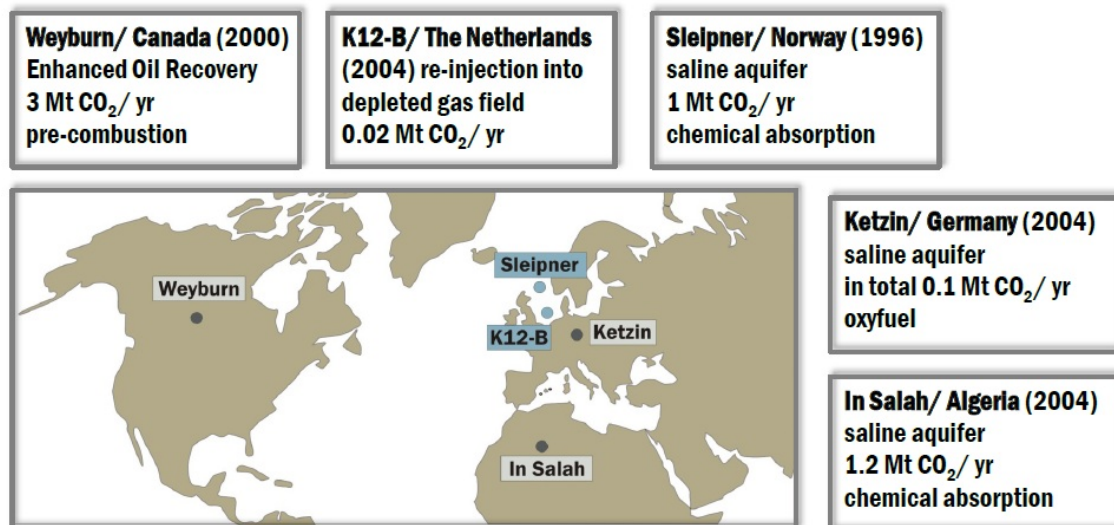


Figure 1.1 The map shows the location of three onshore (including one CCS pilot site in Ketzin, Germany) and two offshore (blue boxes) CCS projects, which are in operation. The year of injection begin, the storage formation, the injection rate, and the separation technology for capturing the CO₂ is given.

The first process involved in CCS is the capture of CO₂ from large point sources, such as fossil fuel power plants, fuel processing plants, refineries, chemical plants, and iron, steel or cement production plants.

1. Introduction

Subsequently, the CO₂ needs to be transported via pipelines, trucks or ships to a suitable storage site, where it is injected in deep geological formations, like non-mineable coal seams, saline aquifers or depleted oil and gas reservoirs (see Fig. 1.2).

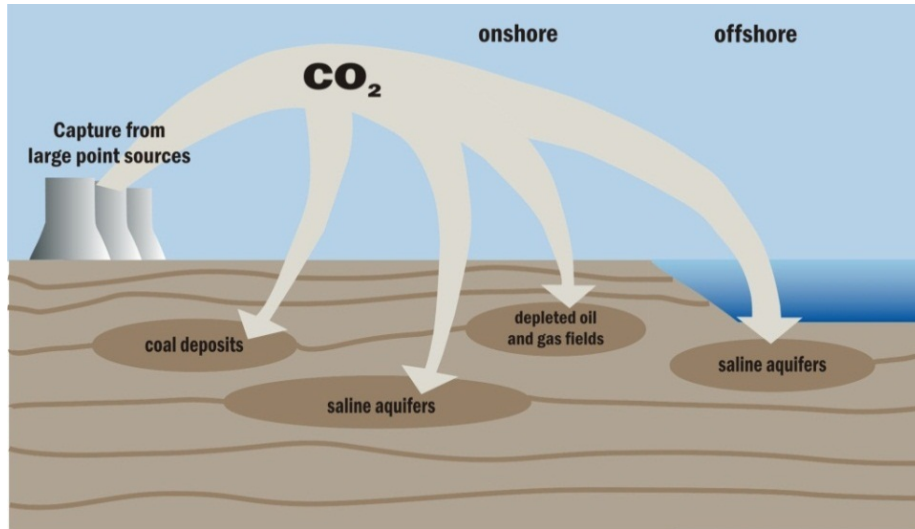


Figure 1.2 Scheme showing potential geological CO₂ storage sites (modified after <http://www.beardall-parry.com/menus/main.asp?PageName=CCS>, access date 01/11/2012).

Estimates of global storage potential are highly uncertain, as it is influenced by many different factors (CO₂ density at reservoir conditions, porosity and permeability of the storage formation, spatial extension of the storage formation (Fang et al., 2010)). The storage capacity of oil and gas fields varies within 900 – 1200 GtCO₂ (Benson and Surles, 2006), whereas saline aquifers show much larger potential. Tab. 1.2 shows a rough estimation for the three main geological storage formations that are explained in detail in chapter 1.2.

Table 1.2 Estimated storage capacities for some geological storage options.

Reservoir type	Lower estimated storage capacity (GtCO ₂)	Upper estimated storage capacity (GtCO ₂)
Oil and gas fields ^a	900	1200
Non-mineable coal seams ^b	3 – 15	200
Deep saline formations ^b	1,000	Uncertain, but possibly 10 ⁴

a) Benson and Surles (2006), b) IPCC (2005)

1. Introduction

Besides the geological storage of CO₂, artificial stores or changing of CO₂ into another form is considered as option for emission reduction. CO₂ can be used as a feedstock in chemical processes for the production of urea, fire extinguishers, in beverages or as an inert agent for food packaging (Xiaoding and Moulijn, 1996). Furthermore, CO₂ is used as a substitute for toxic phosgene during polyurethanes and polycarbonates production (McGhee et al., 1995). In total, about 115 Mt/year CO₂ are used in industry, which is about 0.5 % of the anthropogenic CO₂ emission (~ 29 GtCO₂/year). Because of the little storage capacity, limited storage lifetime of CO₂ in industrial products (months to decades) and the additional required energy for processing steps in industrial production (IPCC, 2005), these technologies provide only a minor contribution to CO₂ storage.

1.1 Technologies for capturing and transportation of CO₂

The first step of CCS is the capture of CO₂ at the source. However, the flue gas, which is produced in power plants by burning fossil fuels, is not only pure CO₂. Several other compounds, such as N₂, CO, NO_x, SO₂, and C_xH_y are included in the gas stream. If the flue gas would be injected directly into the storage formation without separation steps, the required storage volume would be much higher. Furthermore, chemical reactions between reservoir rocks and the additional compounds could lead to severe environmental impacts, such as high mobilization rates of heavy metals. Therefore, compounds are removed from the flue gas during capture processes to get nearly pure CO₂ (98 – 99 %). The capture process requires about 20 – 44 % more primary energy, depending on the applied technology (IPCC, 2005). Three basic systems for capturing the produced CO₂ from large point sources are described in the IPCC report (2005):

- Pre-combustion capture

The fuel is converted into a flue gas, which is composed mainly of carbon monoxide and hydrogen. By the addition of steam, carbon monoxide is converted into CO₂ and additional hydrogen. Both compounds are separated by absorption processes. This capture technology is used in coal-fired power plants.

- Post-combustion capture

The separation of CO₂ from the flue gas is done by liquid absorbers. The most common method (e.g. for processing natural gas or crude oil) is the chemical washing with amine.

1. Introduction

This capture technology is used in steam power plants and gas-fired power plants. This technique can be easily incorporated into already existing power plants.

- Oxy-fuel combustion capture

A flue gas composed mainly of CO₂ and H₂O is produced by using almost pure oxygen instead of air for the combustion. H₂O is removed from CO₂ by condensation.

Currently, post-combustion processes are most frequently used for capturing CO₂ (http://sequestration.mit.edu/tools/projects/index_capture.html, access date 06/11/2012). After CO₂ separation from the flue gas, it has to be transported to suitable storage sites. For the transport of liquid or gaseous CO₂ pipelines, trucks or ships will be used. Due to the large volume occupied by gaseous CO₂, compression or liquefaction of the gas is often performed to increase transport efficiency.

1.2 Storage of CO₂ in deep geological formations

CO₂ will be injected into the storage formation as supercritical fluid, which means $T > 31.1\text{ °C}$ and $p > 7300\text{ kPa}$. The supercritical state is favored as density is much higher compared to liquid state. With increasing density of CO₂ the efficiency of CO₂ storage, defined as amount of CO₂ stored per unit volume (Brennan and Burruss, 2003), increases. Furthermore, the storage safety increases with increasing density, because buoyancy is higher for lighter fluids (Ennis-King and Paterson, 2001). Additionally, the diffusion behavior of a supercritical fluid is much higher compared to gases or liquids. To keep the injected CO₂ in the supercritical state, CO₂ should be injected in average below 800 m, depending on the lithostatic and hydrostatic pressure. Some field sites provide these specific conditions, where CO₂ can be present in the supercritical state, already at lower depth (e.g. Ketzin, Germany, injection depth 630 - 650 m). Potential storage formations for CO₂ can be found in sedimentary basins (offshore and onshore) but they have to fulfill specific requirements (IPCC, 2005; De Figueiredo, 2007):

- reasonable geographical distance between source and storage site,
- sufficient *injectivity* and storage capacity,
- adequate porosity and permeability of the reservoir,
- feasible depth to provide required pressure and temperature conditions,
- well-sealed cap rock above the storage formation (e.g. mudstones, clays, shale, salt or anhydrite beds),

1. Introduction

- stable geological setting (free of fault or shear zones)

(Injectivity: Mass flow rate of CO₂ that can be injected per unit of reservoir thickness and per unit of downhole pressure difference (De Figueiredo 2007))

The most favorable locations for CO₂ storage are depleted gas and oil fields, deep unmineable coal seams, and saline aquifers with storage capacities of 675 – 900, 3 – 200, 1000 – 10⁴ GtCO₂, respectively (IPCC, 2005). Basalts also have been considered to act as possible storage formations, in areas where sedimentary basins are missing, but regarding the IPCC report 2005 their suitability still needs to be evaluated. Therefore, basalts will not be discussed in detail. The possible storage formations are listed in ascending order of their size on a global scale.

Non-mineable coal seams

Coalbeds offer two different porosity systems: numerous heterogeneous pores (with pore sizes ranging from a few Angstroms to over one micrometer) that are distributed homogeneously over the formation, and a network of natural fractures, called *cleats*, that was formed due to shrinking plant material (Shi and Durucan, 2005). If supercritical CO₂ (scCO₂) is injected into a deep coal seam, it will flow through the cleat system and diffuse into the pores, where it is adsorbed onto the surface of the pores (IPCC, 2005). As CO₂ has a higher affinity to coal compared to methane, CO₂ will adsorb (twice as much by volume) onto the coal and release the methane, which can be recovered. Besides the surface sorption of CO₂, physical trapping in natural fractures is considered as one storage option in unmineable coal seams (Shi and Durucan, 2005).

Depleted oil and gas reservoirs and enhanced oil recovery

Abandoned oil and gas fields are one of the most favored storage options because they already demonstrated their safety and integrity over long-term (IPCC, 2005). Gas and oil, which was originally accumulated in these traps, could be now replaced by injected CO₂. The main disadvantage of these storage sites is the enormous amount of existing wells due to prior exploration. Abandoned wells were plugged with cement that could be corroded by the scCO₂. Localization and tight sealing of existing wells can be very difficult and integrity of the caprock has to be monitored in detail.

1. Introduction

Injection of CO₂ into depleted oil fields is also used to recover remaining resources that cannot be extracted by primary production. Besides chemical injection, microbial injection or thermal recovery, gas injection is the most common approach for enhanced oil recovery (EOR). The recovery rate of primary production is usually between 5 – 40% (Holt et al., 1995). An active displacement of the oil by water flooding is used for the secondary recovery and production rates of additional 10 – 20% can be achieved. As the pressure gradient in the formation is not sufficient, some of the oil will remain in the formation and has to be recovered otherwise (Bondor, 1992). The tertiary recovery, with an average production rate of 13.2%, uses CO₂ amongst others as miscible agent (Martin and Taber, 1992; Moritis, 2003). When supercritical CO₂ is injected it will dissolve in the crude oil, which leads to oil swelling and hence, to a reduction of viscosity, which enables a higher recovery (Bondor, 1992).

Saline aquifers

Deep sedimentary formations that are saturated with formation water or brines with high dissolved salt concentrations are the most widely distributed potential storage sites. They often occur in depths that do not contain drinking water. Also high saline concentration does not allow the technical and economical use of the water (Bentham and Kirby, 2005). Exceptions like the Bunter Sandstone Formation in the United Kingdom, which is a drinking water supplier, will not be considered in general as possible storage formation for CO₂ (Bentham and Kirby, 2005). Their large storage capacity makes saline aquifers (e.g. sandstones, limestones) very suitable. The scCO₂ will be stored in depth of about 800 – 1000m, because pressure and temperature need to be high enough to contain CO₂ in the supercritical phase. The formations need to be composed of poorly cemented sands, which are overlaid by thick cap rocks and the porosity and permeability have to be sufficient to provide enough storage capacity. Low permeability would lead to an increase of the fluid pressure, which would result in a limited volume for CO₂ storage. By injecting CO₂, the main part of the pore fluids in the storage formation will be displaced and CO₂ will be stored in the pore space.

Cap rocks

Cap rocks are characterized by high capillary entry pressure, low permeability, high sorption capacity, and high swelling ability (Bildstein et al., 2009; Heath et al., 2009). Clay or shale layers, mudstones or evaporate layers can serve as cap rocks.

1. Introduction

1.3 Trapping mechanisms for injected CO₂

Once CO₂ is injected as a supercritical fluid into a suitable storage formation, different mechanisms contribute to the storage process (Solomon, 2007):

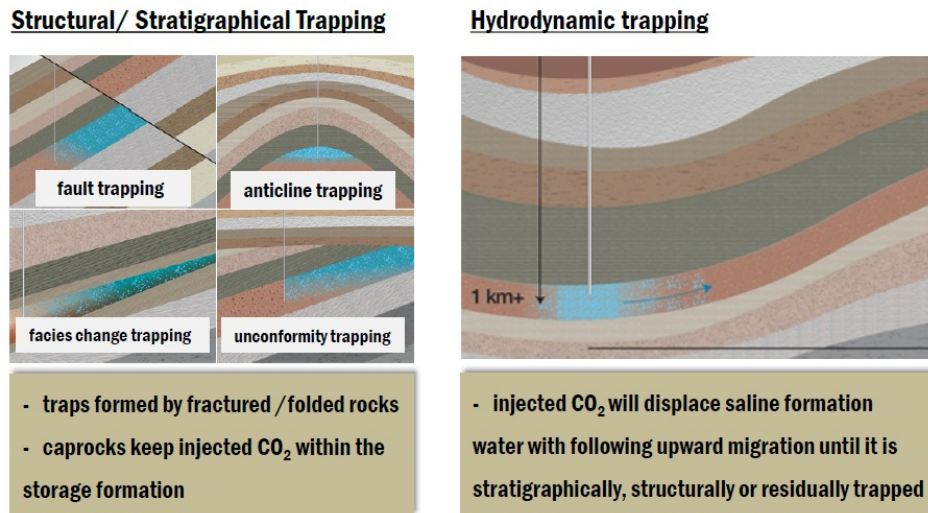
- Permeability trapping by filling up pore space of the storage formation
- Mineral trapping
- Diffusion into the storage formation
- Solubility trapping by dissolution into the formation fluid
- Buoyancy caused by different densities between injected CO₂ and formation fluid
- Fluid flow caused by natural hydraulic gradients
- Migration caused by pressure gradients created by the injection process
- Adsorption of CO₂ onto coal surfaces and organic material

As CO₂ can be stored in different formations it will interact with different formation fluids. Depending on the permeability of these fluids and the fluid flow, migration of injected CO₂ will be different. The quality of migration will be mainly controlled by differences between viscosity of the scCO₂ and the formation fluid, as scCO₂ is by an order of magnitude more viscous than oil or water (Nordbotten et al., 2005). If CO₂ is injected into saline formations or depleted oil reservoirs, it will migrate upwards until the plume has reached a layer with low permeability. This barrier will force the CO₂ plume to migrate laterally (Flett et al., 2007). The main trapping mechanisms can be divided into physical and geochemical processes (see Fig. 1.3), which will always interact and influence each other. A combination of different mechanisms will be most effective. Permanent immobilization of injected CO₂ by conversion into solid phases, adsorption on surfaces in the storage formation or trapping under cap rocks with low permeability is the goal for all CCS sites.

The amount that can be stored by the different trapping mechanisms varies significantly, depending on the storage formation characteristics (mineral trapping – small amounts, residual trapping – large amounts). Also the timeframe between these mechanisms varies from short-term storage (solubility trapping – immediately after trapping) to long-term storage (mineral trapping - hundreds of up to thousand years after injection).

1. Introduction

Physical trapping



Geochemical trapping

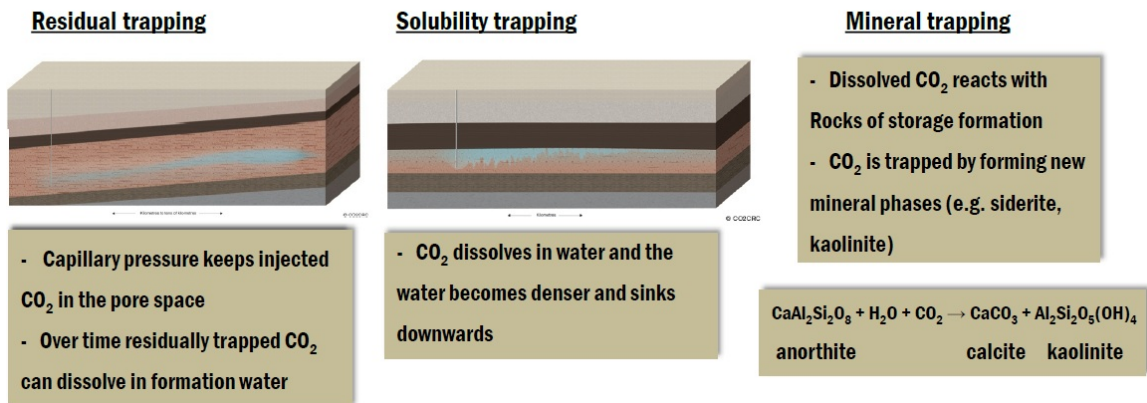


Figure 1.3 CO₂ trapping mechanisms in geological formations divided into physical trapping and geochemical trapping (images provided by the CO2CRC Online Image Library, Cooperative Research Center for Greenhouse Gas Technologies).

1.4 Potentials for CO₂ leakage from storage sites and monitoring concepts

Natural reservoirs for hydrocarbons have shown that gases and fluids can be trapped over millions of years in the underground. Storage times between 5 and 350 million years can be found (Solomon, 2007). Nevertheless, natural formations have leaks and human activities can create pathways for escaping CO₂ as well. It was suggested by several authors that storage sites should be suitable to store CO₂ for at least 1,000 years with an annual loss of less than 0.1% (IPCC, 2005; Wilson and Gerard, 2007; Pruess, 2008).

1. Introduction

According to Song and Zhang (2012) three main modes of leakages can be distinguished:

- *diffusive loss* (migration of CO₂ through the water-saturated pore space of the cap rock via molecular transport)
- *leakage through pore spaces*
- *leakage through faults and fractures*

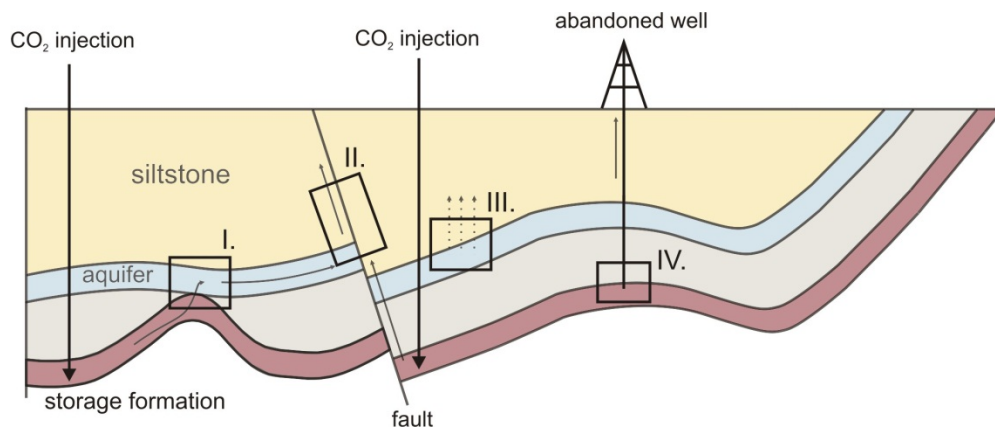


Figure 1.4 Potential leakage pathways for injected CO₂. I. Injected CO₂ can leak through “gaps” in the cap rock into a higher aquifer. II. The injected CO₂ can migrate up dip and can escape along faults and fractures. III. The injection pressure exceeds the capillary pressure and migrates through the overlying formation. IV. The injected CO₂ can leak along old and not tightly plugged abandoned wells (modified after IPCC (2005)).

Buoyancy that causes vertical flow can be an important process contributing to leakage, as the density difference between CO₂ and formation water is relatively large (30-50%) (Solomon 2007). Also anthropogenic factors, like abandoned wells or subsurface production, can affect the storage integrity.

To study potential leakage of CO₂, natural analogues, like cold-water geysers or mofettes, serve as models. They can be found in volcanic and geothermal active settings worldwide, e.g. in the Eifel, Germany (Gal et al., 2011), in the Cheb Basin, Czech Republic (Koch et al., 2008) or at the Colorado Plateau, USA (Evans et al., 2004). Magmatic reservoirs in the underground contain large volumes of gaseous CO₂. If overlying aquifers are highly fractured, CO₂ and other gases (e.g. radon) can migrate to the surface and degas via springs or mofettes.

1. Introduction

Cold-water geysers are in general artificially created if a well is drilled into a confined aquifer containing CO₂-enriched water. The well acts as pathway for the pressurized water to degas to the surface. These natural analogues have been used to improve the understanding of the influence of CO₂ on reservoir rocks and to test different monitoring techniques for CCS field sites (Shipton et al., 2004).

Monitoring concepts for CCS-sites

Before starting to develop monitoring systems, the potential receptors (aquifer, soil zone) for leaking CO₂ have to be identified. If these receptors are monitored, an early detection of a leakage is possible. Numerous studies have been performed to evaluate and test different monitoring methods for a potential CO₂ leakage. Besides the fact that high leakage rates could be a risk for human health and the ecosystem, undetected continuous leaks would not fulfill the aim of the storage facility (Yang et al., 2011). A declaration of the U.S. Department of Energy (Road-Map, 2007) stated that monitoring methods need to be able to detect leaks of 1% of the amount of injected CO₂. So far, no real leakage scenarios have been reported from existing CCS sites. Simulated scenarios, computational simulations and/or natural analogues of degassing CO₂ are used to test monitoring approaches.

As the underground that should be used for CO₂ storage, shows different characteristics in different depths, a subdivision into three different areas of interest is made: I – the surface; II – the shallow zone, and III – the deep underground (see Fig. 1.5). Not every monitoring method can be applied in every depth of the storage formation. Geophysical methods, such as seismic observation or pressure profiles are used in the deep underground to observe the behavior of the injected CO₂ in the reservoir (Torp and Gale, 2004). The accumulation of the injected CO₂ causes significant changes in the seismic signal, which can be clearly detected. The monitoring of the deep underground cannot give information about a possible leakage into upper areas. Therefore, the shallow zone and the surface have to be observed separately. On the surface some direct measurements of the CO₂ flux are performed by the chamber method (Lewicki et al., 2007b) or by Eddy flux methods (Lewicki et al., 2009). In the shallow surface zone, indirect monitoring approaches, e.g. through geochemical parameters have to be applied.

1. Introduction

The decrease of pH, the increase of total inorganic carbon (TIC) and the increase of electrical conductivity can be used as indicators for increasing CO₂ concentrations.

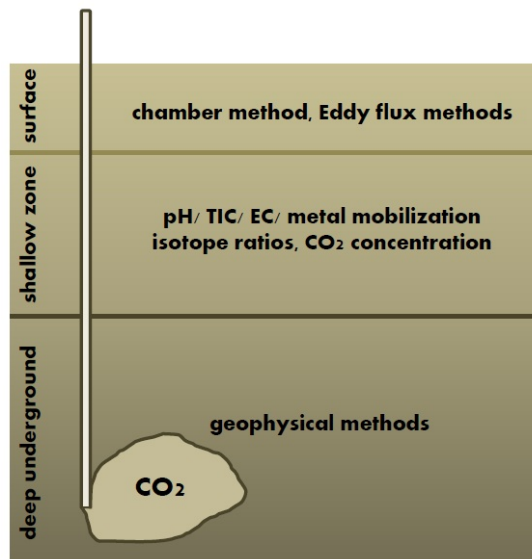


Figure 1.5 Overview of possible monitoring methods of a CO₂ leakage in different depth levels. Most of the methods are indirect measurements (pH, TIC, EC) of the injected CO₂.

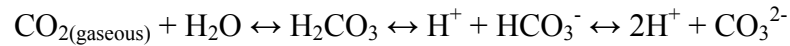
The three key points that a monitoring method needs to meet are (I.) the detection of the presence of a leak, (II.) the determination of the quantity of leakage, and (III.) the localization of the leak. So far, a combination of different monitoring methods is necessary to fulfill all of these requirements. Unfortunately, most monitoring methods do not permit a source identification of CO₂, which is only possible, using stable carbon isotopes. As all natural compounds have a specific isotope signature this can act as a fingerprint (the main principle of source identification by stable isotopes is explained in chapter 1.6). The measurement of stable isotope ratios of CO₂ is a useful tool to get qualitative information about the leak and about the origin of the leaking gas. Due to the high sensitivity of this method, it can be used as early warning approach as well as for long-term monitoring strategies.

1.5 CO₂ in soil and groundwater

CO₂ levels in soil result mainly from bacterial oxidation of plant material and respiration of CO₂ in the root zone. Many different parameters, like soil type, type of vegetation, soil moisture, soil temperature, climate conditions and land use affect the CO₂ levels (Hamada and Tanaka, 2001; Jassal et al., 2004; Oh et al., 2005).

1. Introduction

The CO₂ concentration in soil is about 10- to more than 100-fold greater compared to the CO₂ concentration in the atmosphere (~ 0.036%) (Oh et al., 2005). If gaseous CO₂ is infiltrating the groundwater in the aquifer, it dissolves and the following net reaction takes place:



Higher temperatures support higher dissolution rates of CO_{2(gaseous)} in water. If no buffer (e.g. HCO₃⁻ and CO₃²⁻) is present in the system, pH will decrease. In nearly carbonate-free sites, like the one presented later in this study, the acid buffering potential is quite low, resulting in minimal pHs of 4 (the field site is explained in chapter 2 in detail). pH affects the distribution of the four different TIC species (CO_{2(aq)}, H₂CO₃, HCO₃⁻, and CO₃²⁻). At low pHs, dissolved CO₂ exists mainly as unhydrated CO₂ but it is often expressed as H₂CO₃. Between pH 6.4 and 10.3, HCO₃⁻ is the major species, followed by CO₃²⁻ (Clark and Fritz, 1997). As pHs > 7.5 are not relevant for the studied shallow aquifer, carbonate does not need to be considered.

1.6 Stable carbon isotopes

As already mentioned, stable carbon isotopes can be used to monitor and trace the origin of a CO₂ leakage from an underground storage site into a shallow aquifer.

Stable carbon isotopes in the environment: Stable isotopes are atoms of the same element with different numbers of neutrons. Due to the different mass number, isotopes can be detected mass spectrometrically. Carbon has two stable isotopes - the lighter ¹²C has a natural abundance of 98.93 ± 0.0008% compared to the heavy ¹³C with 1.07 ± 0.08% (de Laeter et al., 2003). The ¹³C/¹²C (δ¹³C) ratios are reported as δ-notation in per mil [‰] relative to the international Vienna PeeDee Belemnite standard with ¹³C/¹²C 0.011237 (Craig, 1957). The ratio of the heavy and the light isotope is characteristic for various compounds of the global carbon cycle as illustrated in Fig. 1.6. Chemical bonds that are formed by lighter isotopes are weaker compared to chemical bonds of heavy isotopes (Bigeleisen and Wolfsberg, 1959). Different bond strengths are a result of a quantum mechanical effect, depending on different zero-point energies of the stable isotopes. The light isotopes have a higher zero-point energy, which enables easier break of chemical bonds. This principle controls the reactivity of isotopes and induces isotope fractionation (Meckenstock et al., 2004).

1. Introduction

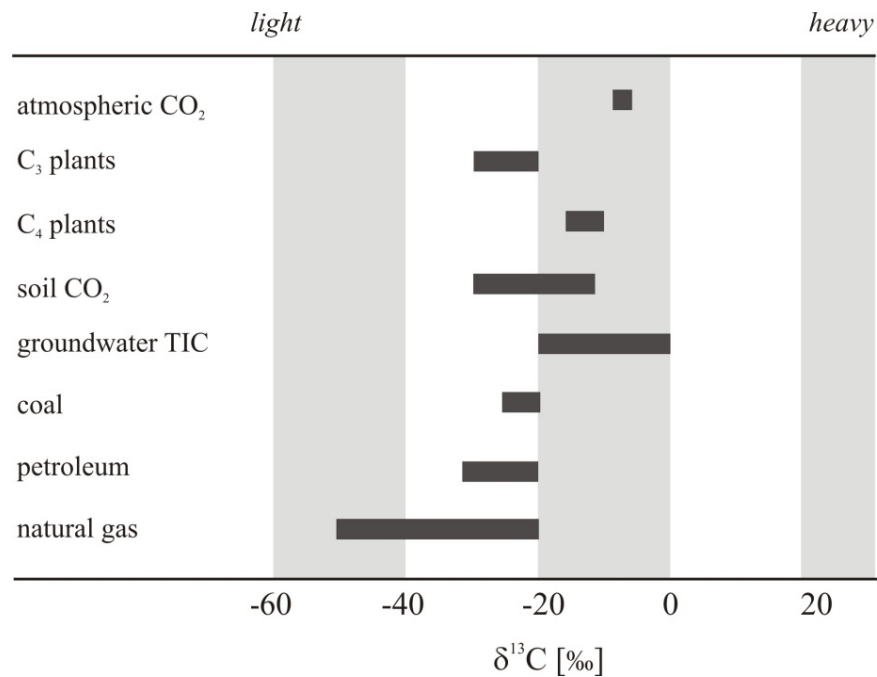


Figure 1.6 Ranges of $\delta^{13}\text{C}$ values for different natural compounds involved in the global carbon cycle (modified after Clark and Fritz (1997)). The more positive the $\delta^{13}\text{C}$ value, the more enriched is the compound in heavy isotopes.

Isotope signature of CO_2 from fossil fuel combustion: The CO_2 that should be stored in the underground will be predominantly produced by burning fossil fuels. These hydrocarbons were formed, amongst others, by buried organic material. During sedimentation, temperature and pressure increased, resulting in the breakdown of organic molecules and the formation of kerogen. Additional thermal alteration of kerogen can lead to the formation of hydrocarbons, in which the isotope signature of the organic material is conserved. Kerogen is often composed of plant material. Over more than 95% of the worldwide biomass is composed of C_3 -plants (Warrick et al., 1986). C_3 -plants use a three-carbon intermediate for CO_2 fixation during photosynthesis. CO_2 diffuses through stomata pores into the plant. Due to the mass difference between the two carbon isotopes, the lighter ^{12}C will diffuse faster compared to ^{13}C . The CO_2 fixation takes place in the stoma of the chloroplasts via the Calvin cycle. This reaction is enzymatically catalysed by the enzyme ribulose-1,5-bisphosphate carboxylase/ oxygenase (RuBisCO), leading to a discrimination of the heavy ^{13}C isotope (Park and Epstein, 1960; Farquhar et al., 1989) (Fig. 1.7). Consequently, C_3 plants are depleted in ^{13}C between 15 and 30‰ compared to the atmosphere (Fig. 1.6).

1. Introduction

Therefore, CO₂ from fossil fuel combustion is often isotopically depleted in $\delta^{13}\text{C}$ (< -25‰) compared to CO₂ in aquifer systems or soil gas (about $\delta^{13}\text{C}$ -20 to 0‰). Also algae are isotopically depleted, which is reflected in the isotope signature of petroleum (see Fig. 1.6).

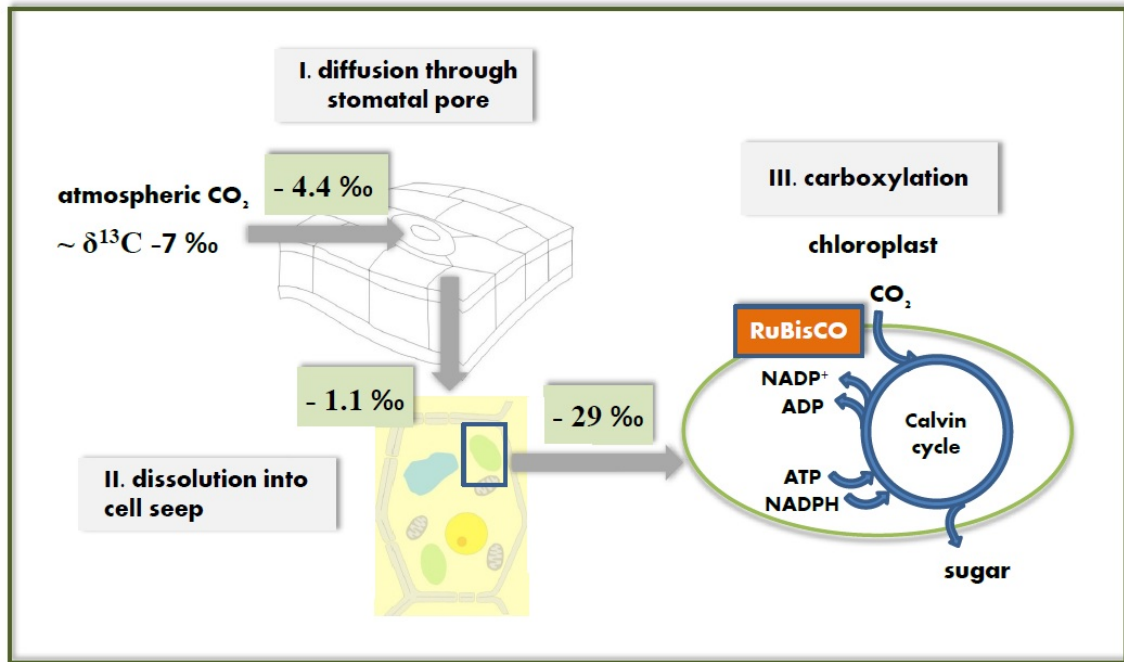


Figure 1.7 ¹³C discrimination during CO₂ uptake and fixation in plant cells. CO₂ fixation takes place in the stoma of the chloroplasts via the Calvin cycle. The enzyme RuBisCO catalyses the first major step of carbon fixation. Values in green boxes indicate that ¹³C is discriminated in the product compared to atmospheric CO₂. Data for isotope fractionation are taken from O'Leary (1988).

Isotope signature of groundwater and soil gas: The natural isotope composition of CO₂ in groundwater is governed by the isotopic composition of CO₂ in the atmosphere, the composition of carbonate minerals, and to some extent, by microbial recycled plant material. On average, ranges between 0 and -20‰ can be found for $\delta^{13}\text{C}$ of groundwater.

The CO₂ in soils is derived from atmospheric CO₂, respiration of plant roots, and the decomposition of organic matter. Isotope ratios of soil CO₂ (gas occupying pore space in a soil) are related to the isotope ratios of the source. Diffusion processes between soil and the atmosphere cause an enrichment of ¹³C of about 4.4 ‰ relative to the source (Cerling et al., 1991; Aravena et al., 1992).

1. Introduction

Therefore, average $\delta^{13}\text{C}$ of soil gas is around -23 ‰ in most C_3 plant areas (see also chapter 3). If the isotope signature of the injected CO_2 and the background (soil gas and groundwater) of the storage site is known and if the difference between both values is significant enough, $\delta^{13}\text{C}$ values might be used as source indicator for CO_2 leaks.

Analysis of stable carbon isotopes

For the analysis of stable carbon isotopes of environmental samples a combination of a conventional gas chromatography (GC) with an isotope-ratio-mass-spectrometer (IRMS) is used. The target compound is separated by a gas chromatograph, which is connected via an interface with an isotope-ratio mass spectrometer (see Fig. 1.8).

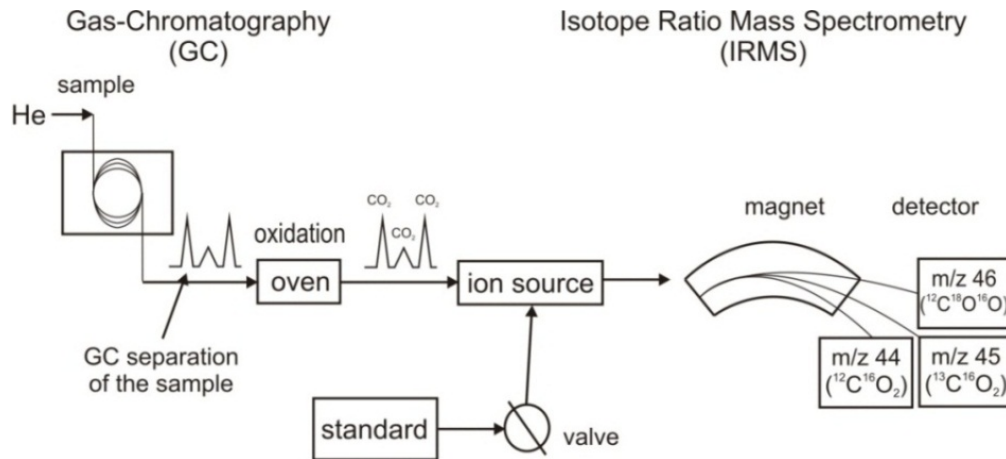


Figure 1.8 Schematic illustration of a GC-IRMS system for analyzing stable carbon isotopes. The standard is a CO_2 gas with a known isotopic signature normed according to the international V-PDB standard (after Fischer (2006)).

For analyzing the isotope ratio of $^{13}\text{C}/^{12}\text{C}$ the organic material has to be oxidized to CO_2 , which is done in the interface that is composed of a combustion oven. If CO_2 is measured directly, combustion is not necessary and the gaseous sample can be injected directly. The isotope signatures are measured via the CO_2 specific masses 44, 45, and 46 with a selective detector of an isotope ratio mass spectrometer. All measured $^{13}\text{C}/^{12}\text{C}$ ratios are reported in delta notation ($\delta^{13}\text{C}$) which is defined:

$$\delta^{13}\text{C} = (\text{R}_{\text{Sample}} - \text{R}_{\text{Standard}} / \text{R}_{\text{Standard}}) \times 1000 \quad (\text{eq. 1.1})$$

where $\text{R}_{\text{standard}}$ and R_{sample} are the isotope ratios in the standard and the sample, respectively.

1.7 The importance of CO₂ for microorganisms

Besides the more dominant and often discussed effects of increasing atmospheric CO₂ concentrations on global climate, the effects of high CO₂ concentrations on microorganisms in the soil surface are less studied. The shallow surface is populated with about one million of bacterial species per gram soil (Kuzyakov and Blagodatskaya, 2012). Microorganisms inhabit areas in the underground that are anthropogenically used, e.g. shallow aquifers for drinking water supply. Furthermore, soils provide important ecosystem services of regulating and supporting functions that are fundamental to life (for a selection see table 1.4) (Daily et al., 1997). Even if these services are often not used directly by humans, they provide the background for human used services and therefore, this aspect needs to be considered (Turbé et al., 2010). Consequently, the question arose, how increasing CO₂ concentrations would affect microorganisms of shallow surface zones and associated soil functions. As leaking CO₂ can migrate from a storage site to the surface, it was necessary to test whether microorganisms are sensitive to elevated CO₂ levels.

Table 1.4 Selected soil ecosystem services ¹(Daily et al., 1997), ²(Dominati et al., 2010)

Supporting	habitat and gene pool ¹
	retention, renewal and delivery of nutrients for plants that contribute to plant growth ^{1,2}
	regulation of major element cycles like carbon and nitrogen ¹
Regulating	disposal of waste and dead organic material ¹
	buffering of the hydrological cycle ¹
	climate regulation through carbon storage ²

Some studies have shown that slightly increased CO₂ concentrations could have a favorable effect on fungal hyphal growth (Bécard and Piché, 1989; Desgranges and Durand, 1990) and on some heterotrophic bacteria (Krebs, 1941). Nevertheless, CO₂ can also act as potential growth inhibitor (Dixon and Kell, 1989). So far, only little is known about the effects of increasing CO₂ concentrations on soil microorganisms. In contrast, numerous studies have been performed with bacteria causing food spoilage or patient infections. In food and medical industry, scCO₂ is used to sterilize food and beverages (Farber, 1991; Enomoto et al., 1997; Dillow et al., 1999).

1. Introduction

This technique is known to kill bacteria very efficiently without damaging the food or medical product. Using scCO₂ for sterilization, it always involves pressures above 7330 kPa but these pressure ranges are not relevant for shallow aquifers. Whereas increasing CO₂ concentrations on plants cause, amongst others, an increase of leaf photosynthesis rates, (Jossi et al., 2006; Taub, 2010), the effect of elevated CO₂ concentration on soil microorganisms has not been studied in detail.

Studies about microbial community changes resulting from long-term exposure to high CO₂ concentrations due to natural CO₂ vents have been done (Oppermann et al., 2010). Furthermore, studies about the response of soil microorganisms on increasing atmospheric CO₂ concentrations were performed (Sadowsky and Schortemeyer, 1997; Freeman et al., 2004; Blagodatskaya et al., 2010). An increase of microbial growth rates with increasing CO₂ concentrations was observed, probably the result of higher carbon input into soil due to elevated rhizodeposition. As these organisms grew under conditions that allowed slow adaptation to elevated CO₂ concentrations, the data cannot be used for statements about effects of suddenly increased CO₂ concentrations like they would occur during CO₂ leakage scenarios. If a decrease of microbial growth with increasing CO₂ concentrations is expected, maybe a disturbance of the ecosystem services has to be considered.

1.8 Objectives of the work and cooperation

Numerous studies have been performed to evaluate CCS technologies as an option to reduce CO₂ emission to the atmosphere. So far, only little has been done to study potential leakages of CO₂ in shallow surface zones. However, these studies are necessary to test and establish monitoring methods, to gain information about the environmental impact of leaking CO₂, and to conduct a proper risk assessment. The aim of the project “*CO₂-Leakage – CO₂ leakage experiment into a near-surface aquifer for testing monitoring concepts and methods*”, in which this work is involved, was the performance of a field test, where CO₂ was injected from the surface into a shallow aquifer, trying to simulate a CO₂ leakage. Different monitoring approaches have been studied and ecophysiological effects of increasing CO₂ concentrations have been investigated. The thesis was subdivided into two working packages with the following objectives:

1. Introduction

Working package I: Development of a monitoring method using stable carbon isotopes

- Monitoring of a simulated CO₂ leakage in a shallow aquifer using stable carbon isotopes;
- validation of this monitoring method for source identification of the leakage;
- enhancement of a soil gas sampling method in the shallow surface and testing if soil gas sampling is an appropriate monitoring tool.

Working package II: Influence of increased CO₂ concentrations on microorganisms

- Investigation of the influence of increasing CO₂ concentrations and increasing pressure on growth and survival of typical aquifer and soil microorganisms;
- assessment of effects of increasing CO₂ concentrations on the proteome of typical aquifer microorganisms.

Working package I

For the performance of a simulated CO₂ leakage into a shallow aquifer it was necessary to find a suitable test location. A suitable location needs: a good connection to the infrastructure, it needs to be free of underground constructions and buildings, it needs to fulfill geological requirements for performing the test, and it needs to be located in an area where the public acceptance for such a research project is given. The design of the injection test and the organization of the project were mainly performed by Dr. Anita Peter from the Institute of Earth Sciences, Department Applied Geology of the CAU Kiel (see chapter 2). Before the injection test could be performed, detailed geophysical investigations of the underground have been performed by Hendrik Lamert, Dr. Ulrike Werban, Helko Kotas, Andreas Schoßland, and Simon Kögler of the Department Monitoring and Exploration Technologies (MET) of the UFZ Leipzig. The technical realization of the CO₂ injection test, the construction and maintenance of the injection system and the modeling of the underground structure of the field site were performed by Matthias Beyer and Ben Heinrich from GICON GmbH Dresden (see chapter 2). Before, during and after the injection test, groundwater samples were taken to study the change of geochemical parameters, like pH, TIC, anions and cations. The sampling campaigns were mainly organized and performed by Hendrik Lamert (Department MET – UFZ, Leipzig) and myself.

1. Introduction

The analyses of the geochemical parameters were performed at the Institute of Earth Sciences at the CAU Kiel and the interpretation of the data was done by Dr. Götz Hornbruch (see chapter 2). The analyses of the concentration of the added tracer SF₆ was performed at a commercial laboratory (ERGO Umweltinstitut GmbH, Dresden) (see chapter 2). Isotopic analyses of the groundwater samples were done by myself.

In addition to the geochemical and isotopic monitoring, geophysical methods, in detail changes in the electrical conductivity, were tested to monitor the leakage of CO₂. The geophysical studies coupled with the testing of multiphase modeling were performed mainly by Hendrik Lamert, Daniel Steinbrückner (MET – UFZ, Leipzig) and Prof. Dr. Helmut Geistlinger (Department Soil Physics – UFZ, Halle) (see chapter 4). For taking soil gas samples from the shallow surface for the isotopic monitoring, a specific sampling device was constructed. The prototype for the soil gas lances was provided by Dr. Ingolf Dumke from the Department Organic Geochemistry and Petrography from the Bundesanstalt für Geowissenschaften und Rohstoffe (BGR) in Hannover. The construction of adapted soil gas lances was done by myself in cooperation with Reinhard Schumann (formerly Department Isotope Biogeochemistry – UFZ, Leipzig) (see chapter 3). Soil gas sampling and analyses were performed by myself.

Working package 2

The second working package should answer the following questions:

- How severe are effects caused by suddenly increasing CO₂ concentrations for specific microorganisms?
- How is growth and survival of non-adapted microorganisms affected?
- How is the expression of proteins affected by suddenly increasing CO₂ concentrations?

Four different model strains (see Tab. 1.4) were used to test the influence of increasing CO₂ concentrations as well as increasing CO₂ concentrations in combination with increasing pressure. These specific strains have been chosen to investigate the effects on microorganisms of diverse ecotypes. Two aerobic and two anaerobic strains, including one sulfate reducer (*D. vulgaris*) and one nitrate reducer (*T. aromatica*) were chosen.

1. Introduction

The variability among the model strains should allow an investigation of CO₂ influences on different temperature-, substrate-, and pHs- depending organisms. The cultivation and survival experiments were performed in the laboratory of the Department Isotope Biogeochemistry – UFZ, Leipzig. Even if many studies about sterilization with scCO₂ have been performed in the framework of modified atmosphere packing for food spoilage bacteria control, the exact mechanisms of CO₂ inhibition are not completely revealed.

Table 1.3 Four model strains used for growth experiments with high CO₂ concentrations and elevated pressure. Growth condition, growth temperature, pH, and growth substrates are listed.

	organisms	substrate	temperature	pH	habitat
Aerobic	<i>Pseudomonas putida</i> F1	acetate	30 °C	7	soil isolate
	<i>Bacillus subtilis</i> 168	glucose	30 °C	7	soil isolate
Anaerobic	<i>Desulfovibrio vulgaris</i> Hildenborough	lactate	37 °C	7	soil isolate
	<i>Thauera aromatica</i> K172	acetate	25 °C	8	sewage sludge isolate

For testing the survival rates of the microorganisms under high CO₂ concentrations and high pressure, specific pressure vessels have been constructed. The construction of the pressure vessels was performed in cooperation with Reinhard Schumann (formerly Department Isotope Biogeochemistry – UFZ, Leipzig) (see chapter 5). To understand the inhibitory mechanisms of CO₂, studies on the proteome of two model organisms have been performed. So far, no studies about the effect of high CO₂ concentrations at atmospheric pressure on the proteomic level have been performed. Therefore, experiments have been conducted to see, if proteins are suppressed or enhanced by increasing CO₂ concentrations. After the growth and survival experiments, investigations on the influence of increasing CO₂ concentrations on the proteome of the model organisms were performed. The measurements of the samples were performed by Kathleen Eismann. The interpretation of the data was mainly performed by Dr. Jana Seifert of the Department Proteomics of the UFZ with support of Dr. Brandon Morris from the University of Freiberg (formerly Department ISOBIO – UFZ) and myself.

**2. Investigation of the geochemical impact of CO₂ on shallow groundwater:
Design and implementation of a CO₂ injection test in Northeast Germany**

2.1 Kurzfassung

Um Aussagen über den geochemischen Einfluss von CO₂ und die Anwendung verschiedener Monitoringmethoden für potentielle CO₂ Leckagen treffen zu können, wurde ein kleinskaliger und zeitlich begrenzter CO₂ Injektionstest in einem flachen Grundwasserleiter durchgeführt. Zur Versuchsplanung und -realisierung war eine detaillierte Standorterkundung, zusammen mit Mehrphasen-Simulationen notwendig. Vor Beginn der CO₂ Injektion wurde ein Monitoring-Netzwerk installiert. Über einen Zeitraum von zehn Tagen wurde über drei Injektionslanzen in einer Tiefe von 18 m in einem quartären Grundwasserleiter CO₂ injiziert. Die Monitoringmethoden umfassten sowohl Grundwasserprobenahmen und Standardanalysen, als auch Spurenelement- und Isotopenanalysen, geoelektrische Bohrlochmessungen, Passivsampler zur temporären Analyse von Kationen und Multiparametersonden zur kontinuierlichen Messung von gelöstem CO₂, pH und elektrischer Leitfähigkeit. Durch die CO₂-Injektion kam es zu einer Zunahme der Gesamtkohlenstoff-Konzentration (TIC) und zu einer pH-Abnahme bis zu einem Wert von 5.1. Außerdem kam es zur Freisetzung von Kationen und Spurenelementen. Sowohl das geoelektrische Monitoring und die Isotopenanalysen, als auch die die Multiparametersonden erwiesen sich als zuverlässige Methoden für das Monitoring von injiziertem CO₂ und/oder einer Veränderung des Grundwassers.

Peter, Anita; Lamert, Hendrik; Beyer, Matthias; Hornbruch, Götz; Heinrich, Ben; Schulz, Alexandra; Geistlinger, Helmut; Schreiber, Ben; Dietrich, Peter; Werban, Ulrike; Vogt, Carsten; Richnow, Hans-Hermann; Großmann, Jochen; Dahmke, Andreas

Published in: Environmental Earth Sciences, 2012, 67 (2), pp 335-349.

2.2 Abstract

A small scale and temporally limited CO₂ injection test was performed in a shallow aquifer to investigate the geochemical impact of CO₂ on shallow aquifers and to apply different monitoring methods. Detailed site investigation together with multiphase simulations were necessary to design the injection experiment and to set up the monitoring network, before CO₂ was injected over ten days at three injection wells at a depth of 18m below surface into a quaternary sand aquifer.

2. Investigation of the geochemical impact of CO₂ on shallow groundwater

Monitoring methods comprised groundwater sampling and standard analyses as well as trace element analyses and isotope analyses; geoelectrical borehole monitoring; passive samplers to analyse temporally integrated for cations and multiparameter probes to measure continuously for dissolved CO₂, pH and electrical conductivity. Due to the injection of CO₂ total inorganic carbon concentrations increased and pH decreased down to 5.1. Associated reactions comprised the release of major cations and trace elements. Geoelectrical monitoring as well as isotope analyses and multiparameter probes proved to be suitable methods to monitor the injected CO₂ and/or the alteration of groundwater.

2.3 Introduction

Leakage from subsurface storage sites is one of the main concerns connected with carbon capture and storage (CCS) technology. One potential risk associated with CO₂ leaking from storage sites is the geochemical alteration of shallow groundwater systems causing a pH decrease and the potential mobilization of heavy metals due to mineral dissolution and / or desorption processes.

Although (Lewicki et al., 2007a) studied intensively sites with naturally occurring CO₂ to understand processes and phenomena of CO₂ leakages from deep formations to the surface, these natural analogues are unlikely to answer urgent questions regarding the impact of CO₂ intrusion on a pristine aquifer that has not been in contact with CO₂. Several studies have investigated either by modelling (Wang and Jaffe, 2004; Zheng et al., 2009; Apps et al., 2010; Wilkin and DiGiulio, 2010) or by laboratory experiments (Little and Jackson, 2010; Lu et al., 2010) the effect of CO₂ on shallow aquifers. Consistently, all report decreasing pH with increasing TIC (total inorganic carbon) and HCO₃⁻ concentrations. Concerning the behaviour of cations, the modelling studies suggest the release of cations like lead, arsenic zinc and other heavy metals due to mineral dissolution (Wang and Jaffe, 2004) and /or due to desorption from surface complexation (Zheng et al., 2009). Both studies emphasize the high sensitivity of relevant modelling parameters, like dissolution and sorption kinetics, on the simulated release of cations, thus they recommend lab and field experiments to gain insight into geochemical processes and parameters.

2. Investigation of the geochemical impact of CO₂ on shallow groundwater

Lab experiments where natural aquifer sediment samples were exposed to CO₂ enriched water showed that concentrations of various metals increased with increasing TIC and decreasing pH (e.g. Ca, Fe, Mn, Ba were reported by (Little and Jackson, 2010); Lu et al. (2010), but other cations decreased with increasing TIC and decreasing pH (e.g. As, Mo, Cr as reported by Little & Jackson (2010)). Some cations are reported to behave in either way, for example aluminium was observed to increase in some experiments (Lu et al., 2010), while Little & Jackson (2010) noticed decreases of aluminium with decreasing pH.

The first and to our knowledge so far only test site, where under field conditions CO₂ was injected into a pristine shallow aquifer is the ZERT site in Montana (Spangler et al., 2010), where CO₂ was injected a depth of 1.1-2.5 m below surface and approximately 0.5-1 m under the groundwater table. Although the aim of this study was monitoring of the unsaturated zone, also intense groundwater sampling was performed at the ZERT site, showing increases in major divalent cation concentrations and increasing trace metal concentrations in groundwater with increasing alkalinity (Apps et al., 2010; Kharaka et al., 2010).

The aim of the present study is to contribute to an improved understanding of the behaviour of CO₂ in shallow groundwater systems as a basis for a sound risk assessment for CCS technology. Therefore, a CO₂ injection experiment was performed during 10 days in March and April 2011 to pursue the following objectives: firstly, to gain insight into the potential geochemical reactions taking place in a shallow, carbonate-free aquifer system that is subject to a CO₂ intrusion. Secondly, to verify whether reactive transport models are capable to predict these reactions in a reliable manner, i.e. whether they are suitable for a sound risk assessment and thirdly, to develop, test and apply different monitoring methods that are appropriate to monitor CO₂ intrusions and / or the geochemical alteration of groundwater due to CO₂ intrusions.

The present paper provides an overview over the test site, the design and operation of the injection experiment and the different monitoring methods applied. Beside groundwater sampling and subsequent analyses, also geoelectrical single-borehole and borehole-borehole measurements, stable isotope analyses of ¹³C/¹²C, continuously operating multiparameter probes including pH, electrical conductivity and CO₂ and passive samplers to monitor for released cations on an integral temporal scale were applied.

2. Investigation of the geochemical impact of CO₂ on shallow groundwater

First results of the different monitoring methods are presented in this paper, while further publications (e.g. Lamert et al. (2012)) will show results of the various methods used in detail and the accompanying modelling studies.

2.4 Test site

The test site is part of a former military airfield, located approximately 100km north of Berlin, in the state of Brandenburg / Germany, close to the town of Wittstock. The test site comprises a fallow plane of approximately 90m by 60m (s. Fig. 2.1). Due to the historical usage as a military airfield, a minor contamination of TCE in the groundwater was found in parts of the test site (concentrations up to 58 µg/L).

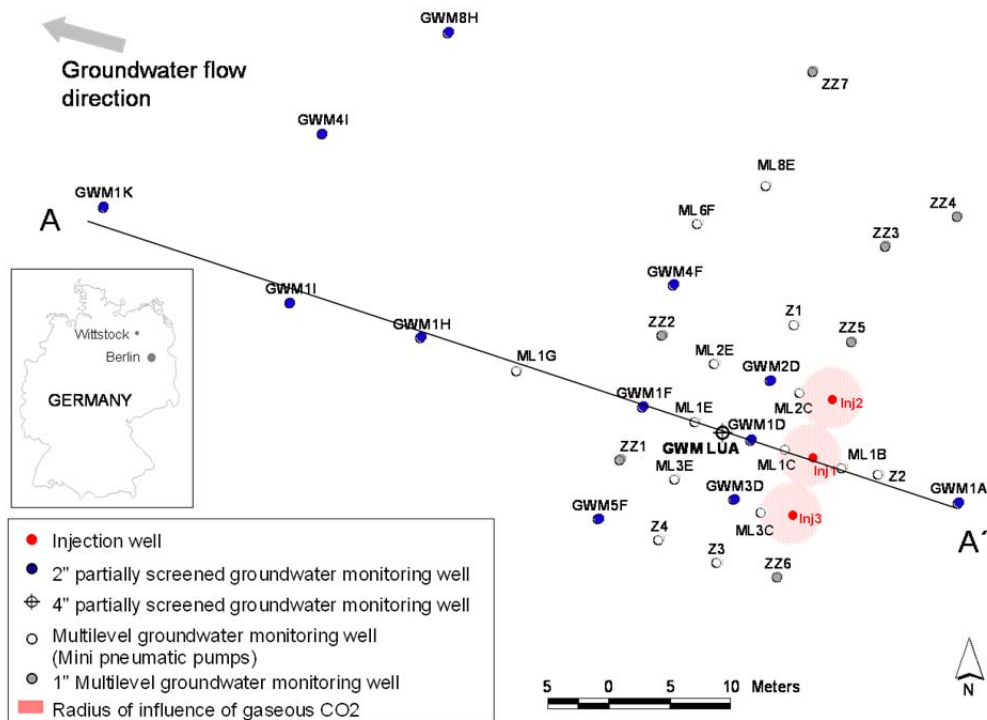


Figure 2.1 Map of test site for CO₂ injection with injection lances, groundwater monitoring wells and intersection line for geological cross section (s. Fig. 2.3).

2.4.1 Geology

A detailed geological characterization of the test site was performed between March 2010 and March 2011. First geoelectrical surveys were performed. Five electric resistivity tomography lines of approximately 250m length and distances of 50m each provided information about the stratigraphic composition of the near subsurface.

2. Investigation of the geochemical impact of CO₂ on shallow groundwater

Based on the resistivity tomography results, relevant locations for Direct Push (DP) soundings were chosen that allow for high resolution vertical profiles of various soil specific properties (Dietrich and Leven, 2006). HPT (hydraulic profiling tool) profiles (Dietrich et al., 2008) were used to derive estimates of hydraulic conductivity (K) based on the ratio of an injected water flow rate and the corresponding pressure response (Q/p). HPT logs that were calibrated by slug-tests as well as sieve analyses served to determine hydraulic conductivities and permeabilities, respectively (see also section 2.5).

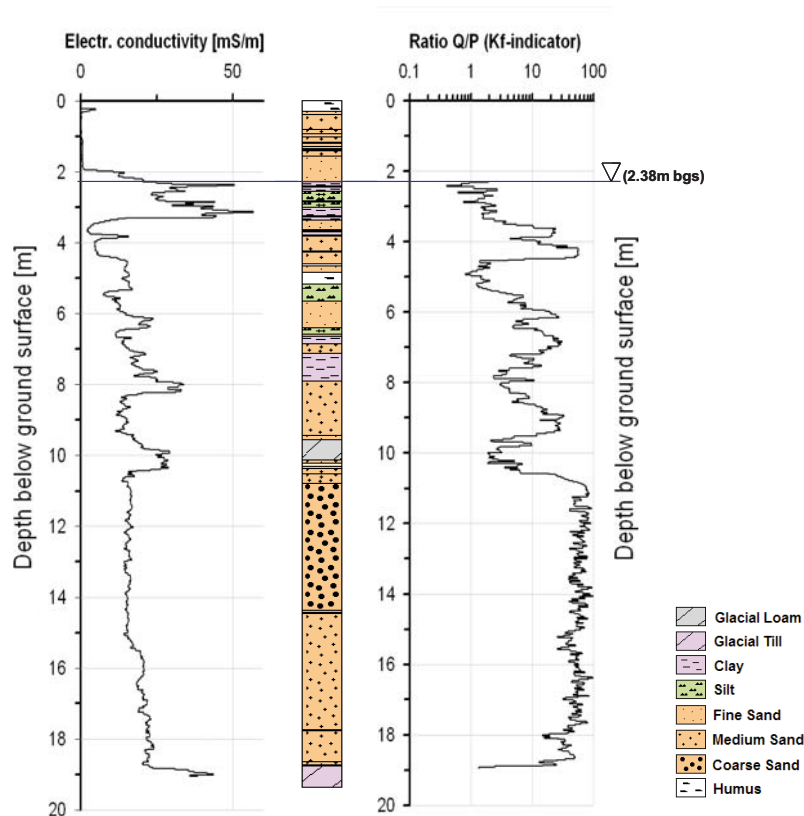


Figure 2.2 EC-log, geological profile and HPT-log located 2m east of injection well Inj1.

Electrical conductivity (EC) loggings (e.g. Schulmeister et al. (2003)) allow for a high resolution stratigraphic interpretation of the sediment. An increase of electrical conductivity indicates an increased share of silt and/or clay particles. In the vicinity of the CO₂ injection wells, additionally sediment cores were taken to validate the EC and HPT logs (see Fig. 2.2). In total, nine DP EC/HPT-soundings together with borehole profiles at 38 locations (see also Fig. 2.1) served as basis for a geologic structure model. A geologic profile and its hydrogeological interpretation are provided in Fig. 2.3 and Tab. 2.1.

2. Investigation of the geochemical impact of CO₂ on shallow groundwater

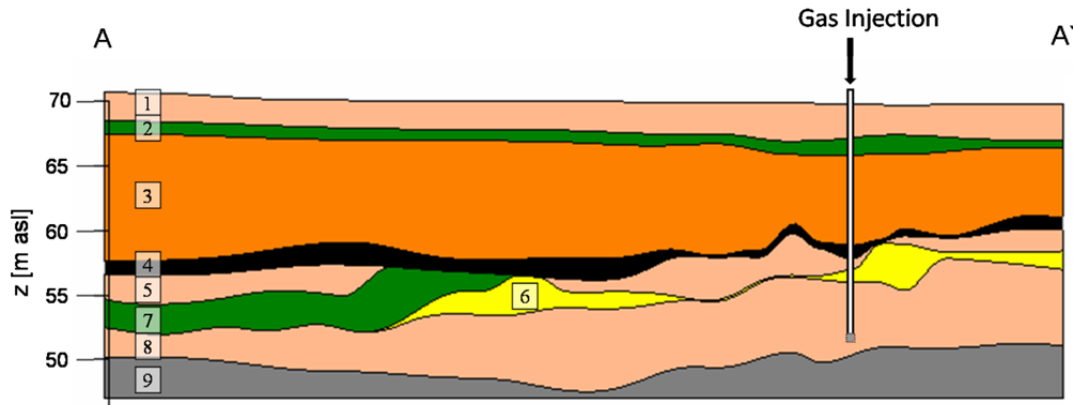


Figure 2.3: Geological profile from A to A' (see Fig. 1) with position of injection lance 1. Layer numbers refer to Tab. 2.1.

Table 2.1 Schematic geological profile at the test site.

Average Layer Depth [m bgl]	Layer No.	Lithological Description	Hydrogeological Classification
0 – 2	1	Sands (primarily medium sand)	unsaturated Zone
2 – 3.5	2	Silt	unsaturated /saturated Zone
3.5 – 11	3	Interbedded sand, silt, clay and humus layers	aquifer 1
11 – 11.5	4	Glacial loam (discontinuous)	aquiclude 1
11.5 – 13.5	5	Medium sand	aquifer 2
13.5 – 15	6	Coarse sand (eastern area)	aquifer 2
13.5 – 16	7	Silt (western area)	local Aquiclude
15 / 16 – 19.5	8	Medium sand, some fine sand	aquifer 2 (injection horizon)
>19.5	9	Glacial till	aquiclude 2

The upper confined aquifer (aquifer 1) at the site is characterized by glacial sediments from the Vistula period, consisting of heterogeneous interbedded sand, silt, clay and humus layers with a thickness of approximately 11 m. Below aquifer 1, glacial loam from the Saale stadium was detected showing varying thicknesses (average of 0.5m) and depths. Apart from few exceptions the loam was extensively detected on the test site, however no glacial loam was found in some drilling samples located in the northwestern, northeastern and southern area. In these areas, hydraulic contact between aquifer 1 and aquifer 2 can be assumed.

2. Investigation of the geochemical impact of CO₂ on shallow groundwater

Generally, the glacial loam is dipping in southwestern direction on the test site. In the eastern part around injection lances Inj1 – Inj3 a dome-like arching was detected (see Fig. 2.3).

Beneath the glacial loam, Saalian sediments of the main groundwater aquifer (aquifer 2) are located. The thickness of aquifer 2 is approximately 8 m. The sediment of this aquifer consists primarily of medium sands with an isolated layer of coarse sand in the eastern part of the test site. The coarse sand is especially developed in the vicinity of the CO₂ injection wells, but tapers off in western direction. Both, medium sands as well as coarse sands are free of carbonates (see (Peter et al., 2011)). In the western area of the test site, a spatially limited silt horizon in the sands of aquifer 2 was encountered which disappears in eastern direction. Due to its extensive and relative homogeneous occurrence, aquifer 2 was chosen as injection horizon for the CO₂. In eight drilling samples glacial till was encountered below aquifer 2 at an average depth of 19.5 m bgl. The glacial till acts as an aquiclude and forms the base of aquifer 2, as well as the lower limit of the geologic structure model. Due to the limited sounding depth (maximum 24 m bgl), the bottom of the glacial till was not detected at the test site.

2.4.2 Hydrogeology

Regional groundwater flow is directed from east to west, towards the river Dosse, which is the drainage located approximately 800 m apart from the injection wells. In order to determine the local groundwater flow direction and flow velocity at the site, six groundwater wells were installed 60 to 160 m away from the injection wells (see also Peter et al., 2011) additionally to the monitoring wells depicted in Fig. 2.1. Groundwater levels measured in March and June 2011 at 25 monitoring wells revealed relatively small hydraulic gradients of about 1.4 ‰ in the eastern part of the test site down to monitoring well GWM 1H, whereas gradients increase west of GWM 1H to approximately 6.8 ‰. The groundwater flow direction derived from the groundwater levels confirm the general flow direction from east to west, however due to very small head differences within the injection area, no reliable conclusion could be made on the local flow direction at the injection lances.

Thus, a salt tracer test using electrical resistivity measurements (see e.g. Hoffmann and Dietrich (2004)) was performed in November 2010 to investigate the local flow regime in the vicinity of the CO₂ injection wells.

2. Investigation of the geochemical impact of CO₂ on shallow groundwater

In the present study, NaCl was added to drinking water to obtain a concentration of 10g/l to realize a clearly difference of the electric conductivity between the local groundwater (about 600 $\mu\text{S}/\text{cm}$) and the injected saline water (about 17 mS/cm). The saline tracer was injected with a constant flow of 0.4 L/min over a period of 84 hours in a depth of 13.2m below ground level into aquifer 2.

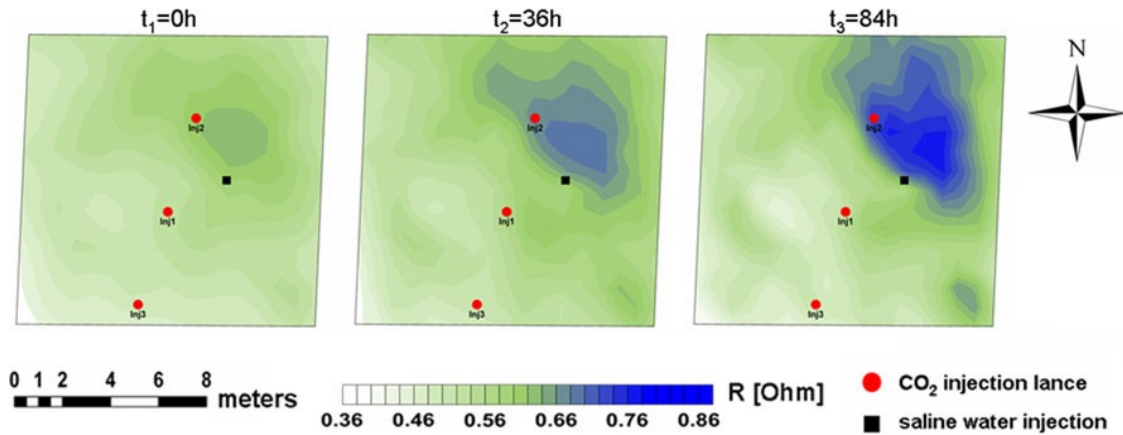


Figure 2.4 Normalized equipotential lines of salt tracer injection at different times. Left: before saline water injection; middle: after 36 hours saline water injection; right: after 84 hours saline water injection.

The movement of the tracer was observed by charging the injected plume and by repeated measurements of equipotential lines at various time steps by electrodes installed at the ground. The resulting shift of normalized equipotential lines indicates a groundwater flow direction towards north-north-west in the vicinity of the central and northern injection wells (Fig. 2.4). Estimates of the local groundwater flow velocity based on tracer test data as well as on hydraulic gradients together with hydraulic conductivity values obtained from sieve analysis and slug-test data revealed groundwater flow velocities of <0.1m/d up to 1m/d.

2.4.3 Monitoring network

In order to allow a spatially dense monitoring of the geochemically altered groundwater, 34 groundwater monitoring wells most of them down gradient of the injection lances were installed (see Fig. 2.1). Four different types of monitoring wells were installed between September 2010 and April 2011: (a) 12 two-inch groundwater monitoring wells using a conventional dry drilling method.

2. Investigation of the geochemical impact of CO₂ on shallow groundwater

The wells were generally screened over a 6m interval, in which the upper end of the screen is located 2 m below the glacial loam, which is the confining top layer of aquifer 2. This interspace between the top end of the screen and the glacial loam should ensure that no gaseous CO₂ that spreads below the glacial loam could escape through the filter screen into the atmosphere. (b) One four-inch groundwater monitoring well was drilled also using dry drilling technology. The larger diameter allows for equipment with multiparameter probes (s. section 4). The filter screen covers 3m (15-18m bgl) in the depth of the injection (18m bgl). (c) Seven one-inch groundwater monitoring wells were installed using SonicDrill technology, thus no annular space filling is needed, as the wells were directly inserted into the collapsing borehole. However, a bentonite sealing was realised at the depth of the glacial loam to prevent CO₂ ascent along the well casing. One meter filter screens were installed at 12.5-13.5m, 14.5-15.5m and 17.5-18.5m depth, so that a depth oriented groundwater sampling using an inflatable packer system could be realised. (d) Pneumatic driven low flow mini pumps were installed directly into the sediment using Direct Push technology. At 10 locations, in each case three pumps were installed at depths of 12, 15 and 18m bgl, at another 4 locations (Z1-Z4) one pump was installed at a depth of approximately 1m below glacial loam.

2.5 Injection test design and operation

Based on multiphase-modeling, the optimal operating conditions for the CO₂-injection test were designed, e.g. injection rate, injection pressure, injection time, and injection regime. The important operational constraint was that the injected CO₂ should remain within the aquifer and breakthrough to the unsaturated zone and atmosphere should be avoided as the focus of the present study lies on the impact of CO₂ on groundwater and the application of monitoring methods for groundwater. Furthermore, it was aimed to produce a coherent plume of dissolved CO₂ in the groundwater in order to enhance the chance to detect CO₂ and/or altered groundwater down gradient of the injection wells.

To design the adequate injection regime, first 2D and then 3D multiphase simulations were performed using TOUGH2 with the ECO2-module for multi-phase simulation (for details see (Pruess et al., 1999; Geistlinger et al., 2009).

2. Investigation of the geochemical impact of CO₂ on shallow groundwater

Based on the geological structure model (see section 2.4), a 3D numerical model of aquifer 2 (consisting of layers no. 4-9 according to Fig. 2.3 and Tab. 2.1) was set up, consisting of 37'125 cells (= 55 × 45 × 15) with a grid spacing of 1 m (see Fig. 2.5a). Key hydraulic parameters for a multiphase-model are horizontal and vertical permeability as well as capillary pressure for each sediment type. The permeability values were taken from sieve analysis and HPT logs (see section 2.4). For each geological layer, the permeability was calculated as mean value over different located values, e.g. the value for the lower medium sand was obtained by averaging 15 different values. For the constitutional relationships, i.e. the permeability-saturation relationship and the capillary-pressure-relationship a van Genuchten model was used (van Genuchten, 1980). The corresponding van-Genuchten parameters α and m were determined by the ROSETTA-database (Simunek and van Genuchten, 1999) and the SOILPROP-database (Mishra and Parker, 1989; Stumpp et al., 2009) and are listed in Tab. 2.2. Best simulation results to obtain a closed coherent dissolved CO₂-plume downstream were achieved using a low injection rate of 10 L CO₂/min at an injection gallery of 3 lances with a distance of 5 m and a continuous injection regime over 10 days.

Table 2.2 Hydraulic parameters of geological layers in aquifer 2.

Layer No. ¹⁾ and description	Porosity [-]	Permeability [m ²]	van-Genuchten α [m ⁻¹]	van-Genuchten m [-]
(4) Glacial loam	0.37	3.1×10^{-15}	7.1×10^{-4}	0.20
(5) Upper medium sand	0.33	2.0×10^{-11}	4.4×10^{-4}	0.39
(6) Coarse sand	0.34	4.2×10^{-11}	7.6×10^{-4}	0.40
(7) Silt	0.37	1.0×10^{-13}	2.7×10^{-4}	0.41
(8) Lower medium sand	0.30	2.6×10^{-11}	2.7×10^{-4}	0.58
(9) Glacial till	0.37	5.1×10^{-16}	7.1×10^{-4}	0.20

¹⁾ Layer numbers correspond to layers in Tab. 2.1/ Fig. 2.3.

2. Investigation of the geochemical impact of CO₂ on shallow groundwater

In Fig. 2.5b the simulated CO₂ gas distribution after 20 days, i.e. 10 days after gas injection had stopped, is depicted for this injection scenario. The gas saturation attains its maximum values at about 5 % at the center line. The blue isolines correspond to 0.5 % gas saturation. Both the maximum and minimum values are realistic values at field scale. The overlapping of the three gas plumes act as a gas wall and suggests that a closed, coherent dissolved CO₂-plume will be produced in the field. This plume was also calculated by TOUGH2, but not presented here. As can be seen from Fig. 2.5b the covering glacial loam layer plays a crucial role in avoiding the breakthrough to the upper aquifer and the atmosphere.

Based on the aforementioned simulation results three injection lances were installed at distances of 5 m perpendicular to groundwater flow using SonicDrill technology, six months before the injection test started. To avoid gas losses through tube fittings, a continuous multichannel tubing system (CMT Solinst, Georgetown, Canada) with an injection screen of 30 cm at a depth of 18 m bgl was used.

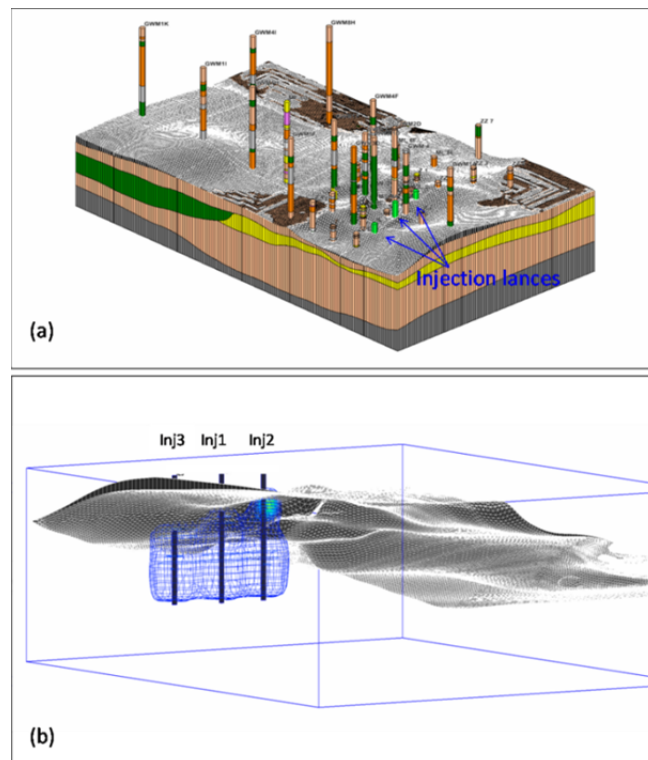


Figure 2.5 (a) Geological structure model showing the model boundaries of the simulated aquifer 2, the locations of the borehole profiles and injection lances (green). (b) 3D simulated gas distribution (blue isolines correspond to 0.5 % gas saturation), accumulating beneath the glacial loam 10 days after stopping the gas injection. Viewing direction is from northeast.

2. Investigation of the geochemical impact of CO₂ on shallow groundwater

At the depth of the glacial loam that acts as an aquiclude between aquifer 1 and 2 bentonite packers were installed to avoid breakthrough of CO₂ along the tubing. To test the tightness of the bentonite sealing optical sensors for O₂ (PreSens, Regensburg, Germany) were installed below and above the glacial loam at the outside of the tubing. Gas injection tests with pressurized air three weeks before the CO₂ injection proved the tightness of the seal, as no oxygen was detected above the glacial loam layer.

Between 29.03.2011 and 09.04.2011 in total 787 kg CO₂ and 0.466 kg SF₆ as a tracer were injected with a low injection pressure approximately equal to the hydrostatic pressure at the three injection lances. This corresponds to injection rates of 10 L CO₂/min and 1.67 mL SF₆/min, respectively, at each lance. As CO₂ was detected in the soil gas in well ZZ5 two days after the beginning of the injection, the injection rate was reduced at injection lance Inj2 from 10 to 7.5 L/min and again after eight days to 5 L/min to avoid losses to the atmosphere. As a counterpart, the injection rate at Inj3 was increased after nine days from 10 to 13.5 L CO₂/min.

2.6 Monitoring of CO₂ and geochemically altered groundwater

Different monitoring methods have been applied to monitor the injected CO₂ and the resulting alteration of groundwater, which also enables recommendations to be derived for monitoring shallow aquifers that might be subject to CO₂ intrusions.

2.6.1 Groundwater sampling and analysis

Thirteen groundwater sampling campaigns were carried out in total - three before, three during and seven after the injection experiment. In total, 669 groundwater samples were taken between November 2010 and October 2011. Groundwater sampling together with recording of on-site parameters (pH, electrical conductivity, redox potential, oxygen and temperature) was performed according to German quality standards (DVWK, 1992, 1997). Groundwater samples were filtrated using 0.45µm cellulose acetate single use filter units and samples for cation analyses were acidified on-site using concentrated HNO₃. Furthermore, alkalinity was determined on-site by titration to quantify carbonate or bicarbonate content of the water samples. Groundwater samples were analysed for TIC/TOC, major cations, anions, ammonium, trace elements, BTEX, chlorinated carbons (PCE, TCE, DCE, VC), ethane, ethene and methane at the Institute for Geosciences of the University of Kiel and for SF₆ at a commercial laboratory.

2. Investigation of the geochemical impact of CO₂ on shallow groundwater

TIC/TOC, BTEX and chlorinated carbon samples were generally analysed within 24-48 h after arrival in Kiel. Samples for trace element analysis were acidified after arrival in the lab with concentrated sub boiled nitric acid and analysed in the ICP-MS laboratory of the Institute for Geosciences at the University of Kiel, according to (Garbe-Schönberg, 1993). The three sampling campaigns prior to the injection test show a rather large spatial variability of most parameters measured at the site (s. Tab. 2.3): pH, electrical conductivity and redox potential varied within 6.2-7.2, 420-1060 $\mu\text{S/cm}$ and 80-457 mV, respectively.

Table 2.3 Statistics of background concentrations of groundwater samples from three sampling campaigns before the injection test: mean, standard deviation, minimum and maximum values and number of samples (n). RP-redox potential; EC – electrical conductivity

	pH	EC [$\mu\text{S/cm}$]	O₂ [mg/L]	RP [mV]	Alkalinity [mg/L]	TOC [mg C/L]	TIC [mg C/L]			
Mean	6.7	631	0.6	276	185.9	2.8	45.1			
SD	0.2	150	1.3	86	59.7	1.0	12.0			
Min	6.2	420	0	80	81.7	1.3	19.4			
Max	7.2	1060	8.7	457	417.9	6.9	69.7			
n	101	99	101	82	86	67	67			

	Cl⁻	NO₃⁻	SO₄²⁻	K	Na	Mg	Ca	Fe	Mn	Si
Mean	20.1	13.7	141.6	2.7	24.2	7.0	107.3	0.18	0.18	4.7
SD	11.0	11.4	38.7	1.1	10.0	1.4	36.5	0.45	0.16	0.9
Min	6.6	0.6	75.8	1.3	12.3	4.3	59.9	0	0	2.7
Max	75.0	62.3	285.0	5.7	74.1	11.0	229.1	2.55	0.60	7.1
n	104	104	104	104	104	104	104	104	104	91

The alteration of groundwater composition due to CO₂ injection is depicted exemplarily for one monitoring well (GWM 2D), located at 5 m down-gradient of an injection well (see Fig. 4.6). The injection of CO₂ leads to an increase in TIC (Fig. 4.6a), which results in a pH decrease (down to 5.4), due to dissolution of CO₂ in water, the formation of carbonic acid and its partial dissociation. Concomitantly, the electrical conductivity increases from approximately 550 $\mu\text{S/cm}$ to more than 700 $\mu\text{S/cm}$, which is a result of cation release, occurring due to pH-dependent cation exchange and mineral dissolution processes. As can be seen in Fig 4.6c, the concentrations of major cations Ca, K, and Mg increase by 24–38 % compared to background values.

2. Investigation of the geochemical impact of CO₂ on shallow groundwater

Sodium, however, decreases by 24 % compared to pre-injection concentrations, indicating either a fixing of sodium due to cation exchange processes or as a result of tailing of the salt tracer test from November 2010. Other trace elements (such as aluminium, silicium, manganese and, to a lesser extent, iron) show significant increases with increasing TIC, revealing relative increases at GWM 2D compared to background values of 184, 126, 116 and 17 %, respectively (Fig. 4.6d). Concentrations of heavy metals like copper, nickel, zinc, barium, cadmium and lead also increased distinctively; however, drinking water levels have not been exceeded due to CO₂ induced concentration increases (with the exception of nickel in two samples). More details on the behaviour of trace metals will be published separately. In general, all trace metals (as well as major cations and anions) attain background values after the CO₂ plume has passed, as can be seen in Fig. 4.6. The relative change in groundwater composition at two additional monitoring wells (GWM 1D–GWM 3D, all located 5 m down-gradient of the injection wells) is shown in a Piper diagram in Fig. 4.7.

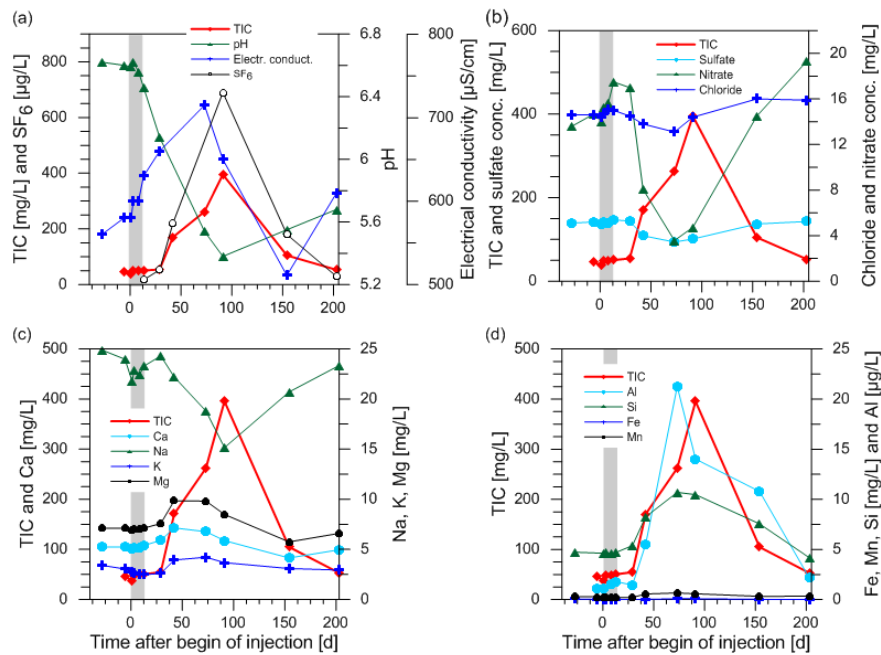


Figure 2.6 Concentration time series at GWM 2D, which is approximately 5m downstream of injection lance Inj2, for total inorganic carbon (TIC) and (a) pH, electrical conductivity and tracer SF₆, (b) sulfate, nitrate and chloride, (c) calcium, sodium, potassium, magnesium and (d) aluminum, silica, iron and manganese. The grey bar indicates the duration of the injection period.

2. Investigation of the geochemical impact of CO₂ on shallow groundwater

The results of two sampling campaigns are depicted in the Piper diagram: a sampling campaign prior to CO₂ injection and the sampling campaign 160 days after injection started, at which the mentioned monitoring wells showed the largest alteration of groundwater composition due to CO₂ injection. The injection of CO₂ led to an increased share of bicarbonate, while the share and absolute concentrations (compare Fig. 4.6b) of other major anions (sulphate and chloride) decreased. Accordingly, the share of divalent cations (mainly calcium and to a lesser extent magnesium) increases, whereas the share of monovalent cations decreases.

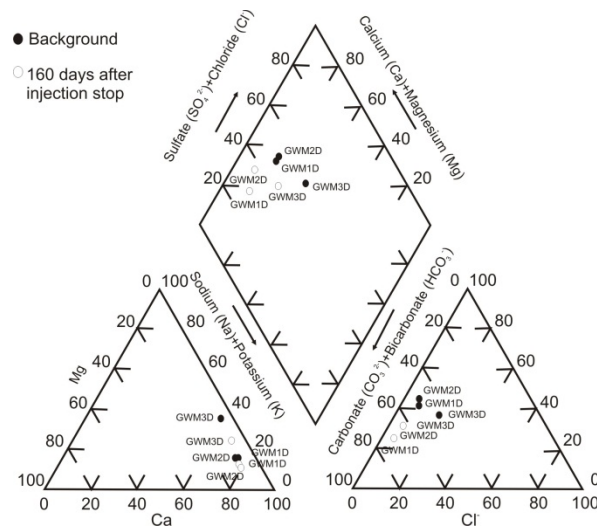


Figure 2.7 Piper diagram for groundwater samples from three monitoring wells (GWM 1D, 2D, 3D) for two sampling campaign, prior to and after the injection test.

2.6.2 Geophysical monitoring

Geoelectrical surveys have been applied for monitoring CO₂ in geological storage formations (e.g. at the CO₂ storage site Ketzin/Germany, described by Kiessling et al. (2010) and for the characterization of natural geological CO₂ leakage sites (Schütze et al., 2012). However, the authors are not aware of other studies using geoelectrical measurements for monitoring gaseous CO₂ and/or altered groundwater caused by a CO₂ intrusion into near subsurface structures. Gaseous CO₂ injection into a groundwater system causes an increased gas phase in the pore space and accordingly increased electrical resistivity. However, the subsequent dissolution and dissociation processes lead to an increase in electrical conductivity, thus a decrease in electrical resistivity.

2. Investigation of the geochemical impact of CO₂ on shallow groundwater

At the test site, three injection lances and 33 monitoring wells were equipped with electrodes for geoelectrical monitoring of CO₂ injection. Ring shape electrodes fixed at pre-defined depths at the outer surface of the HDPE/MDPE well material allow for time efficient, spatially and temporally high resolution monitoring using both borehole and cross-borehole measurements. Geoelectrical monitoring results showed significant changes of electrical resistivity caused by injected CO₂ (Lamert et al., 2012). This data is clearly related to measured field parameters (pH, electrical conductivity), water chemical parameters (TIC) and stable isotope data. Basic principles of geoelectrical monitoring of near subsurface CO₂ intrusions and the results of geoelectrical surveys that were used to monitor the CO₂ injection test are provided by Lamert et al. (2012).

2.6.3 Isotope monitoring

¹³C/¹²C isotope analyses of CO₂ were performed at the site in order to test the hypothesis that isotope signatures can be used to detect and/or identify potential leakages of CO₂ from deep storage sites. Potential CO₂ leakage from deep geological formations affects the carbonate system of overlaying aquifers, thus the challenge is to distinct naturally occurring CO₂ from potential CO₂ leakages, thereby enabling early warning and proper risk assessment to be undertaken. The intention of this study was to develop a monitoring concept based on the stable isotope composition of CO₂, thereby allowing the identification of the CO₂ sources. CO₂ produced by burning fossil fuels is expected to have an isotope composition of the carbon source (oil, coal, gas), which is generally isotopically depleted in $\delta^{13}\text{C}$ (< -25 ‰) compared to CO₂ in natural aquifer systems (about $\delta^{13}\text{C}$ -20 to +10 ‰) (Tissot and Welte, 1984). The natural isotope composition of CO₂ in groundwater is governed by the isotopic composition of CO₂ in the atmosphere, the composition of carbonate minerals and to some extent by microbial recycled plant material. Due to different isotopic compositions of leaking CO₂ from fossil fuel combustion and of CO₂ in aquifers, the isotope ratio might be used as an indicator for CO₂ leaks. The injected CO₂ was isotopically light, thus representing a typical combustion product, to simulate a CO₂ plume from a hypothetically leaking deep CO₂ storage site. The isotopic signature of the CO₂ of the groundwater was monitored for about one year before the injection test, in order to assess significant seasonal variations in the aquifer.

2. Investigation of the geochemical impact of CO₂ on shallow groundwater

When the injection test started, samples were taken in the course of the sampling campaigns, to determine the fate of the injected CO₂. For the sampling 100 ml serum bottles were filled with groundwater and sealed immediately with gas tight butyl stoppers. 15 g NaCl was used to reduce microbial activity. The bottles were stored at 4 °C and the isotope ratio of CO₂ was measured, after acidification with 1 ml 25 % HCl in order to avoid isotope fractionation of CO₂ in the carbonate system. The CO₂ headspace was determined with GC-IRMS in the isotope lab of the Department Isotope Biogeochemistry of the Helmholtz Centre for Environmental Research, Leipzig (settings described in (Fischer et al., 2004)). The groundwater at the field site has an average isotopic signature of δ¹³C -21.9 ± 1.5 ‰, whereas the isotopic signature of the injected carbon dioxide has a significant lighter composition of δ¹³C -30.5 ± 0.4 ‰. The difference of about 9 ‰ was large enough to detect the injected CO₂ and to distinguish it from the natural occurring CO₂. The δ¹³C values of CO₂ of the observation well ML 2C-3 are plotted in Tab. 2.4. Already eight days after the start of the injection test, the CO₂ plume could be detected at this observation well and it took about six month till the CO₂ plume has dissolved.

Table 2.4 δ¹³C values of CO₂ in the groundwater and pH at monitoring well ML 2C-3.

Date of sampling	Days after start of injection	δ¹³C [‰]	pH
02.04.2011	4	-20.92	6.38
06.04.2011	8	-29.87	5.45
12.04.2011	14	-30.44	5.18
28.04.2011	30	-31.50	5.53
11.05.2011	43	-31.50	5.39
28.06.2011	91	-30.19	5.91
30.08.2011	154	-22.07	6.15
19.10.2011	204	-23.04	6.24

In addition, the isotope signature of CO₂ of the soil gas was monitored at the experimental field site. Self-constructed sampling lances, described by (McCarthy and Reimer, 1986), were used. A stainless steel tube with a thin capillary tube inside (total volume 2.2 ml) was pushed one meter into the ground and soil gas samples were taken with a gas-tight syringe and transferred into evacuated glass vials.

2. Investigation of the geochemical impact of CO₂ on shallow groundwater

The background signature of the soil gas was -19.5 ± 2.1 ‰ and no seasonal variations were observed. Due to the presence of the glacial loam in about 10 meters depth, a migration of the injected CO₂ towards the surface was obviously retarded. The monitoring of the 53 sampling points confirmed this assumption and no changes of the isotopic ratio in the soil gas were observed. During the injection test a minor leakage of CO₂ occurred at one of the injection lances, which could be detected immediately in the soil gas samples from around this area. This observation showed that the sampling procedure is also possible for the detection of leakage in the very shallow subsurface.

2.6.4 Multiparameter Probes

In four monitoring wells, the multi-parameter probe (MPP) CDT*plus* (UIT GmbH Dresden, Germany) was used to continuously measure basic groundwater parameters, i.e. pressure, pH, electrical conductivity (EC) and temperature. In one of the wells, an additional CO₂ probe was installed. The purpose of the probes, besides continuous measurement and thus exact determination of first and peak arrivals of CO₂ and/or chemically altered groundwater, was to test their practicability for long-term monitoring in groundwater systems that are potentially subject to CO₂ intrusions. Another advantage of measuring on-site parameters and CO₂ in situ at the monitoring well is the prevention of CO₂ losses due to degassing during groundwater pumping to the surface.

Three probes have been installed in two-inch groundwater monitoring wells down-gradient of the CO₂ injection lances (GWM 2D, GWM 3D and GWM 4F: see Fig. 2.1) in the lower aquifer 2 at a depth of about 17 m bgl, where changes in pH, EC and TIC were expected. One probe that is supplemented with a sensor for CO₂ measurements has been installed in GWM 1D. The herein used CO₂ sensor detects the dissolved CO₂ concentration in the groundwater following the Severinghaus method (Severinghaus and Bradley, 1958). The electrode combines an Ag/AgCl reference electrode for pH and a glass membrane electrode, which is stringed with a polymer membrane permeable only to CO₂. The groundwater CO₂ partial pressure equilibrates through the membrane and is measured in terms of the resulting pH of the inner bicarbonate solution. This relationship is used to recalculate the dissolved CO₂ concentration in the groundwater. In combination with the pH value the carbonate speciation can be estimated as well.

2. Investigation of the geochemical impact of CO₂ on shallow groundwater

Although CO₂ probes have been used to measure continuously CO₂ in soil gas or air (e.g. Jones et al. (2009)), to the authors knowledge, CO₂ concentrations have not been measured continuously in-situ in groundwater before.

The monitoring phase started about one month in advance of the CO₂ injection test to record the background and time-dependent parameter variations. Recent publications on numerical and field studies (Wang and Jaffe, 2004; Zheng et al., 2009; Apps et al., 2010; Fahrner et al., 2012), as well as reactive transport simulations within this project (Hornbruch et al. in prep.) suggest a decrease in pH to levels in the range of 5.4 to 6 and an increase of EC in the range of hundreds of $\mu\text{S}/\text{cm}$ at similar field conditions. These values mainly depend on the amount of buffering minerals like calcite or iron hydroxides, gaseous CO₂ saturation and depth. Fig. 2.8 shows the time series of pH, EC and TIC (calculated from measured dissolved CO₂ concentrations) over the entire test period at GWM 1D from the MPP compared to standard groundwater samples. There are some differences to the results of the groundwater samples: the significant lower values of TIC in the groundwater samples compared to the MPP data is probably caused by degassing of CO₂ during sampling and potentially by subsequent losses during transport and lab analyses (Fig. 2.8a). The latter effects lowering the TIC concentrations were avoided by determination of alkalinity by field titration. The alkalinity and measured pH of the groundwater served to calculate TIC and as can be seen in Fig. 2.7a these values are in significant better agreement with the MPP data in particular at high concentrations. This indicates that TIC concentrations obtained by titration and pH measurements in the field were more reliable in contrast to TIC measurements performed in the lab.

Fig. 2.8b shows the temporal course of pH at GWM 1D and GWM 2D obtained by MPP measurements and from in-situ determination of pH during groundwater sampling campaigns. Although both wells are 5 m apart from an injection well, GWM 1D shows a significantly faster response to CO₂ injection: within 5 days after starting the injection, the pH measured at GWM 1D drops to 5.5; whereas in GWM 2D, it took about three to four weeks longer to arrive at a similar pH value. Differences between MPP measurements and pH values taken during groundwater sampling probably arise due to different sampling volumes: unlike the probe that exclusively measured water in the well, the pH measured during sampling represents a mixed sample recorded after approximately 1 h of pumping, which results in a spatial average around the well.

2. Investigation of the geochemical impact of CO₂ on shallow groundwater

The EC values (data not shown) reveal an increase of only 100 $\mu\text{S}/\text{cm}$ during the injection period of 10 days to a maximum of ca. 550 $\mu\text{S}/\text{cm}$ after 98 days. This is due to the low content of buffering minerals, as sediment analyses showed (Peter et al., 2011). The use of MPP was helpful for continuously monitoring CO₂ induced geochemical impacts over a long time period. However due to the relative high frequency of sampling campaigns at the test site and the associated insertion and removal of probes to obtain groundwater samples from the monitoring wells, the probes seem to be more susceptible to failure.

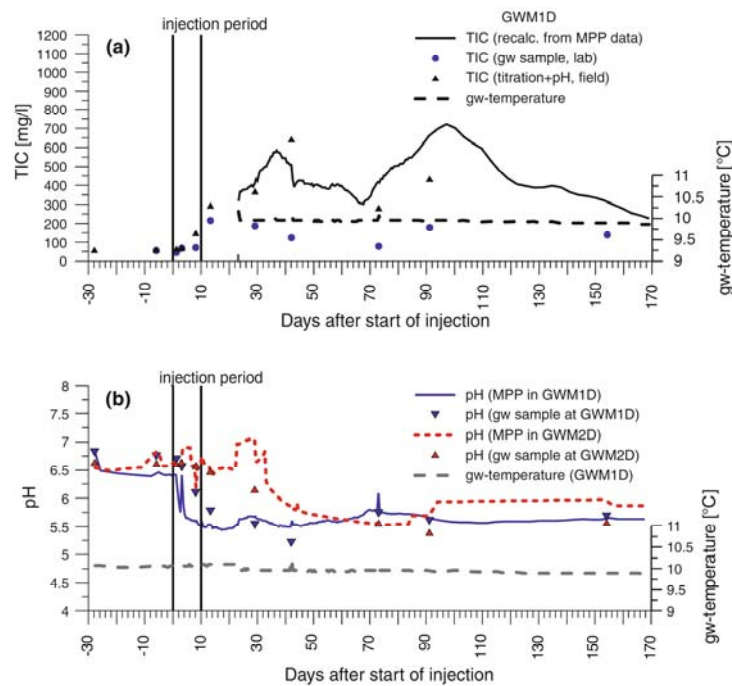


Figure 2.8 Comparison of (a) TIC and (b) pH values measured by multiparameter probes (MPP) and obtained from groundwater sampling. TIC from MPP is calculated from sensor measuring dissolved CO₂.

2.6.5 Passive samplers

Passive samplers that allow for cost-effective, temporally integrated monitoring of relevant environmental parameters have been used for various applications in the past (Namieśnik et al., 2005). While most of the passive samplers used so far sampled organic compounds (e.g. Verreydt et al. (2010)), passive samplers for heavy metals have been applied in the past primarily as an extraction method for improved lab analyses (e.g. Brumbaugh et al. (2002)).

2. Investigation of the geochemical impact of CO₂ on shallow groundwater

In the present study, passive samplers were applied for sampling of cations and heavy metals, using a system as described in de Jonge and Rothenberg (2005) and Rozemeijer et al. (2010). Two different adsorber resins were used to sample for cations and specifically for heavy metals, respectively - one is a cation exchange adsorber material and the other a chelat-complexing type of resin (SorbiCell TM, Denmark). Each adsorber resin is located within a cartridge that is open at both sites, to allow water to flow through. Together with the resin, a tracer salt is placed at the outlet of the cartridge, whose disappearance enables a volume estimate of the water volume that flowed through the system. Results of the passive samplers exposed in the field and of lab experiments on sorption behaviour of different adsorber resins will be published in a future paper.

2.7 Discussion

In the following section, the design and implementation of the injection test is discussed and experiences, recommendations and limitations are given concerning both the technical design of the test and the monitoring methods. Concerning the design and installation of a test site for a gas injection experiment at a hitherto non-investigated field site, a hierarchical approach using first large-scale methods (i.e. geophysical methods), and then subsequently smaller scale methods (i.e. Direct Push-methods using various in situ measurement techniques) was proven to be suitable. This iterative and adaptive procedure (including field site investigations, data analyses and multiphase modelling to establish dimensions of the injection test and monitoring network) continued up until the injection period was stopped, with additional monitoring wells having been drilled based on updated field observations and model simulations.

Regarding the technical realization of the injection wells, it has been proven advantageous to install the injection lances firstly using minimally invasive Direct Push-technologies. Thus, no annular space filling is required, which could provide potential preferential pathways for upward gas migration. Impermeable layers were tightened in the annular space using bentonite seals. Secondly, it was advantageous to install the injection lances at least several weeks in advance of the injection test, so that the sediment and sealing could reconsolidate, closing or minimizing preferential pathways along the outside of the injection wells.

2. Investigation of the geochemical impact of CO₂ on shallow groundwater

Injection tests using compressed air together with oxygen sensors installed on the outer walls of the wells at different depths have been shown to be valuable for proving sediment consolidation and seal tightness. To further improve experimental process understanding, the installation of pH sensors and pressure sensors on the outer walls of the injection wells would also have been useful, as it was not desirable to perform groundwater sampling in the direct vicinity (< 2.5 m) of the injection wells to avoid potential preferential pathways for upward gas migration. Thus, pH and pressure sensors here would have allowed for direct measurement of pH effects and potential pressure head changes, occurring due to CO₂ injection, as the latter were not observed in the monitoring wells 5 m apart from the injection wells.

Concerning monitoring methods, the various monitoring well types performed differently: comprehensive blank sampling of tap water and mineral water showed that the pneumatic driven mini pumps (imw, Tübingen, Germany), installed directly into the sediment, led to increased concentrations for some trace metals (zinc, copper, lead and cadmium), as did the inflatable packer system used to sample the 1''-monitoring wells. Only the submersible pump MP1 (Grundfos, Erkrath, Germany) used in the 2'' and 4'' wells yielded reliable blank concentrations for all measured trace metals. These results will be presented in detail in an additional paper on trace metal mobilization due to CO₂ injection (Peter et al., currently in preparation). Furthermore, the injection experiment confirmed the susceptibility of TIC measurements in the groundwater, especially at high TIC concentrations. Measurements using the directly in the monitoring well-installed CO₂ probe, yielded highest concentrations of TIC, as expected. At wells in close vicinity to the injection lances, groundwater sampling resulted in CO₂ degassing, so that TIC concentrations obtained by titration of alkalinity in the field already revealed decreased concentrations, compared to concentrations measured using the CO₂ sensor in the well. Results of TIC measurements from lab analyses yielded the lowest concentration values, due to further losses occurring due to transportation and samples being warmed to room temperature.

All methods tested to detect either CO₂/TIC in groundwater or the geochemical alteration of groundwater due to CO₂ intrusions were applied at a small-scale, densely equipped test site, which does not reflect a realistic monitoring network at a real CCS site. However, some conclusions concerning the applicability of these methods at large-scale CCS sites can be drawn from this injection experiment.

2. Investigation of the geochemical impact of CO₂ on shallow groundwater

As other authors (e.g. Chalatumyk and Gunter (2005)) have shown, monitoring strategies for CCS sites comprise different methods for all potentially affected compartments (i.e. from the reservoir formation up to the atmosphere), each covering a different scale. In order to cope with the large scales necessary to monitor a CCS site, hierarchical monitoring strategies are appropriate. Cortis et al. (2008) suggested a two-step approach for (1) detecting and locating CO₂ seepage(s) using large-scale monitoring on a fixed grid and (2) for pinpointing and quantifying the seepage using smaller-scale methods on a flexible dynamic monitoring grid. Although Cortis et al. (2008) developed their concept for monitoring the unsaturated zone and atmosphere this concept can be extended to all compartments included in environmental CCS monitoring. Methods suitable for a large-scale monitoring scheme on a fixed grid should either comprise methods covering large scales (e.g. eddy covariance towers, airborne monitoring) or they should effectively monitor vulnerable areas on a smaller scale, like faults or abandoned boreholes. Thus, groundwater monitoring methods become suitable either for small-scale monitoring of ‘a priori’ selected vulnerable areas on a permanent fixed monitoring grid (case 1) or for pinpointing leakages on a dynamic monitoring grid (case 2). With regard to effective and economical groundwater monitoring methods, either multiparameter probes installed in monitoring wells measuring pH and/or CO₂ or geoelectrical monitoring at boreholes (see also Lamert et al. (2012)) seem to be suitable methods. Furthermore, groundwater sampling and analyses for basic parameters such as TIC, pH, anions and cations seem appropriate for targeting and identifying leakages into aquifers and additional analyses for isotope signatures, in order to identify CO₂ sources.

Finally, an important lesson learned during this research project was that early and transparent communication of planned research activities with local authorities, regulators and especially with the local public is a crucial prerequisite for successful and undisturbed operation of even small scale pilot projects.

2.8 Summary

A 10-day CO₂ injection experiment into a shallow aquifer was performed to investigate geochemical impact on groundwater and to test different monitoring methods.

2. Investigation of the geochemical impact of CO₂ on shallow groundwater

Careful ‘a priori’ site characterization and test design via multiphase simulations was necessary to obtain an optimally equipped test site, optimized injection rates and optimal distances between injection wells. Monitoring included groundwater sampling and subsequent standard analyses, as well as trace element and isotope analyses; geoelectrical borehole monitoring and the use of passive samplers and multi-parameter probes both installed in the wells.

CO₂ injection led to an increase in total inorganic carbon (TIC), mainly consisting of bicarbonate, and to a decrease of pH down to 5.1. Geochemical reactions comprised of a release of cations and trace elements, whereas anions were observed to decrease. Geoelectrical borehole monitoring was able to detect groundwater alteration (see also Lamert et al. (2012)) and ¹³C/¹²C isotope analyses revealed a clear deviation from background values of up to 10.5 %. Multi-parameter probes that continuously measured CO₂, pH and electrical conductivity revealed that TIC analyses in the lab seem to be less reliable than values obtained by the multi-parameter probe in the wells or by field titration and pH measurements.

As the intension of this paper is to provide an overview of the injection test itself and the monitoring methods applied, detailed results concerning the individual methods will be published in additional papers.

2.9 Acknowledgements

This project was funded by the German Ministry of Education and Research within the Priority Program *Geotechnologies*, Funding number 03G0670A-C. Furthermore we thank the municipality of Wittstock and the Brandenburgische Boden GmbH for supporting the project.

3. Monitoring of a simulated CO₂ leakage in a shallow aquifer using stable carbon isotopes

3. Monitoring of a simulated CO₂ leakage in a shallow aquifer using stable carbon isotopes

3.1 Kurzfassung

Während eines Feldversuches nahe der Stadt Wittstock, Deutschland wurde eine künstliche CO₂ Leckage in einem flachen Grundwasserleiter durchgeführt und mit Hilfe stabiler Kohlenstoffisotope überwacht. Ca. 400 000 L CO₂ wurden in eine Tiefe von 18 m über einen Zeitraum von zehn Tagen injiziert. Sowohl in Grundwasser- als auch in Bodengasproben wurde das ¹³C/¹²C Verhältnis von CO₂ gemessen, um Aussagen über die räumliche Verteilung der CO₂-Fahne treffen zu können und um die Anwendbarkeit und Zuverlässigkeit dieser Detektionsmethode für potentielle CO₂ Leckagen, z.B. von CCS Anlagen (Carbon Capture and Storage) zu evaluieren. Die Isotopensignatur des injizierten CO₂ (δ¹³C ca. -30 ‰) unterschied sich von der Hintergrundsignatur des CO₂ (δ¹³C ca. -21 ‰). Die künstliche CO₂ Fahne konnte über einen Zeitraum von 204 Tagen detektiert werden. Die Ergebnisse belegten, dass das Monitoring mittels stabiler Isotope für eine Quellenidentifizierung genutzt werden kann. Des Weiteren eignet sich die Methode zur Detektion einer potenziellen CO₂ Migration aus der Speicherformation in einen oberflächennahen Grundwasserleiter bzw. in den obersten Bodenhorizont. Eine Voraussetzung für die Anwendung dieser Methode ist ein signifikanter Unterschied, zwischen den Isotopensignaturen des natürlichen Hintergrundes und des injizierten CO₂.

Schulz, Alexandra; Vogt, Carsten; Lamert, Hendrik; Peter, Anita; Heinrich, Ben; Dahmke, Andreas; Richnow, Hans-Hermann.

Published in: Environmental Science and Technology, 2012, 46 (20); pp 11243-11250.

3.2 Abstract

Artificial carbon dioxide leakage into a shallow aquifer was monitored, based on stable carbon isotope measurements, at a field site near the town of Wittstock, Brandenburg, Germany. About 400 000 L of CO₂ were injected into a shallow aquifer at 18 m depth over ten days.

3. Monitoring of a simulated CO₂ leakage in a shallow aquifer using stable carbon isotopes

The ¹³C/ ¹²C ratios of CO₂ were measured in groundwater and soil gas samples in order to monitor the distribution of the injected CO₂ plume and to evaluate the feasibility and reliability of this approach to detect potential CO₂ leakages, e.g. from CCS sites (Carbon Capture and Storage). The isotope composition of the injected CO₂ (δ¹³C around -30 ‰) could be distinct from the background CO₂ (δ¹³C around -21 ‰) and the artificial CO₂ plume could be monitored over a time of more than 204 days. The results demonstrate that this stable isotope monitoring approach could be used to identify CO₂ sources and to detect potential CO₂ migration from a CCS site into overlying shallow aquifers or even into the upper subsurface. A prerequisite for this is a significant difference between the isotope ratios of the natural background and the injected CO₂.

3.3 Introduction

The development of the Carbon Capture and Storage (CCS) technology, wherein carbon dioxide (CO₂) is sequestered indefinitely in underground storage areas, has progressed rapidly in recent years. This technology is considered an option for the reduction of CO₂ emissions to the atmosphere (Holloway, 2001; Orr, 2009). The potential for leakage of stored CO₂ through faults, boreholes, or permeable rock formations into shallow aquifers is one concern associated with CCS (Oldenburg and Unger, 2003; IPCC, 2005; Little and Jackson, 2010). Until now, no direct observations of leakage from a CO₂ storage site existed. Thus only natural and/or industrial analogues were used to predict the effects of CO₂ leakage in shallow groundwater. A review by Lemieux (Lemieux, 2011) pointed out the necessity of further field studies to establish data for the behaviour of CO₂ in a shallow aquifer. Monitoring tools for detecting potential leakages of CO₂ from CCS sites in deep geological formations are needed for the development of early warning systems, for assessing the tightness of cap rocks, and for a rigorous evaluation of risks associated with CCS technology.

Thus far, several methods have been developed for measuring CO₂ concentrations associated with underground leakage. In the near-surface environment for example, the chamber method is used, which is based on measurements of CO₂ accumulations at the potential leakage site (Lewicki et al., 2007b), whereas eddy-flux methods analyse net CO₂ leakage flux over a large area using a fast CO₂ analyser (Lewicki et al., 2009). Parameters like pH and/or electrical conductivity allow for the monitoring of overall CO₂ flux in shallow aquifers, but source identification is not possible.

3. Monitoring of a simulated CO₂ leakage in a shallow aquifer using stable carbon isotopes

On the one hand, the problem is insufficient spatial resolution for realistic monitoring tools; on the other hand, the discrimination between biogenic and fossil sources of CO₂ is an unresolved disadvantage for both techniques. Stable carbon isotope analysis has the potential to address both of these shortcomings. CO₂ occurs naturally in both aquifers and in the shallow soil zone. The challenge for a CCS monitor seeking to provide early warning or conduct risk assessment is to distinguish naturally present CO₂ from potential underground CO₂ leakage. The geochemistry of a shallow aquifer will be affected by the upward migration of CO₂ from a storage site.

Batch-reactor experiments (Lu et al., 2010), computational simulations (Carroll et al., 2009; Fahrner et al., 2011; Humez et al., 2011; Fahrner et al., 2012), and a small-scale field study at the ZERT (Zero Emission Research and Technology) site (Kharaka et al., 2010; Spangler et al., 2010) all suggest the mobilization of cations from the host rock, pH decrease, and electrical conductivity increase following an underground CO₂ release. These parameters have the potential to be used as indirect indicators of CO₂ intrusion (Fahrner et al., 2012). However, measurements of CO₂ concentration or indirect parameters can both be distorted by naturally occurring spatial and temporal variations in the CO₂ inventory of soil-aquifer systems. This impedes upon the ability to reliably identify CO₂ sources, and suggests the necessity of isotope monitoring to allow the clear attribution of detected CO₂ to its source.

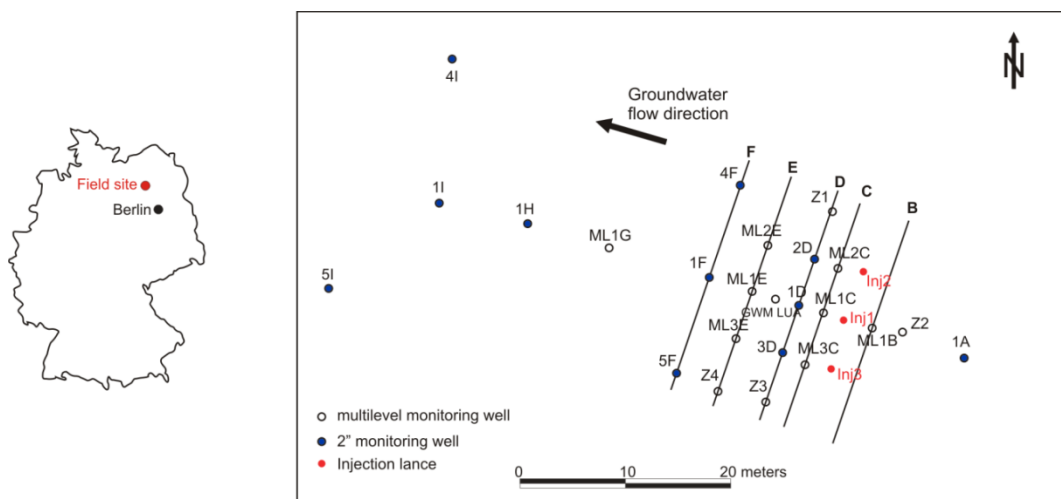


Figure 3.1 Map of Germany with the field site in the north-east (left), and detailed plan for the monitoring field of the CO₂ injection test site. The plan is showing the installed monitoring wells and the three CO₂ injection lances (red) (modified after (Peter et al., 2012)). The control levels (B-F) are explained in more detail in the text.

3. Monitoring of a simulated CO₂ leakage in a shallow aquifer using stable carbon isotopes

Several researchers have used and established a stable carbon isotope approach to determine changes in fluid isotope composition due to CO₂ injection (Emberley et al., 2004) or to quantify ionic trapping of injected CO₂ as HCO₃⁻ (Raistrick et al., 2006). Furthermore, the isotope signature of CO₂ was used for baseline monitoring before CO₂ injection to detect anomalous locations that could act as possible leakage pathways (Klusman, 2006). Additionally, at the ZERT site a laser-based analyser capable of measuring both CO₂ concentrations and isotope ratios was used to monitor a controlled subsurface CO₂ release event (McAlexander et al., 2011).

In this study, the behaviour of an artificially generated gaseous CO₂ plume, caused by a controlled and temporally limited CO₂ injection experiment, was monitored by stable carbon isotope analysis. The natural isotopic composition of CO₂ in groundwater is determined by the isotopic composition of CO₂ in the atmosphere, the composition of carbonate minerals, and by microbial recycled plant material. Conversely, the CO₂ to be stored in the underground sites is produced by the combustion of fossil fuels and has the isotope composition of the carbon source (i.e., oil, coal, or gas). This source is generally more isotopically depleted in δ¹³C (< -25 ‰) than CO₂ found in aquifer systems (δ¹³C - 20 to +10 ‰) (Clark and Fritz, 1997). Naturally CO₂-rich springs, related to volcanic activities or admixture with mantle-derived CO₂ generally have isotope ratios of between -11.5 and 0.5 ‰ (Griesshaber et al., 1992; Yoshimura et al., 2004; Du et al., 2006). A study of CO₂-rich waters in general showed an average value of -2.8 ‰ (Redondo and Yélamos, 2005). These results show that even at field sites with naturally increased groundwater-CO₂ concentrations, interference from the background isotope signatures with the injected CO₂ isotope signatures cannot be expected. Therefore, the different isotope ratios of carbon dioxide in shallow confined aquifers can aid in discriminating between carbon sources.

A CO₂ leakage scenario was simulated at a field site in Germany by injecting carbon dioxide into a shallow aquifer (Peter et al., 2011; Lamert et al., 2012). To test whether the CO₂ plume of a leaking CCS site could be assessed, spatial and temporal development of the plume was monitored in several ways: the isotope composition of CO₂ in soil gas and groundwater samples, geochemical parameters (pH, total inorganic carbon - TIC, electric fluid conductivity), and geoelectrics for the groundwater samples. 397,938 L CO₂ (787 kg) were injected 18 m below ground level (bgl) into a shallow aquifer over a period of ten days.

3. Monitoring of a simulated CO₂ leakage in a shallow aquifer using stable carbon isotopes

Groundwater sampling and soil gas measurements were performed to determine whether the released CO₂ migrated from the aquifer to the upper soil horizon and whether it was possible to detect migrating CO₂ within a reasonable time frame. The overall goal was to determine whether stable isotope measurement of CO₂ is a reliable monitoring tool for detecting potential leakage events from CCS sites. A further aim was to test and evaluate the application of the soil gas sampling system as a routine monitoring method.

3.4 Injection test and sampling methods

3.4.1 Field Site

The injection experiment was performed at a former military airfield about 100 km north of Berlin in the state of Brandenburg, Germany (Fig. 1). The subsurface is composed of Quaternary sediments, specifically of fine to coarse sands, silt, clay, and glacial loam of the Saale and Vistula ice age. Two aquifers are present up to the investigation depth of about 20 m below ground level (bgl), both of which were relevant for the injection test. The upper confined aquifer (aquifer 1) is characterized by heterogeneously distributed interbedded sand and silt layers and has an average thickness of about 11 m. Glacial loam with a highly variable thickness averaging 0.5 m separates the upper aquifer from the lower aquifer (aquifer 2). Aquifer 2 ranges from 11.5 – 19.5 m bgl, and is the main groundwater aquifer. It consists of a carbonate-free, relatively homogeneous medium-to-coarse sand formation, with hydraulic conductivities in the range of $4.5 - 6.8 \cdot 10^{-4} \text{ m s}^{-1}$ (Peter et al., 2011). The lower part of aquifer 2 (16 – 19.5 m bgl) was chosen as the injection horizon. Glacial till underlies aquifer 2 and acts as an aquitard. In some profiles of the northwestern, northeastern, and southern area, no glacial loam was found, thus hydraulic contact between aquifers 1 and 2 can be assumed. The regional groundwater flow direction is westward with a north-west tendency. The groundwater flow velocity varies between $< 0.1 \text{ m d}^{-1}$ up to 1 m d^{-1} (for a more detailed description of the field site and the geochemical parameters refer to (Peter et al., 2011; Lamert et al., 2012)).

3. Monitoring of a simulated CO₂ leakage in a shallow aquifer using stable carbon isotopes

3.4.2 Injection test

The CO₂ injection was performed in aquifer 1, which was chosen due to its relatively homogenous composition. The isotope ratio of the injected CO₂ was -30.5 ± 0.4 ‰ (Westfalen AG), to mimic a CO₂ source generated by fossil fuel combustion. The injection lances were screened over 0.2 m at 18 m to ensure a depth-defined CO₂ injection. Three injection lances with a lateral spacing of 5 m were installed perpendicularly to the regional groundwater flow direction (Fig. 3.1). The injection rate averaged 10 L of CO₂ min⁻¹ at normal temperature and low injection pressure (approximately equal to hydrostatic pressure) at each injection lance. In total 397,938 L (1 bar, 0 °C) of CO₂ were injected over ten days. In addition, SF₆ gas (70.24 L) was used as a conservative tracer and was mixed with the CO₂. The injection test took place over a ten-day period in March and April of 2011. The settings were chosen according to multiphase simulations (Lamert et al., 2012), which predicted complete dissolution of the injected CO₂ in the groundwater while the plume ascended to the confining upper boundary of the aquifer. Thirty-four observation wells of differing diameters were installed. To assess potential CO₂ leakage at the monitoring wells themselves, CO₂ surface gas flow measurements were performed at the surface using a LICOR CO₂ surface flow measurement system. For more detailed information about the design of the injection test and the monitoring network refer to (Lamert et al., 2012).

3.4.3 Soil gas sampling in the unsaturated zone

Soil gas samples were taken using self-constructed sampling lances which were first described by McCarthy and Reimer (McCarthy and Reimer, 1986). The 1.45 m sampling devices (refer to SI for detailed description) were constructed of stainless steel with an outer diameter of 14.3 mm and an inner diameter of 5.0 mm. The lances were pushed manually with a percussion hammer approximately 1.10 m into the ground to ensure a constant sampling depth. This depth was chosen to minimize the influence of the upper soil horizon due to soil respiration in the root zone and exchange with the atmosphere. The soil gas samples were taken with a 5 mL gas-tight glass syringe and transferred into evacuated glass vials, which were sealed gas-tight with butyl rubber stoppers and aluminium crimp seals. The samples were kept cool and stored at about 4 °C and measured within four days of sampling using a gas chromatograph – isotope ratio mass spectrometer (GC-IRMS).

3. Monitoring of a simulated CO₂ leakage in a shallow aquifer using stable carbon isotopes

3.4.4 Groundwater sampling

Groundwater samples were taken during 13 sampling campaigns, with three campaigns taking place prior to injection, three during, and seven taking place after the injection experiment. Groundwater sampling was performed according to German quality standards (DIN 38402 A13, DVWK information sheet 245 and DVGW W112/2011). Site parameters such as pH, temperature, oxygen concentration, electrical conductivity and redox potential were also recorded at each sampling campaign using a universal pocket meter (Multi 350i, WTW). The groundwater samples for the analyses of stable carbon isotopes of CO₂ were transferred into sterilized 200 mL glass bottles amended with 15 g NaCl to suppress microbiological activity. The bottles were closed gas-tight with butyl rubber stoppers and aluminium crimp seals and were stored at 4 °C. Samples were measured within four days of sampling using a GC-IRMS. Alkalinity was also analyzed on-site using potentiometric titration with 0.1 M HCl to quantify the carbonate and bicarbonate content of the water samples. The Institute for Geoscience at the University of Kiel analyzed the water samples for TIC/ TOC, major cations, anions, trace elements, BTEX, and chlorinated hydrocarbons. The gas-chromatographic analyses for SF₆ were carried out at a commercial laboratory (ERGO Umweltinstitut GmbH).

3.4.5 Measurement settings for stable carbon isotope analyses of CO₂

The ¹³C/¹²C ratios of gaseous CO₂ in the headspace of the groundwater samples were measured after each sampling campaign. In addition the ¹³C/¹²C ratios of the dissolved inorganic carbon were measured after acidification with concentrated HCl to obtain a pH between one and two to ensure a complete transfer of the dissolved CO₂ into the gas phase and to avoid isotope fractionation effects related to the carbonate system. Analysis of the carbon isotope ratios of the CO₂ was performed with a GC-IRMS in which a gas chromatograph (6890 Series, Agilent Technology, USA) is coupled via a combustion device to an isotope ratio mass spectrometer (Finnigan MAT 253, Thermofinnigan Bremen). The headspace samples (50 to 100 µl) were injected into the GC using a gas-tight syringe (Hamilton, USA). The GC was equipped with a CP-Porabond Q column (50 m x 0.32 mm x 0.5 µm, Varian, USA) and the samples were held at a constant temperature of 40 °C and a helium-flow rate of 2 ml min⁻¹.

3. Monitoring of a simulated CO₂ leakage in a shallow aquifer using stable carbon isotopes

Samples were each measured three times and a statistical standard deviation of ≤ 0.5 ‰ was always achieved for the described settings. All measured ¹³C/¹²C ratios are reported in delta notation ($\delta^{13}\text{C}$) which is defined:

$$\delta^{13}\text{C} = (R_{\text{Sample}} - R_{\text{Standard}} / R_{\text{standard}}) \times 1000 \quad (\text{eq. 3.1})$$

where R_{standard} and R_{sample} are the isotope ratios in the standard and the sample, respectively. The values are reported relative to the international Vienna Pee Dee Belemnite (VPDB) standard (Coplen, 1996). A simple mixing model was used to verify that the decreased isotope ratios of groundwater samples resulted from the addition of isotopically-light injected CO₂. The following equation was used:

$$A^{13}\delta_{(B)} + (1-A)^{13}\delta_{(I)} = ^{13}\delta_{(M)} \quad (\text{eq. 3.2})$$

where $^{13}\delta_{(B)}$ is the isotope signature of the background, $^{13}\delta_{(I)}$ is the isotope signature of the injected CO₂ and $^{13}\delta_{(M)}$ is the isotope signature after the injection, and A and 1-A are the mixing ratios of the background isotope ratio and the isotope ratio of the injected CO₂, respectively (Fischer et al., 2004).

3.5 Results

3.5.1 Stable carbon isotope ratios of the soil gas

Monitoring of the background-CO₂ isotope ratio in the soil gas began about nine months prior to the injection of isotopically-light CO₂ into the aquifer, to assess potential seasonal variations (SI-Tab. 1). After three sampling campaigns (May 2010, November 2010, March 2011), an average isotope ratio of -19.5 ± 2.13 ‰ was measured and no significant seasonal variations were observed. Minor deviations of the CO₂ isotope ratio were observed at some sampling points (e.g. ML 1B with -16.8 ‰ ± 0.61 ‰ and x12 with -16.7 ‰ ± 0.42 ‰), but these values were still well outside the range of the injected CO₂ (-30.5 ± 0.4 ‰) and thus could be easily distinguished as background CO₂. The distribution of the $\delta^{13}\text{C}$ values of the CO₂ in the soil gas at 1.1 m depth displayed relative homogeneity over the entire field site (Fig. 3.2, A).

During the injection test, decreased isotope ratios of the CO₂ present in soil gas were detected at the northern injection lance *Inj2*. It is assumed that the injected CO₂ migrated back to the surface via preferential flow paths from underground.

3. Monitoring of a simulated CO₂ leakage in a shallow aquifer using stable carbon isotopes

The input of injected CO₂ into the soil gas system was detected immediately at soil gas sampling points ML 2C, GWM 2D, and x9 in close proximity to the injection lance (Fig. 3.2, B). At these locations, the isotope ratios immediately decreased to $-28.1 \text{ ‰} \pm 0.02 \text{ ‰}$, $-27.0 \text{ ‰} \pm 0.13 \text{ ‰}$, and $-27.7 \text{ ‰} \pm 0.22 \text{ ‰}$, respectively. Due to the construction of the injection lances, it was not possible to use the LICOR surface flow measurement system to measure the CO₂ flow rate.

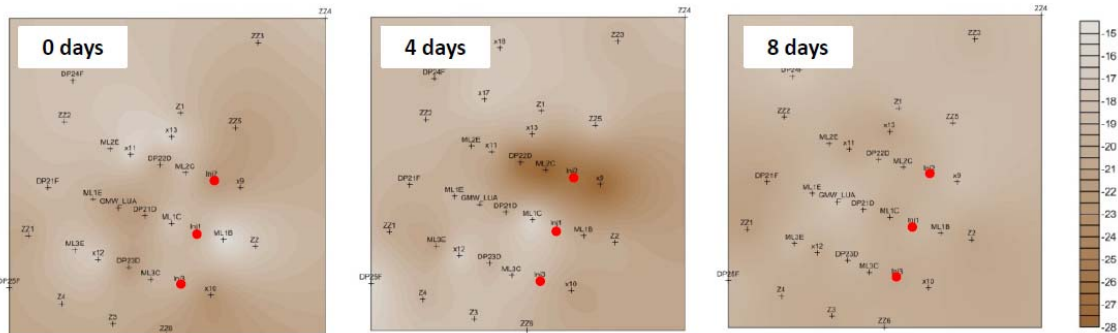


Figure 3.2 Contour maps showing the distribution of $\delta^{13}\text{C}$ values of CO₂ [‰] in soil gas before, during, and after (from left to the right) the injection of isotopically light CO₂ in March/April 2011. Relatively homogeneously distributed values were observed before and after the injection of CO₂. During the injection, a slight leakage occurred at the northern injection lance Inj2, which was detected immediately in the soil gas samples taken in the close vicinity of the leak.

Additionally, neither the GA94 gas analyzer nor the Testo 535 system was able to provide reliable data, as concentration could only be measured after dilution with atmospheric air. As a result, the soil gas isotope ratios were the sole indicators allowing detection of CO₂ leakage. The leakage of CO₂ was repaired and the CO₂ injection rate reduced to avoid further direct leakage of CO₂ at this sampling point. At the next sampling campaign, four days later, the isotope ratios had returned to background values (Fig. 3.2, C), indicating that the leaked CO₂ had infiltrated only the pore space of the soil and had equilibrated with the isotope composition of the surrounding air relatively quickly. During the remaining sampling campaigns, no changes in the $\delta^{13}\text{C}$ values of the soil gas CO₂ were measured and no enriched values below of -23.1 ‰ were detected.

3. Monitoring of a simulated CO₂ leakage in a shallow aquifer using stable carbon isotopes

3.5.2 Stable carbon isotope ratios of the groundwater

Ten groundwater sampling campaigns were performed after the initiation of CO₂ injection (SI-Tab. 3.2). The sampling of both groundwater and soil gas began about nine months before the injection test. Three sampling campaigns were performed to measure the background isotope ratio of the groundwater to assess seasonal variations. The average isotope ratio for the background across all three sampling campaigns was $-21.9 \pm 1.4 \text{ ‰}$ (Fig. 3.3), with no significant seasonal variations. The isotope ratio distribution displayed relative homogeneity over the entire monitoring field. The contour maps with the isotope ratios plotted show the section of the monitoring field featuring the observation wells that were influenced by the injected CO₂ (Fig. 3.3). The other wells at greater distances are not shown as the isotope ratio remained constant over the entire monitoring period.

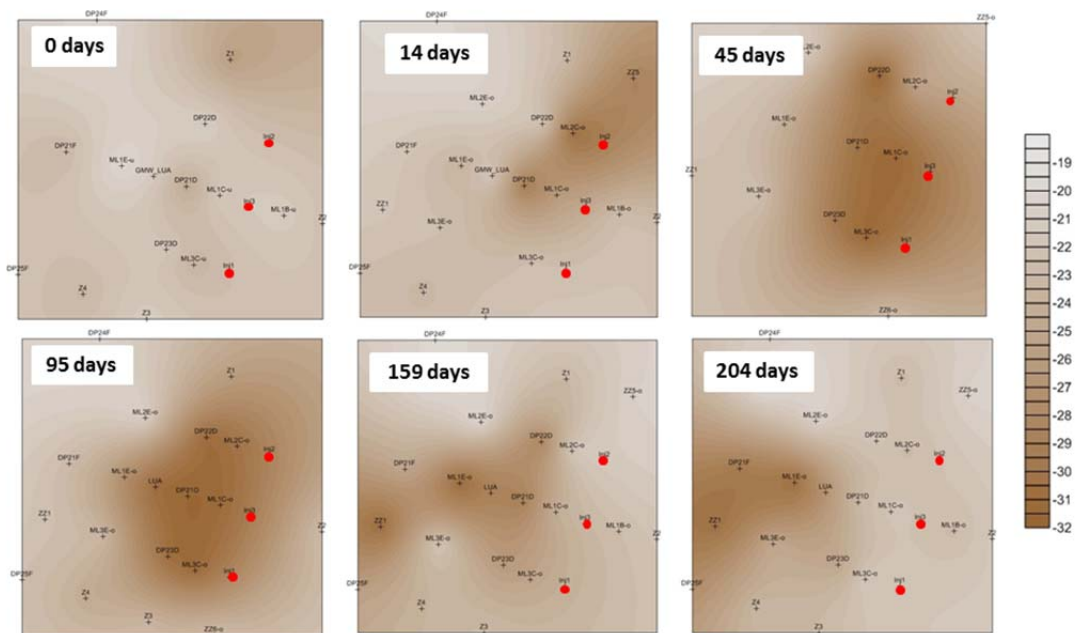


Figure 3.3 Distribution of $\delta^{13}\text{C}$ values of CO_2 [‰] in groundwater from the start of the CO_2 injection until the final sampling campaign at day 204. The numbers in boxes indicate the number of days after the beginning of the injection test. The red spots show the location of the CO_2 -injection lances.

Beginning four days after CO_2 injection, depleted isotope ratios of about $-29.9 \text{ ‰} \pm 0.32 \text{ ‰}$ were measured at the multilevel well *ML 2C*, located about 2.5 meters from the northern injection lance *Inj2* in control plane *C*.

3. Monitoring of a simulated CO₂ leakage in a shallow aquifer using stable carbon isotopes

At the next sampling, ten days later, the isotopically-light injected CO₂ had reached the middle well in control plane *D* (about five meters away from injection lance *Inj1*) which showed an isotope ratio of $-29.1 \text{ ‰} \pm 0.20 \text{ ‰}$. The migration of the injected CO₂ was west-oriented, in line with the direction of local groundwater flow. This migration continued and after 45 days isotope ratios had decreased to $-29.8 \text{ ‰} \pm 0.29 \text{ ‰}$ throughout control plane *D*. In the final sampling campaign, 204 days after injection, the injected CO₂ had reached control planes *E* and *F*, where isotope ratios of $-29.8 \text{ ‰} \pm 0.11 \text{ ‰}$ and $-29.6 \text{ ‰} \pm 0.17 \text{ ‰}$ respectively, were detected. In control plane *F*, only the western and south-western observation wells (*GWM 1F*, *GWM 5F*, *ZZ1*) were affected by injected CO₂. The northern wells (*ZZ2*, *GWM 4F*) showed no change in isotope ratios. During this period, the δ -values in control planes *C* and *D* gradually increased to values observed before injection. In control plane *C* isotope ratios reached values of $-22.4 \pm 0.74 \text{ ‰}$, a near-complete return to the measured background value prior to CO₂ injection ($-21.9 \pm 1.4 \text{ ‰}$), and in control plane *D* isotope ratios had risen back to $-23.7 \pm 1.46 \text{ ‰}$. Control planes *A* and *B* were never affected by the injected CO₂, as they are located upgradient of the injection lances with respect to groundwater flow. As the injected CO₂ migrated with the groundwater flow direction, these observation wells were not influenced by the injected CO₂.

In addition to isotope ratios, physicochemical parameters including pH, TIC, concentration of the SF₆ tracer, and electrical fluid conductivity of groundwater samples were measured (Fig. 3.4) for comparison with detected isotope ratios. The physicochemical parameters displayed correlation with the measured isotope ratios. With depletion of isotope ratios, pH also decreases to minimal values of about 5.2. Electrical conductivity was significantly influenced by the injected CO₂, evidenced by an increase from 470 to 680 $\mu\text{S}/\text{cm}$ (Fig. 3.4) was found when the injected CO₂ had reached the specific monitoring well. The TIC values also increased with decreasing isotope ratios (Fig. 4.4), but due to the degassing of the samples during sampling and transportation to the lab, these values are subject to greater variability (see (Lamert et al., 2012) for discussion of different TIC measurements). In one well the CO₂ concentration was measured directly using a probe. The comparison of the TIC values obtained by titration directly in the field and the TIC values calculated using the CO₂ concentration and the pH showed a good correlation. Therefore, we assumed the measured TIC values to be a proxy for the CO₂ concentration.

3. Monitoring of a simulated CO₂ leakage in a shallow aquifer using stable carbon isotopes

The distribution of the SF₆ concentrations correlated well with the distribution of the isotope ratios (SI-Tab. 3) and higher SF₆ concentrations being associated with more negative isotope ratios.

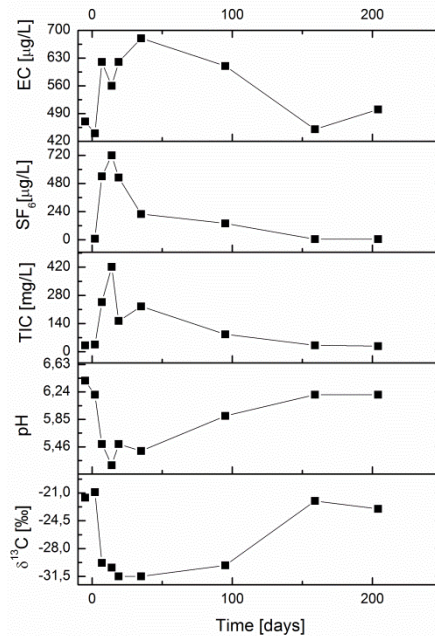


Figure 3.4 Various parameters for the shallowest sampling level (13 meters) of the multilevel well ML2C in the northern part of the monitoring field. In addition to the parameters that were measured in the field (pH, electrical conductivity), the total inorganic carbon content, the concentration of the tracer SF₆ and the isotopic ratios are given for all sampling campaigns.

Additionally, the mixing model, which is based on the isotope ratios of the groundwater samples, showed that nearly all of the CO₂ detected in the groundwater samples of control planes *C*, *D*, and *E* was a result of added CO₂ from injections. The isotope ratios of $-30.8 \text{ ‰} \pm 0.17 \text{ ‰}$, $-30.6 \text{ ‰} \pm 0.04 \text{ ‰}$, and $-30.9 \text{ ‰} \pm 0.37 \text{ ‰}$, respectively, correspond closely to the isotope ratio of the injected CO₂ ($-30.5 \pm 0.04 \text{ ‰}$). At none of the three control planes a relevant indication for dilution of isotope ratios was observed. In control plane *F*, about 20 meters in the main groundwater flow direction from the injection lances, a slight dilution in the amount of the arriving CO₂ was detected. The isotope ratios at the observation wells in control plane *F* ranged between $-25.9 \pm 0.16 \text{ ‰}$ and $-29.6 \text{ ‰} \pm 0.17 \text{ ‰}$, whereas at observation well *ZZI*, located between *1F* and *5F*, no dilution was detected. These results show that the major part of the injected CO₂ moved consistently westward with the groundwater flow.

3. Monitoring of a simulated CO₂ leakage in a shallow aquifer using stable carbon isotopes

According to the carbonate species distribution, at a pH of 5 only 5 % of the CO₂ is presents as HCO₃⁻, and the amount of CO₃²⁻ is negligible. It can therefore be assumed that the overwhelming majority of the CO₂ will be present as aqueous dissolved CO₂ and a fractionation between the different CO₂ species can be neglected.

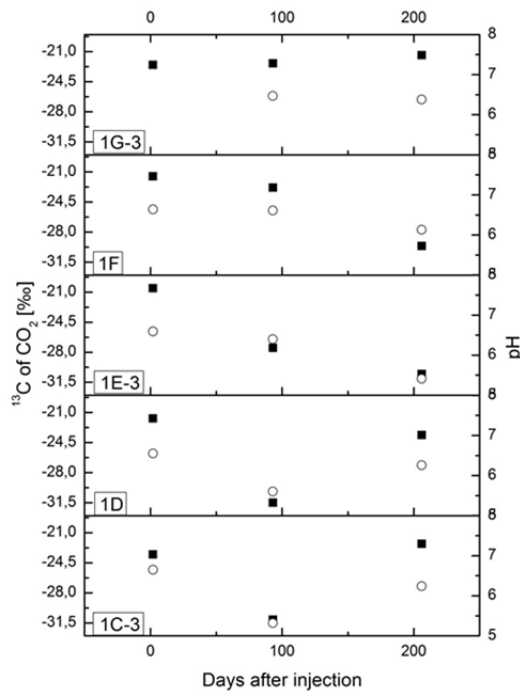


Figure 3.5 The variation of the isotope ratio (circles) of five specific wells along a cross-section in correlation with the variation of the pH (squares). Well ML1C-3 is the closest well to the injection lance; well ML1G-3 is about 25 meters away (see figure 1). At first, the two closest wells showed indication of the injected CO₂ while no change either in pH or isotope ratio was measured at the monitoring well farthest away from the injection well.

3.6 Discussion

The monitoring of carbon dioxide leakage in a shallow aquifer and in the upper soil zone using stable carbon isotopes can make an important contribution to the proper risk assessment of Carbon Capture and Storage technology. The measurement of the stable carbon isotope ratios of CO₂ in groundwater and soil gas allows distinction between the different sources of the CO₂. The identification of the leakage source is of some importance, especially in cases where several CCS sites are in close proximity. In the case of leakage, aquifers are possible receptors of upwardly migrating CO₂ plumes.

3. Monitoring of a simulated CO₂ leakage in a shallow aquifer using stable carbon isotopes

The CO₂ is expected to display conservative behavior in shallow aquifers lacking a carbonate mineral matrix, and our data suggest that the isotope fingerprint of CO₂ leakage events may be detectable over long time frames. Thus, confined shallow aquifers might be prime zones for monitoring CO₂ leakage with stable isotope techniques.

Factors affecting the isotope ratios of soil gas

So far, relatively few data are available for carbon isotope ratios of soil gas (CO₂ that occupies the pore space in a the soil matrix) (Amundson et al., 1998). Most of the measurements have been performed for soil-respired CO₂ (the flux of CO₂ moving through the soil). This study concentrates on carbon isotope ratios of both soil gas and groundwater to monitor the behavior of an artificially created CO₂ plume. The CO₂ in soils is derived from three sources: respiration of plant roots, atmospheric CO₂, and the decomposition of organic matter. The isotope ratios of background CO₂ in this study did not show significant seasonal variation related to periods of higher photosynthetic activity in the soil gas, as the sampling depth of 1.1 m was below the region of root respiration. We can therefore conclude that root respiration does not significantly influence the isotope ratios of CO₂ of deeper soil zones. At the field site, C₃ plants were dominant (e.g. *Achillea millefolium*, *Echium vulgare*) and according to Amundson (Amundson et al., 1998) the ¹³C ratios of the flora will dominate the carbon isotope chemistry of the soil (average δ¹³C values of C₃ plants = -27 ‰ (Deines, 1980)). As the background CO₂ within the soil gas is slightly depleted in ¹³C (-21.5 ± ‰) compared to the atmosphere, it is assumed that a mixture of atmospheric gas exchange and the decomposition of organic material is responsible for the isotope ratios of the soil gas CO₂.

Detection of CO₂ leakage using soil gas

On only one sampling campaign isotopically-light CO₂ in soil gas was recorded, at three specific sampling points. We can thus conclude that the injected CO₂ remained below the aquitard (10 m bgl), which operated as a barrier between the two aquifers over the entire monitoring field. The isotopically-light CO₂ that was detected in the soil gas at these three points is thought to have originated directly from a leak at one of the injection lances.

3. Monitoring of a simulated CO₂ leakage in a shallow aquifer using stable carbon isotopes

The leak most likely occurred at the injection lance and then migrated into the pore space of the adjacent soil. In the initial phase of the experiment, decreased isotope ratios in the groundwater samples were not detected at these locations, so it can be assumed that the isotopically-light CO₂ never reached the upper aquifer. The results of the soil gas monitoring convincingly demonstrate the ability to detect small CO₂ leaks in the vadose zone employing isotope analysis. Nevertheless, a high sampling frequency is necessary because the diffusion of soil gas and gaseous exchange with the atmosphere lead to a relatively fast dilution of the isotope signal.

Behavior of CO₂ in the aquifer

In contrast to soil gas, the retention time of injected CO₂ in groundwater is much longer and the sampling frequency can therefore be reduced. As the westward migration of the injected CO₂ corresponded to the groundwater flow direction, it can be assumed that a substantial amount of the injected CO₂ was distributed via dissolution and subsequent migration in the groundwater. Nevertheless, gas transport must also be taken into account, as geoelectrical monitoring showed clear evidence of upward migration and subsequent accumulation of the gas below the aquitard (Lamert et al., 2012). Several monitoring wells were equipped with multi-level packers, which allowed the vertical monitoring of the distribution of isotopically-light CO₂ in groundwater (SI-Fig. 2). The aquifer section into which the CO₂ was injected is composed of relatively homogeneous sand but with differences in grain size over the depth profile. Coarser grain sizes in the upper and lower sampling levels may account for the spatial distribution of groundwater containing dissolved isotopically-light CO₂. Therefore, the migration of the CO₂ plume along flow paths with higher permeability is likely. In contrast, in areas composed of sediments of typically low hydraulic conductivity, a slower migration of the dissolved isotopically-light CO₂ was found (see geological profile in Lamert et al. (2012)).

In general, the relatively long retention time of the CO₂ plume in control planes *C* and *D* fit the hypothesis for dissolution of CO₂ in groundwater and subsequent migration of the plume with the groundwater stream. In this case the CO₂ plume moved with the groundwater flow and was only slowly diluted. The slow migration of the CO₂ plume corresponds well with the low groundwater flow velocity of 0.07 – 0.1 m d⁻¹.

3. Monitoring of a simulated CO₂ leakage in a shallow aquifer using stable carbon isotopes

Evaluation of the stable isotope approach

According to the mass balance of the isotope ratios measured in groundwater, monitoring method becomes more sensitive the larger the difference between the isotope ratio of the background and the injected CO₂ is. At a difference of only 5 ‰ (e.g., from background CO₂ at -25 ‰ and CO₂ from fossil fuel combustion at -30 ‰), about six times more isotopically-light CO₂ would be necessary to decrease the isotope ratio of the groundwater by 1 ‰. The smaller the difference in isotope ratios, the more injected CO₂ is necessary to create an observable change, thus this monitoring method is only applicable in case of sufficiently large difference between isotope ratios. Additionally, the isotope ratio of the CO₂ to be stored underground must be known in advance to make this method applicable.

Another aspect that determines the applicability of this monitoring method is the absence of carbonates in the sediments. When carbonates are present in the groundwater, the pH would be buffered, at least in the early stages of a CO₂ leakage event, and a shift to a higher HCO₃⁻ concentration would be the result. Consequently, a higher amount of injected CO₂ would be necessary to determine a change in the isotope ratios. Further in case of carbonate rich soils an isotope exchange with the matrix has to be taken into account which is not covered by this investigation.

In addition, this monitoring concept can only be considered reliable in cases where there is no significant exchange between the atmosphere and the aquifer; otherwise isotope fractionation would need to be considered. If a large degassing would occur while sampling isotope fractionation would play a role but it was not the case for this study. The presence of an aquitard, especially for shallow aquifers, decrease exchange processes with the atmosphere and simplify the interpretation of isotope composition as well as the sensitivity of ¹³CO₂ monitoring. If no aquitard exists, the monitoring in deeper aquifers may avoid disturbances of the isotope signal in the groundwater by atmospheric influences. If the monitoring approach were based only on physicochemical parameters like pH, the identification of the CO₂ source would not be possible, indicating the possibility that a change in these parameters (e.g. due to the input of salt or organic material into the groundwater) could lead to a misinterpretation. Furthermore, spatial resolution should always be taken into account.

3. Monitoring of a simulated CO₂ leakage in a shallow aquifer using stable carbon isotopes

Large-scale approaches based on a fixed grid would be necessary for rough detection of CO₂ seepage whereas small-scale approaches, like isotope monitoring, would be useful for pin-pointing and identifying the leakage source (Cortis et al., 2008).

Implications

This study was performed on a small scale, thus a direct extrapolation and up scaling of these results to a real leakage scenario may be a challenge. Nevertheless, the observed results do clearly show that stable carbon isotope analysis is a reliable and fast-responding tool to detect CO₂ leakage from a storage site as measured in either groundwater or soil gas. This study thus may serve as proof-of-concept and establishes data that can provide a foundation for further research and eventual application.

3.7 Acknowledgement

This project was funded by the German Federal Ministry of Education and Research (Grant: 03G0670C) in the context of the project “CO₂ injection into a near surface aquitard for evaluating monitoring concepts and methods”. We thank R. Dumke from the BGR, Hannover for providing us with the prototype of the soil gas lances and we thank R. Schumann for the construction and maintenance of the adapted soil gas lances.

3.8 Supporting information

Isotope ratios [‰] of soil gas for three sampling campaigns before and during the CO₂ injection (SI-Tab. 3.1). Sampling campaigns, number of taken samples and the lowest measured isotope ratio of each campaign (SI-Tab. 3.2). Isotope ratios and SF₆-concentration of groundwater samples for all sampling campaigns (SI-Tab. 3.3). Schematic of a self-constructed soil gas sampling lance (SI-Fig. 3.1). Profile of one monitoring well with different sampling depths and a correlation with the distribution of isotope ratios in the specific depth (SI-Fig. 3.2).

4. Feasibility of geoelectrical monitoring and multiphase modelling for process understanding of gaseous CO₂ injection into a shallow aquifer

4. Feasibility of geoelectrical monitoring and multiphase modelling for process understanding of gaseous CO₂ injection into a shallow aquifer

4.1 Kurzfassung

Potentielle Wegsamkeiten im Untergrund können zu einer Migration von gasförmigem CO₂ aus geologischen Speicherschichten in einen oberflächennahen Aquifer führen. Infolgedessen ist die Verfügbarkeit geeigneter Monitoringmethoden für potentielle CO₂ Austritte, sowohl in tiefen geologischen Formationen, als auch in flachen Horizonten, eine Voraussetzung für die Entwicklung der Carbon Capture and Storage Technologie. Geoelektrische Überwachungen wurden bei einem kleinskaligen, zeitlich begrenzten CO₂-Injektionsversuch in einem ungestörten, flachen Grundwasserleiter durchgeführt. Zusätzlich wurde die Anwendbarkeit einer Multiphasenmodellierung getestet, um sowohl komplexe nichtlineare, mehrphasige Fließprozesse, als auch das elektrische Verhalten teilweise gesättigter, heterogener, poröser Medien zu beschreiben. Es wurde gezeigt, dass geoelektrische Methoden für das Monitoring von injiziertem CO₂ und geochemisch verändertem Grundwasser geeignet sind. Im Feldversuch wurden mit Hilfe geoelektrischer Messmethoden, signifikante Variationen in der elektrischen Leitfähigkeit im Bereich von 15 – 30 % detektiert. Standortspezifische Bedingungen (z.B. geologische Beschaffenheit, Grundwasserzusammensetzung) führen jedoch zu starken Variationen der elektrischen Leitfähigkeit im Untergrund, was wiederum die Zuverlässigkeit geoelektrischer Monitoringmethoden beeinflusst. Die Daten des Monitorings lieferten erste Ergebnisse bezüglich Migrations- und Akkumulationsprozessen von gasförmigem CO₂. Es konnte gezeigt werden, dass geoelektrisches Monitoring, zusammen mit Multiphasenmodellierung, eine geeignete Methode zum Verständnis der Migration von Gasphasen und von Massentransferprozessen, die durch das Eindringen von CO₂ in ein flaches Grundwasserleitersystem entstehen, ist.

*Lamert, Hendrik; Geistlinger, Heinrich; Werban, Ulrike; Schütze, Claudia, Peter, Anita; Hornbruch, Götz; **Schulz, Alexandra**; Pohlert, Marco; Kalia, S.; Großmann, Jochen; Dahmke, Andreas, Dietrich, Peter.*

Published in: Environmental Earth Sciences, 2012, 67, pp 447-462

4. Feasibility of geoelectrical monitoring and multiphase modelling for process understanding of gaseous CO₂ injection into a shallow aquifer

4.2 Abstract

Potential pathways in the subsurface may allow upwardly migrating gaseous CO₂ from deep geological storage formations to be released into near surface aquifers. Consequently, the availability of adequate methods for monitoring potential CO₂ releases in both deep geological formations and the shallow subsurface is a prerequisite for the deployment of Carbon Capture and Storage technology. Geoelectrical surveys are carried out for monitoring a small-scale and temporally limited CO₂ injection experiment in a pristine shallow aquifer system. Additionally, the feasibility of multiphase modeling was tested in order to describe both complex non-linear multiphase flow processes and the electrical behavior of partially saturated heterogeneous porous media. The suitability of geoelectrical methods for monitoring injected CO₂ and geochemically altered groundwater was proven. At the test site, geoelectrical measurements reveal significant variations in electrical conductivity in the order of 15–30 %. However, site-specific conditions (e.g., geological settings, groundwater composition) significantly influence variations in subsurface electrical conductivity and consequently, the feasibility of geoelectrical monitoring. The monitoring results provided initial information concerning gaseous CO₂ migration and accumulation processes. Geoelectrical monitoring, in combination with multiphase modeling, was identified as a useful tool for understanding gas phase migration and mass transfer processes that occur due to CO₂ intrusions in shallow aquifer systems.

4.3 Introduction

An approach currently being developed with the aim of reducing CO₂ emissions into the atmosphere is CCS technology (Carbon Capture and Storage). The main concern associated with CCS is that CO₂ from storage reservoir formations (such as deep saline aquifers or depleted oil and gas fields) may leak due to permeable cover sediments or natural and artificial pathways, such as faults or well structures. These potential pathways may allow upwardly migrating gaseous CO₂ to be released into near surface aquifers or even into the atmosphere (surface leakage), which would reduce the efficiency of CCS. Moreover, a potential leakage of CO₂ from storage sites could have detrimental effects on the surrounding environment and even upon human health (Oldenburg and Unger, 2003; Hollaway et al., 2007; Lewicki et al., 2007a).

4. Feasibility of geoelectrical monitoring and multiphase modelling for process understanding of gaseous CO₂ injection into a shallow aquifer

Computational simulations (Carroll et al., 2009; Fahrner et al., 2011; Humez et al., 2011), batch-reactor experiments (Lu et al., 2010) and a small-scale field study at the ZERT site (Kharaka et al., 2010) describe significant changes of aquifer geochemistry (e.g., mobilization of cations from the host rock, pH decrease, electrical conductivity increase) in the groundwater system after CO₂ intrusion.

Consequently, in the context of sound risk assessment, the availability of adequate methods for the detection and monitoring of potential CO₂ release is a prerequisite for the deployment of CCS technology, in both deep geological formations and the shallow subsurface (Wilson et al., 2007). To monitor injected CO₂ in deep geological formations, geophysical methods are currently applied (Torp and Gale, 2004). Geoelectrical methods are a promising tool for monitoring subsurface processes, which induce temporal or spatial variations of electrical conductivity. Some case studies have already been performed using geoelectrical methods for monitoring the CO₂ storage test site Ketzin/ Germany (Kießling et al., 2010) and for the characterization of natural geological CO₂ leakage sites (Schütze et al., 2012).

In our case study, a controlled CO₂ injection experiment was performed by injecting gaseous CO₂ into a pristine shallow aquifer, with the aim of further improving the understanding of CO₂ behavior in shallow groundwater systems (Peter et al., 2012b). During a period of 10 days in 2011, 787 kg in total of gaseous CO₂ was injected into a near surface aquifer at a depth of 18 m below ground surface. One of the main objectives of this field study was to design and test different monitoring methods to detect potential CO₂ release in near subsurface groundwater systems. For this purpose, three CO₂ injection lances and 34 monitoring wells were installed and additionally equipped with electrodes to allow spatially and temporally high resolution monitoring of subsurface processes caused by CO₂ intrusion. To perform a CO₂ gas injection experiment in partially saturated heterogeneous porous media, understanding and control of complex non-linear multiphase flow processes is essential. The general objective of the present paper is to improve the understanding of transport processes monitored during the performed CO₂ injection experiment with respect to analogue processes, which might occur during a CO₂ leakage from deep storage reservoirs.

4. Feasibility of geoelectrical monitoring and multiphase modelling for process understanding of gaseous CO₂ injection into a shallow aquifer

In this context, a more detailed focus of this work could be outlined as follows (1) to prove and describe the feasibility of geoelectrical methods for monitoring CO₂ intrusions into near subsurface structures and (2) to test the feasibility of the multiphase model TOUGH2 (Pruess et al., 1999), to describe the gas flow patterns and the electrical behavior of partially saturated heterogeneous porous media. Therefore, the goal of the modeling study is to answer whether or not TOUGH2 is able to describe experimentally measured geoelectrical breakthrough curves and additionally, whether TOUGH2 can adequately describe the gas flow patterns or at least the average gas phase distribution within a heterogeneous aquifer.

4.4 Geoelectrical monitoring of subsurface processes

4.4.1 An overview of physical parameters affecting electrical conductivity

In this section, rock-physical basic principles for geoelectrical monitoring are presented with respect to CO₂ intrusion into a shallow aquifer system. Due to the lower pressure regime present in shallow aquifers, potentially upward migrating supercritical CO₂ from deep geological formations changes into its gas phase. Gaseous CO₂ intrusion into shallow groundwater systems generally causes increased gas phase content in the soil pore space, which accordingly leads to decreased bulk electrical conductivity of the subsurface. However, a subsequent dissolution of CO₂ leads to a formation of carbonic acid, which generally leads to decreased pH values. This is followed by an increase of electrical fluid conductivity. Following (Rein et al., 2004), potential effects of factors inducing variations of electrical conductivity in the subsurface are discussed, i.e., gas and soil water content, concentration variation of ions in groundwater, and temperature. An empirical, widely used equation for estimating the electrical conductivity of partly saturated rocks was developed by Archie (1942), which assumed that the electrical conductivity of the soil matrix is negligible:

$$\sigma_{ps} = \sigma_f \frac{1}{F} S_w^n \quad (\text{eq. 4.1})$$

where σ_{ps} denote electrical conductivity of partly saturated rocks (subsurface); σ_f electrical conductivity of fluid; F formation resistivity factor; S_w water saturation; n exponent of saturation (often assumed: $n = 2$, e.g., (Archie, 1942). With [according to Dachnov (Schön, 1996)]:

4. Feasibility of geoelectrical monitoring and multiphase modelling for process understanding of gaseous CO₂ injection into a shallow aquifer

$$F = \frac{a}{\phi^m} \quad (\text{eq. 4.2})$$

where ϕ denote porosity; m exponent of cementation; a empirical coefficient, see also Schön (1996). However, in the presence of an electrical conductive matrix (e.g., clay-rich sediments), the corresponding component of electrical conductivity is not negligible. A list of appropriate studies and models investigating matrix conductivity as a component of rock conductivity is provided by Schön (1996). Taking the electrical conductivity of the matrix into account, a more general equation for σ_{ps} is:

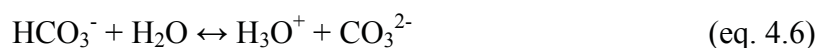
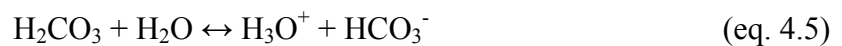
$$\sigma_{ps} = \sigma_f \frac{1}{F} S_w^n + \sigma_m \quad (\text{eq. 4.3})$$

where σ_m denote electrical conductivity of the soil matrix. According to equation 4.3, parameters, which generally might be affected by a CO₂ intrusion, are water saturation S_w and fluid conductivity σ_f . Naturally, large variations of water saturation S_w are expected in the area of groundwater table fluctuations as well as in the upper part of the unsaturated zone (soil moisture content). However, gas intrusion into the saturated zone firstly induces decreasing water saturation in the pore space, which is in turn associated with an increase in electrical resistivity (reciprocal of conductivity) of the subsurface. According to (Rein et al., 2004), a calculated variation in water saturation from 100 to 95 % results in a conductivity decrease of about 10 %, whilst a change in water saturation from 100 to 80 % leads to a conductivity decrease of about 36 %.

Fluid conductivity σ_f is primarily characterized by the geological background, which affects the composition of ions dissolved in groundwater. Basically, CO₂ intrusion in water (H₂O) leads to dissolution processes depending on pressure and temperature:



The subsequent dissociation of carbonic acid in water:



and the geochemical alteration of groundwater due to CO₂ intrusion, which strongly depends on mineral and groundwater composition, affect the electrical fluid conductivity (see also (Kharaka et al., 2010; Lu et al., 2010; Fahrner et al., 2011).

4. Feasibility of geoelectrical monitoring and multiphase modelling for process understanding of gaseous CO₂ injection into a shallow aquifer

Electrical conductivity of the fluid can be estimated by ionic mobility and ion concentrations (Keller, 1966):

$$\sigma_f = Fa \sum_{i=1}^{N_i} C_i^{eq} v_i \quad (\text{eq. 4.7})$$

where Fa denotes Faraday Constant; C_i^{eq} equivalent concentration of ion i ; v_i the temperature depended mobility of ion i . Equation 4.7 neglects the interaction of ions. This simplification does not account for the activity coefficient, which relates activities to molal concentrations (Appelo and Postma, 1993). This is justified for fluids containing low salt concentrations, which are associated with low ionic strengths. Ionic fluid composition is changing due to CO₂ intrusion into an aquifer system. According to equation 4.7 changes of equivalent concentrations of present ions lead to variations in fluid conductivity. However, σ_f variations in response to a CO₂ intrusion depend on various factors, i.e., variations in depth, groundwater dynamic, initial groundwater composition, mineralogy of the host rock, and CO₂ intrusion rate (Fahrner et al., 2011). Fahrner et al. (2011) calculated the geochemical impact of CO₂ intrusion upon the electrical conductivity of groundwater by using different scenarios including varying conditions. For a shallow freshwater aquifer with calcite present, Fahrner et al. (2011) calculated a significant increase of fluid conductivity in the order of 1 mS/cm. The presence or lack of calcite was identified as a major geochemical factor inducing electrical conductivity variations of groundwater in the case of CO₂ intrusion, as the solubility of carbonates increases with increasing content of dissolved CO₂. For an equivalent scenario in the absence of calcite, the increase of fluid conductivity was less pronounced due to the low dissociation rate of dissolved carbonic acid.

Detailed information on CO₂ dissociation processes and the carbonate-equilibrium-system are given, e.g., in Appelo and Postma (1993). The electrical conductivity of a fluid can generally be estimated using equation 4.7. However, dynamic geochemical processes (e.g., cation exchange processes) associated with site-specific conditions (e.g., presence or absence of buffering materials) must be taken into account when assess variations in fluid conductivity caused by CO₂ intrusion.

4. Feasibility of geoelectrical monitoring and multiphase modelling for process understanding of gaseous CO₂ injection into a shallow aquifer

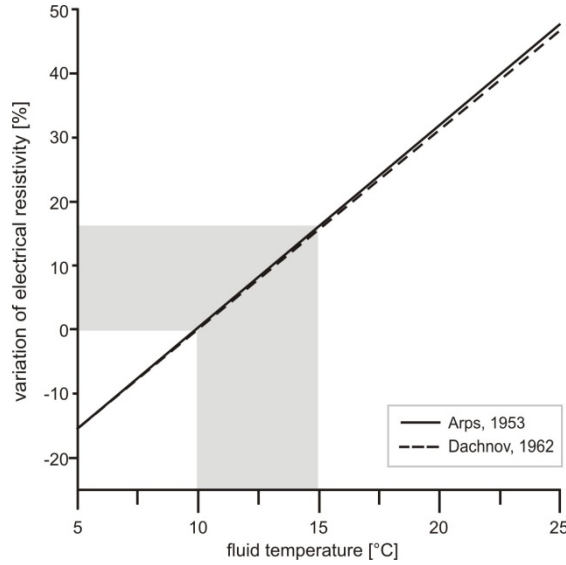


Figure 4.1 Relative variation of electrical fluid resistivity due to temperature variation. Approximation according to Arps (1953) and Dachnov (Schön 1996), reference temperature: 10 °C.

Due to deep geological storage of CO₂ and the associated potential upward migration of gaseous CO₂, temperature variations may also influence σ_f (Fig. 4.1). Variations of electrical conductivity caused by temperature changes can be approximated according to empirical equations presented by Arps (1953):

$$\sigma_f(T_1) = \sigma_f(T_0) \frac{T_1 + 21.5}{T_0 + 21.5} \quad (\text{eq. 4.8})$$

where T_0 , T_1 denote fluid temperature at time t_0 and t_1 ; $\sigma_f(T_0)$, $\sigma_f(T_1)$ denote electrical conductivity of the fluid at temperature T_0 , T_1 in (°C). And by Dachnov (Schön, 1996):

$$\sigma_f(T_1) = \sigma_f(T_0) \frac{1 + \alpha_T (T_1 - 18)}{1 + \alpha_T (T_0 - 18)} \quad (\text{eq. 4.9})$$

where α_T denotes temperature coefficient, for temperatures about 18 °C is $\alpha_T \approx 0.025$ °C⁻¹. For example, temperature changes of 5 °C result in a relative electrical resistivity variation of approx. 16 % (Fig. 4.1). The three parameters described above - variations in water saturation, changing ion content in groundwater, and temperature variations - significantly influence the electrical conductivity of variable saturated porous media. However, the impact strength of each parameter depends on numerous conditions (e.g., geological settings, depth, and groundwater composition) and is thus highly site specific (see also Kolditz et al. (2012)).

4. Feasibility of geoelectrical monitoring and multiphase modelling for process understanding of gaseous CO₂ injection into a shallow aquifer

4.4.2 *An overview of geoelectrical time-lapse monitoring of subsurface processes*

Geoelectrical methods allow time efficient as well as temporal and spatially high resolution monitoring of hydrodynamic subsurface processes. Generally, surveys using electrodes installed in boreholes at selected depths of interest (e.g., tracer injection horizon) are more suitable than using electrodes installed at the ground surface level. This is due to the fact that the latter are usually more influenced by external perturbations, i.e., changes in air temperature or soil moisture (e.g. Binley et al. (2002); Rein et al. (2004)). The sensitivity distribution of a four-electrode array (two current and two potential electrodes) configuration primarily denotes regions, which are sensitive to the measurement. Typical behavior reveals that the highest sensitivities occur in the vicinity of the electrodes (e.g., Knödel et al. (2007)). Electrodes located at wells in the injection horizon are placed nearby or within the altered groundwater, which commonly results in better spatial and temporal resolution. Geoelectrical measurements allow conclusions about varying electrical parameters and thus, help the assessment of hydrodynamic subsurface processes. For monitoring variations of electrical parameters in the subsurface, two approaches can be used. Firstly, determining variations of absolute values:

$$\Delta\sigma_{ps} = \sigma_{ps}^{t,1} - \sigma_{ps}^{t,0} \quad (\text{eq. 4.10})$$

where $\Delta(\sigma_{ps})$ denotes the variation of electrical conductivity of partly saturated rock at time step $t = 0$ and $t = 1$. According to equations 4.1, 4.2 and 4.3, electrical variations of partly saturated rocks are induced by variations of fluid conductivity and water saturation:

$$\Delta(\sigma_{ps}) = (\sigma_f^{t,1} (S_w^n)^{t,1} - \sigma_f^{t,0} (S_w^n)^{t,0}) F^{-1} = \Delta(\sigma_f S_w^n) F^{-1} \quad (\text{eq. 4.11})$$

Using absolute values for monitoring variations of electrical parameters, $\Delta(\sigma_{ps})$ also depends upon the formation resistivity factor F and accordingly on geological heterogeneities (see equation 4.11). Generally, F might be assumed to be constant over time. However, due to mineral dissolution and chemical precipitation, F may be variable (Huq et al., 2012). For the assumption that F is constant over time, no alteration processes of the sediment structure occur. Consequently, for conditions with constant F and constant $\Delta\sigma_f$, parameters ΔS_w^n and $\Delta(\sigma_{ps})$ are linearly related (equation 4.11).

4. Feasibility of geoelectrical monitoring and multiphase modelling for process understanding of gaseous CO₂ injection into a shallow aquifer

The second approach for monitoring variations of electrical parameters determines relative values, e.g., determination of ratios that correspond to variations relative to $\sigma_{ps}^{t,0}$:

$$\sigma_{ps}^{t,1} / \sigma_{ps}^{t,0} = \frac{\sigma_f^{t,1} F^{-1} (S_w^n)^{t,1} + \sigma_m}{\sigma_f^{t,0} F^{-1} (S_w^n)^{t,0} + \sigma_m} \quad (\text{eq. 4.12})$$

This approach seems more complex. When matrix conductivity is negligible ($\sigma_m \ll \sigma_f^{t,z} F^{-1} (S_w^n)^{t,z}$). Equation 4.12 can be simplified (assuming that F is constant over time):

$$\sigma_{ps}^{t,1} / \sigma_{ps}^{t,0} \approx \frac{\sigma_f^{t,1} (S_w^n)^{t,1}}{\sigma_f^{t,0} (S_w^n)^{t,0}} \quad (\text{eq. 4.13})$$

This assumption depends strongly on site-specific geological and mineralogical conditions (e.g., presence of clay-rich sediments) and must consequently be assessed for each field site. However, according to equation 4.13 using relative values, determined variations do not depend on F . The approach using absolute variation (equation 4.11) could generally be used for homogeneous geological conditions. In geological conditions with negligible matrix conductivity a more appropriate approach is the second one [equation 4.12, 4.13; Dietrich (1999)]. Consequently, the choice of which approach should be taken is site dependent.

4.5 CO₂ injection scenario: test site and test setup

In order to prove the feasibility of geoelectrical measurements for monitoring CO₂ intrusion scenarios in shallow aquifer systems, a field study was carried out at a former military airfield near the town of Wittstock. The test site is located approx. 100 km north of Berlin, in the state of Brandenburg (Germany). At the test site, a plane fallow land, the geological conditions are primarily characterized by glacial or glacial-fluvial unconsolidated Quaternary sediments. Based on a detailed field site investigation, information on stratigraphic composition was collected using Direct Push soundings (Dietrich and Leven, 2006; Leven et al., 2011; Vienken et al., 2012), as well as drilling samples (see also Peter et al. (2011); Peter et al. (2012b)). The stratification of the uppermost aquifer (aquifer 1) consists of interbedded strata composed of sands, silts, clays and humus with total thickness of about 11 m. Glacial loam is underlying aquifer 1. According to drilling results, the depth and thickness (in average 0.5 m) of the loam is highly variable.

4. Feasibility of geoelectrical monitoring and multiphase modelling for process understanding of gaseous CO₂ injection into a shallow aquifer

At the test site, aquifer 2 extends approx. 11.5–19.5 m below ground level (bgl). Due to its large extent in depth and relatively homogeneous composition, the sandy sediments of this aquifer were chosen as an appropriate injection horizon for the gaseous CO₂ (Fig. 4.2). Glacial till is underlying aquifer 2 and forms the base of the CO₂ injection horizon.

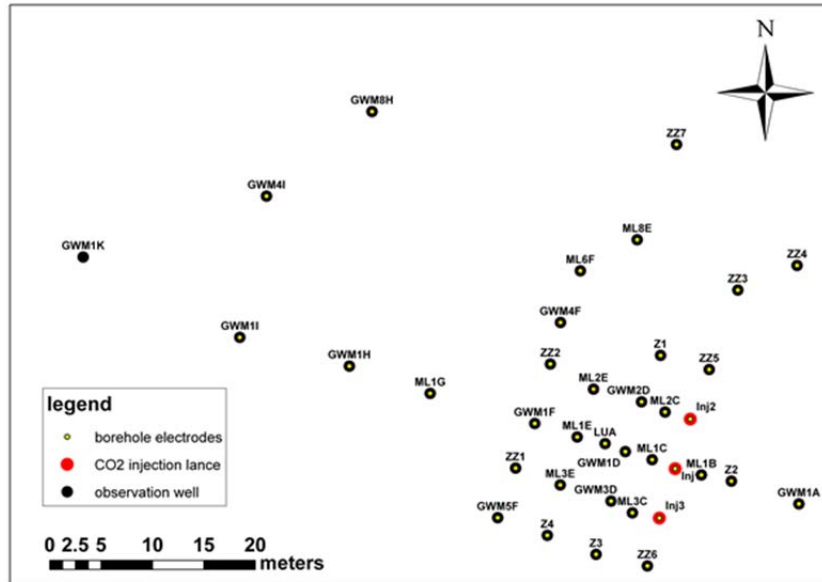


Figure 4.2 a) Test site Wittstock. Regional groundwater flow is directed from GWM 1A to GWM 1I, roughly from east to west. b) Schematic geological profile and schematic illustration of a well equipped with electrodes.

Collected data resulted in a detailed geological structure model of the test site. The geological structure model for the injection horizon is described in detail by Peter et al. (2012b). It consists of six different layers from top to bottom: (1) glacial loam, (2) upper medium sand layer, (3) coarse sand layer in the eastern part, (4) silt layer in the Western part, (5) lower medium sand layer, and (6) continuous boulder clay layer. Regional groundwater flow direction is roughly directed from east to west. The average pore water velocity (subsequently referred to as ‘groundwater flow velocity’) varies within the range 0.1 up to 1 m day⁻¹. In order to perform the field test, three CO₂ injection lances and 34 monitoring wells in total were installed at the test site, oriented perpendicular to regional groundwater flow direction (Fig. 4.2). One of the main operational constraints was to produce a coherent plume of dissolved CO₂ in groundwater. Injection lances (1.1” continuous 3-channel tubing) were installed using minimally invasive Direct Push technologies and are screened over 0.2 m at a depth of 18 m to realize a depth-defined CO₂ injection.

4. Feasibility of geoelectrical monitoring and multiphase modelling for process understanding of gaseous CO₂ injection into a shallow aquifer

Injection lances were installed several weeks in advance of the injection period with the aim that the sediment may reconsolidate again, thereby minimizing potential preferential pathways along the well. The design and implementation of the injection experiment is described in detail by Peter et al. (2012b).

Between 29.03.2011 and 08.04.2011, 787 kg CO₂ in total was injected with a low injection pressure (approximately equal to the hydrostatic pressure) simultaneously at the three injection lances into aquifer 2. This corresponds to injection rates of 10 L CO₂/min (at standard pressure and temperature) at each injection well. Altogether, four different types of monitoring wells were installed to implement an extensive monitoring set-up for the CO₂ injection experiment (see Peter et al. (2012b)). They allow for groundwater sampling before, during and after the CO₂ injection scenario. Additionally, injection lances and 33 monitoring wells are equipped with a total of 300 ring-shaped copper electrodes for implementing geoelectrical surveys. The electrodes fixed at the outer surface of the HDPE/MDPE well material are installed in predefined depths between 8.0 m and 18.5 m bgl, thus allowing for an electrical resistivity monitoring covering the entire thickness of aquifer 2 (Fig. 4.2b). In this manner, borehole and cross-borehole measurements are realized. Generally, the spacing of the electrodes was selected to be 1 and 1.5 m, respectively. Monitoring wells GWM 1D, GWM 2D and GWM 3D are equipped with additional electrodes to realize an electrode spacing of 0.75 m. These electrodes allow a more detailed detection of potentially accumulating gaseous CO₂ beneath the glacial loam.

4.5.1 Geoelectrical monitoring of the performed CO₂ injection scenario

In the presented field study, variations in apparent electrical resistivity of the subsurface are monitored by using multichannel resistivity equipment and were converted into apparent electrical conductivity values (σ_a). Extensive geoelectrical monitoring was performed by repeating a predefined measuring cycle with all installed electrodes. Monitoring was performed by using different 4-point arrays (Wenner, Schlumberger, gradient, and dipole– dipole). A temporal resolution of the electrical resistivity data of 120 min was realized. Geoelectrical monitoring began approximately 1 day before the CO₂ injection scenario was started, in order to obtain baseline values.

4. Feasibility of geoelectrical monitoring and multiphase modelling for process understanding of gaseous CO₂ injection into a shallow aquifer

Monitoring during and after the CO₂ injection period was carried out during an initial campaign, followed by additional ‘shorter time frame’ field campaigns (Tab. 4.1), which became necessary due to the low regional groundwater flow velocity of approximately 0.05 m/day.

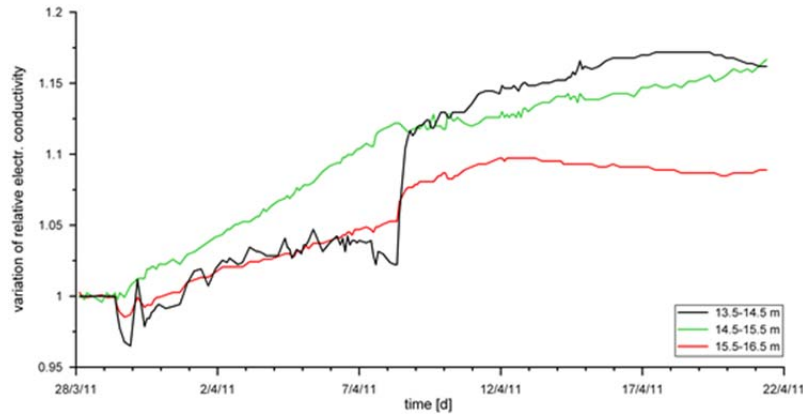


Figure 4.3 Temporal variation of apparent conductivity (σ_a) relative to baseline measurements at well ML 1C (1.1" diameter well) during Monitoring Campaign 1; electrode configuration: Wenner (AMNB). Depths (meter below ground level) of potential electrodes M–N are given in the legend. The bottom of glacial loam layer is located 12.0 m bgl.

In this manner, approximately 350 monitoring cycles (including about 4,200 measurements each) were performed. Electrodes fixed at pre-defined depths at discrete wells allowed high resolution geoelectrical monitoring of the CO₂ injection scenario to take place. Measurements at various time intervals are normalized to corresponding values of mean baseline measurements (see equation. 4.12; 4.13). This approach was used due to the fact that matrix conductivity is negligible in the identified sandy CO₂ injection horizon at the test site. Assuming the formation resistivity factor F is constant over time, the geoelectrical observed variations are caused by variations of σ_f and (see equation 4.13). Temperature in aquifer 2 was measured using multi-parameter probes. Temperature variations were determined to be in the order of 0.1 °C and have been neglected for geoelectrical monitoring (see also Peter et al. (2012b); Fig. 1).

The first interpretation step carried out during process monitoring was to use breakthrough curves from borehole measurements to analyze variations of σ_a at a total of 36 wells. Breakthrough curves of borehole measurements (single spacing at discrete wells) are used since variations of σ_a can be quickly determined in high resolution over the entire test site (see also Fig. 4.2).

4. Feasibility of geoelectrical monitoring and multiphase modelling for process understanding of gaseous CO₂ injection into a shallow aquifer

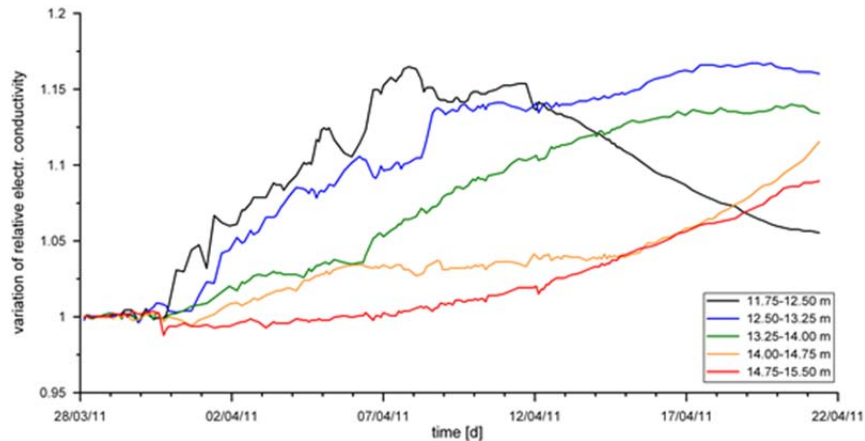


Figure 4.4 Temporal variation of apparent conductivity (σ_a) relative to baseline measurements at well GWM1D (2" diameter well) during Monitoring Campaign 1; electrode configuration: Wenner (AMNB). Depths (meter below ground level) of potential electrodes M–N are given in the legend. The bottom of glacial loam layer is located approx. 11 m bgl.

Highest variations in σ_a were observed in the area between the three injection lances down to well ML 1G. Based on extensive geoelectrical monitoring, single spacing borehole measurements at three wells ML 1C (1.100 diameter well), GWM 1D (200 diameter well), and ML 1E (1.100 diameter well) were exemplarily selected and will be presented in this paper. The effects of the radius of monitoring wells with respect to the geoelectrical measurements are negligible. The breakthrough curves from the configuration arrays used (Wenner, Schlumberger, gradient, dipole–dipole) show similar behavior and provided comparable results. However, Wenner array results are presented because the noise of the Wenner data is generally minor lower.

The selected wells are located along the regional groundwater flow path 2.5, 5 and 10 m distance apart from the central CO₂ injection lance Inj1, respectively (Fig. 4.2). Immediately after gaseous CO₂ injection started, significant variations in σ_a at well ML 1C (located 2.5 m away from injection lance 1) were detected (Fig. 4.3). Using a single electrode spacing of 1.0 m, the most likely explanation for the initial decrease of σ_a is increased gas saturation in the pore space (see also section 4.4). This effect is subsequently followed by an increase of σ_a up to approx. 17 %, which might be caused by dissolution and dissociation processes of CO₂ in the groundwater, as well as subsequent geochemical processes, e.g., cation exchange processes. A significant ‘step-like increase’ in σ_a was detected on 8th April, when gaseous CO₂ injection was stopped.

4. Feasibility of geoelectrical monitoring and multiphase modelling for process understanding of gaseous CO₂ injection into a shallow aquifer

This effect was most pronounced at potential electrodes installed at depths of 13.5 and 14.5 m (black curve in Fig. 4.3). Furthermore, the “step-like” increase of σ_a was detected by each of the aforementioned configuration arrays used during a period of approx. 5 h, representing measurements recorded over three successive time intervals.

The initial σ_a decrease after CO₂ injection began and the significant step-like increase in σ_a (in the order of 10 % for the uppermost Wenner array) after injection stopped, showing the gas phase dynamics caused by gaseous CO₂ injection. These effects indicate rapid gas ascent towards the glacial loam layer, representing an impermeable geological layer overlying the injection horizon. Monitoring well GWM 1D is located at a distance of 5 m from the central injection lance towards regional groundwater flow direction (Fig. 4.2). First and most significant variations in σ_a were measured at electrodes located directly below glacial loam (black and blue curve in Fig. 4.4). The most likely explanation for this is the occurrence of upwardly migrated and subsequently accumulated gaseous CO₂ below the impermeable loam layer, which lead to the formation of a gaseous CO₂ pool. Using a single electrode spacing of 0.75 m at the potential electrodes located in depths of 12.50 and 13.25 m, electrical conductivity variations of approx. 17 % were measured during Monitoring Campaign 1 (Fig. 4.4). Monitoring well ML 1E is located 10 m away from the central CO₂ injection lance towards the main groundwater flow direction (Fig. 4.2). Until Monitoring Campaign 3, geoelectrical measurements yielded no significant variations in σ_a . However, during the fourth campaign σ_a variations of approx. 12 % and during the fifth campaign σ_a variations up to 32 % were measured (Fig. 4.5). Field parameters of groundwater samples are used to validate geoelectrical breakthrough curves. Values for pH and EC (σ_f) of groundwater samples taken from 15 m depth are illustrated in Fig. 4.5. At well ML 1E (depths: 15 m bgl), pH values decreased from 6.4 to 5.2 and σ_f of groundwater samples increased from about 500 to 800 $\mu\text{S}/\text{cm}$.

In addition to geoelectrical monitoring results (σ_a), field parameters of water samples also indicate significant alteration in groundwater chemistry caused by the injected CO₂. Geoelectrical monitoring results and field parameters are clearly related (Fig. 4.5). Geoelectrical measurements at monitoring wells ML 1C, GWM 1D and ML 1E showed significant variations of σ_a .

4. Feasibility of geoelectrical monitoring and multiphase modelling for process understanding of gaseous CO₂ injection into a shallow aquifer

The geoelectrical results of ML 1C clearly demonstrate the interaction of both contrary processes affecting subsurface electrical conductivity: increased gas saturation in the pore space and a higher ion concentration.

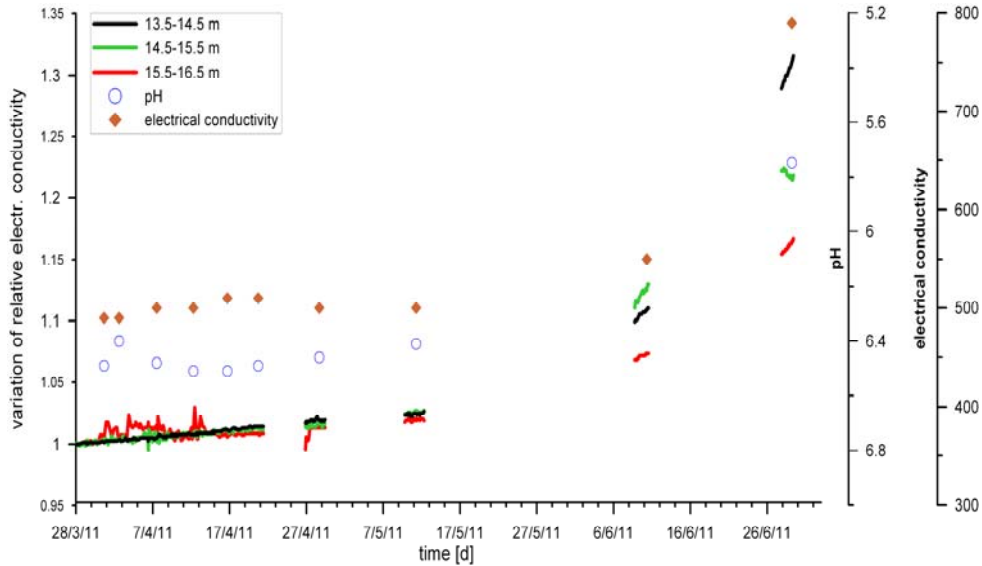


Figure 4.5 Field parameters of groundwater samples (symbols) and temporal variation of apparent conductivity (σ_a) relative to baseline measurements (solid lines) at well ML1E (1.1" diameter well); electrode configuration: Wenner (AMNB). Depths (meter below ground level) of potential electrodes M–N are given in the legend. The bottom of glacial loam layer is located 12.1 m bgl.

Furthermore, geoelectrical monitoring results of ML 1C and GWM 1D indicate a rapid upward migration of gaseous CO₂ associated with accumulation processes below the glacial loam layer. Possible upward migration paths are discrete gas channels within the sediment and potential pathways at the outside of installed wells. However, only using geoelectrical monitoring results for comprehensive understanding of gas phase migration processes is difficult. Therefore, a complementary multiphase modeling was performed.

4.6 Multiphase modeling with TOUGH2

4.6.1 Mathematical and numerical basis

The TOUGH2 program was chosen for multiphase modeling, since it can sufficiently describe the spatial and temporal gas saturation of our bench-scale experiments (Geistlinger et al., 2009).

4. Feasibility of geoelectrical monitoring and multiphase modelling for process understanding of gaseous CO₂ injection into a shallow aquifer

The agreement between theoretical and experimental results was excellent. Our conclusion was that the average gas flow behavior is adequately described by the TOUGH2 program. Furthermore, TOUGH2 is capable of taking realistic stochastic permeability fields into account, which can be implemented relatively easily by the permeability modifier concept. In real field scenarios, stochastic permeability fields will have a significant impact on the gas flow process. One focus of this modeling study is to investigate if the continuum model TOUGH2 (Pruess, 2005; Geistlinger et al., 2009) can adequately describe the gas flow pattern or at least the average gas phase distribution within a heterogeneous aquifer. A second focus of the modeling study is to answer whether or not the widely accepted multiphase model TOUGH2 is able to describe experimental breakthrough curves (BTCs).

Most of the field studies in literature on CCS are based on continuum models (see references in Hesse et al. (2008); Pruess (2008); Cinar (2009)). These models assume that the complex multiphase flow processes can be averaged over a representative elementary volume (REV) and that the essential features of the flow process can be described on a REV scale. There is an ongoing controversy in literature, if continuum models are able to adequately describe the complex flow patterns observed in heterogeneous porous media, especially the channelized stochastic flow pattern. From both bench-scale and field-scale experiments, there is overwhelming evidence that the injected gas flows through single stochastic gas channels. Based on Selker's stochastic hypothesis (Selker et al., 2007), a gas channel is caused by a Brownian-motion process during gas injection. Therefore, pore-scale heterogeneity will determine the shape of individual stochastic gas channels. Since continuum models average over pore-scale heterogeneity, they are in principle unable to describe the channelized flow patterns (see for details Geistlinger et al. (2009)).

On the other hand, there are many studies on air sparking, which are based on continuum modeling (see references in McCray (2000); Thomson and Johnson (2000)). To date, it is not clear under which conditions a continuum model can describe the essential features of complex gas flow patterns. TOUGH2 is an established multiphase program tested for different benchmark problems and is often used in CCS field studies (Pruess, 2008; Class, 2009).

4. Feasibility of geoelectrical monitoring and multiphase modelling for process understanding of gaseous CO₂ injection into a shallow aquifer

It is important to develop a “real world”-continuum model, since geological heterogeneity is a key driver on all scales (pore scale, bench scale, and field scale) for stochastic gas flow patterns. Therefore, conditioned parameter fields are used to map the real geological and hydraulic properties of the test site to a numerical model.

Firstly, in order to be consistent, a short overview of the TOUGH2 mathematical model and its numerical basis is presented. The volumetric fluxes of the two phases or fluids, water q_w and gas q_g , are given by generalized Darcy laws:

$$q_w = \frac{k k_{rw}}{\mu_w} \nabla(P_w - \rho_w g z) \quad (\text{eq. 4.14a})$$

$$q_g = \frac{k k_{rg}}{\mu_g} \nabla(P_g - \rho_g g z) \quad (\text{eq. 4.14b})$$

where w and g stands for water and gas, k absolute permeability, k_r relative permeability, P pressure, μ viscosity, ρ density, g earth's gravity acceleration. The concept of relative permeability is based on the assumption that all immiscible phases can flow simultaneously through the REV of the porous medium. The flow equations of phase i in a multiphase flow system, which are solved by TOUGH2 numerically, are obtained by substituting the volumetric flux into the continuity equation:

$$\frac{\partial(\rho_w S_w \phi)}{\partial t} + \nabla \left(-\rho_w \frac{k * k_{rw}}{\mu_w} \nabla(P_w - \rho_w g z) \right) = I_w \quad (\text{eq. 4.15a})$$

$$\frac{\partial(\rho_g S_g \phi)}{\partial t} + \nabla \left(-\rho_w \frac{k * k_{rg}}{\mu_g} \nabla(P_g - \rho_g g z) \right) = I_g \quad (\text{eq. 4.15b})$$

where S denotes the phase saturation, ϕ porosity, I injection rate. The difference between water phase pressure and gas phase pressure is called capillary pressure p_c . In order to solve the system of partial differential equations, the constitutive relationships between gas saturation, permeability and the capillary pressure are needed. For this purpose, the van Genuchten–Mualem (e.g. van Genuchten (1980) model was used, which is described by the following equations:

4. Feasibility of geoelectrical monitoring and multiphase modelling for process understanding of gaseous CO₂ injection into a shallow aquifer

$$k_{rw}(S_g) = (S_g)^{0.5} [1 - (1 - S_g^{1/m})^m] \quad (\text{eq. 4.16a})$$

$$p_c(S_g) = \rho_w g h(S_g) = \frac{\rho_w g}{\alpha} (S_g^{-1/m} - 1)^{1/n} \quad (\text{eq. 4.16b})$$

where α denotes inverse capillary head, $m = 1 - 1/n$, n van Genuchten parameter. For numerical simulations, we used the equation-of-state (EOS) module ECO2N. The ECO2N-module can describe the physico-chemical processes of a single CO₂-rich phase, in our case the gaseous CO₂ phase. The more recent EOS-module ECO2M (Pruess, 2011) is able to describe a single (aqueous or CO₂-rich) phase, as well as two- and three-phase mixtures of aqueous, liquid CO₂ and gaseous CO₂ phases.

Since we are only interested in the flow behavior of an injected CO₂ gas phase within a shallow aquifer and its dissolution into the groundwater, both modules describing the same processes. These EOS-modules were designed for applications related to geologic sequestration of CO₂ in saline aquifers. The used module includes a comprehensive description of the thermodynamics and thermo-physical properties of H₂O–NaCl–CO₂ mixtures. Flow processes can be modeled isothermally or non-isothermally, and phase conditions represented may include a single (aqueous or CO₂-rich) phase, as well as two-phase mixtures. Hence, the following physico-chemical processes are described by TOUGH2–ECO2N: (1) gas injection, which leads both, to gas flow and water flow, as well as (2) CO₂ dissolution into the groundwater and its transport processes. In this context, it is important to note that for gas dissolution, local partitioning equilibrium condition is assumed.

4.6.2 *Creating heterogeneous parameter fields*

Both heterogeneous permeability and capillary pressure fields may have a strong impact on gaseous and dissolved CO₂-distribution, and therefore on the time course of the different BTCs at different locations. Based on extensive field site investigation at the test site (section 4.5, Peter et al. (2012b)), the geological structure model of the CO₂ injection horizon consists of six different layers (Tab. 4.2). For each geological layer, the heterogeneous permeability field was derived using a conditioned Gaussian field with an exponential covariance function and a correlation length of 5 m.

4. Feasibility of geoelectrical monitoring and multiphase modelling for process understanding of gaseous CO₂ injection into a shallow aquifer

Table 4.1 Hydraulic parameters of different geological layers at the test site (see also Peter et al. (2012b)).

Layer	Porosity (-)	Permeability (m ²)	Van Genuchten α (m ⁻¹)	Van Genuchten m (-)
(1) Glacial loam	0.37	3.1×10^{-15}	7.1×10^{-4}	0.20
(2) Upper medium sand	0.33	$2.0 \pm 0.6 \times 10^{-11}$	4.4×10^{-4}	0.39
(3) coarse sand	0.34	$4.2 \pm 0.6 \times 10^{-11}$	7.6×10^{-4}	0.40
(4) Silt	0.37	1.0×10^{-13}	2.7×10^{-4}	0.41
(5) Lower medium sand	0.30	$2.6 \pm 1.3 \times 10^{-11}$	2.7×10^{-4}	0.58
(6) Boulder clay	0.37	5.1×10^{-16}	7.1×10^{-4}	0.20

For conditioning the sequential Gaussian simulation was used (Deutsch and Journel, 1998). The capillary pressure field was obtained by Leverett scaling (Leverett, 1940). Key hydraulic parameters for a multiphase model are horizontal and vertical permeability and the capillary pressure for each sediment type. The permeability values are taken from sieve analysis, slug tests and HPT (hydraulic profiling tool) logs (Dietrich et al., 2008).

Permeability was calculated according to Hazen (e.g., Knödel et al. (2007)), based on a total number of 42 sieve analyses. Comparison with relative permeability obtained by HPT logs was used to perform a consistency check. For each geological layer, permeability was calculated as a mean value over different located values. The variance was used to generate the conditioned stochastic permeability field. The corresponding van Genuchten parameters α and m for each layer were determined using the ROSETTA database (Schaap, 2002) and the SOILPROP database (Stumpp et al., 2009). All parameters are listed in Tab. 4.2. Porosity was determined by directly measuring the bulk and rock volume. The 3D-numerical grid consists of 60,000 cells (=100 9 30 9 20) with a grid spacing of 1 m. The conditioned heterogeneous permeability and capillary pressure fields are shown in Fig. 4.6. From local measurements of the hydraulic potential, a local groundwater velocity of 0.4 m/d was estimated.

4. Feasibility of geoelectrical monitoring and multiphase modelling for process understanding of gaseous CO₂ injection into a shallow aquifer

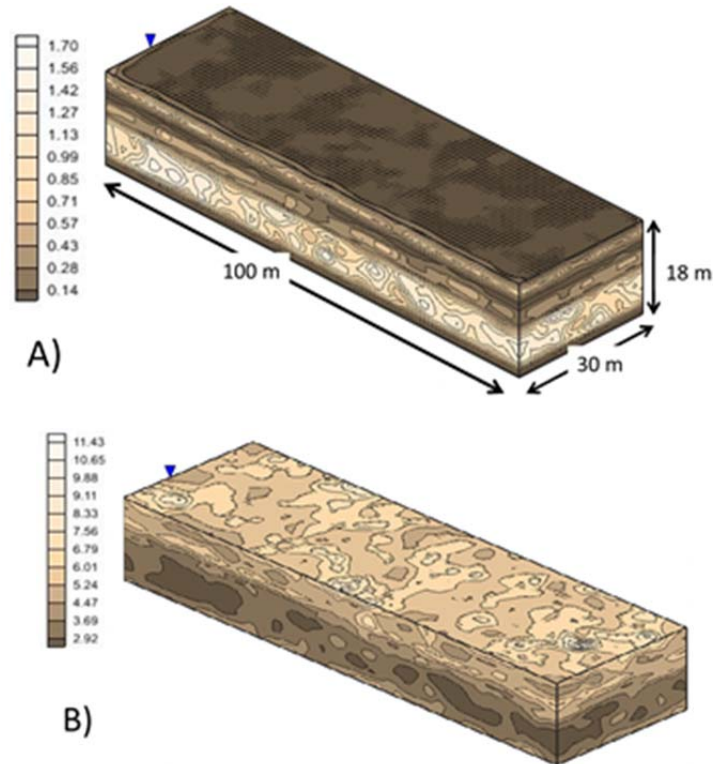


Figure 4.6 a) Heterogeneous permeability for the test site: values of the color scale are given in 10-10 m², b) Simulated capillary pressure distribution: values of color scale are given in kPa.

4.6.3 CO₂ injection scenario: distribution of gaseous CO₂ and dissolved CO₂

The calibration of geoelectrical breakthrough curves was achieved during various trial-and-error attempts. Since the central injection lance and the monitoring wells ML 1C–GWM 1D are located nearly along a flow path, a 2D-cross-section of the 3D-model was considered, i.e., a 100 m x 1 m x 20 m model cut along the center line. There are two main differences between 2D and 3D that can influence the spatial gas flow pattern: (1) the injection rate and (2) the anisotropy caused by the heterogeneous permeability field. To take into account a realistic 2D-injection rate, we conducted a dimensional transformation. For the same injection rate of 10 L/min as was used for the 3D-model, gas saturation and radius of influence are overstated by a geometry factor of about $\pi R^2/2R\Delta x$ (= volume of paraboloid/ volume of 2D-slice). Consequently, the 2D-injection rate was scaled, i.e., a rate of 2 L/min instead of 10 L/min was applied. In order to check our scaled injection rate and the influence of the anisotropy, we also ran the 3D-model for special test cases.

4. Feasibility of geoelectrical monitoring and multiphase modelling for process understanding of gaseous CO₂ injection into a shallow aquifer

We found that the 2D-simulation yields almost the same BTC-curves as the 3D-model. A more elaborated 3D-theory is currently under preparation. In Fig. 4.7, an aquifer cross-section of 20 m x 20 m is shown. The upper row of Fig. 4.7 shows the distribution of gaseous CO₂ and the lower row shows dissolved CO₂ at 5, 10 and 20 days after CO₂ injection started for the aquifer section Inj1-ML 1C-GWM 1D (Fig. 4.2). The red square in S_g (10 days)-image indicates the CO₂ injection point (18 m bgl). Black squares indicate positions of installed electrodes at wells ML 1C and GWM 1D, from left to right.

4.6.4 CO₂ injection scenario: simulating breakthrough curves

Experimental data showing breakthrough curves of geoelectrical monitoring results (σ_a), simulated BTCs are calculated for corresponding positions (nodes) at wells ML 1C and GWM 1D and show values for σ_{ps} . Using geoelectrical monitoring data, a higher spatial resolution could be achieved. However, it can be assumed that in first approximation the presented geoelectrical BTCs show the typical behavior of accordant local varying subsurface conductivity σ_{ps} . Since the focus of the modeling study was to investigate if the continuum model TOUGH2 is able in principle to describe experimental breakthrough curves, we assume that σ_a & σ_{ps} in order to compare the experimental BTCs with the simulated data. A more detailed analysis of geoelectrical data could be carried out but goes beyond the scope of this paper.

The electrical conductivity of a partially saturated porous medium is a complex non-linear function of gas saturation and is given by equation 4.13. However, this is just a rough estimation, since the dynamic distribution of the gas phase plays a key role for connectivity of different sections of the pore space. During injection, channelized coherent gas flow is established in the vicinity of the injection wells and the adjacent water phase is also moved by friction forces. This will have a significant effect on σ_{ps} . However, the gas plume may move upwards even after gas injection is stopped, driven by buoyancy forces—as long as the gas channels do not collapse. Hence, for static residual gas saturation, a smaller impact on the electrical conductivity is expected due to lower gas saturation and lower static water phase. Wenner arrays, e.g., at ML 1C 13.5–14.5 m (black curve in Fig. 4.3) detected this change in the gas phase dynamics as a ‘step-like increase’ of σ_a . However, only the upper Wenner electrodes significantly detected the gas phase dynamic processes (Fig. 4.3).

4. Feasibility of geoelectrical monitoring and multiphase modelling for process understanding of gaseous CO₂ injection into a shallow aquifer

The most likely explanation for this is the development of a gas pool underneath the glacial loam layer, which either encloses the upper electrodes or is in the vicinity of them (Fig. 4.7, upper row: gas saturation at 10 days).

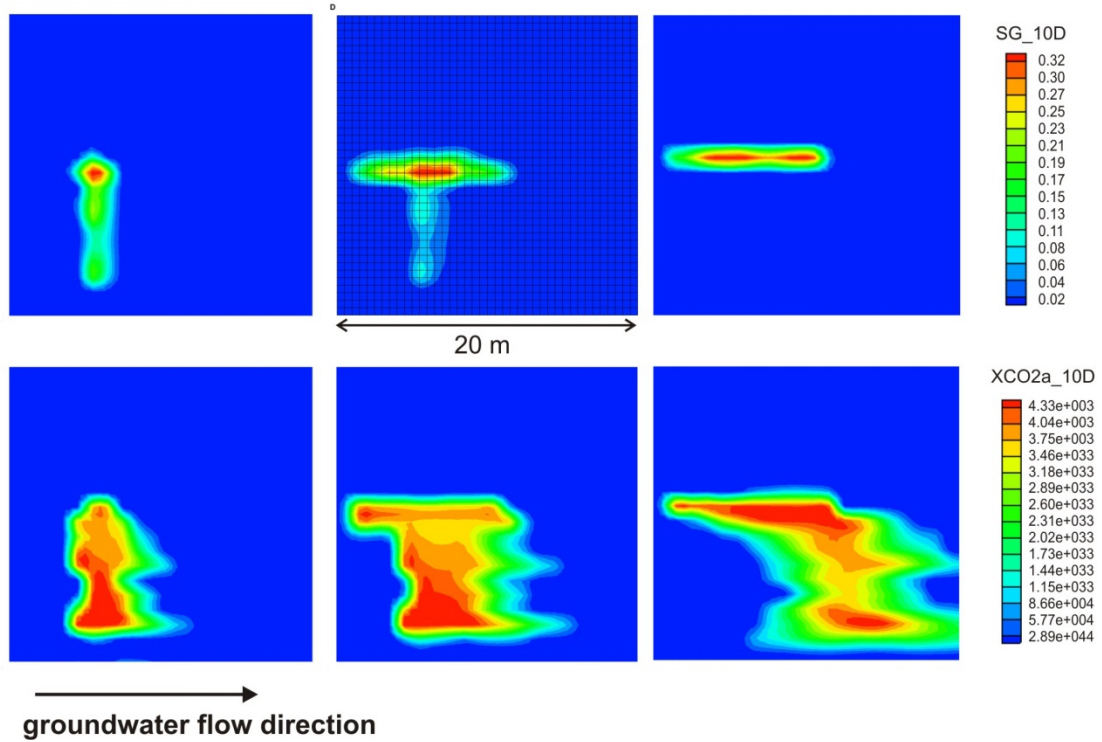


Figure 4.7 Upper row saturation gaseous CO₂ (%); lower row dissolved CO₂ as mol-fraction X_{CO₂} (mol/mol), both at t = 5, 10, and 20 days after CO₂ injection started; red square in S_g (10 days)-image indicates the CO₂ injection point (18 m bgl), black squares indicate positions of installed electrodes at wells ML 1C and GWM 1D from left to right.

Since geoelectrical measurements provide information over a certain matrix volume, the gas saturation or number of gas channels in this volume had to be high enough so that the saturation effects become significant enough to enable detection. Usually, isotropic paraboloids are assumed when designing gas injection tests (see e.g. Peter et al. (2012b) One important question is whether or not applied multiphase models can adequately describe such ‘step-like’ behavior. Based on Faraday’s law and the fact that dissolved CO₂ species are the main ions in the water phase, a reasonable linear proportionality of σ_f on the CO₂-mol fraction X_{CO₂}, i.e., $\sigma_f(\text{CO}_2) X_{\text{CO}_2w}$ was assumed. For calculating the relative electrical conductivity of the fluid, the following empirical function was used (compare with equation 11b):

4. Feasibility of geoelectrical monitoring and multiphase modelling for process understanding of gaseous CO₂ injection into a shallow aquifer

$$\sigma_{f,rel} = \frac{X_{CO_2}^0 + X_{CO_2}}{X_{CO_2}^0 + \Delta f(X_{CO_2})} \quad (\text{eq. 4. 17})$$

where $\Delta f = (1 - a) X_{CO_2}$ is a correction term. The constants a and $X_{CO_2}^0$ are unknown parameters and have to be determined by the experimental BTCs. One could choose the Δf -term zero and use $X_{CO_2}^0$ as the only unknown fitting parameter. However, this would only describe relative conductivity change and not yield the correct time scale (= time at which the maximum conductivity is reached). To describe the experimental time scale, the second fitting parameter a is required. The focus of this paper is to investigate if multiphase modeling is able to help us understand and explain the key characteristics of geoelectrical BTCs. We found that the parameter set, for $a = 0.15$ and $X_{CO_2}^0 = 1.9 \cdot 10^{-4}$, respectively, can explain the characteristic change of σ_a and the breakthrough time. In a future paper, we will present a more elaborated 3D-theory including a best fit algorithm for each BTC. It is obvious that different parameter sets for different curves make sense, since the dissolved CO₂ of different BTCs has traveled through different aquifer sections. Based on equations (4.13, 4.17) and assuming that $S_g = 0$, the BTCs of relative σ_{ps} at different depths for GWM 1D and ML 1C are calculated (Fig. 4.8). According to Fig. 4.7, most of the Wenner arrays (=BTC-sampling points) do not “experience” gaseous CO₂, i.e., the change of the fluid conductivity $\sigma_f(\text{CO}_2)$ is the only impact on σ_{ps} . When interpreting Fig. 4.8 as well as comparing Fig. 4.8 with Fig. 4.4 (experimental BTCs), it can be seen that both show a relative change of electrical conductivity in the order of 10 to 15 %. This characteristic shows that the assumption $\sigma_a \approx \sigma_{ps}$ is justified for the purpose of the modeling study. However, when comparing experimental and simulated BTCs, this simplification must be taken into account.

The comparison between the uppermost experimental curve of GWM 1D and the theoretical curves at 11 and 12 m show reasonable agreement. The slope of the experimental curve is less compared to the slope of the theoretical curve. One evident reason is the heterogeneous permeability field that has, in reality, a broader distribution and a lower mean value than the theoretical one. This would lead to smaller pore water velocities and a broader spectrum of arrival times and slopes of the BTCs. Small-scale heterogeneity could lead to more pronounced fingering of the dissolved CO₂-front and hence to a weaker concentration gradient. As previously mentioned, the correlation length of clusters with similar permeability values is 5 m.

4. Feasibility of geoelectrical monitoring and multiphase modelling for process understanding of gaseous CO₂ injection into a shallow aquifer

Compared to model dimension, this correlation length yields relatively large permeability clusters. A more elaborate study should consider stochastic permeability fields with different and smaller correlation lengths.

Another reason for the different arrival times of the experimental and theoretical BTCs is the strong influence of the heterogeneous gas flow pattern during gas injection. To understand this influence, firstly the time development of the gas plume has to be discussed (Fig. 4.7, upper row). Considering the shape of the gas plume after 10 days injection, the gaseous CO₂ has accumulated below the glacial loam and the front of the gas plume has moved about 5 m in 10 days. This represents the mean gas phase velocity, which is nearly independent of the groundwater velocity, since the same extension of the gas plume is also established against groundwater flow direction.

Based on this simulated gas distribution, measurements using the upper electrodes of monitoring wells ML 1C and GWM 1D can be said to be influenced by the gas phase. This is in fact the case for ML 1C-BTCs, since the upper experimental BTC shows the indicative step-like behavior (black curve in Fig. 4.3). Using the upper electrodes of GWM 1D, this step-like behavior was not detected. However, early arrival of the uppermost BTC at well GWM 1D (black curve in Fig. 4.4) is a strong indicator that the gas phase velocity adds to groundwater and for upward migration of gaseous CO₂ in the vicinity of the injection wells up to the overlying glacial loam layer. The arrival times at all deeper BTCs are more time-delayed. In addition to gaseous CO₂ distribution, the dissolved CO₂-distribution (Fig. 4.7, lower row) also has a strong impact upon BTCs. As can be seen from the heterogeneous distribution, the theoretical BTC of well GWM 1D at a depth of about 14 m has the shortest arrival time (Fig. 4.8). The theoretical BTCs in the middle of the investigated depths (13, 14 m) exhibit an earlier arrival time compared to the BTC below the glacial loam (Fig. 4.8). This strongly contradicts the experimental arrival times (Fig. 4.4), i.e., the arrival times increase from top to bottom. For two depths, 11 m (black curves) and 13 m (green curves), this comparison between experimental and theoretical curves is also shown in Fig. 4.9. The theoretical curve at depth 13 m arrives earlier than that of the curve at a depth of 11 m and vice versa for the experimental curves.

4. Feasibility of geoelectrical monitoring and multiphase modelling for process understanding of gaseous CO₂ injection into a shallow aquifer

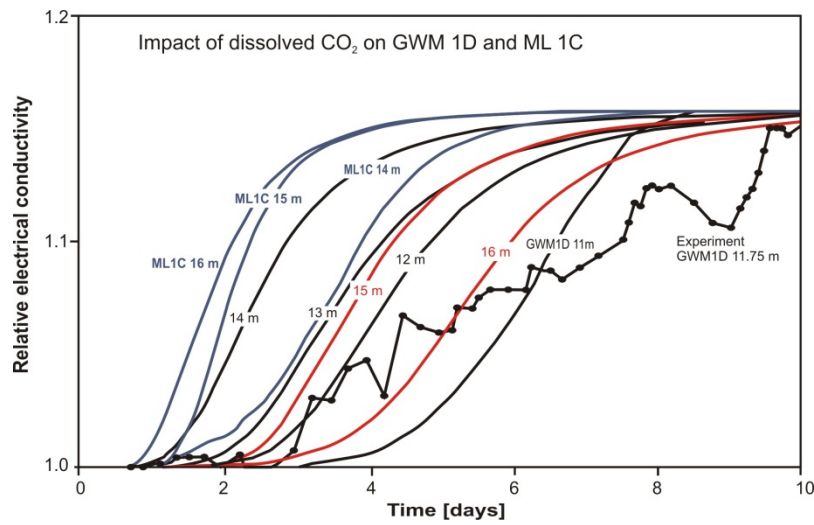


Figure 4.8 Relative conductivity (σ_{ps}) for monitoring wells GWM 1D (black and red curves) and ML 1C (blue curves) at different depths. For monitoring well GWM 1D the experimental curve (σ_a) is shown for depth of approx. 11.75 m (black curve with squares).

The same inverse behavior can be recognized for the BTCs of monitoring well ML 1C (Fig. 4.3, blue curves in Fig. 4.8). Consequently, the multiphase model is unable to explain the time evolution of the dissolved CO₂. The reason for this discrepancy is the local equilibrium approach (LEA) for mass transfer processes. However, most of the multiphase models that are currently used in literature (see references in Class, 2011) in order to carry out prognoses or risk analysis for CCS technology are based on LEA. Good agreement between experimental BTCs and the gas phase distribution shows that the multiphase model correctly simulates the time evolution of the gas phase. If the buoyancy-driven gas phase velocity within the single stochastic gas channels is too fast, no partitioning equilibrium can be established along the pathway from the injection point to the gas pool. Only if the mass transfer process is kinetically limited, the experimental BTCs can be understood.

4. Feasibility of geoelectrical monitoring and multiphase modelling for process understanding of gaseous CO₂ injection into a shallow aquifer

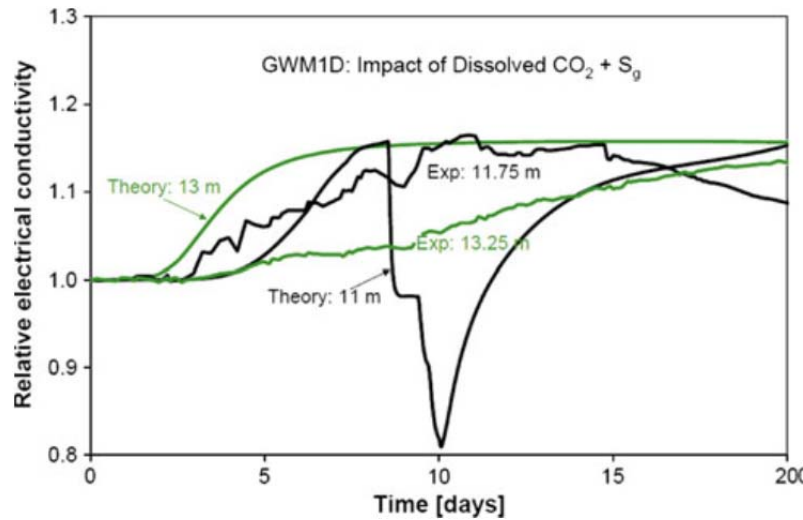


Figure 4.9 Comparison of experimental (σ_a) and theoretical conductivity (σ_{ps}) relative to baseline measurements at well GWM 1D for two different depths: 11 m (black curves) and 13 m (green curves).

Now, returning to the important question of whether or not the multiphase model is able to adequately describe the experimentally observed ‘step-like behavior’. The only theoretical BTC, which ‘‘experiences’’ the gaseous phase is the BTC of well GWM 1D, representing a depth of 11 m. Calculating this BTC ($S_g = 0$, $n = 2$) according to equation (4.13), it exhibits a ‘step-like behavior’ due to temporal variation of the gas saturation (Fig. 4.9). Such behavior is a rather sensitive indicator of the temporal evolution of the gas saturation. The most likely explanation for the two-step BTC is due to two subsequent saturation fronts with $S_{g1} \setminus S_{g2}$, which move through the sampling point of BTC-11 m and are caused by the heterogeneous flow field. Comparing the theoretical curve at 11 m with the upper experimental curve (potential electrodes located at depths of 11.75 and 12.50 m) such a step like behavior is not observed. The most likely explanation is due to the channelized flow behavior. Gas flows through discrete gas channels, whereas the continuum model TOUGH2 ‘‘smeared’’ the gas channels over a certain averaged volume, e.g., cell volume of 1 m³. Hence, the model experiences a gas channel as averaged gas saturation over the cell volume. If this gas channel is too small compared to significant sensitivity volume of the Wenner array, then the gas flow behavior, i.e., the gas channel, will be not detected. Possible pathways for observed rapid gas migration are stochastic gas channels and potential preferential pathways at the outside of installed wells.

4. Feasibility of geoelectrical monitoring and multiphase modelling for process understanding of gaseous CO₂ injection into a shallow aquifer

4.7 Summary and concluding remarks

It was shown that geoelectrical monitoring in combination with multiphase modeling is a useful tool for understanding gas phase migration processes and mass transfer processes. A multiphase model has to be based on a real heterogeneous geological structure model. Parameter fields have to be conditioned on experimental data sets, in order to map the real aquifer to the model aquifer. For the first time, we found that the ‘step-like behavior’ of electrical conductivity for both experimental and theoretical BTCs is a rather sensitive indicator for temporal variations of the gas phase. Due to the gaseous CO₂ injection into the injection horizon at depth of 18 m bgl, gaseous CO₂ flows relatively fast (see also Oldenburg and Lewicki (2006) through discrete gas channels upwards to the glacial loam layer and a gas pool is formed. Along the temporally gas channels, no local equilibrium can be reached between gaseous CO₂ and dissolved CO₂. Therefore, a multiphase model that is based on LEA (local equilibrium approach) overestimates dissolved CO₂ (lower row in Fig. 4.7). Since most of the multiphase models that are currently used in CCS technology for prognoses and risk analysis are based on LEA, we urgently recommend checking the theoretical results by performing in situ measurements of both, gas phase distribution and dissolved CO₂ distribution. Further main conclusions include:

- Geoelectrical measurements provided significant variations of σ_a in the order of 15 to 30 %. Hence, this field study has shown the feasibility of geoelectrical measurements for monitoring CO₂ intrusions into shallow aquifers. However, at the presented wells, electrodes were placed at a maximum distance of 1 m apart from each other within the injection horizon. The experimental monitoring setup used permits the detection of small-scale variations in both σ_a (geoelectrical breakthrough curves) and σ_f (groundwater sampling). In order to apply this monitoring strategy at real CCS sites, this approach has to be adapted for significantly larger areas, i.e., several km² (see also Singh et al. (2012)).
- In this field study, it has been proven that it is highly beneficial to install electrodes for geoelectrical borehole monitoring below an impermeable geological layer, allowing detection of rapid variations in σ_a due to upwardly migrated gaseous CO₂.

4. Feasibility of geoelectrical monitoring and multiphase modelling for process understanding of gaseous CO₂ injection into a shallow aquifer

Additionally, interpretation of geoelectrical breakthrough curves allows rapid initial process understanding. Consequently, this approach is a promising tool for borehole monitoring at CCS sites.

- The injection horizon used is only affected by the injected CO₂. Other sources, which might have an impact upon electrical conductivity (e.g., input of fertilizers, saline water intrusion) are negligible at the test site. Such external factors may lead to ambiguity in terms of geoelectrical monitoring and must be considered when monitoring CCS sites. Field parameters of groundwater samples should be used to obtain additional information showing that potentially observed variation in σ_a are caused by leaked CO₂ or not.
- The application and feasibility of geoelectrical monitoring of CO₂ intrusions strongly depends upon site-specific conditions with respect to dynamic (geochemical) processes, as well as the measuring setup used. Consequently for each field site, a specific characterization of relevant parameters must be implemented (see also Kolditz et al. (2012)). Generally, hydraulic and electrical properties are not constant in space due to heterogeneous structures in the subsurface.

Hence, the inference from measured geoelectrical data to variation in σ_f is ambiguous. Geoelectrical monitoring is applicable for detecting the zone of varying electrical conductivity, but for quantitative conclusions, additional information is required (e.g., from groundwater sampling).

4.8 Acknowledgement

We would like to thank the town of Wittstock and the Brandenburgische Boden GmbH for supporting this project. This study was funded by the German Ministry of Education and Research (BMBF) within the Priority Program Geotechnologies, funding numbers 03G0670A-C.

5. Effects of high CO₂ concentrations on typical aquifer microorganisms

5.1 Kurzfassung

Um Informationen über eine CO₂-Leckage, aus einem tiefen geologischen CO₂ Speicher in einen flachen Grundwasserleiter zu sammeln, wurde der Einfluss von erhöhten CO₂-Konzentrationen auf das Wachstum und die Überlebenszahl von umweltrelevanten Mikroorganismen untersucht. Die CO₂-Konzentration in der Gasphase variierte zwischen atmosphärischen Bedingungen und 80 % CO₂ für die aeroben Stämme *Pseudomonas putida* F1 und *Bacillus subtilis* 168 und bis zu 100 % für die anaeroben Stämme *Thauera aromatica* K172 and *Desulfovibrio vulgaris* Hildenborough. Ansteigende CO₂-Konzentrationen führten zu einer Verzögerung der lag-Phase, zu reduzierten Wachstumsraten und zu verringerten Zellzahlen; mit zunehmender CO₂-Konzentration nahmen die Effekte zu. Zusätzliche Versuche mit erhöhten Drücken (1 – 5000 kPa) und erhöhten CO₂-Konzentrationen sollten in-situ Bedingungen in einer tiefen CO₂-Speicherformation simulieren. Innerhalb von 24 Stunden nahmen die Lebendzellzahlen bei Drücken ≥ 1000 kPa signifikant ab. Damit wurde ein tödlicher Effekt der Kombination von erhöhtem Druck und erhöhten CO₂-Konzentrationen gezeigt.

Schulz, Alexandra; Vogt, Carsten; Richnow, Hans-Hermann.

Published in: Environmental Pollution, 2012, 169, pp 27-34.

5.2 Abstract

We have investigated the effect of increasing CO₂ concentrations on the growth and viability of environmentally relevant microorganisms to obtain information for a leakage scenario of CO₂ into shallow aquifers related to the capture and storage of CO₂ in deep geological sections. CO₂ concentrations in the gas phase varied between atmospheric conditions and 80 % CO₂ for the aerobic strains *Pseudomonas putida* F1 and *Bacillus subtilis* 168 and up to 100 % CO₂ for the anaerobic strains *Thauera aromatica* K172 and *Desulfovibrio vulgaris* Hildenborough. Increased CO₂ concentrations caused prolonged lag-phases, reduced growth rates, and diminished cell yields; the extent of this effect was proportional to the CO₂ concentration. Additional experiments with increasing CO₂ concentrations and increasing pressure (1-5000 kPa) should simulate situations occurring in deep CO₂ storage sites.

5. Effects of high CO₂ concentrations on typical aquifer microorganisms

Living cell numbers decreased significantly within 24 hours at pressures ≥ 1000 kPa, demonstrating a severe lethal effect for the combination of high pressure and increasing CO₂ concentrations.

5.3 Introduction

In recent decades, the concentration of carbon dioxide in the atmosphere has increased significantly as a result of anthropogenic emission. One option for the reduction of the carbon dioxide emission is Carbon Capture and Storage (CCS), the capture of carbon dioxide from large emission sources and storage in deep geological structures, e.g. saline Permian sandstone aquifers such as Rotliegend strata (IPCC, 2005). Leakage of carbon dioxide from an underground storage site into a near surface aquifer is one concern associated with the CCS technology. The complete tightness of a CO₂ reservoir in geological strata has been questioned (Wu et al., 2010) and semi-analytical models have shown that if cracks and crevices are present in cap rock formations of the storage site, a leakage of free phase CO₂ can be a significant pathway for losing sequestered CO₂ (Saripalli and McGrail, 2002). The upwardly migrating CO₂ can reach shallow aquifers located over deep CO₂ storage sites, and chemical, geological and/or microbiological changes may be induced in the soil environment as well as in the shallow groundwater, which can be a source of drinking water (Wu et al., 2010). A pH decrease, mineral dissolution and a change in the growth of characteristic microorganisms are some of the potential risks of a leakage scenario. Proper risk assessment for proposed CO₂ storage sites should include simulated leakage scenarios and exploration of the impacts of increasing CO₂ concentrations on indigenous microorganisms.

Several studies have previously examined changes in microbial communities induced by long-term exposure to CO₂ (Freeman et al., 2004; Blagodatskaya et al., 2010; Oppermann et al., 2010). These ecosystems had the chance to adapt to these conditions and therefore the effects of a possible leakage into aquifer environments are difficult to predict. Consequently, a study on the reaction of soil microorganisms towards a sudden increase of the CO₂ concentration is necessary. Furthermore, to the best of our knowledge, a detailed study on the change of the growth characteristics of microbial soil organisms due to elevated CO₂ concentrations has not been performed.

5. Effects of high CO₂ concentrations on typical aquifer microorganisms

In the present study, the effects of different CO₂ concentrations on the growth and viability of aerobic and anaerobic microorganisms were investigated. Microbial strains (*Pseudomonas putida*, *Bacillus subtilis*, *Desulfovibrio vulgaris*, and *Thauera aromatica*), routinely detected in shallow aquifers, were used to investigate the consequences of a CO₂ leakage from a deep geological storage site. These strains were used as model organisms to study the principal effects of high CO₂ concentrations on environmentally relevant microbes. Here, we address questions associated with how the growth and survival rates of aerobic and anaerobic microorganisms change in response to suddenly elevated CO₂ concentrations. Furthermore, variable stress responses of microorganisms of various ecotypes (aerobes, nitrate reducer, sulfate reducer) towards increased CO₂ concentrations are discussed. In addition, as a worst case scenario for CO₂ leakage, we examined the influence of high CO₂ partial pressures on the viability of typical for the different ecotypes. All experiments are performed with pure cultures under favourable growth (temperature, medium, carbon source) conditions to study the specific influence of CO₂ and to exclude disturbing side effects.

5.4 Material and methods

5.4.1 Microorganisms and culture media

Bacillus subtilis sbsp. *subtilis* strain 168, *Pseudomonas putida* strain F1, *Desulfovibrio vulgaris* strain Hildenborough and *Thauera aromatica* strain K172 were obtained from the German Collection of Microorganisms and Cell Cultures (DSMZ; Braunschweig, Germany). *B. subtilis* and *P. putida* were cultivated in a modified, phosphate-buffered Brunner mineral medium (2.44 g/L Na₂HPO₄; 1.52 g/L KH₂PO₄; 0.50 g/L (NH₄)₂SO₄; 0.20g/L MgSO₄ × 7 H₂O; 0.05 g/L CaCl₂ × 2 H₂O; 1 mL/L trace element solution 10; 5 mL/L vitamin solution) with glucose [5 mM] or acetate [5 mM] as substrates. Cultures were grown at 30 °C and pH 7 in an orbital shaker at 150 rpm. *D. vulgaris* was cultured under anoxic conditions in the same Brunner mineral medium (see above) at pH 7 and 37 °C. After autoclaving at 121 °C for 20 minutes, the medium was purged with nitrogen to remove oxygen. Na₂SO₄ [20 mM] was provided as the terminal electron acceptor, the medium was amended with 1mL/L selenite-tungsten solution (0.5 g/L NaOH, 3 mg/L Na₂SeO₃ × 5 H₂O; 4 mg/L Na₂WO₄ × 2 H₂O), and lactate [10 mM] was the sole carbon and energy source.

5. Effects of high CO₂ concentrations on typical aquifer microorganisms

T. aromatica was cultured in a modified anoxic Brunner mineral medium at pH 8 and 25 °C; the medium was prepared anoxically as described above. KNO₃ [8 mM] and 1mL/L of a selenite-tungsten solution (see medium for *D. vulgaris*) were amended, and acetate [5 mM] was provided as the sole carbon and energy source. Generally, additional solutions were added from sterile oxalic (for *P. putida*, *B. subtilis*) or anoxic (for *T. aromatica*, *D. vulgaris*) stock solutions using sterile plastic syringes, which were nitrogen-flushed in case of anoxic media. Pre-cultures for growth experiments were grown in 118 mL glass bottles, sealed gas-tight with butyl rubber stoppers. 20 % of carbon dioxide was already added into the pre-cultures of *D. vulgaris* to achieve the best growth conditions. For maintenance, all strains were re-inoculated into fresh medium once per week. All chemicals were of reagent-grade quality and obtained from Merck and Sigma-Aldrich.

5.4.2 Growth experiments under different CO₂ concentrations at ambient pressure

The growth experiments were conducted in 30 mL glass tubes. Each tube was filled with 4.5 mL of Brunner mineral medium modified for each strain (see 2.1) and closed with gas-tight butyl rubber stoppers. The medium was purged with gas mixtures of N₂ and CO₂ with compositions between approximately 0 (refers to no amendment of CO₂) to approximately 100 % CO₂ by using a mass flow controller (EL-FLOW, Bronkhorst High-Tech, Germany). Each glass vial was purged with the appropriate gas mixture for 15 minutes to receive a full saturation of the atmosphere and the medium.

For the aerobic experiments using *B. subtilis* and *P. putida*, 20 % O₂ was added by removing the adequate headspace volume with a gas-tight syringe and replacing it with the appropriate volume of pure O₂. The O₂ concentrations were monitored using O₂ sensors (sensor type PSt3, detection limit 0.03 %, PreSens, Germany). The CO₂ concentration was increased up to 100 % in the head space for experiments with the anaerobic organisms *D. vulgaris* and *T. aromatica*. After autoclaving, the medium was inoculated with 0.5 mL of a freshly grown culture to achieve an initial OD₆₆₀ of at least 0.015 (0.04 ± 0.006 for *P. putida*, 0.027 ± 0.008 for *B. subtilis*, 0.018 ± 0.007 for *D. vulgaris* and 0.016 ± 0.003 for *T. aromatica*). The microorganisms were subsequently grown at the previously described growth temperatures (25 °C for *T. aromatica*, 30 °C for *B. subtilis* and *P. putida*, 37 °C for *D. vulgaris*) on an orbital shaker at 150 rpm.

5. Effects of high CO₂ concentrations on typical aquifer microorganisms

As the focus of this study was to investigate the effects caused by elevated CO₂ concentrations, we used the appropriate growth temperature for each organism to exclude disturbing side effects. The optical density was measured every two hours at a wavelength of 660 nm with a UV/ VIS spectrophotometer (Pharmacia LKB Novaspec II) for up to 90 hours. The glass vials were placed directly into the spectrophotometer to ensure constant measurements during the course of the experiments. The growth rate μ was calculated as follows:

$$\mu = \frac{2.303(\log OD_2 - \log OD_1)}{(t_2 - t_1)} \quad (\text{eq. 5.1})$$

where OD values are chosen such that OD_1 is two times OD_2 with the corresponding time points t (see Tab. 4.1) (Widdel, 2010). At the end of the experiments, the viable cell numbers were determined using the Most Probable Number method (MPN). 96-well microtiter plates (Nunc, Denmark) with a volume of 300 μl per well were filled with 200 μl of Brunner medium modified for each strain and inoculated with 100 μl dilutions from 10^{-4} - 10^{-10} . The cell numbers and the 95 % confidence limit on the log of the MPN were computed using a computer program designed by Robert Blodgett based on the normal approximation previously described (Haldane, 1939; Garthright and Blodgett, 1996). The relative inhibitory effect (RI) of CO₂ was calculated according to Enfors and Molin (Enfors and Molin, 1981) as follows:

$$RI = [(r_c - r_{CO_2}) / r_c] \times 100 \quad (\text{eq. 5.2})$$

where r_c and r_{CO_2} are the growth rates for the control and the specific CO₂ concentrations respectively. In order to exclude an influence of substrate limitation on cell growth, HPLC measurements were performed with glucose and acetate for *P. putida*, *B. subtilis* and *T. aromatica* every two hours for the duration of the experiments. HPLC analyses were performed on a Shimadzu 10A HPLC equipped with an RID detector and a VA 300/ 7.8 Nucleogel ION 300 OA column (Macherey & Nagel, Germany) using an eluent of 0.005 N H₂SO₄ at a flow rate of 0.6 mL/min.

5.4.3 Viability experiments under CO₂ stress at high pressure

For the high-pressure experiments, two self-made pressure vessels of stainless steel with a volume of 0.56 L, on which a maximum pressure of 7500 kPa can be applied, were used (Fig. 1).

5. Effects of high CO₂ concentrations on typical aquifer microorganisms

The maximum temperature used for the experiments was 38 °C. The pressure vessels were placed in a water bath with a compact low temperature thermostat (RM6 Lauda, Germany), allowing temperature adjustment for the different growth conditions.

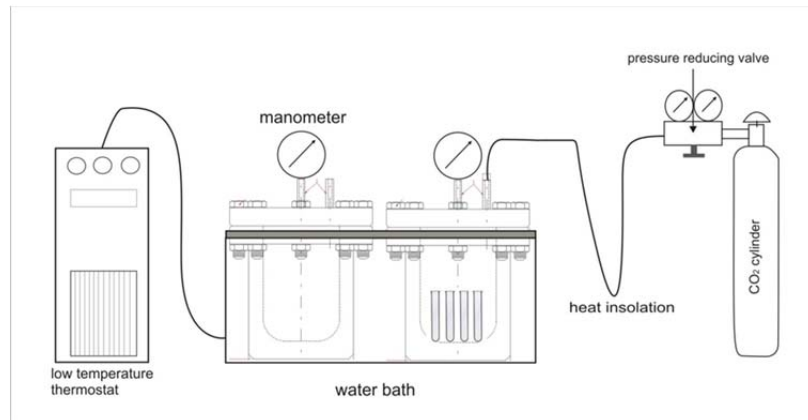


Figure 5.1 Experimental set up for growth experiments with CO₂ at high pressure. The two stainless steel pressure vessels were placed in a water bath and connected to a thermostat. The pressure was applied by using CO₂ cylinders and a pressure-reducing valve permitting pressure up to 7500 kPa.

Seven glass vials with a volume of 30 mL were filled with 10 mL of inoculum from a freshly grown culture, closed with silicon stoppers and aluminium grip seals, and placed in one vessel. Two needles were placed into the stopper of each glass vial to allow for pressure equilibration between the media in the glass vials and the pressure vessel. The vessel was closed gas tight with a torque wrench by applying a force of first 25 Nm and then 50 Nm. The vessels containing anaerobic strains were purged with carbon dioxide for 5 minutes. A pressure of 500, 1000, 2000, 3000, 4000 and 5400 kPa was applied to each vessel using pressure reducing valves. The O₂ content was controlled before and after the experiment using optical O₂ sensors (sensor type PSt3, PreSens, Germany). The pressure was maintained for 24 hours and released as slowly as possible. MPN assays were performed after each run on three parallels of each pressure vessel, as described above. In addition to the pressure experiments with carbon dioxide, the same pressure experiments were performed with pure nitrogen and pressures of up to 7500 kPa, to distinguish between pressure-induced effects on the microorganisms or effects caused by both pressure and increasing carbon dioxide concentrations.

5.5 Results

5.5.1 Influence of pH on growth and viability

For the investigation of the effects of CO₂ on microbial growth, culture experiments were conducted in a phosphate-buffered medium in order to reduce the effects of pH decrease on the microbial metabolism. The addition of gaseous CO₂ to the phosphate-buffered mineral medium still resulted in a decrease of the pH from an initial value of 7.0 to a minimum pH of 6.3 for *P. putida*, 6.3 for *B. subtilis*, 6.2 for *T. aromatica* and 6.4 for *D. vulgaris*, respectively (see table 5.1). Thus, to investigate the inhibitory effect of the low pH alone on microbial growth, experiments with all four strains were conducted using mineral medium in which the pH was adjusted to 6 by the addition of HCl (0.5 M). In these preliminary experiments, the cultures were not amended with additional CO₂. *P. putida*, *B. subtilis* and *D. vulgaris* showed slightly decreased growth rates and, with the exception of *D. vulgaris*, slightly diminished growth yields at the lower pH (Fig. 5.2).

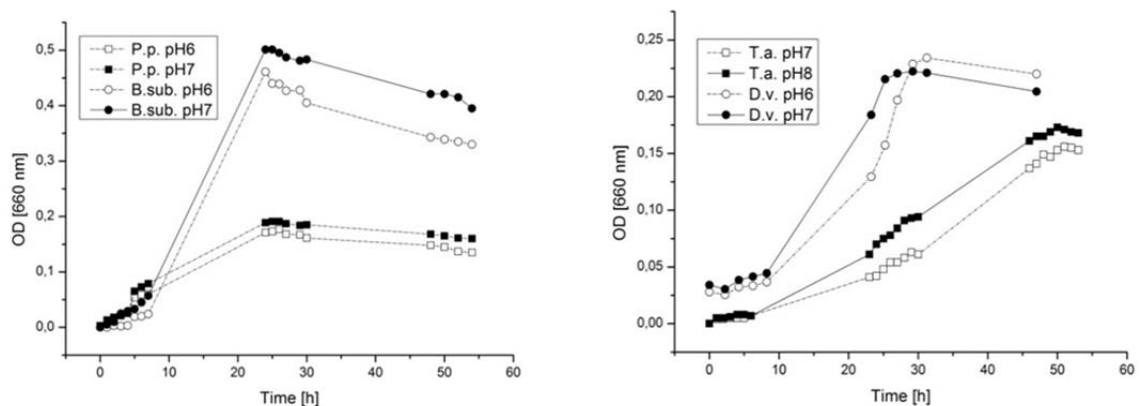


Figure 5.2 Comparison of growth at different pH values for *P. putida* and *B. subtilis* (left) and for *D. vulgaris* and *T. aromatica* (right). The pH in the medium was reduced by the addition of HCl (0.5 M).

T. aromatica grew poorly when the pH was decreased from 7 to 6 (Fig. SI-1). Therefore, the buffer concentration of the mineral medium was adjusted and the initial pH was increased from 7 to 8. After addition of CO₂, the pH decreased from 8 to 7. The growth at pH 7 was only slightly reduced compared to the growth rate at pH 8 (Fig. 5.2). In summary, all tested microorganisms grew fairly well in the pH ranges used later in the CO₂ stress experiments.

5. Effects of high CO₂ concentrations on typical aquifer microorganisms

Hence, experimentally observed effects could be attributed to elevated CO₂ concentrations. Experiments at lower pH values (to a minimum of 4) showed significant inhibition of growth for all four strains (Fig. SI-1).

Table 5.1 The relative inhibitory effect (RI) of CO₂ and the growth rate μ for CO₂ concentrations from 0 – 100% for the investigated microorganisms.

CO ₂ [%]	aerobic										anaerobic					
	<i>P. putida</i>					<i>B. subtilis</i>					<i>D. vulgaris</i> (sulfate-reducing)		<i>T. aromatica</i> (nitrate-reducing)			
	pH	RI [%]	μ [h ⁻¹]	pH	RI [%]	μ [h ⁻¹]	pH	RI [%]	μ [h ⁻¹]	CO ₂ [%]	pH	RI [%]	μ [h ⁻¹]	pH	RI [%]	μ [h ⁻¹]
0	7.18	0	0.52 ± 0.16	7.1	0	0.59 ± 0.03	7.09	0	0.48 ± 0.16	0	6.96	0	0.11 ± 0.03	8.00	0	0.06 ± 0.01
50	6.58	54.8 ± 21.6	0.32 ± 0.14	6.56	25.4 ± 21.0	0.44 ± 0.09	6.38	17.3 ± 7.1	0.39 ± 0.09	50	6.65	7.3 ± 2.5	0.09 ± 0.01	6.96	11.8 ± 2*	0.05 ± 0.01
60	6.52	79.5 ± 8.7	0.13 ± 0.03	6.53	n.m.	n.m.	6.31	25.9 ± 7.3	0.35 ± 0.12	70	6.60	40.9 ± 9	0.05 ± 0.01	6.91	40.7 ± 4.6*	0.04 ± 0.02
70	6.51	84.0 ± 8.1	0.10 ± 0.03	6.49	n.m.	n.m.	6.31	32.8 ± 10.8	0.31 ± 0.09	90	6.41	57.1 ± 2*	0.05 ± 0.004	6.84	51.2 ± 5.7	0.03 ± 0.002
80	6.48	86.4 ± 3.8	0.07 ± 0.01	6.37	75.1 ± 3.3	0.15 ± 0.01	6.25	46.3 ± 3.4	0.25 ± 0.09	100	6.35	77.6 ± 5.5	0.03 ± 0.01	6.79	83.7 ± 11.9	0.02 ± 0.01

n.m. not measured

*the standard deviation was calculated based on three replicates as no repetition experiments were performed

5. Effects of high CO₂ concentrations on typical aquifer microorganisms

5.5.2 Cell growth and viability under different CO₂ concentrations at ambient pressure

Three obvious changes were observed when high CO₂ concentrations were applied to the strains. First, the lag-phase was significantly prolonged for all four strains. In particular, the lag phase for *P. putida* increased from one to eight hours, and from two to seven hours for *B. subtilis* (Fig. 5.3). For the sulfate-reducing *D. vulgaris*, the prolongation of the lag-phase was even more pronounced and increased from nine to twenty-three hours (Fig. 5.3). For *T. aromatica* lag-phases at ambient conditions varied between four and six hours but after addition of 100 % CO₂ lag-phase and exponential growth phase could not be distinguished anymore as the growth rate decreased significantly (Fig. 5.3). The second observation was a notable decrease in the growth rate (μ) with increasing CO₂ concentrations. Finally, it was observed that the growth yields, in the presence of CO₂ concentrations higher than 60%, decreased for all four strains (Fig. 5.3).

A comparison of the MPN values (in the presence of 80 % CO₂) with the non-amended CO₂ controls at the end of each experiment showed a reduction in MPN counts by 22.7 ± 0.2 % for *P. putida* and by 51.6 ± 5.5 % for *B. subtilis*. MPN counts for *D. vulgaris* and *T. aromatica* decreased by 86.6 ± 4.9 and 84.9 ± 11.3 %, respectively. The calculation of the relative inhibitory effect of CO₂ (RI) also showed a different response of the four strains to increasing CO₂ concentrations (Tab. 5.1). The most pronounced effect at lower CO₂ concentrations (50 %) was observed for *P. putida* leading to an inhibitory effect of 68.8 %. The anaerobic strains were less affected at 80 % CO₂ compared to the aerobic one, which showed that the tolerance level to CO₂ stress is different for the four used strains.

To investigate if different substrates affect cellular growth at different CO₂ concentrations, glucose was used in place of acetate for *P. putida* cultures. When *P. putida* was grown on glucose as the sole energy source, the growth rates for 0 % and 80 % CO₂ were comparable to those observed during growth on acetate (Fig. 5.3). A significant difference was observed at 50 % CO₂, where the inhibitory effect for glucose was much smaller compared to acetate. Glucose-grown cultures had higher final OD₆₀₀ values, due to the higher amount of energy available from this substrate in the given concentrations (Fig. 5.3).

5. Effects of high CO₂ concentrations on typical aquifer microorganisms

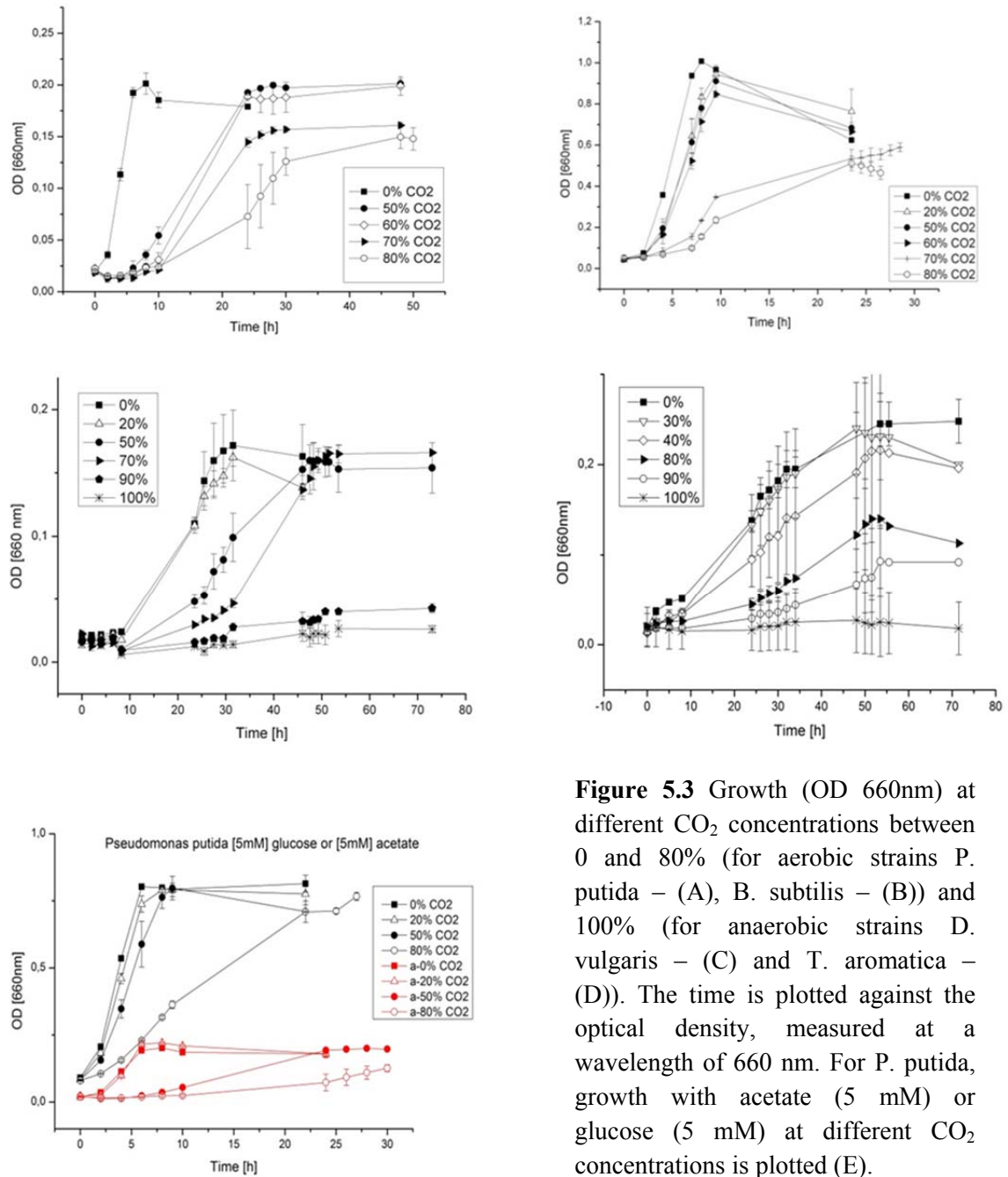


Figure 5.3 Growth (OD 660nm) at different CO₂ concentrations between 0 and 80% (for aerobic strains *P. putida* – (A), *B. subtilis* – (B)) and 100% (for anaerobic strains *D. vulgaris* – (C) and *T. aromatica* – (D)). The time is plotted against the optical density, measured at a wavelength of 660 nm. For *P. putida*, growth with acetate (5 mM) or glucose (5 mM) at different CO₂ concentrations is plotted (E).

Substrate consumption by *P. putida* was significantly reduced at CO₂ concentrations of 80%, compared to no CO₂ addition, and acetate uptake effectively stopped at the highest carbon dioxide levels (see supplementary information). Another aspect to be considered was, whether O₂ limitation leads to a reduction of growth for the aerobic strains. The O₂ concentration was measured in the gas and liquid phase for aerobic cultures, using O₂ sensors. Oxygen consumption during the growth experiments was significantly higher for *B. subtilis* compared with *P. putida* (Fig. SI-2).

5. Effects of high CO₂ concentrations on typical aquifer microorganisms

The O₂ concentration for *P. putida* (growing on acetate) for 0% CO₂ decreased from an initial concentration of 0.46 mM in the liquid phase down to 0.29 mM, compared to a decrease from 0.41 mM down to 0.19 mM in the presence of 80% CO₂. A reduction from 0.5 mM to 0.01 mM was observed in the liquid phase for *B. subtilis* (growing on glucose) at 0% CO₂, compared with a decrease from 0.43 mM to 0.07 mM when provided with an atmosphere consisting of 80% CO₂.

5.5.3 Cell viability under CO₂ stress at high pressure

Freshly grown cells were incubated at elevated pressures in self-constructed stainless steel vessels (see Fig. 5.1) and the pressure was increased up to 5000 kPa for CO₂ and up to 7500 kPa for the control experiments using pure nitrogen. These control experiments were performed to distinguish between the effect of the elevated pressure itself, and the combination of high CO₂ concentrations and pressure. The results of these experiments are shown in Fig. 5.4.

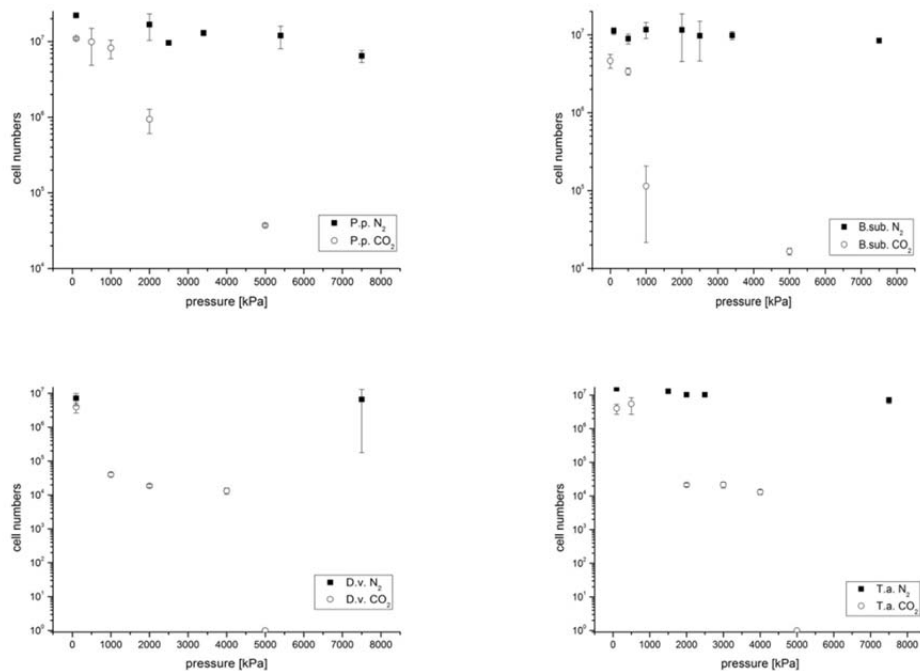


Figure 5.4 MPNs of the tested strains after incubation at high pressure and elevated CO₂ concentrations. To examine a negative effect of the pressure itself on the viability of the cells, control experiments were performed with pure nitrogen and no CO₂ amendments. For the anaerobic strains *T. aromatica* and *D. vulgaris*, all cells were killed at a pressure of 5000 kPa (no growth corresponds to the value one for the log scale) and elevated CO₂ concentrations. A significant number of *P. putida* and *B. subtilis* cells still survived at 5000 kPa pressure.

5. Effects of high CO₂ concentrations on typical aquifer microorganisms

When cells were incubated for 24 hours in the presence of pure nitrogen at pressures up to 5000 kPa, a reduction in MPNs of 59%, 12% and 33% was observed for *P. putida*, *B. subtilis* and *T. aromatica*, respectively compared to the 0 kPa control experiments. When the pressure was further increased up to 7500 kPa, an MPN reduction of 57% for *P. putida* and of 25% for *B. subtilis* was observed, compared to the 0 kPa experiments. The strictly anaerobic *D. vulgaris* was less affected by pressure, and an MPN reduction of only 8% at 7500 kPa was observed, whereas MPNs were reduced by 55% for the facultative anaerobic *T. aromatica*.

In contrast, when pressure (100-5000 kPa) was combined with increased CO₂ concentrations, the MPNs decreased by about 99% for *P. putida* and for *B. subtilis* and by 100 % for *T. aromatica* and *D. vulgaris*. Thus, while no living cells were observed for the anaerobic strains after the pressure experiment with CO₂, viable cells were recovered for the aerobic strains. Here, *P. putida* seems to be more resistant to the CO₂ - pressure treatment compared to *B. subtilis*: at a pressure of 1000 kPa, the MPN value was reduced by 97.6% for *B. subtilis*, in contrast to a reduction of only 25.3% for *P. putida*. Also the pH decreased significantly with increasing pressure compared to the control experiments with nitrogen (Tab. S5-1). For 5000 kPa the pH was reduced to about 5.63 for *P. putida*, 5.56 for *B. subtilis*, 5.90 for *D. vulgaris* and 5.33 for *T. aromatica*.

5.6 Discussion

The potential risk of CO₂ leakage from a geological sequestration site or from CO₂-driven geothermic probes into the groundwater, and the impacts on the ecological system, might be very diverse and the response of various bacterial communities will differ strongly. Several studies have addressed the effect of pressurized CO₂ on spoilage bacteria in the food and medical industry, where bacteria have the potential to lead to food spoilage and patient infection (Farber, 1991; Enomoto et al., 1997; Dillow et al., 1999). However, little is known about the influence of CO₂ on environmentally relevant microorganisms in shallow aquifers overlying geological CO₂ sequestration sites. In this study, we address this scenario by determining the effects of different CO₂ concentrations on two aerobic and two anaerobic model organisms (*P. putida*, *B. subtilis*, *T. aromatica*, *D. vulgaris*), all of which are typically present in shallow aquifers.

5. Effects of high CO₂ concentrations on typical aquifer microorganisms

Carbon dioxide that infiltrates a freshwater aquifer under oxidizing conditions and under atmospheric pressure will have an immediate impact on water chemistry, leading to a reduction in pH and an increase in the concentration of total dissolved solids. The respective ratios of different CO₂ chemical species (CO₂, HCO₃⁻, H₂CO₃, CO₃²⁻) will vary as a function of the aqueous pH and the geochemical composition of the aquifer matrix. Generally, a pH decrease will lead to an increase in the relative portion of CO₂, while the portion of HCO₃⁻ will decrease. At pH values below eight, as investigated in this study, the concentration of carbonate ions can be neglected (Yagi and Yoshida, 1977). Although an increase in carbonic acid may be buffered by carbonate dissolution, a decrease of aqueous pH will be the result of CO₂ addition, in any case; likely changing the composition of the microbial community and exerting selective pressure for microbial cells able to adapt to the more acidic conditions. For example, the four model organisms used in our study grew only poorly at pH values of 5 or lower (Fig. SI 1). Therefore, the leakage of CO₂ into an unbuffered aquifer would influence the composition of the microbial community much more than leakage into an aquifer with a high buffering capacity and a pH decrease down to 5 or even lower would be very likely for unbuffered groundwater.

On the other hand, considering Permian sandstones as possible storage sites for CO₂ in Germany, the carbonate rocks of the overlaying basal Zechstein should be taken into account (e.g. the lower *Werra Carbonate Subformation* Thuringian Basin). Aquifers composed of a carbonate rock matrix will have a natural buffering capacity for the leaking CO₂, and therefore the key microbial changes will be dominated by the increased CO₂ partial pressure and not by the pH alteration. Hence, the goal of the present study was to investigate the direct metabolic effects of increased CO₂ concentrations and pressures. Therefore, we have adjusted the pH of our culture medium by using a phosphate buffer generally to values allowing the test organisms to grow unaffected by extreme pH values. Before the experiments with increased CO₂ concentrations were performed, we investigated if the used strains can grow under the absence of externally provided CO₂, since previous studies have shown that some organisms need CO₂ for growth due to essential heterotrophic CO₂ fixation reactions (Valley and Rettger, 1927; Walker, 1932; Wood et al., 1941; Feisthauer et al., 2008). In our experiments, all strains were able to grow without an external CO₂ supply; probably, the inoculum contained low but sufficient CO₂ concentrations for an immediate restart of growth.

5. Effects of high CO₂ concentrations on typical aquifer microorganisms

The calculated inhibitory effect of CO₂ showed that the aerobic strains are more sensitive to CO₂ stress compared with the anaerobic strains (Tab. 1). Differential responses to increased CO₂ concentrations among the four model strains may partially be explained by the different incubation temperatures. *T. aromatica* (cultivated at 25 °C) showed no growth at 100% CO₂ compared to *D. vulgaris* (cultivated at 38 °C) possibly because CO₂ solubility increases with lower temperatures (1.5 g/L H₂O at 24.8 °C and only 1.2 g/L H₂O at 34.6 °C (Morrison and Billett, 1952)). King & Nagel (1967) proposed the displacement of O₂ by CO₂ as a reason for the reduced growth rate of microorganisms but this could not be confirmed, as the O₂ concentration never became a rate limiting factor in our experiments. However, other researchers have shown that the impact of elevated CO₂ concentrations is more severe under O₂-limited conditions (Molin, 1983), which could lead to a shift towards communities dominated by microaerophilic or anaerobic organisms implying that aerobic organisms of O₂ depleted aquifers are even more affected by a CO₂ leakage. Most authors explain the effect of CO₂ as an alteration of cell membrane properties (Sears and Eisenberg, 1961). The effect of phospholipid solubilisation by liquid CO₂ should be more pronounced in the membrane of Gram-negative microorganisms due to the presence of two membranes.

Furthermore, Gram-positive microorganisms have a thick layer of peptidoglycan, that may slow the diffusion of carbon dioxide into the cell (Oulé et al., 2010). Therefore, several studies proposed a higher resistivity of Gram-positive microorganisms towards CO₂ stress (Stier et al., 1981; Oulé et al., 2010). However, this hypothesis could not be confirmed in a pressure range between 100 and 5400 kPa. Further suggestions for the mode of physiological effects of CO₂ are a penetration of CO₂ into the membrane, resulting in a decrease of intracellular pH (Ballestra et al., 1996), a direct influence on physicochemical properties of enzymes e.g. carboxylases/ decarboxylases (Spilimbergo and Bertucco, 2003) and an alteration of the cell membrane, including effects on nutrient uptake and absorption properties (Jones and Greenfield, 1982).

We will investigate the putative cellular effects of CO₂ on our model organisms in future studies on a proteomic level to receive information about the influence of increased CO₂ concentrations on the activation or repression of specific proteins.

5. Effects of high CO₂ concentrations on typical aquifer microorganisms

A preliminary study with *Pseudomonas fluorescens* as model strain suggested that, based on results of respiration tests, adaptive enzyme synthesis does not occur in response to higher CO₂ concentrations (Gill and Tan, 1979). Previous experiments with samples from freshwater aquifers showed also an increase of alkali and alkaline metal (Li, Rb, Sr, Mg, Ca/ Mn, Fe, Co, Ni, Zn – increase after 2 weeks of exposure to CO₂) concentrations (Little and Jackson, 2010). As the concentration of the metals increased significantly immediately after an exposure of the freshwater of an aquifer to CO₂ under oxidized conditions and atmospheric pressure, the influence of increased metal concentrations in combination with high CO₂ concentrations on the growth behaviour of microorganisms should be investigated in future studies as well.

Besides the pH effect, the effect of pressure itself was tested and the results demonstrated that pressure can reduce the viability of the tested strains, but the effects are in the order of one magnitude at maximum and not strain specific. Only the combination of pressure and increased CO₂ leads to a dramatic reduction in cellular growth and detected MPN counts. Therefore, especially for deeper aquifers and for areas with higher lithostatic pressure gradients, CO₂ leakage can be more severe when both, high pressure and increased CO₂ concentrations are present. Extrapolating these observations, the average lithostatic and hydrostatic pressure (*i.e.* an increase of 350 kPa for every 10 m increase in depth, if the groundwater table equates the ground level and the average matrix density is 2.5 times the density of the water) at a depth of 50 m would significantly inhibit microbial activity in the presence of high CO₂ concentrations.

In summary, it can be concluded that the effect of CO₂ is not strain specific (for the investigated organisms) or dependent upon the electron acceptor present in the system, as nitrate- and sulfate-reducing organisms showed similar reactions to the CO₂ stress. Potential leakage rates of up to 10% of the injected CO₂ are predicted (Knox et al., 2003) and growth experiments with 10% CO₂ showed that these CO₂ concentrations without pressure influence have no significant obvious influence on the cell viability. Nevertheless, leakages may enhance CO₂ concentration in aquifers to levels where toxic effects can be expected and elevated CO₂ concentrations in combination with pressures ≥ 1000 kPa already lead to a dramatic decrease in cell viability. Long-term studies are necessary to make clear statements about the microbial responses and the adaptation abilities to increased CO₂ concentrations in shallow aquifers.

5. Effects of high CO₂ concentrations on typical aquifer microorganisms

This study provides principal information on the influence of suddenly increasing CO₂ concentrations on the viability of microorganisms present in shallow aquifers. This information can be used for a proper risk assessment, which is necessary to evaluate the Carbon Capture and Storage technology.

5.7 Acknowledgement

This project was funded by the German Federal Ministry of Education and Research (Grant: 03G0670C) under the context of the project “CO₂ injection into a near surface aquitard for evaluating monitoring concepts and methods”. We thank R. Schumann for construction and maintenance of the high pressure reactors, Denise Przybylski for the HPLC measurements, Roshani Sitaula for help in the laboratory and Jana Rakoczy, Angela Woods and Brandon Morris for English correction.

5.8 Supporting information

Comparison of the pH values for the pressure experiments with CO₂ and N₂ (SI-Tab. 5.1). Different solubility of CO₂ at atmospheric pressure and different temperatures (SI-Tab. 5.2). Growth of the different strains at different pHs (SI-Fig. 5.1). Dissolved oxygen concentration in mg/L for the two aerobic strains *Pseudomonas putida* and *Bacillus subtilis* (SI-Fig. 5.2). Acetate and glucose consumption at various concentration of CO₂ by *P. putida* during the experiment (SI-Fig. 5.3). Relative inhibitory effect (RI) is plotted against the CO₂ concentration for the four different model organisms (SI-Fig. 5.4).

6. Changes in the proteome of soil bacteria induced by elevated CO₂ concentrations

6.1 Kurzfassung

Die Speicherung von CO₂ in tiefen geologischen Formationen wird als eine Möglichkeit zur Reduzierung steigender CO₂ Konzentrationen in der Atmosphäre betrachtet. Eine mögliche Leckage von CO₂ in oberflächennahe Grundwasserleiter könnte die physiologischen Leistungen umweltrelevanter Mikroorganismen beeinträchtigen. Toxische Effekte erhöhter CO₂-Konzentrationen auf Mikroorganismen wurden oft beschrieben, aber die exakte Wirkweise von CO₂ ist wenig verstanden. Globale Proteinanalysen sollten diese Frage klären. Hierfür wurden der nitratreduzierende Stamm *Thauera aromatica* K172 und der aerobe Stamm *Pseudomonas putida* F1 in Gegenwart von 0, 50 oder 80% CO₂ mit Acetat als alleiniger Kohlenstoff- und Energiequelle kultiviert und die Proteinexpressionen nach erfolgtem Wachstum verglichen. Die Proteinextrakte wurden mittels Orbitrap LTQ Massenspektrometrie analysiert. Veränderungen der Proteinexpression wurden über eine statistische Analyse der gemessenen Peptidintensitäten detektiert. Bei beiden Stämmen veränderte sich die Expression von Proteinen unter dem Einfluss erhöhter CO₂-Konzentrationen signifikant ($p < 0.05$): 270 Proteine waren in *P. putida* betroffen und 37 Proteine in *T. aromatica*. Die verändert exprimierten Proteine sind an der Translation, der Acetatverwertung, am Membrantransport und an der zellulären Stressantwort beteiligt. Diese Ergebnisse liefern erste Hinweise auf die Ursachen des reduzierten Wachstums und somit der toxischen Wirkung erhöhter CO₂-Konzentrationen.

Schulz, Alexandra; Seifert, Jana; Vogt, Carsten; Morris, Brandon; Richnow, Hans-Hermann.

In preparation

6.2 Abstract

As a result of increasing CO₂ concentrations in the atmosphere, the storage of CO₂ in deep geological formations is considered. One of the major disadvantages of the CCS technique is a potential leakage of CO₂ into shallow aquifers, leading to harmful effects on living organisms, e.g. microbial communities.

6. Changes in the proteome of soil bacteria induced by elevated CO₂ concentrations

Toxic effects of high CO₂ concentrations on microorganisms have been often described, but the exact mode of action is less well understood. To assess this question, global proteomic analyses were performed on the soil bacteria *Thauera aromatica* K172 and *Pseudomonas putida* F1, affected by CO₂ atmospheres of 0, 50, and 80 percent during growth with acetate under oxic (*P. putida*) or nitrate-reducing conditions (*T. aromatica*). Proteins were analyzed using an LTQ Orbitrap mass spectrometer. The measured peptide intensities were used to conduct a statistical analysis of protein changes in *T. aromatica* and *P. putida*, respectively. Significant changes in protein expression were observed in both strains at elevated CO₂ concentrations. In total 270 and 37 proteins were significantly affected ($p < 0.05$) in *P. putida* and *T. aromatica*, respectively. Proteins related to protein translation, acetate metabolism, membrane transport and cellular stress response were altered. These results give some first indications for the reduced growth and hence for the toxic mode of elevated CO₂ concentrations.

6.3 Introduction

The increasing concentrations of CO₂ in the atmosphere has raised questions how to avoid further CO₂ emissions. One idea for reducing the CO₂ emission to the atmosphere is the capture and storage of CO₂ (CCS) in deep geological formations (IPCC, 2005). However, if there are cracks, crevices or abandoned wells present in the cap rock, the stored CO₂ has the potential to leak into shallow aquifers (Wu et al., 2010). The emerging effects of high CO₂ concentrations on indigenous microbial communities are difficult to estimate. Several researchers have examined the changes in microbial communities as a result of long-term exposure to CO₂ (Freeman et al., 2004; Blagodatskaya et al., 2010; Oppermann et al., 2010) but these communities were most often adapted to the new environmental conditions. The question about how a rapid increase of CO₂ concentrations would influence growth was not addressed. Nevertheless, this aspect has to be taken into account in order to consider potential leakage scenarios from an underground CO₂ storage site. We have recently determined how high CO₂ concentrations affect the growth and viability of ecophysiologicaly different typical soil bacteria (two aerobic strains, one nitrate reducer, one sulfate reducer), (Schulz et al., 2012). Generally, reductions of growth rate and growth yield were observed.

6. Changes in the proteome of soil bacteria induced by elevated CO₂ concentrations

Similar results were received in studies related to the food and medical industry, where CO₂ is known as potential bacteriostatic agent (Farber, 1991; Enomoto et al., 1997; Dillow et al., 1999). Several hypotheses exist about the mode of operation of high CO₂ concentrations on microorganisms. Ballestra et al. (1996) and others have suggested a decrease of the internal pH due to diffusive transport of CO₂ into a cell accompanied by dissociation, damaging the metabolic processes by suppressing key metabolic enzymes (Ballestra et al., 1996; Bertoloni et al., 2006). Alteration of cell membrane properties, accompanied by effects on nutrient uptake and absorption properties were also proposed (Sears and Eisenberg, 1961; Jones and Greenfield, 1982). Disruption of the intracellular electrolyte balance by CO₂ was suggested (Damar and Balaban, 2006; Garcia-Gonzalez et al., 2007), along with a direct influence on physicochemical properties of enzymes (e.g. carboxylases/ decarboxylases) (Spilimbergo and Bertucco, 2003).

Debates about physiological effects of CO₂ treatment led to studies on protein changes induced by supercritical CO₂ (scCO₂) concentrations (T > 31.1°C, p > 73 300 kPa), and down-regulation of enzymes involved in cell metabolism after scCO₂ treatment was reported (Kim et al., 2009). A decrease of protein content by about 182 proteins after scCO₂ treatment was also observed by Liao et al. (2011). This was explained by a possible damage of the cytoplasmic membrane and a subsequent leakage of the proteins into the supernatant. To the best of our knowledge, protein studies with non-supercritical CO₂ have been only performed with major food crops (rice, barley, wheat, soybean, potato); the protein concentration decreased for every crop with increasing CO₂ concentrations (Taub et al., 2008). In the present study, growth experiments with CO₂ concentrations from 0 to 100% have been conducted for one aerobic (*Pseudomonas putida* F1) and one nitrate-reducing strain (*Thauera aromatica* K172) in order to determine the effects of CO₂ on the metabolism on a proteomic level. Therefore, label-free quantification of the proteins was performed with both strains to compare global differences in protein expression.

6.4 Material and methods

6.4.1 Microorganisms and culture media

Pseudomonas putida strain F1 and *Thauera aromatica* strain K172 were obtained from the German Collection of Microorganisms and Cell Cultures (DSMZ; Germany).

6. Changes in the proteome of soil bacteria induced by elevated CO₂ concentrations

P. putida was cultivated in a phosphate-buffered mineral medium (2.44 g/L Na₂HPO₄; 1.52 g/L KH₂PO₄; 0.50 g/L (NH₄)₂SO₄; 0.20g/L MgSO₄ x 7 H₂O; 0.05 g/L CaCl₂ x 2 H₂O; 1 mL/L trace element solution 10; 5 mL/L vitamin solution) with acetate [5 mM] as sole carbon and energy source. Cultures were grown at 30°C and pH 7 in an orbital shaker at 150 rpm. *T. aromatica* was cultured in the same but slightly modified mineral medium. The medium was additionally amended with 1mL/L selenite-tungsten solution (0.5 g/L NaOH, 3 mg/L Na₂SeO₃ x 5 H₂O; 4 mg/L Na₂WO₄ x 2 H₂O) and flushed with nitrogen to remove oxygen; the pH was adjusted to 8. KNO₃ [8 mM] was provided as the terminal electron acceptor, and acetate [5 mM] was the sole carbon and energy source. *T. aromatica* was cultivated in an orbital shaker at 150 rpm at 25°C. For labeling experiment with ¹⁵N, (NH₄)₂SO₄ was substituted with ¹⁵N labeled NH₄Cl [50 mg/L]. Generally, additional solutions were added from sterile oxic (for *P. putida*) or anoxic (for *T. aromatica*) stock solutions using sterile plastic syringes, which were nitrogen-flushed in case of anoxic media. Pre-cultures for growth experiments were grown in 118 mL glass bottles, sealed gas-tight with butyl rubber stoppers. For maintenance, all strains were re-inoculated into fresh medium once per week.

6.4.2 Growth experiments under different CO₂ concentrations at ambient pressure

The growth experiments were performed in 30 mL glass tubes in three replicates for each condition. Each tube was filled with 4.5 mL of mineral medium modified for each strain (see 2.1) and closed with gas-tight butyl rubber stoppers. The medium was purged with gas mixtures of N₂ and CO₂ with compositions of approximately 0% (refers to no amendment of CO₂), 50% and 80% CO₂ by using a mass flow controller (EL-FLOW, Bronkhorst High-Tech, Germany). Each glass vial was purged with the appropriate gas mixture for 15 minutes to receive a full saturation of the atmosphere and the medium. For the aerobic experiments using *P. putida*, 20% O₂ was added by removing the adequate headspace volume with a gas-tight syringe and replacing it with the appropriate volume of pure oxygen. The oxygen concentrations were monitored using oxygen sensors (sensor type PSt3, detection limit 0.03%, PreSens, Germany). The vials were inoculated with a freshly grown culture.

6. Changes in the proteome of soil bacteria induced by elevated CO₂ concentrations

For the incubation with ¹⁵NH₄, the inoculum was centrifuged two times (Eppendorf centrifuge 5403) at 10000 rpm for 20 minutes at 10°C and washed with 0.9% NaCl solution to remove remaining unlabeled nitrogen components. Growth curves of the inoculated vials were determined by measurement of the optical density at a wavelength of 660 nm every two hours with a UV/ VIS spectrophotometer (Pharmacia LKB Novaspec II). The glass vials were placed directly into the spectrophotometer to ensure constant measurements during the course of the experiments.

6.4.3 Sample preparation for protein analysis

At the end of the log-phase of the growth experiment the cells were harvested from each vial by centrifuging three times at 10000 rpm for 10 minutes at 4 °C (SIGMA centrifuge 3K30). Afterwards, the cells were frozen in liquid nitrogen for five minutes and stored in a -20 °C freezer before they were analyzed by mass spectrometry.

6.4.4 Differential Proteomics

Global proteomic analysis was performed on the two strains to compare differences in protein expression as affected by the different applied CO₂ concentrations. Proteins were extracted using a standard SDS-based extraction protocol and separated on a one-dimensional gel. The gel was cut in five equal bands and proteins were digested with trypsin in-gel overnight at 37°C. The eluted peptides of each band were analyzed using an LTQ Orbitrap XL mass spectrometer (Thermo Scientific) coupled to a nanoAcquity UPLC (Waters) as described in Bastida et al. (2010). Raw files of three biological replicates of each strain were processed using Max Quant (Cox and Mann, 2008). Genome sequences from *P. putida* strain F1 and *Aromatoleum aromaticum* strain EbN1, respectively were used as database. Z-scores of LFQ intensities were used to conduct a statistical analysis of protein changes in *P. putida* and *T. aromatica*, respectively in response to elevated CO₂ concentrations. Statistical analyses were performed using MATLAB version 7.11.0.584 (R2010b). LFQ intensities from MaxQuant were log₂ -transformed before further analysis. After transformation, the intensities still did not meet the assumption of normality required for traditional analysis of variance (ANOVA, Fig. 6.3). Therefore, non-parametric Kruskal-Wallis one-way ANOVAs were performed on three replicates from the zero, fifty, and eighty percent carbon dioxide for each protein identified in the *P. putida* and *T. aromatica* cultures, respectively.

6. Changes in the proteome of soil bacteria induced by elevated CO₂ concentrations

If the mean LFQ intensity for each protein varied significantly between CO₂ levels (*i.e.* the null hypothesis of equal means was rejected, $\alpha < 0.05$), Mann-Whitney ranked-sum *post hoc* analysis was used to determine which sample (CO₂ level) was significantly different. To see if the incorporation of labeled ¹⁵N was successful, the relative isotope abundance was calculated. For getting results about changes in protein expression the *labeling ratio* was used, which is a ratio between the intensities of ¹⁴N and ¹⁵N.

6.5 Results

6.5.1 Growth curves of the different strains under different CO₂ concentrations

The growth of both strains was affected by high CO₂ concentrations. Specifically, the lag-phase of *P. putida* increased from 0.5 hour to five hours in the labeled and unlabeled medium respectively in the presence of 80% CO₂ (see Fig. 6.1). Furthermore, the growth yields decreased for about 25% ± 8.4% at a CO₂ concentration of 80% in the unlabeled and for about 38% ± 17.4% in the labeled medium. For *T. aromatica* the lag-phase varied between five to 10 h at ambient conditions, but increased CO₂ concentrations complicated the differentiation between the lag-phase and the exponential growth phase because optical density decreased below 0.05 (see Fig. 6.2). Also the decrease in growth yield was very significant for *T. aromatica*. In the unlabeled medium, growth yields decreased by about 84 ± 4.5% in the presence of 80% CO₂ compared to ambient conditions and by about 80 ± 7.4% in the labeled medium.

The results of the growth experiments showed clearly different behaviors for *P. putida* and *T. aromatica* under increased CO₂ concentrations. A pronounced negative effect (prolonged lag-phases and growth rates, reduced growth yields) on the growth of ecophysiological different typical soil bacteria, including *P. putida* and *T. aromatica*, was previously reported (Schulz et al., 2012). In this study, also the effects of decreasing pH, a lack of oxygen, or a lack of carbon substrates were addressed (Schulz et al., 2012). To get a deeper insight into the mechanism of CO₂ toxicity, we examined the proteome of CO₂-influenced and non-influenced cells.

6. Changes in the proteome of soil bacteria induced by elevated CO₂ concentrations

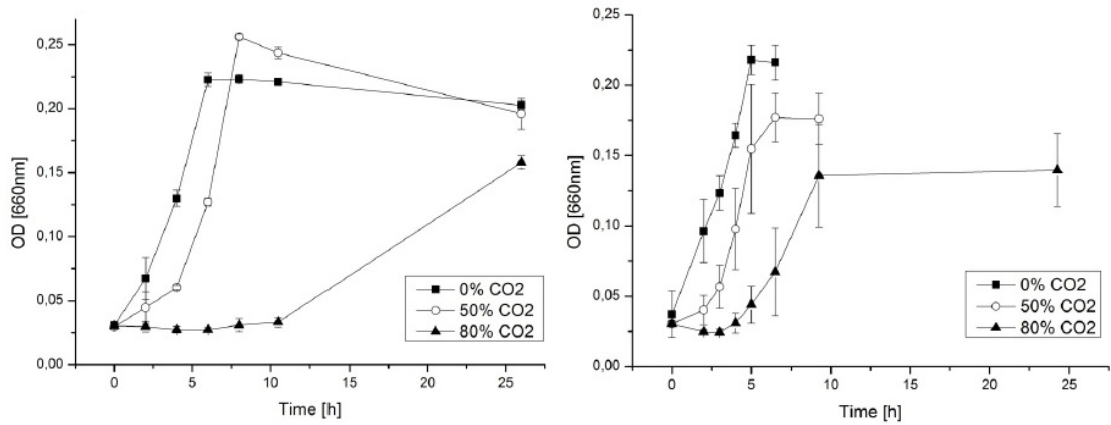


Figure 6.1 Growth curves of *P. putida* F1 for 0, 50 and 80% CO₂ with unlabeled Brunner medium (left graph) and with ¹⁵N-labeled Brunner medium (right graph).

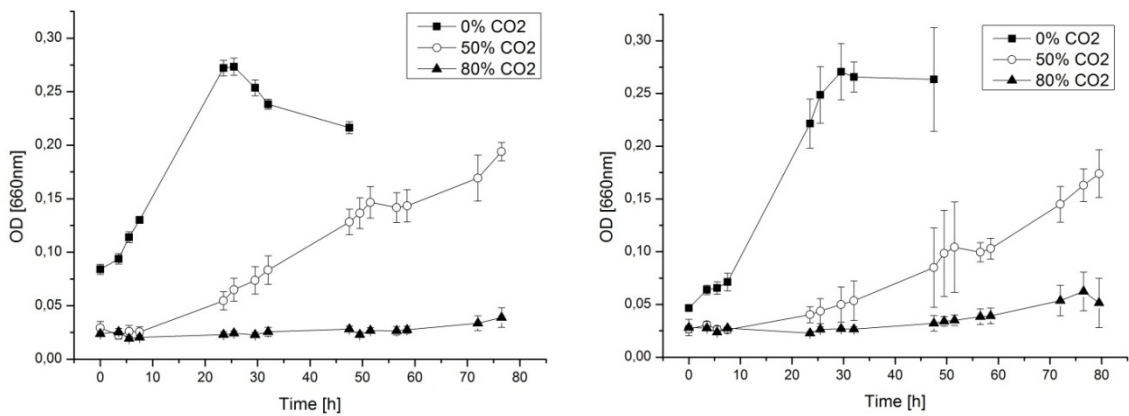


Figure 6.2 Growth curves of *T. aromatica* for 0, 50 and 80% CO₂ with unlabeled Brunner medium (left graph) and with ¹⁵N-labeled Brunner medium (right graph).

6.5.2 Protein data

In total 1300 proteins of *P. putida* and 350 proteins of *T. aromatica* were identified and quantified. Global and significant changes in protein expression were detected in both *T. aromatica* and *P. putida* while growing in the presence of increased CO₂ headspace amounts. The dynamic range of proteins detected in *P. putida* was much greater than for *T. aromatica* (see Fig. 6.3). This led to a greater number of detected protein changes in *P. putida*. Non-parametric Kruskal-Wallis one-way ANOVA detected 270 proteins to be significantly affected by CO₂ in *P. putida* at the $\alpha < 0.05$ level, and 414 proteins at the $\alpha < 0.10$ level.

6. Changes in the proteome of soil bacteria induced by elevated CO₂ concentrations

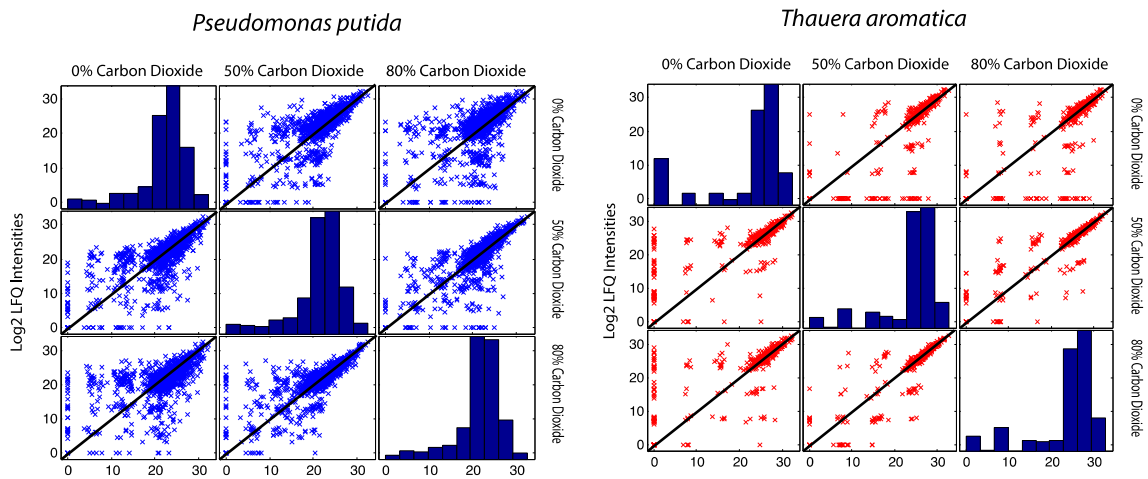


Figure 6.3 Protein changes in *P. putida* F1 (left) and *T. aromatica* K172 (right) in the presence of different headspace concentrations of CO₂ (0, 50, and 80%). Data points above or below the central diagonal line show differences between CO₂ levels. Histograms along the diagonal show the distribution of Log₂-transformed LFQ intensities for replicates.

Table 6.1 ¹⁵N (% average) incorporation for selected proteins at different headspace carbon dioxide concentrations for *P. putida*.

0% CO ₂	50% CO ₂	80% CO ₂	Protein
95.9%	95.5%	95.7%	acetyl-CoA synthetase [gi 229328219; <i>Ps. putida</i> F1]
94.9%	95.3%	94.7%	bifunctional aconitate hydratase 2/2 methylisocitrate dehydratase [gi 161936356; <i>Ps. putida</i> F1]
93.8%	93.6%	93.5%	isocitrate lyase [gi 148546986; <i>Ps. putida</i> F1]
95.3%	94.4%	93.8%	2-oxoglutarate dehydrogenase [gi 148546903; <i>Ps. putida</i>]
94.7%	95.0%	94.2%	50S ribosomal protein L3 [gi 148545739; <i>Ps. putida</i> F1]
95.0%	94.9%	94.9%	30S ribosomal protein S2 [gi 148549392; <i>Ps. putida</i>]
95.7%	95.6%	95.2%	Outer membrane porin [gi 148545505; <i>Ps. putida</i>]
95.5%	94.6%	94.9%	Outer membrane porin [gi 14854647; <i>Ps. putida</i>]
94.8%	94.8%	95.0%	Outer membrane porin [gi 148546165; <i>Ps. putida</i>]
96.1%	96.1%	n.d.	extracellular solute-binding protein [gi 148546164; <i>Ps. putida</i> F1]

6. Changes in the proteome of soil bacteria induced by elevated CO₂ concentrations

For *T. aromatica*, 37 proteins were significantly different between experimental conditions at the $\alpha < 0.05$ level, and 129 proteins when considered significant at the $\alpha < 0.10$ level. For further discussion we will only focus on the $\alpha < 0.05$ level.

It was observed for all samples of *P. putida* that the incorporation of the labeled ¹⁵N was always between 93 and 96%, which means that the unlabeled nitrogen was nearly fully substituted by the labeled ¹⁵N (see table 6.1).

Table 6.2 shows the labeling ratios for selected proteins under different headspace CO₂ concentrations. For *P. putida* it was observed that the aconitate hydratase and 2-oxoglutarate dehydrogenase, both related to the TCA cycle and thus acetate metabolism, were the most abundant proteins under 50% and 80% CO₂ headspace concentration and only minor changes have been observed compared to the control with 0% CO₂. Proteins, related to initiation and progression of protein translation (30S ribosomal protein S2, 50S ribosomal protein L3) were less abundant at 80% CO₂. The labeling ratio of outer membrane porins decreased proportionally with increasing CO₂ concentration (Table 6.2).

Table 6.2 Labeling ratios for selected proteins at different headspace CO₂ concentrations for *P. putida* F1.

0% CO ₂	50% CO ₂	80% CO ₂	Protein
0.987	0.962	0.351	acetyl-CoA synthetase [gi 229328219; <i>Ps. putida</i> F1]
0.908	0.948	0.919	bifunctional aconitate hydratase 2/2 methylisocitrate dehydratase [gi 161936356; <i>Ps. putida</i> F1]
0.979	0.964	0.840	isocitrate lyase [gi 148546986; <i>Ps. putida</i> F1]
0.890	0.878	0.910	2-oxoglutarate dehydrogenase [gi 148546903; <i>Ps. putida</i>]
0.870	0.747	0.769	50S ribosomal protein L3 [gi 148545739; <i>Ps. putida</i> F1]
0.873	0.856	0.714	30S ribosomal protein S2 [gi 148549392; <i>Ps. putida</i>]
0.792	0.711	0.614	outer membrane porin [gi 148545505; <i>Ps. putida</i>]
0.721	0.552	0.286	outer membrane porin [gi 14854647; <i>Ps. putida</i>]
0.660	0.531	0.127	outer membrane porin [gi 148546165; <i>Ps. putida</i>]
0.849	0.770	n.d.	extracellular solute-binding protein [gi 148546164; <i>Ps. putida</i> F1]

6. Changes in the proteome of soil bacteria induced by elevated CO₂ concentrations

This suggests membrane stability and permeability effects of elevated CO₂ levels on passive transport of ions and small molecules controlled by porins. Extracellular solute-binding protein (GI 148546164), regions of which play a role in dipeptide import, was significantly lower abundant at elevated CO₂ concentration, the labeled protein was not identified in all 80% cultures (Table 6.2). The labeling ratio of outer membrane porins decreased proportionally with increasing CO₂ concentration (Table 6.2). This suggests membrane stability and permeability effects of elevated CO₂ levels on passive transport of ions and small molecules controlled by porins. Extracellular solute-binding protein (GI 148546164), regions of which play a role in dipeptide import, was significantly lower abundant at elevated CO₂ concentration, the labeled protein was not identified in all 80% cultures (Table 6.2). As only such a little number of proteins of *T. aromatica* was affected by increasing CO₂ concentrations, the evaluation of the data is very difficult and should be supported by additional experiments.

6.6 Discussion

Several previous studies have shown that high CO₂ concentrations negatively affect the metabolism of microorganisms. From an enzymatic point of view, it can be expected that rates of carboxylation/decarboxylation differ under the influence of CO₂, as shown by Wimpenny (1969). However, the influence of CO₂ probably extends beyond enzymes involved in carboxylation reactions; many other cellular processes might be affected (Jones and Greenfield, 1982). For example, increased CO₂ has been shown to increase the rate of succinate formation in *E. coli* (Elsden, 1938). The significance of this response is however probably dependent upon the carbon source used for growth.

In this study, acetate was used as a growth substrate for *P. putida* and *T. aromatica*. In both strains, acetate is metabolized via the TCA cycle, using either oxygen (*P. putida*) or nitrate (*T. aromatica*) as electron acceptor. Our results suggest that the energy metabolism of *P. putida* was significantly impaired by increasing CO₂ concentrations, indicated by the lowered expression of a key enzyme of the energy metabolism, acetyl-CoA synthetase (see table 6.2). Acetyl-CoA synthetase catalyzes the formation of acetyl-CoA from acetate and coenzyme A in *P. putida* and *T. aromatica* and is the pacemaker of the energy metabolism during growth with acetate.

If the activity of acetyl-CoA synthetase is reduced, the TCA cycle is restrained, leading to a decreased production of reducing equivalents needed for energy production via

6. Changes in the proteome of soil bacteria induced by elevated CO₂ concentrations

ATP synthase, and finally leading to a low energy charge of the cells. In contrast, a minor increase in the labeling ratio of the 2-oxoglutarate dehydrogenase was observed, another key enzyme of the TCA cycle, responsible for catalyzing the conversion of 2-oxoglutarate to succinyl-CoA and CO₂ downstream in the cycle. Bacterial 2-oxoglutarate dehydrogenase is induced by AMP (Strumilo, 2005) hence conditions of low energy charge, which might be the reason for the enzymes induction under CO₂ stress. On the other hand, the expression of isocitrate lyase, a key enzyme of the glyoxylate cycle bypassing the two decarboxylation steps of the TCA cycle, was also lowered with increasing CO₂ concentrations, indicating that the metabolic activity of the cells was generally lowered. The high abundance of aconitate hydratase under all tested conditions might be due to the postulated enzymes' function to increase the carbon flow in the TCA during metabolism of acetate (Emer et al., 2009). With acetate as sole substrate, it is generally expected that cells have limited means to re-oxidize NADH and use amino acid-related pathways to either synthesize more NAD⁺, or to feed carbon skeleton intermediate needs. Indeed, there is some evidence in the current study for amino acid production increasing proportionally with CO₂ concentrations but these results have to be confirmed by additional experiments.

Additionally a lowered synthesis of proteins involved in the ribosomal protein synthesis machinery (30S ribosomal protein S2, 50S ribosomal protein L3) was observed under CO₂ stress, which might be a consequence of the restricted energy metabolism. As a result it would lead to a disturbance of protein synthesis, which would result in generally lowered growth rates.

Our work has shown that lower growth yields were observed with increased carbon dioxide in the headspace (Fig. 6.1 and 6.2; (Schulz et al., 2012)). This effect has also been seen for *Klebsiella aerogenes* grown in a chemostats (Teixeira de Mattos et al., 1984). This study demonstrated that high CO₂ concentrations influence both the energetics and metabolism of cellular processes. Tan and Gill (1982) showed that carbon dioxide greatly impacted substrate uptake in *Ps. aeruginosa*. It seems that the main reason for carbon dioxide efficacy is the ability of carbon dioxide to freely penetrate bacterial membranes.

This process will likely impact internal pH, thereby affecting enzymatic equilibria or reaction dynamics (Wolfe, 1980). Cellular responses to this process would be expected to be global and involve a large number of cellular enzymes. In addition, CO₂ can alter

6. Changes in the proteome of soil bacteria induced by elevated CO₂ concentrations

the solubility of proteins, making insoluble proteins soluble, and thereby have dramatic consequences for cellular processes and homeostasis (Mitz 1957, 1978). CO₂ is also highly reactive with amines (Edsall, 1969), binding reversibly to amino acids, peptides, and proteins. These reactions cause charge and tertiary structure changes to proteins (Mitz, 1979).

In summary, the proteomic analysis of *T. aromatica* and *P. putida* demonstrate that CO₂ affects proteins related to all functional categories of cellular processes. It was shown that large portions of the proteome are significantly affected by increased CO₂ in the headspace. Further studies would be needed to determine the exact impact of CO₂; however we have conclusively shown that growth yield decreases and the proteomic changes dramatically when both cultures are grown in the presence of high CO₂ concentrations. Therefore, leakages scenarios that lead to high CO₂ concentrations will always impair indigenous microbial communities.

6.7 Acknowledgement

This project was funded by the German Federal Ministry of Education and Research (Grant: 03G0670C) under the context of the project “CO₂ injection into a near surface aquitard for evaluating monitoring concepts and methods”. We want to thank Kathleen Eismann for preparing the samples for LC-MS/MS measurements.

7. Final discussion and outlook

7. Final discussion and outlook

7.1 Evaluation of the monitoring approach

The capture and storage of CO₂ is one considered option for reducing the CO₂ concentration in the atmosphere, but this technology is still afflicted with some uncertainties. For conducting a proper risk assessment, including probabilities and consequences, reliable monitoring methods have to be established. According to the European Commission Decision about monitoring guidelines for greenhouse gas emissions, the monitoring of a CCS site shall be based on the following main principles (Commission-Decision, 2007):

- Completeness: monitoring should cover all process- and combustion-emissions
- Consistency: monitoring data have to be comparable over time
- Transparency: different methods should be used to quantify the amount of stored CO₂ and a reproduction of the determination has to be possible
- Trueness: accuracy of emission detection has to be as high as possible
- Cost effectiveness: accuracy of applied monitoring methods has to be balanced against additional costs

Furthermore, monitoring should provide an early warning by leakage detection and an optimization of the storage efficiency. So far, no standard protocols exist for an effective monitoring strategy, as many site-specific factors will influence the proceeding. Also the question about the timeframe of a monitoring campaign is still under discussion. In a review of White et al. (2003) it was suggested that monitoring of a CCS site should be performed for more than 1000 years, whereas others suggested that monitoring is no longer required if it can be confirmed that the injected CO₂ plume is not moving any longer (Chow et al., 2003). Regardless of the period of time of monitoring, all long-term approaches need cost-effective and easily applicable methods. These methods need to detect not only rapid losses of CO₂ but also the continuous leakage rates that will occur in small quantities at nearly every storage site. The IPCC report on CCS (2005) gives a summary about the release rates of CO₂ from natural storage analogues and EOR sites. For CO₂ trapped in sedimentary basins, the average release fraction is below 10⁻⁷ per year (Baines and Worden, 2001; Stevens et al., 2001) and for EOR sites, where surface flux measurements have been performed, the released fraction is near zero (Moritis, 2002; Klusman, 2003).

7. Final discussion and outlook

So far, only one example for wellbore failure is known from a natural gas storage facility in Kansas, USA, where about 3000 t of CO₂ have been released (Lee, 2001).

Strong effects on respiratory physiology occur at CO₂ concentrations of more than 2% in ambient air. 7 – 10% CO₂ can cause unconsciousness and death. Therefore, monitoring techniques that detect a leakage directly from the storage site are necessary to prevent further migration of escaping CO₂. In addition, near-surface monitoring needs to be applied to ensure the completeness of the monitoring approach. Technologies from oil and gas industry can be used for monitoring injection rates and pressures but further development is necessary to fit the specific needs of a CCS site. For monitoring the subsurface distribution of CO₂, natural analogues have been used, but they can only give indications for CO₂ migration. As the geological character of natural analogues is usually different compared to CCS sites (IPCC, 2005), they are not adequate to mirror the migration of CO₂ from the storage formation to the near-surface. Furthermore, it is not possible to perform a baseline monitoring at natural analogues and therefore, the use of comparative approaches is not possible.

Monitoring technologies can be divided into direct (tracers, geochemical measurements, isotope measurements) and indirect techniques (seismic, well logs, electrical measurements). For monitoring CO₂ fluxes in air, infrared gas analyzers are applied (Pickles and Cover, 2004). In table 7.1 the four different monitoring approaches are compared that have been applied during the field test described in this study (see chapter 2). Geochemical measurements include pH, major cations and anions, trace elements and field parameters like temperature, electrical conductivity and dissolved oxygen. The isotope monitoring approach is based on the comparison of the isotope signature of the sample before and after the injection of CO₂. It is a comparative approach and therefore it requires a detailed baseline monitoring. Seasonal variations (e.g. due to higher photosynthetic production rates during summer) of the isotope signature of the background have to be known in advance to ensure that induced changes of the isotope signature are caused by CO₂ leaked from a CCS reservoir. As baseline monitoring is so important for this approach, it cannot be introduced if the storage of CO₂ is already running. Another important aspect of knowing the isotope signature of the natural background is that a significant difference between injected and natural CO₂ is required for applying this method. The important aspect of this method is an easy identification of the source of CO₂.

Table 7.1 Comparison of different monitoring approaches used in the presented field experiment.

	Geochemical Monitoring		Isotope Monitoring		Geoelectrical borehole Monitoring		Tracer SF ₆
	monitoring well	Lateral distribution	soil gas	groundwater	monitoring well	monitoring well	
Requirement	monitoring well		no requirements	monitoring well	monitoring well	monitoring well	monitoring well
Spatial resolution	Lateral distribution		lateral: good vertical: poor		Good for a small area; not practicable for large fields		Lateral distribution
Baseline monitoring	required		required	required	required		not required
Quantification	Possible with TIC*		possible	possible	not possible		not possible
Source identification	not possible		possible	possible	not possible		not possible
Environmental risks	no		no	no	no		SF ₆ is a greenhouse gas with high GWP
Feasibility			Difference of isotope ratios	Difference of isotope ratios	Depending on site-specific conditions		

* Measurement of TIC concentration is not always reliable

7. Final discussion and outlook

Furthermore, sampling, especially of soil gas, is very easy to handle and can be applied at nearly every field site without intensive preliminary preparation. However, GC-IRMS is required for measuring the samples. When comparing the different approaches it can be concluded that a combination of different methods will be the most reliable monitoring strategy. Artificial tracers like SF₆ should be avoided, as SF₆ is also a greenhouse gas with a high global warming potential (see table 1.1, chapter 1). Due to the very time-consuming measurement and the little spatial applicability, the range of application for geoelectrical monitoring is somehow limited. Geochemical approaches can be complicate, if the filed site has a complex geochemical characteristic. The more heterogeneous the field site, the less reliable is this monitoring approach. Only a combination of different geochemical parameters, like pH, TIC or EC can be used for the monitoring, as the intensity of single parameters strongly depends on aquifer mineralogy (Peter et al., 2012a). A combination of geochemical analyses together with isotope analyses will provide a reliable monitoring strategy to assess potential CO₂ leakage from a storage site into the near-subsurface.

7.2 Implementation of the isotope monitoring approach to other field site scenarios

The detection of CO₂ leakage from a storage site into the shallow surface is not the only field of application for isotope monitoring approaches. As the isotope ratio of carbon is very characteristic for different compounds (see chapter 1.6), the isotope monitoring method can also be used for e.g. mapping contaminations of BTEX compounds. For example, during the microbial degradation of benzene, CO₂ that is depleted in ¹³C, is produced. The isotopically lighter CO₂ can be measured in soil gas samples taken in the shallow surface. This would be a very simple and fast approach to get a good overview about the distribution of a specific compound at a contaminated field site. Furthermore, isotope monitoring is not only a good method for detecting spatial resolution of compounds; also depth oriented profiles can be obtained if sampling is conducted in monitoring wells.

As the access to fossil fuels is more and more limited, new technologies have been tested and discussed to achieve higher recovery rates. Hydraulic fracturing is one of these technologies. A fracturing fluid is injected into the storage formation to increase the formation pressure. Consequently cracks are formed and natural gas can be recovered.

7. Final discussion and outlook

Water is the main fracturing fluid but also scCO₂ is considered to act as a fracturing fluid. Studies showed that the breakdown pressure for scCO₂ is lower compared to water. Furthermore, scCO₂ generates more three-dimensional cracks rather than flat planes (Ishida et al., 2012) so that efficiency can be increased. The fracking technology is also afflicted with numerous uncertainties and evaluations of possible risks as well as proper monitoring methods are required. If CO₂ is injected into the formation and the hydrogeological setting is known, the isotope monitoring approach can be used to observe if the fracturing fluid has migrated into shallow aquifers.

7.3 Further steps in the investigation of microorganisms concerning elevated CO₂ concentrations

The growth experiments have shown that growth of the microorganisms is restrained with increasing CO₂ concentrations. As high CO₂ concentrations cause lower pHs, a selection of microorganisms that can tolerate more acidic conditions within the microbial community has to be considered. This loss in biodiversity can also affect ecosystem processes, including ecosystem services (Griffiths et al., 2000). Other researchers claim that it is not so much a question of biodiversity rather than a question of community composition and individual species (Wardle, 1999). Therefore, long-term studies should be conducted to see, whether microorganism are able to adapt to elevated CO₂ stress and regulate their growth rate to “normal” levels again. Additionally, experiments with spore forming microorganisms (*B. subtilis*) should be performed to investigate, if the level of spore formation increases due to the induced CO₂ stress and if the spores are capable of the new growth conditions. Even if the investigation of growth rates and growth yields of microorganisms present in shallow aquifers cannot be used as monitoring approach (simply too time consuming), these investigations will help to evaluate possible consequences of leakage scenarios on the ecosystem.

The studies on CO₂ induced changes on protein expression have shown that more experiments and data are necessary to confirm the observed trends. Furthermore, it has to be investigated if the detected effects can be generalized for all aerobic and also for anaerobic microorganisms. Even if no cell death was achieved under ambient pressure, harmful effects of increased CO₂ concentrations have been observed.

8. References

- Alexandratos, N.**, 1988. World Agriculture: Towards 2000. Pinter Publisher, London.
- Amundson, R., Stern, L., Baisden, T., Wang, Y.**, 1998. The isotopic composition of soil and soil-respired CO₂. *Geoderma* 82, 83-114.
- Appelo, C.A.J., Postma, D.**, 1993. Geochemistry, groundwater and pollution. Balkema Publisher, Amsterdam, the Netherlands
- Apps, J., Zheng, L., Zhang, Y., Xu, T., Birkholzer, J.**, 2010. Evaluation of potential changes in groundwater quality in response to CO₂ leakage from deep geologic storage. *Transport in Porous Media* 82, 215-246.
- Aravena, R., Schiff, S.L., Trumbore, S.E., Dillon, P.I., Elgood, R.**, 1992. Evaluating dissolved inorganic carbon cycling in a forested lake watershed using carbon isotopes. *Radiocarbon* 34.
- Archie, G.E.**, 1942. The electrical resistivity log as an aid in determining some reservoir characteristics. *Pet. Trans.* 146, 54-62.
- Arps, J.J.**, 1953. The effect of temperature on the density and electrical resistivity of sodium chloride solutions *Trans. Am. Inst. Min. Metall. Eng.* 198.
- Arrhenius, S.**, 1896. On the influence of carbonic acid in the air upon the temperature on the ground. *Philosophical Magazine and Journal of Science* 41, 237-279.
- Baines, S.J., Worden, R.H.**, 2001. Geological CO₂ disposal. Understanding the long-term fate of CO₂ in naturally occurring accumulations. In: Williams, D.J., Durie, R.A., McMullan, P., Paulson, C.A.J., Smith, A. (Eds.). 5th International Conference on Greenhouse Gas Control Technologies (GHGHT-5). CSIRO Publishing, Collingwood, Victoria, Australia, Cairns, Australia, pp. 311-316.
- Ballestra, P., Da Silva, A.A., Cuq, J.L.**, 1996. Inactivation of *Escherichia coli* by carbon dioxide under pressure. *Journal of Food Science* 61, 829-836.
- Bastida, F., Rosell, M., Franchini, A.G., Seifert, J., Finsterbusch, S., Jehmlich, N., Jechalke, S., Von Bergen, M., Richnow, H.H.**, 2010. Elucidating MTBE degradation in a mixed consortium using a multidisciplinary approach. *FEMS Microbiology Ecology* 73, 370-384.
- Batjes, N.H.**, 1999. Management options for reducing CO₂-concentrations in the atmosphere by increasing carbon sequestration in the soil. Wageningen, The Netherlands, p. 126.
- Bécard, G., Piché, Y.**, 1989. Fungal growth stimulation by CO₂ and root exudates in vesicular-arbuscular mycorrhizal symbiosis. *Applied and Environmental Microbiology* 55, 2320-2325.
- Benson, S.M., Surles, T.**, 2006. Carbon dioxide capture and storage: an overview with emphasis on capture and storage in deep geological formations. *Proceedings of the IEEE* 94, 1795-1805.
- Bentham, M., Kirby, M.**, 2005. CO₂ storage in saline aquifers. *Oil & Gas Science and Technology - Rev. IFP* 60, 559-567.
- Bertoloni, G., Bertucco, A., De Cian, V., Parton, T.**, 2006. A study on the inactivation of micro-organisms and enzymes by high pressure CO₂. *Biotechnology and Bioengineering* 95, 155-160.
- Bigeleisen, J., Wolfsberg, M.**, 1959. Theoretical and experimental aspects of isotope effects in chemical kinetics. *Adv. Chem. Phys.* 1, 15-76.
- Bildstein, O., Jullien, M., Crédoz, A., Garnier, J.**, 2009. Integrated modeling and experimental approach for caprock integrity, risk analysis, and long term safety assessment. *Energy Procedia* 1, 3237-3244.
- Binley, A., Winship, P., West, L.J., Pokar, M., Middleton, R.**, 2002. Seasonal variation of moisture content in unsaturated sandstone inferred from borehole radar and resistivity profiles. *Journal of Hydrology* 267, 160-172.
- Blagodatskaya, E., Blagodatsky, S., Dorodnikov, M., Kuzyakov, Y.**, 2010. Elevated atmospheric CO₂ increases microbial growth rates in soil: results of three CO₂ enrichment experiments. *Global Change Biology* 16, 836-848.
- Bondor, P.L.**, 1992. Applications of carbon dioxide in enhanced oil recovery. *Energy Conversion and Management* 33, 579-586.

8. References

- Brennan, S.T., Burruss, R.C.**, 2003. Specific sequestration volumes: a useful tool for CO₂ storage capacity assessment. p. 14.
- Brumbaugh, W.G., Petty, J.D., Huckins, J.N., Manahan, S.E.**, 2002. Stabilized liquid membrane device (SLMD) for the passive, integrative sampling of labile metals in water. *Water, Air, & Soil Pollution* 133, 109-119.
- Canadell, J.G., Pataki, D., Gifford, R.M., Houghton, R.A., Luo, Y., Raupach, M.R., Smith, P., Steffen, W.**, 2007. Saturation of the terrestrial carbon sink. In: Canadell, J.G., Pataki, D.E., Pitelka, L.F. (Eds.). *Terrestrial Ecosystems in a Changing World*. Springer, Berlin, pp. 59-78.
- Carroll, S., Hao, Y., Aines, R.**, 2009. Geochemical detection of carbon dioxide in dilute aquifers. *Geochemical Transactions* 10, 4.
- Cerling, T.E., Solomon, D.K., Quade, J., Bowman, J.R.**, 1991. On the isotopic composition of carbon in soil carbon dioxide. *Geochimica et Cosmochimica Acta* 55, 3403-3405.
- Chalaturnyk, R., Gunter, W.D.**, 2005. Geological storage of CO₂: time frames, monitoring and verification. In: Wilson, E., Monea, M. (Eds.). *Seventh international conference on Greenhouse Gas Technologies (GHGT-7)*, Vancouver, Canada.
- Chow, J.C., Watson, J.G., Benson, S.M., Hidy, G.M., Gunter, W.D., Penkala, S.J., White, C.M.**, 2003. Separation and capture of CO₂ from large stationary sources and sequestration in geological formations. *Journal of the Air & Waste Management Association* 53, 1172-1183.
- Cinar, Y.**, 2009. Experimental study of CO₂ injection into saline formations. *SPE* 14, 588-594.
- Clark, I., Fritz, P.**, 1997. *Environmental Isotopes in Hydrogeology*. CRC Press LLC.
- Class, H.**, 2009. Intercomparison of codes and models - how can we improve reliability and understanding of model predictions for CO₂ storage? Workshop on modeling and risk assessment of geological storage of CO₂, Longyear-byen, Svalbar.
- Commission-Decision**, 2007. Establishing guidelines for the monitoring and reporting of greenhouse gas emissions pursuant to Directive 2003/87/EC of the European Parliament and of the Council. In: Union, E. (Ed.). 2007/589/EC. *Official Journal of the European Union*, Brussels, Belgium, p. 85.
- Coplen, T.B.**, 1996. New guidelines for reporting stable hydrogen, carbon, and oxygen isotope-ratio data. *Geochimica et Cosmochimica Acta* 60, 3359-3360.
- Cortis, A., Oldenburg, C., M., Benson, S.M.**, 2008. The role of optimality in characterizing CO₂ seepage from geological carbon sequestration sites. *International Journal of Greenhouse Gas Control* 2, 640-652.
- Cox, J., Mann, M.**, 2008. MaxQuant enables high peptide identification rates, individualized p.p.b.-range mass accuracies and proteome-wide protein quantification. *Nature Biotechnology* 26, 1367-1372.
- Craig, H.**, 1957. Isotopic standards for carbon and oxygen and correction factors for mass-spectrometric analysis of carbon dioxide. *Geochimica et Cosmochimica Acta* 12, 133-149.
- Cunnold, D.M., Steele, L.P., Fraser, P.J., Simmonds, P.G., Prinn, R.G., Weiss, R.F., Porter, L.W., O'Doherty, S., Langenfelds, R.L., Krummel, P.B., Wang, H.J., Emmons, L., Tie, X.X., Dlugokencky, E.J.**, 2002. In situ measurements of atmospheric methane at GAGE/AGAGE sites during 1985-2000 and resulting source inferences. *J. Geophys. Res.* 107, 4225.
- Daily, G., C., Matson, P.A., Vitousek, P.M.**, 1997. Ecosystem services supplied by the soil. In: Daily, G., C. (Ed.). *Nature's services: Societal dependence on natural ecosystems* Island Press, Washington DC, pp. pp 113-132.
- Damar, S., Balaban, M.O.**, 2006. Review of dense phase CO₂ technology: microbial and enzyme inactivation, and effects on food quality. *Journal of Food Science* 71, R1-R11.
- De Figueiredo, M.A.**, 2007. The liability of carbon dioxide storage. *Engineering Systems Division*. Massachusetts Institute of Technology, p. 417.
- de Jonge, H., Rothenberg, G.**, 2005. New device and method for flux-proportional sampling of mobile solutes in soil and groundwater. *Environmental Science & Technology* 39, 274-282.

8. References

- de Laeter, J.R., Böhlke, J.K., de Bièvre, P., Hidaka, H., Peiser, H. S., Rosman, K.J.R., Taylor, P.D.P.**, 2003. Atomic weights of the elements: Review 2000. Pure Appl. Chem. International Union of pure and applied chemistry.
- Deines, P.**, 1980. The isotopic composition of reduced organic carbon. In: Fritz, P., Fontes, J.C. (Eds.). Handbook of Environmental Isotope Geochemistry, 1. The Terrestrial Environment. Elsevier, Amsterdam, pp. 329-406.
- Desgranges, C., Durand, A.**, 1990. Effect of pCO₂ on growth, conidiation, and enzyme production in solid-state culture on *Aspergillus niger* and *Trichoderma viride* TS. Enzyme and Microbial Technology 12, 546-551.
- Deutsch, C.V., Journel, A.G.**, 1998. GSLIB: Geostatistical software library and user's guide Oxford University Press, Oxford.
- Dietrich, P.**, 1999. Konzeption und Auswertung gleichstromgeoelektrischer Tracerversuche unter Verwendung von Sensitivitätskoeffizienten. Tübinger geowissenschaftliche Arbeiten: Reihe C, Hydro-, Ingenieur- und Umweltgeologie. Institut und Museum für Geologie und Paläontologie, Tübingen.
- Dietrich, P., Butler, J.J., Faiß, K.**, 2008. A rapid method for hydraulic profiling in unconsolidated formations. Ground Water 46, 323-328.
- Dietrich, P., Leven, C.**, 2006. Direct push-technologies. In: Kirsch, R. (Ed.). Groundwater geophysics. Springer, Berlin, pp. 321-340.
- Dillow, A.K., Dehghani, F., Hrkach, J.S., Foster, N.R., Langer, R.**, 1999. Bacterial inactivation by using near- and supercritical carbon dioxide. Proc. Natl. Acad. Sci USA 96, 10344-10348.
- Dixon, N.M., Kell, D.B.**, 1989. The inhibition by CO₂ of the growth and metabolism of microorganisms. Journal of Applied Bacteriology 67, 109-136.
- Dixon, R.K.**, 1997. Special issue - Climate change impacts and response options in Eastern and Central Europe - Foreword. Clim. Change 36, 1-2.
- Dominati, E., Patterson, M., Mackay, A.**, 2010. A framework for classifying and quantifying the natural capital and ecosystem services of soils. Ecological Economics 69, 1858-1868.
- Du, J., Cheng, W., Zhang, Y., Jie, C., Guan, Z., Liu, W., Bai, L.**, 2006. Helium and carbon isotopic compositions of thermal springs in the earthquake zone of Sichuan, Southwestern China. Journal of Asian Earth Sciences 26, 533-539.
- DVWK**, 1992. Entnahme und Untersuchungsumfang von Grundwasserproben. Merkblatt zur Wasserwirtschaft DVWK 128.
- DVWK**, 1997. Tiefenorientierte Probenahme aus Grundwassermessstellen. Merkblätter zur Wasserwirtschaft DVWK 245.
- Elsden, S.R.**, 1938. The effect of CO₂ on the production of succinic acid by *Bact. coli* commune. Biochemistry 32, 187-193.
- Emberley, S., Hutcheon, I., Shevalier, M., Durocher, K., Gunter, W.D., Perkins, E.H.**, 2004. Geochemical monitoring of fluid-rock interaction and CO₂ storage at the Weyburn CO₂-injection enhanced oil recovery site, Saskatchewan, Canada. Energy 29, 1393-1401.
- Emer, D., Krug, A., Eikmanns, B.J., Bott, M.**, 2009. Complex expression control of the *Corynebacterium glutamicum* aconitase gene: identification of RamA as a third transcriptional regulator besides AcnR and RipA. Biotechnol. 140, 92-98.
- Enfors, S.-O., Molin, G.**, 1981. The influence of temperature on the growth inhibitory effect of carbon dioxide on *Pseudomonas fragi* and *Bacillus cereus*. Canadian Journal of Microbiology 27, 15-19.
- Ennis-King, J., Paterson, L.**, 2001. Reservoir engineering issues in the geological disposal of carbon dioxide in deep saline formations. 5th International Conference on Greenhouse Gas Control Technologies, Cairns, Australia pp. 290-295.
- Enomoto, A., Nakamura, K., Nagai, K., Hashimoto, T., Hakoda, M.**, 1997. Inactivation of food microorganisms by high-pressure carbon dioxide treatment with or without explosive decompression. Biosci. Biotechnol. Biochem. 61, 1133-1137.
- Evans, J.P., Heath, J., Shipton, Z.K., Kolesar, P.T., Dockrill, B., Williams, A., Kirchner, D., Lachmar, T.E., Nelson, S.T.**, 2004. Natural leaking CO₂-charged

8. References

- systems as analogs for geologic sequestration sites. 3rd annual Conference on Carbon Capture and Sequestration, Alexandria, VA.
- Fahrner, S., Schaefer, D., Dahmke, A.,** 2011. Reactive transport modeling to assess geochemical monitoring for detection of CO₂ intrusion into shallow aquifers. *Energy Procedia* 4, 3155-3162.
- Fahrner, S., Schäfer, D., Dahmke, A.,** 2012. A monitoring strategy to detect CO₂ intrusion in deeper freshwater aquifers. *International Journal of Greenhouse Gas Control* 9, 262-271.
- Fang, Y., Baojun, B., Dazhen, T., Dunn-Norman, S., Wronkiewicz, D.,** 2010. Characteristics of CO₂ sequestration in saline aquifers. *Petroleum Science* 7, 83-92.
- Farber, J.M.,** 1991. Microbiological aspects of modified - atmosphere packaging - a review. *Journal of Food Protection* 54, 58-70.
- Farquhar, G.D., Ehleringer, R., Hubic, K.T.,** 1989. Carbon isotope discrimination and photosynthesis. *Annu. Rev. Plant Physiol. Plant Mol. Biol.* 40, 503-537.
- Feisthauer, S., Wick, L.Y., Kästner, M., Kaschabek, S.R., Schlömann, M., Richnow, H.H.,** 2008. Differences of heterotrophic ¹³CO₂ assimilation by *Pseudomonas knackmussii* strain B13 and *Rhodococcus opacus* 1CP and potential impact on biomarker stable isotope probing. *Environmental Microbiology* 10, 1641-1651.
- Fischer, A.,** 2006. Charakterisierung des mikrobiellen Schadstoffabbaus in kontaminierten Grundwasserleitern mit Hilfe stabiler Isotope. Mathematisch-Naturwissenschaftliche Fakultät. Christian-Albrechts-University Kiel, p. 289.
- Fischer, A., Vieth, A., Kn, Iler, K., Wachter, T., Dahmke, A., Richnow, H.-H.,** 2004. Charakterisierung des mikrobiellen Schadstoffabbaus mithilfe von isotopenchemischen Methoden. *Grundwasser* 9, 159-172.
- Flett, M., Gurton, R., Weir, G.,** 2007. Heterogeneous saline formations for carbon dioxide disposal: Impact of varying heterogeneity on containment and trapping. *Journal of Petroleum Science and Engineering* 57, 106-118.
- Freeman, C., Kim, S.-Y., Lee, S.-H., Kang, H.,** 2004. Effects of elevated atmospheric CO₂ concentrations on soil microorganisms. *The Journal of Microbiology* 42, 267-277.
- Gal, F., Brach, M., Braibant, G., Jouin, F., Michel, K.,** 2011. CO₂ escapes in the Laacher See region, East Eifel, Germany: application of natural analogue onshore and offshore geochemical monitoring. *International Journal of Greenhouse Gas Control* 5, 1099-1118.
- Garbe-Schönberg, C.-D.,** 1993. Simultaneous determination of thirty-seven trace elements in twenty-eight international rock standards by ICP-MS. *Geostandards Newsletter* 17, 81-97.
- Garcia-Gonzalez, L., Geeraerd, A.H., Spilimbergo, S., Elst, K., Van Ginneken, L., Debevere, J., Van Impe, J.F., Devlieghere, F.,** 2007. High pressure carbon dioxide inactivation of microorganisms in foods: The past, the present and the future. *International Journal of Food Microbiology* 117, 1-28.
- Garthright, W.E., Blodgett, R.J.,** 1996. Confidence intervals for microbial density using serial dilutions with MPN estimates. *Biometrical Journal* 38, 489-505.
- Geistlinger, H., Lazik, D., Krauss, G., Vogel, H.-J.,** 2009. Pore-scale and continuum modeling of gas flow pattern obtained by high-resolution optical bench-scale experiments. *Water Resour. Res.* 45, W04423.
- Gill, C.O., Tan, K.H.,** 1979. Effect of carbon dioxide on growth of *Pseudomonas fluorescens*. *Applied and Environmental Microbiology* 38, 237-240.
- Griesshaber, E., O'Nions, R.K., Oxburgh, E.R.,** 1992. Helium and carbon isotope systematics in crustal fluids from the Eifel, the Rhine Graben and Black Forest, F.R.G. *Chemical Geology* 99, 213-235.
- Griffiths, B.S., Ritz, K., Bardgett, R.D., Cook, R., Christensen, S., Ekelund, F., Sorensen, S.J., Baath, E., Bloem, J., de Ruiter, P.C., Dolfing, J., Nicolardot, B.,** 2000. Ecosystem response of pasture soil communities to fumigation-induced microbial diversity reductions: an examination of the biodiversity-ecosystem function relationship. *Oikos* 90, 279-294.
- Gruber, N., Friedlingstein, P., Field, C.B., Valentini, R., Heimann, M., Richey, J.E., Romero-Lankao, P., Schulze, D., Chen, C.-T.A.,** 2004. The vulnerability of

8. References

- the carbon cycle in the 21st century: An assessment of carbon-climate human interactions. In: Field, C.B., Raupach, M.R. (Eds.). *The Global Carbon Cycle: Integrating Humans, Climate, and the Natural World*. Island Press, Washington (DC), pp. 45-76.
- Haldane, J.B.S.**, 1939. Sampling errors in the determination of bacterial or virus density by the dilution method. *Journal of Hygiene* 39, 289-293.
- Hamada, Y., Tanaka, T.**, 2001. Dynamics of carbon dioxide in soil profiles based on long-term field observation. *Hydrological Processes* 15, 1829-1845.
- Hansen, J., Johnson, D., Lacis, A., Lebedeff, S., Lee, P., Rind, D., Russell, G.**, 1981. Climate impact of increasing atmospheric carbon dioxide. *Science* 213, 957-966.
- Heath, J., McPherson, B., Phillips, F., Cooper, S., Dewers, T.**, 2009. Natural helium as a screening tool for assessing caprock imperfections at geologic CO₂ storage sites. *Energy Procedia* 1, 2903-2910.
- Hesse, M.A., Orr, F.M., Tchelepi, H.A.**, 2008. Gravity currents with residual trapping. *Journal of Fluid Mechanics* 611, 35-60.
- Hoffmann, R., Dietrich, P.**, 2004. Geoelektrische Messungen zur Bestimmung von Grundwasserfließrichtungen und -geschwindigkeiten. *Grundwasser* 9, 194-200.
- Hollaway, S., Pearce, J., Hards, V., Ohsumi, T., Gale, J.**, 2007. Natural emissions of CO₂ from the geosphere and their bearing on the geological storage of carbon dioxide. *Energy* 32, 1194 - 1201.
- Hollaway, S.**, 2001. Storage of fossil fuel-derived carbon dioxide beneath the surface of the earth. *Annu. Rev. Energy Environ.* 26, 145-166.
- Holt, T., Jensen, J.L., Lindeberg, E.**, 1995. Underground storage of CO₂ in aquifers and oil reservoirs. *Energy Conversion and Management* 36, 535-538.
- Humez, P., Audigane, P., Lions, J., Chiaberge, C., Bellenfant, G.**, 2011. Modeling of CO₂ leakage up through an abandoned well from deep saline aquifer to shallow fresh groundwaters. *Transport in Porous Media* 90, 153-181.
- Huq, F., Blum, P., Marks, M., Nowak, M., Haderlein, S., Grathwohl, P.**, 2012. Chemical changes in fluid composition due to CO₂ injection in the Altmark gas field: preliminary results from batch experiments. *Environmental Earth Sciences* 67, 385-394.
- Indermuhle, A., Stocker, T.F., Joos, F., Fischer, H., Smith, H.J., Wahlen, M., Deck, B., Mastroianni, D., Tschumi, J., Blunier, T., Meyer, R., Stauffer, B.**, 1999. Holocene carbon-cycle dynamics based on CO₂ trapped in ice at Taylor Dome, Antarctica. *Nature* 398, 121-126.
- IPCC**, 2001. *Climate Change 2001: The scientific basis*. In: Houghton, J.T., Ding, Y., Griggs, D.J., Noguer, M., van der Linden, P.J., Dai, X., Maskell, K., Johnson, C.A. (Eds.), Cambridge, UK, p. 881.
- IPCC**, 2005. *IPCC Special Report on Carbon Dioxide Capture and Storage*. Working Group III of the Intergovernmental Panel on Climate Change, Cambridge, United Kingdom and New York, NY, USA.
- IPCC**, 2007. *Fourth Assessment Report - Climate Change 2007: Synthesis Report*. In: Pachauri, R.K., Reisinger, A. (Eds.), Geneva, Switzerland, p. 104.
- Ishida, T., Aoyagi, K., Niwa, T., Chen, Y., Murata, S., Chen, Q., Nakayama, Y.**, 2012. Acoustic emission monitoring of hydraulic fracturing laboratory experiment with supercritical and liquid CO₂. *Geophysical Research Letters* 39, 16309-16315.
- Jassal, R.S., Black, T.A., Drewitt, G.B., Novak, Gaumont-Guay, D., Nestic, Z.**, 2004. A model of the production and transport of CO₂ in soil: predicting soil CO₂ concentrations and CO₂ efflux from a forest floor. *Agriculture and Forest Meteorology* 124, 219-236.
- Jones, D.G., Barlow, T., Beaubien, S.E., Ciotoli, G., Lister, T.R., Lombardi, S., May, F., Möller, I., Pearce, J.M., Shaw, R.A.**, 2009. New and established techniques for surface gas monitoring at onshore CO₂ storage sites. *Energy Procedia* 1, 2127-2134.
- Jones, R.P., Greenfield, P.F.**, 1982. Effect of CO₂ on yeast growth and fermentation. *Enzyme and Microbial Technology* 4, 210-222.
- Jossi, M., Fromin, N., Tarnawski, S., Kohler, F., Gillet, F., Aragno, M., Hamelin, J.**, 2006. How elevated pCO₂ modifies total and metabolically active

8. References

- bacterial communities in the rhizosphere of two perennial grasses grown under field conditions. *FEMS Microbiology Ecology* 55, 339-350.
- Keeling, R.F., Piper, S.C.**, 2009. Atmospheric CO₂ records from sites in the SIO air sampling network. . *Trends: A Compendium of Data on Global Change*. Carbon Dioxide Information Analysis Center, Oak Ridge National Laboratory, U.S. Department of Energy.
- Keller, G.V.**, 1966. *Electrical methods in geophysical prospecting*. Pergamon Press, New York.
- Khalil, M.A.K.**, 1999. Non-CO₂ greenhouse gases in the atmosphere. *Annu. Rev. Energy Environ.* 24, 645-661.
- Khalil, M.A.K., Shearer, M.J., Rasmussen, R.A.**, 1996. Atmospheric methane over the last century. *World Resource Review* 8, 481-492.
- Kharaka, Y., Thordsen, J., Kakouros, E., Ambats, G., Herkelrath, W., Beers, S., Birkholzer, J., Apps, J., Spycher, N., Zheng, L., Trautz, R., Rauch, H., Gullickson, K.**, 2010. Changes in the chemistry of shallow groundwater related to the 2008 injection of CO₂ at the ZERT field site, Bozeman, Montana. *Environmental Earth Sciences* 60, 273-284.
- Kiessling, D., Schmidt-Hattenberger, C., Schuett, H., Schilling, F., Krueger, K., Schoebel, B., Danckwardt, E., Kummerow, J.**, 2010. Geoelectrical methods for monitoring geological CO₂ storage: First results from cross-hole and surface-downhole measurements from the CO₂SINK test site at Ketzin (Germany). *International Journal of Greenhouse Gas Control* 4, 816-826.
- Kim, S.R., Kim, H.T., Park, H.J., Kim, S., Choi, H.J., Hwang, G.-S., Yi, J.H., Ryu, D.H., Kim, K.H.**, 2009. Fatty acid profiling and proteomic analysis of *Salmonella enterica* serotype Typhimurium inactivated with supercritical carbon dioxide. *International Journal of Food Microbiology* 134, 190-195.
- Klusman, R.W.**, 2003. A geochemical perspective and assessment of leakage potential for a mature carbon dioxide-enhanced oil recovery project and as a prototype for carbon dioxide sequestration; Rangely field, Colorado. *AAPG Bulletin* 87, 1485-1507.
- Klusman, R.W.**, 2006. Detailed compositional analysis of gas seepage at the National Carbon Storage Test Site, Teapot Dome, Wyoming, USA. *Applied Geochemistry* 21, 1498-1521.
- Knödel, K., Lange, G., Voigt, H.-J.**, 2007. *Environmental geology. Handbook of field methods and case studies*. Springer, Berlin.
- Knorr, W.**, 2009. Is the airborne fraction of anthropogenic CO₂ emissions increasing? *Geophys. Res. Lett.* 36, L21710.
- Knox, P.R., Paine, J.G., Hovorka, S.D.**, 2003. Optimal geological environments for carbon dioxide disposal in brine formations (saline aquifers) in the United States - Pilot experiment in the Frio Formation, Houston Area. The University of Texas at Austin, Bureau of Economic Geology, Austin, p. 54.
- Koch, U., Bräuer, K., Heinicke, J., Kämpf, H.**, 2008. The gas flow at mineral springs and mofettes in the Vogtland/NW Bohemia: an enduring long-term increase. *Geofluids* 8, 274-285.
- Kolditz, O., Bauer, S., Beyer, C., Böttcher, N., Dietrich, P., Görke, U.-J., Kalbacher, T., Park, C.-H., Sauer, U., Schütze, C., Shao, H., Singh, A., Taron, J., Wang, W., Watanabe, N.**, 2012. A systematic benchmarking approach for geologic CO₂ injection and storage. *Environmental Earth Sciences* 67, 613-632.
- Kuzyakov, Y., Blagodatskaya, J.**, 2012. Elevated CO₂ affects microbial competition in soil. In: http://www.aec.uni-bayreuth.de/MICROSOM_3.pdf (Ed.). British Publisher, pp. http://www.aec.uni-bayreuth.de/MICROSOM_3.pdf.
- Kyoto Protocol**, 1998. Kyoto protocol to the United Nations Framework Convention on Climate Change. United Nations.
- Lamert, H., Geistlinger, H., Werban, U., Schütze, C., Peter, A., Hornbruch, G., Schulz, A., Pohlert, M., Kalia, S., Beyer, M., Großmann, J., Dahmke, A., Dietrich, P.**, 2012. Feasibility of geoelectrical monitoring and multiphase modeling for process understanding of gaseous CO₂ injection into a shallow aquifer. *Environmental Earth Sciences* 67, 447-462.
- Le Quéré, C., Andres, R.J., Boden, T., Conway, T., Houghton, R.A., House, J.S., Marland, G., Peters, G.P., van der Werf, G., Ahlström, A., Andrew, R.M., Bopp, L., Canadell, J.G., Ciais, P., Doney, S.C.,**

8. References

- Enright, C., Friedlingstein, P., Huntingford, C., Jain, A.K., Jourdain, C., Kato, E., Keeling, R.F., Klein Goldewijk, K., Levis, S., Levy, P., Lomas, M., Poulter, B., Raupach, M.R., Schwinger, J., Sitch, S., Stocker, B.D., Viovy, N., Zaehle, S., Zeng, N.**, 2012. The global carbon budget 1959–2011. *Earth System Science Data* 5, 1107-1157.
- Le Quere, C., Raupach, M.R., Canadell, J.G., Marland, G.e.a.**, 2009. Trends in the sources and sinks of carbon dioxide. *Nature Geoscience* 2, 831-836.
- Lee, A.M.**, 2001. Hutchinson gas explosions - unraveling a geologic mystery. 26th Annual KBA/ KIOGA Oil and Gas Law Conference pp. 3-1 - 3-29.
- Lemieux, J.-M.**, 2011. Review: The potential impact of underground geological storage of carbon dioxide in deep saline aquifers on shallow groundwater resources. *Hydrogeology Journal* 19, 757-778.
- Leven, C., Weiß, H., Vienken, T., Dietrich, P.**, 2011. Direct-Push-Technologien – Effiziente Untersuchungsmethoden für die Untergrundkundung. *Grundwasser* 16, 221-234.
- Leverett, M.C.**, 1940. Capillary behavior in porous solids. *AIME* 142, 152-169.
- Levin, I.**, 2012. The balance of the carbon budget. *Nature* 488, 35-36.
- Lewicki, J., Birkholzer, J., Tsang, C.-F.**, 2007a. Natural and industrial analogues for leakage of CO₂ from storage reservoirs: identification of features, events, and processes and lessons learned. *Environmental Geology* 52, 457-467.
- Lewicki, J.L., Hilley, G.E., Fischer, M.L., Pan, L., Oldenburg, C.M., Dobeck, L., Spangler, L.**, 2009. Eddy covariance observations of surface leakage during shallow subsurface CO₂ releases. *J. Geophys. Res.* 114, D12302.
- Lewicki, J.L., Oldenburg, C.M., Dobeck, L., Spangler, L.**, 2007b. Surface CO₂ leakage during two shallow subsurface CO₂ releases. *Geophys. Res. Lett.* 34, L24402.
- Liao, H., Zhang, F., Hu, X., Liao, X.**, 2011. Effects of high-pressure carbon dioxide on proteins and DNA in *Escherichia coli*. *Microbiology* 157, 709-720.
- Little, M.G., Jackson, R.B.**, 2010. Potential impacts of leakage from deep CO₂ geosequestration on overlying freshwater aquifers. *Environmental Science and Technology* 44, 9225-9232.
- Lu, J., Partin, J., Hovorka, S., Wong, C.**, 2010. Potential risks to freshwater resources as a result of leakage from CO₂ geological storage: a batch-reaction experiment. *Environmental Earth Sciences* 60, 335-348.
- Martin, F.D., Taber, J.J.**, 1992. Carbon dioxide flooding. *Journal of Petroleum Technology* 44, 396-400.
- McAlexander, I., Rau, G.H., Liem, J., Owano, T., Fellers, R., Baer, D., Gupta, M.**, 2011. Deployment of a carbon isotope ratiometer for the monitoring of CO₂ sequestration leakage. *Analytical Chemistry* 83, 6223-6229.
- McCarthy, J.H., Jr., Reimer, G.M.**, 1986. Advances in soil gas geochemical exploration for natural resources: some current examples and practices. *J. Geophys. Res.* 91, 12327-12338.
- McCray, J.E.**, 2000. Mathematical modeling of air sparging for subsurface remediation: state of the art. *Hazard Mater* 72, 237-263.
- McGhee, W., Riley, D., Christ, K., Pan, Y., Parnas, B.**, 1995. Carbon dioxide as a phosgene replacement: synthesis and mechanistic studies of urethanes from amines, CO₂, and alkyl chlorides. *The Journal of Organic Chemistry* 60, 2820-2830.
- Meckenstock, R.U., Morasch, B., Griebler, C., Richnow, H.H.**, 2004. Stable isotope fractionation analysis as a tool to monitor biodegradation in contaminated aquifers. *Journal of Contaminant Hydrology* 75, 215-255.
- Miller, B.R., Huang, J., Weiss, R.F., Prinn, R.G., Fraser, P.J.**, 1998. Atmospheric trend and lifetime of chlorodifluoromethane (HCFC-22) and the global tropospheric OH concentration. *J. Geophys. Res.* 103, 13237-13248.
- Mishra, S., Parker, J.C.**, 1989. A user's guide to SOILPROP., Blacksburg.
- Molin, G.**, 1983. Combined carbon dioxide inhibition and oxygen limitation of the growth of *Pseudomonas fragi* 72 in batch and continuous culture. *Journal of General Microbiology* 129, 2885-2891.
- Moritis, G.**, 2002. Enhanced oil recovery. *Oil and Gas Journal* 100, 43-47.

8. References

- Moritis, G.**, 2003. CO₂ sequestration adds new dimension to oil, gas production. *Oil and Gas Journal* 101, 71-83.
- Morrison, T.J., Billett, F.**, 1952. 730. The salting-out of non-electrolytes. Part II. The effect of variation in non-electrolyte. *Journal of the Chemical Society (Resumed)*, 3819-3822.
- Namieśnik, J., Zabiegała, B., Kot-Wasik, A., Partyka, M., Wasik, A.**, 2005. Passive sampling and/or extraction techniques in environmental analysis: a review. *Analytical and Bioanalytical Chemistry* 381, 279-301.
- Nordbotten, J.M., Celia, M.A., Bachu, S., Dahle, H.K.**, 2005. Semianalytical solution for CO₂ leakage through an abandoned Well. *Environmental Science & Technology* 39, 602-611.
- O'Leary, M.H.**, 1988. Carbon isotopes in photosynthesis. *BioScience* 38, 328-336.
- Oh, N.-H., Kim, H.-S., Richter Jr, D.D.**, 2005. What regulates soil CO₂ concentrations? A modeling approach to CO₂ diffusion in deep soil profiles. *Environmental Engineering Science* 22, 38-45.
- Oldenburg, C., Lewicki, J.**, 2006. On leakage and seepage of CO₂ from geologic storage sites into surface water. *Environmental Geology* 50, 691-705.
- Oldenburg, C., Unger, A.**, 2003. On leakage and seepage from geologic carbon sequestration sites: Unsaturated zone attenuation. *Vadose Zone J* 2, 287 - 296.
- Olivier, J.G.J., Janssens-Maenhout, G., Peters, J.A.H.W.**, 2012. Trends in global CO₂ emissions; 2012 Report. The Hague: PBL Netherlands Environmental Assessment Agency; Ispra: Joint Research Centre.
- Oppermann, B.I., Michaelis, W., Blumenberg, M., Frerichs, J., Schulz, H.M., Schippers, A., Beaubien, S.E., Krüger, M.**, 2010. Soil microbial community changes as a result of long-term exposure to a natural CO₂ vent. *Geochimica et Cosmochimica Acta* 74, 2697-2716.
- Orr, F.M.**, 2009. Onshore geologic storage of CO₂. *Science* 325, 1656-1658.
- Oulé, M.K., Dickman, M., Arul, J.**, 2010. Microbicidal effect of pressurized CO₂ and the influence of sensitizing additives. *European Journal of Scientific Research* 41, 570-582.
- Park, R., Epstein, S.**, 1960. Carbon isotope fractionation during photosynthesis. *Geochimica et Cosmochimica Acta* 21, 110-126.
- Pearson, P.N., Palmer, M.R.**, 2000. Atmospheric carbon dioxide concentrations over the past 60 million years. *Nature* 406, 695-699.
- Peter, A., Dahmke, A., Hornbruch, G., Lamert, H., Schulz, A., Vogt, C., Richnow, H.H., Dietrich, P., Werban, U., Geistlinger, H., Lazik, D., Großmann, J., Beyer, M., Schreiber, B., Heinrich, B.**, 2012a. Abschlussbericht zum Forschungsvorhaben 03G0670A-C Verbundprojekt UR II: „CO₂-Leckage“ CO₂-Leckageversuch in einem oberflächennahen Grundwasserleiter zur Erprobung von Monitoringkonzepten und –methoden.
- Peter, A., Hornbruch, G., Dahmke, A.**, 2011. CO₂ leakage test in a shallow aquifer for investigating the geochemical impact of CO₂ on groundwater and for developing monitoring methods and concepts. *Energy Procedia* 4, 4148-4153.
- Peter, A., Lamert, H., Beyer, M., Hornbruch, G., Heinrich, B., Schulz, A., Geistlinger, H., Schreiber, B., Dietrich, P., Werban, U., Vogt, C., Richnow, H.-H., Großmann, J., Dahmke, A.**, 2012b. Investigation of the geochemical impact of CO₂ on shallow groundwater: design and implementation of a CO₂ injection test in Northeast Germany. *Environmental Earth Sciences* 67, 335-349.
- Pickles, W., Cover, W.**, 2004. Hyperspectral geobotanical remote sensing for CO₂ storage monitoring. U.S. Department of Energy of the University of California.
- Prinn, R., Cunnold, D., Rasmussen, R., Simmonds, P., Alyea, F., Crawford, A., Fraser, P., Rosen, R.**, 1990. Atmospheric emissions and trends of nitrous oxide deduced from 10 years of ALE-GAGE data. *J. Geophys. Res.* 95, 18369-18385.
- Pruess, K.**, 2005. ECO2N: a THOUGH2 fluid property module for mixtures of water, NaCl, and CO₂. Lawrence Berkeley National Laboratory, CA. Earth Sciences Div., Berkeley.
- Pruess, K.**, 2008. On CO₂ fluid flow and heat transfer behavior in the subsurface, following leakage from a geologic storage

8. References

- reservoir. *Environmental Geology* 54, 1677-1686.
- Pruess, K.**, 2011. ECO2M: a THOUGH2 fluid property module for mixtures of water, NaCl, and CO₂, including super- and subcritical conditions, and phase change between liquid and gaseous CO₂. Lawrence Berkeley National Laboratory, Berkeley, Calif.
- Pruess, K., Oldenburg, C.M., Moridis, G.**, 1999. TOUGH2 user's guide. Version 2.0, Berkeley.
- Raistrick, M., Mayer, B., Shevalier, M., Perez, R.J., Hutcheon, I., Perkins, E., Gunter, B.**, 2006. Using chemical and isotopic data to quantify ionic trapping of injected carbon dioxide in oil field brines. *Environmental Science and Technology* 40, 6744-6749.
- Redondo, R., Yélamos, J.G.**, 2005. Determination of CO₂ origin (natural or industrial) in sparkling bottled waters by ¹³C/¹²C isotope ratio analysis. *Food Chemistry* 92, 507-514.
- Rein, A., Hoffmann, R., Dietrich, P.**, 2004. Influence of natural time-dependent variations of electrical conductivity on DC resistivity measurements. *Journal of Hydrology* 285, 215-232.
- Road-Map**, 2007. Carbon Sequestration Technology Road Map and Program Plan. In: Energy, U.S.D.o. (Ed.). National Energy Technology Laboratory, Washington DC.
- Rockstrom, J., Steffen, W., Noone, K., Persson, A., Chapin, F.S., Lambin, E.F., Lenton, T.M., Scheffer, M., Folke, C., Schellnhuber, H.J., Nykvist, B., de Wit, C.A., Hughes, T., van der Leeuw, S., Rodhe, H., Sorlin, S., Snyder, P.K., Costanza, R., Svedin, U., Falkenmark, M., Karlberg, L., Corell, R.W., Fabry, V.J., Hansen, J., Walker, B., Liverman, D., Richardson, K., Crutzen, P., Foley, J.A.**, 2009. A safe operating space for humanity. *Nature* 461, 472-475.
- Rozemeijer, J., van der Velde, Y., de Jonge, H., van Geer, F., Broers, H.-P., Bierkens, M.**, 2010. Application and evaluation of a new passive sampler for measuring average solute concentrations in a catchment scale water quality monitoring study. *Environmental Science & Technology* 44, 1353-1359.
- Sadowsky, M., Schortemeyer, M.**, 1997. Soil microbial responses to increased concentrations of atmospheric CO₂. *Global Change Biology* 3, 217-224.
- Saripalli, P., McGrail, P.**, 2002. Semi-analytical approaches to modeling deep well injection of CO₂ for geological sequestration. *Energy Conversion & Management* 43, 185-198.
- Sarmiento, J., L., Gruber, N.**, 2002. Sinks for anthropogenic carbon. *Physics Today* 55, 30-36.
- Schaap, H.**, 2002. Rosetta database. University of Arizona.
- Schön, J.H.**, 1996. Physical properties of rocks: fundamentals and principles of petrophysics. Pergamon Press, New York.
- Schulmeister, M.K., Butler, J.J., Healey, J.M., Zheng, L., Wysocki, D.A., McCall, G.W.**, 2003. Direct-push electrical conductivity logging for high-resolution hydrostratigraphic characterization. *Ground Water Monitoring & Remediation* 23, 52-62.
- Schulz, A., Vogt, C., Richnow, H.-H.**, 2012. Effects of high CO₂ concentrations on ecophysiologicaly different microorganisms. *Environmental Pollution* 169, 27-34.
- Schütze, C., Sauer, U., Beyer, K., Lamert, H., Bräuer, K., Strauch, G., Flechsig, C., Kämpf, H., Dietrich, P.**, 2012. Natural analogues: a potential approach for developing reliable monitoring methods to understand subsurface CO₂ migration processes. *Environmental Earth Sciences* 67, 411-423.
- Schuur, E.A.G., Bockheim, J., Canadell, J.G., Euskirchen, E., Field, C.B., Goryachkin, S.V., Hagemann, S., Kuhry, P., Lafleur, P.M., Lee, H., Mazhitova, G., Nelson, F.E., Rinke, A., Romanovsky, V.E., Shiklomanov, N., Tarnocai, C., Venevsky, S., Vogel, J.G., Zimov, S.A.**, 2008. Vulnerability of permafrost carbon to climate change: implications for the global carbon cycle. *BioScience* 58, 701-714.
- Sears, D.F., Eisenberg, R.M.**, 1961. A model representing a physiological role of CO₂ at the cell membrane. *Journal of General Physiology* 44, 869-887.
- Selker, J., Niemet, M., McDuffie, N., Gorelick, S., Parlange, J.-Y.**, 2007. The local geometry of gas injection into saturated homogeneous porous media. *Transport in Porous Media* 68, 107-127.
- Severinghaus, J.W., Bradley, A.F.**, 1958. Electrodes for blood pO₂ and pCO₂

8. References

- determination. *Journal of Applied Physiology* 13, 515-520.
- Shi, J., Q., Durucan, S.**, 2005. CO₂ storage in deep unmineable coal seams. *Oil & Gas Science and Technology - Rev. IFP* 60, 547-558.
- Shipton, Z.K., Evans, J.P., Kirchner, D., Kolesar, P.T., Williams, A.P., Heath, J.**, 2004. Analysis of CO₂ leakage through "low-permeability" faults from natural reservoirs in the Colorado Plateau, southern Utah. In: Baines, S.J., Worden, R.H. (Eds.). *Geological storage of carbon dioxide*. Geological Society, London, pp. 43-58.
- Simunek, J., van Genuchten, M.T.**, 1999. HYDRUS 2D software, version 2.0. International Groundwater Modeling Center, Colorado.
- Singh, A.K., Pilz, P., Zimmer, M., Kalbacher, T., Görke, U.J., Kolditz, O.**, 2012. Numerical simulation of tracer transport in the Altmark gas field. *Environmental Earth Sciences* 67, 537-548.
- Solomon, S.**, 2007. Carbon dioxide storage: Geological security and environmental issues - case study on the Sleipner gas field in Norway. In: Bellona (Ed.). *The Bellona Foundation*, p. 128.
- Song, J., Zhang, D.**, 2012. Comprehensive review of caprock-sealing mechanisms for geologic carbon sequestration. *Environmental Science & Technology*.
- Spangler, L., Dobeck, L., Repasky, K., Nehrir, A., Humphries, S., Barr, J., Keith, C., Shaw, J., Rouse, J., Cunningham, A., Benson, S., Oldenburg, C., Lewicki, J., Wells, A., Diehl, J., Strazisar, B., Fessenden, J., Rahn, T., Amonette, J., Barr, J., Pickles, W., Jacobson, J., Silver, E., Male, E., Rauch, H., Gullickson, K., Trautz, R., Kharaka, Y., Birkholzer, J., Wielopolski, L.**, 2010. A shallow subsurface controlled release facility in Bozeman, Montana, USA, for testing near surface CO₂ detection techniques and transport models. *Environmental Earth Sciences* 60, 227-239.
- Spilimbergo, S., Bertucco, A.**, 2003. Non-thermal bacterial inactivation with dense CO₂. *Biotechnology and Bioengineering* 84, 627-638.
- Stevens, S., Kuuskraa, V., Gale, J.**, 2001. Sequestration of CO₂ in Depleted Oil and Gas Fields: Global capacity, costs and barriers. *Proceedings of the 5th Annual Greenhouse Gas Technology Conference*.
- Stier, R.F., Bell, L., Ito, K.A., Shafer, B.D., Brown, L.A., Seeger, M.L., Allen, B.H., Porcuna, M.N., Lerke, P.A.**, 1981. Effect of modified atmosphere on *C. botulinum* toxigenesis and the spoilage microflora of Salmon fillets. *Journal of Food Science* 46, 1639-1642.
- Strumilo, S.**, 2005. Short-term regulation of the alpha-ketoglutarate dehydrogenase complex by energy-linked and some other effectors. *Biochemistry (Moscow)* 70, 726-729.
- Stumpp, C., Engelhardt, S., Hofmann, M., Huwe, B.**, 2009. Evaluation of pedotransfer functions for estimating soil hydraulic properties of prevalent soils in a catchment of the Bavarian Alps. *European Journal of Forest Research* 128, 609-620.
- Sturges, W.T., Wallington, T.J., Hurley, M.D., Shine, K.P., Sihra, K., Engel, A., Oram, D.E., Penkett, S.A., Mulvaney, R., M., B.C.A.**, 2000. Trifluoromethyl sulfur pentafluoride (SF₅CF₃) and sulfur hexafluoride (SF₆) from Dome Concordia. *Trends: A Compendium of Data on Global Change*. Carbon Dioxide Information Analysis Center, Oak Ridge National Laboratory, Oak Ridge, Tenn., U.S.A.
- Tan, K.H., Gill, C.O.**, 1982. Physiological basis of CO₂ inhibition of a meat spoilage bacterium, *Pseudomonas fluorescens*. *Meat Science* 1.
- Tans, P.**, 2012. Trends in atmospheric carbon dioxide. In: Laboratory, U.S.D.o.C.-N.O.a.A.A.E.S.R. (Ed.). <http://www.esrl.noaa.gov/gmd/ccgg/trends/index.html#global>.
- Tarnocai, C., Canadell, J.G., Schuur, E.A.G., Kuhry, P., Mazhitova, G., Zimov, S.**, 2009. Soil organic carbon pools in the northern circumpolar permafrost region. *Global Biogeochem. Cycles* 23, GB2023.
- Taub, D.**, 2010. Effects of rising atmospheric concentrations of carbon dioxide on plants. *Nature Education Knowledge* 3.
- Taub, D.R., Miller, B., Allen, H.**, 2008. Effects of elevated CO₂ on the protein concentration of food crops: a meta-analysis. *Global Change Biology* 14, 565-575.

8. References

- Teixeira de Mattos, M.J., Plomp, P.J.A.M., Neijsseln, O.M., Tempest, D.W.**, 1984. Influence of metabolic end-products on the growth efficiency of *Klebsiella aerogenes* in anaerobic chemostat culture. *Antonie van Leeuwenhoek* 50, 461-472.
- Thomson, N.R., Johnson, R.L.**, 2000. Air distribution during in situ air sparging: an overview of mathematical modeling. *Journal of Hazardous Materials* 72, 265-282.
- Tissot, B.P., Welte, D.H.**, 1984. Petroleum formation and occurrence. Springer, Berlin.
- Torp, T.A., Gale, J.**, 2004. Demonstrating storage of CO₂ in geological reservoirs: The Sleipner and SACS projects. *Energy* 29, 1361-1369.
- Turbé, A., De Toni, A., Benito, P., Lavelle, P., Lavelle, P., Ruiz, N., Van der Putten, W.H., Labouze, E., Mudgal, S.**, 2010. Soil biodiversity: functions, threats and tools for policy makers. Bio Intelligence Service, IRD, and NIOO, Report for European Commission (DG Environment).
- Valley, G., Rettger, L.F.**, 1927. The influence of carbon dioxide on bacteria. *Journal of Bacteriology* 14, 101-137.
- van Genuchten, M.T.**, 1980. A closed-form equation for predicting the hydraulic conductivity of unsaturated soils. *Soil Sci. Soc. Am. J.* 44, 892-898.
- Verreydt, G., Bronders, J., Van Keer, I., Diels, L., Vanderauwera, P.**, 2010. Passive samplers for monitoring VOCs in groundwater and the prospects related to mass flux measurements. *Ground Water Monitoring & Remediation* 30, 114-126.
- Vienken, T., Leven, C., Dietrich, P.**, 2012. Use of CPT and other direct push methods for (hydro-) stratigraphic aquifer characterization — a field study. *Canadian Geotechnical Journal* 49, 197-206.
- Walker, H.H.**, 1932. Carbon dioxide as a factor affecting lag in bacterial growth. *Science* 76, 602-604.
- Wang, S., Jaffe, P.R.**, 2004. Dissolution of a mineral phase in potable aquifers due to CO₂ releases from deep formations; effect of dissolution kinetics. *Energy Conversion and Management* 45, 2833-2848.
- Wardle, D.A.**, 1999. Biodiversity, ecosystem and interactions that transcend the interface. *Trends in Ecology and Evolution* 14, 125-127.
- Warrick, R.A., Gifford, R.M., Parry, M.L.**, 1986. Assessing the response of food crops to the direct effects of increased CO₂ and climatic change. In: B. Bolin, J.J., B. R. Döös, Warrick, R. A. (Ed.). *SCOPE 29 - The Greenhouse Effect, Climatic Change, and Ecosystem*.
- Watson, R.T., Zinyowera, M.C., Moss, R.H.**, 1996. Climate change impacts 1995. Impacts, adaptations and mitigation of climate change: scientific-technical analyses. Cambridge University Press, Cambridge.
- White, C.M., Strazisar, B.R., Granite, E.J., Hoffman, J.S., Pennline, H.W.**, 2003. Separation and capture of CO₂ from large stationary sources and sequestration in geological formations—coalbeds and deep saline aquifers. *Journal of the Air & Waste Management Association* 53, 645-715.
- Widdel, F.**, 2010. Theory and measurement of bacterial growth. University Bremen, p. 11.
- Wilkin, R.T., DiGiulio, D.C.**, 2010. Geochemical impacts to groundwater from geologic carbon sequestration: controls on pH and inorganic carbon concentrations from reaction path and kinetic modeling. *Environmental Science & Technology* 44, 4821-4827.
- Wilson, E., Friedmann, S., Pollak, M.**, 2007. Research for deployment: incorporating risk, regulation, and liability for carbon capture and sequestration. *Environ Sci Technol* 41, 5945 - 5952.
- Wilson, E.J., Gerard, D.**, 2007. Carbon capture and sequestration: integrating technology, monitoring and regulation. Blackwell Publishing, Ames, IA.
- Wimpenny, J.W.T.**, 1969. Oxygen and carbon dioxide as regulators of microbial growth and metabolism. In: Meadow, P., Pirt, S.J. (Eds.). *Microbial Growth*. Cambridge: Cambridge University Press, pp. 161-197.
- Wolfe, S.K.**, 1980. Use of CO₂-enriched and CO₂-enriched atmospheres for meats, fish and produce. *Food Technology* 34, 55-58.
- Wood, H.G., Werkman, C.H., Hemingway, A., Nier, A.O.**, 1941. Heavy carbon as a tracer in heterotrophic carbon dioxide assimilation. *Journal of Biological Chemistry* 139, 365-376.
- Wu, B., Shao, H., Hu, Z.W., Tang, Y.J., Jun, Y.-S.**, 2010. Viability and metal reduction of *Shewanella oneidensis* MR-1

8. References

under CO₂ stress: Implications for ecological effects of CO₂ leakage from geologic CO₂ sequestration. *Environmental Science and Technology* 44, 9213-9218.

Xiaoding, X., Moulijn, J.A., 1996. Mitigation of CO₂ by chemical conversion: plausible chemical reactions and promising products. *Energy & Fuels* 10, 305-325.

Yagi, H., Yoshida, F., 1977. Desorption of carbon dioxide from fermentation broth. *Biotechnology and Bioengineering* 19, 801-819.

Yang, Y.-M., Small, M.J., Ogretim, E.O., Gray, D.D., Bromhal, G.S., Strazisar, B.R., Wells, A.W., 2011. Probabilistic design of a near-surface CO₂ leak detection system. *Environmental Science & Technology* 45, 6380-6387.

Yoshimura, K., Liu, Z., Cao, J., Yuan, D., Inokura, Y., Noto, M., 2004. Deep source CO₂ in natural waters and its role in extensive tufa deposition in the Huanglong Ravines, Sichuan, China. *Chemical Geology* 205, 141-153.

Zheng, L., Apps, J.A., Zhang, Y., Xu, T., Birkholzer, J.T., 2009. On mobilization of lead and arsenic in groundwater in response to CO₂ leakage from deep geological storage. *Chemical Geology* 268, 281-297.

9. Acknowledgements

Even if it is not possible to name everybody that helped me finishing this work, I want to express my thanks to some of them. First, I want to thank my supervisor **Dr. Hans Hermann Richnow** for giving me the opportunity to do my PhD at the UFZ. Furthermore, I want to thank **Prof. Andreas Dahmke** for the good cooperation and for giving me the chance to submit and defend my thesis at the Institute of Applied Geosciences at the CAU Kiel. Special thanks go to my second supervisor **Dr. Carsten Vogt**. His calm and patient character helped me a lot during the work on the project. He was always willing to listen to my questions, concerns and complains and he helped me a lot in finding the focus of the thesis. I want to thank **Dr. Anita Peter** for the good organization and coordination of the whole project. Additional thanks go to **Hendrik Lamert**, who was a great partner within the project. Thanks for the interesting and exciting weeks of field work and for sharing beer, Glühwein and junk food. I also want to thank **Helko Kotas** and **Andreas Schoßland** for making the field work always so funny and lively.

Besides my supervisors, I want to thank many people from the Department Isotope Biogeochemistry from the UFZ. The working atmosphere was great and my colleagues helped me during all the ups and downs. Special thanks go to **Marie, Conrad, Steffen, Nuria, Kristina and Arne**. I enjoyed the lunch breaks, the coffee breaks and I have to thank you that you always listened so patient to my bad jokes without casting me out. It was great to share all the experiences with you. I also want to thank **Jana R.** for sharing all the gossip and for being there when I needed it. I need to thank **Frau Paul** for her fantastic organization of all the paper work and for the conspirative knitting meetings. Furthermore I want to thank **Uschi** for the nice chats in the morning, for her help in the isotope lab and for taking care of my health.

I want to thank **my family**, who supported me with fantastic food and wine and who always trusted in me and never complained when I didn't have enough time to visit. I want to thank my close friends **Franziska** and **Johannes** for being true and reliable friends and for supporting me with their understanding and motivation during all the time. Finally, I want to thank **Frank** for letting me know that there are more important things in life than work, for teaching me how to have real breakfast, for laughing loud about my bad jokes and for telling even worse ones, and for the feeling that I can trust in the future.

10. List of publications

10.1 Articles and manuscripts

- (1) **Schulz, Alexandra**; Vogt, Carsten; Lamert, Hendrik; Peter, Anita; Heinrich, Ben; Dahmke, Andreas; Richnow, Hans-Hermann. Monitoring of a simulated CO₂ leakage in a shallow aquifer using stable carbon isotopes. *Environmental Science and Technology*, 2012, 46 (20); pp 11243-11250.
- (2) **Schulz, Alexandra**; Vogt, Carsten; Richnow, Hans-Hermann. Effects of high CO₂ concentrations on ecophysiologicaly different microorganisms. *Environmental Pollution*, 2012, 169, pp 27-34.
- (3) Lamert, Hendrik; Geistlinger, Heinrich; Werban, Ulrike; Schütze, Claudia, Peter, Anita; Hornbruch, Götz; **Schulz, Alexandra**; Pohlert, Marco; Kalia, S.; Großmann, Jochen; Dahmke, Andreas, Dietrich, Peter. Feasibility of geoelectrical monitoring and multiphase modeling for process understanding of gaseous CO₂ injection into a shallow aquifer. *Environmental Earth Sciences*, 2012, 67, pp 447-462
- (4) Peter, Anita; Lamert, Hendrik; Beyer, Matthias; Hornbruch, Götz; Heinrich, Ben; **Schulz, Alexandra**; Geistlinger, Helmut; Schreiber, Ben; Dietrich, Peter; Werban, Ulrike; Vogt, Carsten; Richnow, Hans-Hermann; Großmann, Jochen; Dahmke, Andreas. Investigation of the geochemical impact of CO₂ on shallow groundwater: design and implementation of a CO₂ injection test in Northeast Germany. *Environmental Earth Sciences*, 2012, 67 (2), pp 335-349.
- (5) **Schulz, Alexandra**; Seifert, Jana; Vogt, Carsten; Morris, Brandon; Richnow, Hans-Hermann. Changes in the proteome of soil bacteria induced by elevated CO₂ concentrations. In preparation

10.2 Conference posters

- (1) **Schulz, Alexandra**; Vogt, Carsten; Richnow, Hans-H. (2010): Simulation of carbon dioxide leakage into a shallow aquifer and resulting effects on characteristic microorganisms. i-SUP Innovation for Sustainable Production, Bruges, Belgium.
- (2) **Schulz, Alexandra**; Vogt, Carsten; Richnow, Hans-H. (2010): Simulation of carbon dioxide leakage into a shallow aquifer and resulting effects on characteristic microorganisms. GeoDarmstadt, Darmstadt.
- (3) **Schulz, Alexandra**; Vogt, Carsten; Richnow, Hans-H. (2012): Simulation of carbon dioxide leakage into a shallow aquifer and resulting effects on characteristic microorganisms. VAAM Jahrestagung der Vereinigung für Allgemeine und Angewandte Mikrobiologie, Tübingen.

10. List of publications

- (4) Lamert, Hendrik; Werban, Ulrike, **Schulz Alexandra**; Steinbrueckner, Daniel; Peter, Anita; Hornbruch, Götz; Dahmke, Andreas; Beyer, Matthias; Heinrich, Ben; Großmann, Jochen; Dietrich, Peter (2011) CO₂ injection test in a shallow aquifer – Monitoring by using different technologies. AGU (American Geophysical Union) Fall Meeting, 05. - 09.12.2011, San Francisco.
- (5) Lamert, Hendrik; Werban, Ulrike; **Schulz, Alexandra**, Peter, Anita; Hornbruch, Götz; Dahmke, Andreas; Schreiber, B; Beyer, Matthias; Heinrich, Ben; Großmann, Jochen; Dietrich, Peter (2011) CO₂ injection test in a shallow aquifer – Evaluation of DC geoelectrics for process monitoring. Statusseminar Geotechnologien, 20.-21.09.2011, Potsdam.
- (6) Lamert, Hendrik; Werban, Ulrike; **Schulz, Alexandra**, Peter, Anita; Hornbruch, Götz; Dahmke, Andreas; Beyer, Matthias; Heinrich, Ben; Großmann, Jochen; Dietrich, Peter; CO₂ injection test in a shallow aquifer – Using DC Geoelectrics for process monitoring. 72. Jahrestagung der Deutschen Geophysikalischen Gesellschaft (DGG), 05. - 08. 3. 2012, Hamburg.
- (7) Peter, Anita; Hornbruch, Götz; Lamert, Hendrik; Werban, Ulrike; Beyer, Matthias; Geistlinger, Helmut; Richnow, Hans; Vogt, Carsten; **Schulz, Alexandra**; Lazik, Detlef; Großmann, Jochen; Dietrich, Peter; Schäfer, D.; Dahmke, Andreas (2010): CO₂ leakage test in a shallow aquifer for investigating the geochemical impact of CO₂ on groundwater and for developing monitoring methods and concepts. Poster at GHGT10 Greenhouse Gas Technologies 2010, Amsterdam, the Netherlands.

10.3 Talks

- (1) **Schulz, Alexandra**; Vogt, Carsten; Peter, Anita; Lamert, Hendrik, Heinrich, Ben; Richnow, Hans-H. (2011): Monitoring of a simulated carbon dioxide leakage into a shallow aquifer using stable carbon isotopes. AIG, Symposium on Applied Isotope Geochemistry, Tarragona, Spanien.
- (2) **Schulz, Alexandra**; Vogt, Carsten; Richnow, Hans-H.; Lamert, Hendrik, Peter, Anita; (2012): Stable isotope monitoring of a simulated carbon dioxide leakage in a shallow aquifer. HIGRADE Conference, Leipzig, Germany.
- (3) Lamert, Hendrik; Dietrich, Peter; Werban, Ulrike; Schütze, Claudia; Steinbrueckner, Daniel; **Schulz, Alexandra**; Peter, Anita; Hornbruch, Götz; Großmann, Jochen; Beyer, Matthias (2011) CO₂ injection test in a shallow aquifer: Using DC geoelectrics for process monitoring. 1st International Workshop on Geoelectrical Monitoring (GELMON), 30.11.-02.12.11, Vienna.

10. List of publications

- (4) **Schulz, Alexandra**; Vogt, Carsten; Richnow, H.; Peter, Anita; Lamert, Hendrik; Beyer, Matthias; Hornbruch, Götz; Heinrich, Ben; Geistlinger, Helmut; Werban, Ulrike; Dietrich, Peter; Großmann, Jochen; Dahmke, Andreas (2010): „Vorstellung des Forschungsvorhabens „CO₂-Injektionsversuchs in einen oberflächennahen Aquifer zur Erprobung von Monitoringmethoden und –konzepten – Mikrobiologische Versuche und Isotopenmonitoring“. Öffentliche Informationsveranstaltung im Rathaus Wittstock.
- (5) Peter, Anita; Hornbruch, Götz; Lamert, Hendrik; Werban, Ulrike; Beyer, Matthias; Geistlinger, Helmut; Richnow, Hans; Vogt, Carsten; **Schulz, Alexandra**; Lazik, Detlef; Großmann, Jochen; Dietrich, Peter; Schäfer, D.; Dahmke, Andreas (2010): “CO₂ leakage test in a shallow aquifer for investigating the geochemical impact of CO₂ on groundwater and for developing monitoring methods and concepts.” Institute for Geoscience, University Copenhagen, Denmark.
- (6) Peter, Anita; Lamert, Hendrik; Beyer, Matthias; Hornbruch, Götz; Heinrich, Ben; **Schulz, Alexandra**; Geistlinger, Helmut; Werban, Ulrike; Dietrich, Peter; Vogt, Carsten; H. Richnow; Großmann, Jochen; Dahmke, Andreas (2011): “CO₂-Injection test in a shallow Forschungsvorhaben 03G0670A-C Abschlussbericht Seite 70 aquifer to investigate the geochemical impact on groundwater and to test monitoring methods”, Statusseminar Geotechnologien am GFZ in Potsdam.
- (7) **Schulz, Alexandra**; Vogt, Carsten; Richnow, H.; Peter, Anita; Lamert, Hendrik; Beyer, Matthias; Hornbruch, Götz; Heinrich, Ben; Geistlinger, Helmut; Werban, Ulrike; Dietrich, Peter; Großmann, Jochen; Dahmke, Andreas (2012): „Ergebnisse der mikrobiellen Untersuchungen und des Isotopenmonitorings im Rahmen des CO₂-Injektionsversuchs in einen oberflächennahen Aquifer“. Öffentliche Informationsveranstaltung zum Abschluss des Projektes im Rathaus Wittstock.

11. Curriculum vitae**Personal details**

Date of birth	11. June 1983
Place of birth	Halle/ Saale, Germany
Address	Mozartstraße 21, 04107 Leipzig

Education

09.2009 - today	PhD at the Helmholtz-Centre for Environmental Research – UFZ, Department Isotope Biogeochemistry
04.2004 - 07.2009	Martin-Luther University Halle-Wittenberg, Germany Geology/ Palaeontology ▪ Diploma/ Master
01.2009 - 03.2009	Visiting scholar at the University of Pretoria, South Africa
01.2008 - 07.2008	Diploma Thesis at the Technical University of Darmstadt, Germany
08.2007 - 12.2007	Institute of Geomaterial Sciences
08.1994 - 06.2003	ERASMUS at the Université de la Réunion
2003	Abitur/ Latina August Hermann Francke Gymnasium Halle/ Saale

Work experiences

11.2012	Interpreter for Explore Resources
11.2009 - 11.2011	Interpreter for Great Basin Gold Ltd.
07.2011 - 08.2011	Internship at the Helmholtz-Centre for Environmental Research – UFZ, Leipzig, Germany Department of Lake Research
10.2006 - 07.2009	Student assistant at the Institute of Mineralogy and Geochemistry at the Martin-Luther University Halle-Wittenberg, Germany
11.2008	Interpreter for Yukon Nevada Gold Corp.
02.2007 - 03.2007	Internship at the Centre of Material Analysis in Lauf, Germany

Eidesstattliche Erklärung

Hiermit erkläre ich, dass die vorliegende Arbeit von mir selbständig angefertigt wurde, abgesehen von der Beratung durch meine Betreuer und unter Anwendung der entsprechend gekennzeichneten Hilfsmittel und Literaturangaben. Mit Ausnahmen der gekennzeichneten Teile ist die Arbeit noch nicht veröffentlicht oder zur Veröffentlichung eingereicht. Die Arbeit ist unter Einhaltung der Regeln guter wissenschaftlicher Praxis der Deutschen Forschungsgemeinschaft entstanden.

Die Arbeit wurde bisher weder im In- noch im Ausland in gleicher oder ähnlicher Form einer anderen Prüfungsbehörde vorgelegt.

Leipzig, den 25. Januar 2013

Dipl.-Geologin Alexandra Schulz

Appendix A

Investigation of the geochemical impact of CO₂ on shallow groundwater: design and implementation of a CO₂ injection test in Northeast Germany

Peter, Anita; Lamert, Hendrik; Beyer, Matthias; Hornbruch, Götz; Heinrich, Ben; Schulz, Alexandra; Geistlinger, Helmut; Schreiber, Ben; Dietrich, Peter; Werban, Ulrike; Vogt, Carsten; Richnow, Hans-Hermann; Großmann, Jochen; Dahmke, Andreas

Environmental Earth Sciences, 2012, 67 (2), pp 335-349

Investigation of the geochemical impact of CO₂ on shallow groundwater: design and implementation of a CO₂ injection test in Northeast Germany

Anita Peter · Hendrik Lamert · Matthias Beyer · Götz Hornbruch · Ben Heinrich ·
Alexandra Schulz · Helmut Geistlinger · Ben Schreiber · Peter Dietrich · Ulrike Werban ·
Carsten Vogt · Hans-Hermann Richnow · Jochen Großmann · Andreas Dahmke

Received: 28 November 2011 / Accepted: 17 April 2012
© Springer-Verlag 2012

Abstract A small scale and temporally limited CO₂ injection test was performed in a shallow aquifer to investigate the geochemical impact of CO₂ upon such aquifers and to apply and verify different monitoring methods. Detailed site investigation coupled with multi-phase simulations were necessary to design the injection experiment and to set up the monitoring network, before CO₂ was injected over a ten-day period at three injection wells, at a depth of 18 m below surface level into a quaternary sand aquifer located close to the town of Wittstock in Northeast Germany. Monitoring methods comprised groundwater sampling and standard analyses, as well as

trace element analyses and isotope analyses; geoelectrical borehole monitoring; passive samplers to analyse temporally integrated for cations and multi-parameter probes that can measure continuously for dissolved CO₂, pH and electrical conductivity. Due to CO₂ injection, total inorganic carbon concentrations increased and pH decreased down to a level of 5.1. Associated reactions comprised the release of major cations and trace elements. Geoelectrical monitoring, as well as isotope analyses and multi-parameter probes proved to be suitable methods for monitoring injected CO₂ and/or the alteration of groundwater.

Keywords Carbon sequestration · CO₂ leakage · Risk assessment · Groundwater monitoring

A. Peter (✉) · G. Hornbruch · A. Dahmke
Institute for Geosciences, University of Kiel,
Ludewig-Meyn-Str. 10, 24118 Kiel, Germany
e-mail: anita.peter@gpi.uni-kiel.de

H. Lamert · P. Dietrich · U. Werban
Department Monitoring and Exploration Technologies,
Helmholtz Centre for Environmental Research - UFZ,
Permoserstr. 15, 04318 Leipzig, Germany

M. Beyer · B. Heinrich · B. Schreiber · J. Großmann
GICON GmbH, Tiergartenstr. 48, 01219 Dresden, Germany

A. Schulz · C. Vogt · H.-H. Richnow
Department of Isotope Biogeochemistry,
Helmholtz Centre for Environmental Research - UFZ,
Permoserstr. 15, 04318 Leipzig, Germany

H. Geistlinger
Department of Soil Physics, Helmholtz Centre
for Environmental Research - UFZ, Theodor-Lieser-Str. 4,
06120 Halle, Saale, Germany

P. Dietrich
Center for Applied Geoscience, University of Tübingen,
Hölderlinstr. 12, 72074 Tübingen, Germany

Introduction

Leakage from subsurface storage sites is one of the main concerns connected with carbon capture and storage (CCS) technology. One potential risk associated with CO₂ leaking from storage sites is the geochemical alteration of shallow groundwater systems, causing a pH decrease and the potential mobilization of heavy metals due to mineral dissolution and/or desorption processes.

Although Lewicki et al. (2007) intensively studied sites with naturally occurring CO₂ to understand processes and phenomena of CO₂ leakages from deep formations into the surface, these natural analogues are unlikely to answer urgent questions regarding the impact of CO₂ intrusion on a pristine aquifer that has not as yet been in contact with CO₂. Several studies have investigated either by modelling (e.g. Wang and Jaffe 2004; Zheng et al. 2009; Apps et al. 2010; Wilkin and Digiulio 2010) or by laboratory experiments (e.g. Little and Jackson 2010; Lu et al. 2010) the

effect of CO₂ on shallow pristine aquifers. Consistently, all report decreasing pH with increasing TIC (total inorganic carbon) and HCO₃⁻ concentrations. Concerning the behaviour of cations, the modelling studies suggest that the release of cations such as lead, arsenic, zinc and other heavy metals occurs due to mineral dissolution (Wang and Jaffe 2004) and/or due to desorption from surface complexation (Zheng et al. 2009). Both studies emphasize the high sensitivity of relevant modelling parameters, such as dissolution and sorption kinetics, on the simulated release of cations, thus they recommend performing lab and field experiments, to gain an insight into the geochemical processes and parameters. Lab experiments, where natural aquifer sediment samples were exposed to CO₂ enriched water, showed that concentrations of various metals increased with increasing TIC and decreasing pH (e.g. Ca, Fe, Mn, Ba were reported by Little and Jackson 2010 and Lu et al. 2010); however, other cations decreased with increasing TIC and decreasing pH (e.g. As, Mo, Cr as reported by Little and Jackson 2010). Some cations are reported to behave in either way, for example, aluminium was observed to increase in some experiments (Lu et al. 2010), while Little and Jackson (2010) noticed decreases of aluminium with decreasing pH.

The first and to our knowledge so far only test site, where CO₂ was injected into a pristine shallow aquifer under field conditions is the ZERT site in Montana (Spangler et al. 2010), where CO₂ was injected at a depth of 1.1–2.5 m below surface level and approximately 0.5–1 m under the groundwater table. Although the aim of the study was to monitor the unsaturated zone, intense groundwater sampling was also performed at the ZERT site, showing increases in major divalent cation concentrations and increasing trace metal concentrations in groundwater with increasing alkalinity (Kharaka et al. 2010; Zheng et al. 2012).

The aim of the present study is to further understand the CO₂ behaviour in shallow groundwater systems, as a basis for sound risk assessment of CCS technology. Therefore, a CO₂ injection experiment was performed during a 10-day period in March and April 2011, with the following objectives: firstly, to gain an insight into the potential geochemical reactions taking place in a shallow, carbonate-free aquifer system that is subject to CO₂ intrusion. Secondly, to verify whether reactive transport models are capable of predicting these reactions in a reliable manner, i.e. whether they are suitable for sound risk assessment and thirdly, to develop, test and apply different monitoring methods that are appropriate to monitor CO₂ intrusions and/or the geochemical alteration of groundwater due to CO₂ intrusions.

The present paper provides an overview of the test site, the design and operation of the injection experiment and

the different monitoring methods applied. Besides groundwater sampling and subsequent analyses, geoelectrical single-borehole and borehole-borehole measurements, stable isotope analyses of ¹³C/¹²C, continuously operating multi-parameter probes including pH, electrical conductivity and CO₂ and passive samplers were also applied to monitor released cations on an integral temporal scale. First results from the different monitoring methods are presented in this paper, while further publications (e.g. Lamert et al. 2012) will present in detail results of the various methods used and the accompanying modelling studies.

Test site

The test site is part of a former military airfield, located approximately 100 km north of Berlin, in the state of Brandenburg/Germany, close to the town of Wittstock. The test site is a fallow plane of approximately 90 m × 60 m (see Fig. 1). Due to its historical usage as a military airfield, minor TCE contamination was found in the groundwater in parts of the test site (concentrations up to 58 µg/L).

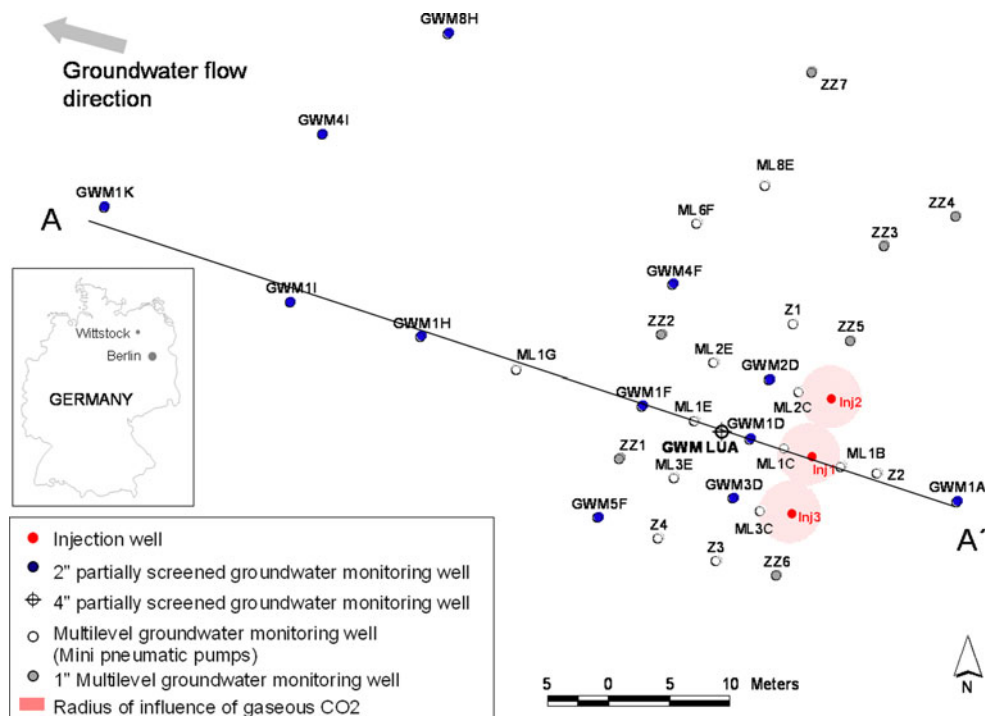
Geology

A detailed geological characterization of the test site was performed between March 2010 and March 2011. Firstly, geoelectrical surveys were performed. Five electrical resistivity tomography profiles (of approximately 250 m length and 20 m distance each) provided initial information about the stratigraphic composition of the near subsurface. Based on the resistivity tomography results, relevant locations for direct push (DP)-soundings were selected to obtain high resolution vertical profiles of various soil-specific properties (Dietrich and Leven 2006).

Hydraulic profiling tool (HPT) profiles (Dietrich et al. 2008) were used to derive estimates of hydraulic conductivity (K) based on the ratio of injected water flow rate and the corresponding pressure response (Q/p). The higher the ratio Q/p , the higher the relative hydraulic conductivity of the sediment. The relative K values of the HPT logs were calibrated using slug-tests and sieve analyses (see also “[Injection test design and operation](#)”), resulting in vertical profiles of absolute hydraulic conductivities.

Electrical conductivity (EC) loggings (e.g. Schulmeister et al. 2003) allow for a high resolution characterization of electrical properties of these sediments, which can be interpreted with respect to lithostratigraphy. An increase in electrical conductivity indicates the presence of an increased proportion of silt and/or clay particles. In order to validate the EC and HPT logs, sediment cores were taken in the vicinity of the CO₂ injection wells (see Fig. 2).

Fig. 1 Map of test site for CO₂ injection with injection lances, groundwater monitoring wells and intersection line for geological cross-section (see Fig. 3)



As EC and HPT logs are generally anti-proportionally related (i.e. high EC values correspond to low permeable layers, i.e. to low HPT values), both profiles clearly relate to the geological profile obtained from the sediment core: for example in both profiles, the glacial loam 10 m below surface level can be clearly identified.

In total, nine DP EC/HPT-soundings together with borehole profiles at 38 locations (see also Fig. 1) served as a basis for the geological structure model. A geological profile and its subsequent hydro-geological interpretation is provided in Fig. 3 and Table 1.

The upper confined aquifer (aquifer 1) at the site is characterized by glacial sediments from the Vistula period, consisting of heterogeneous inter-bedded sand, silt, clay and humus layers, with a thickness of approximately 11 m. Below aquifer 1, glacial loam from the Saale stadium was detected which is of varying thicknesses (average of 0.5 m) and depths. Apart from a few exceptions, the loam could be extensively detected on the test site, however no glacial loam was found in some drilling samples located in the northwestern, northeastern and southern areas. In these areas, hydraulic contact between aquifer 1 and aquifer 2 can be assumed. Generally, the glacial loam is dipping in a south-westernly direction on the test site. In the eastern part near to the injection lances Inj1–Inj3, a dome-like arching of the glacial loam was detected (see Fig. 3).

Beneath the glacial loam, Saalian sediments of the main groundwater aquifer (aquifer 2) can be found. The thickness of aquifer 2 is approximately 8 m. The sediment of this aquifer consists primarily of medium sands with an

isolated layer of coarse sand in the eastern part of the test site. Coarse sand is especially present in the vicinity of the CO₂ injection wells, however tapers off towards the western direction. Both medium and coarse sands found here are free of carbonates (see Peter et al. 2011). In the western area of the test site, a spatially limited silt horizon within the sands of aquifer 2 was discovered, which is not present in the eastern side of the aquifer. Due to its extensive and relatively homogeneous occurrence, aquifer 2 was chosen as injection horizon for the CO₂.

Glacial till was encountered in eight drilling samples below aquifer 2, at an average depth of 19.5 m bgl. The glacial till acts as an aquiclude and forms the base of aquifer 2, as well as the lower limit of the geological structure model. Due to the limited sounding depth (maximum 24 m bgl), the base of the glacial till was not detected at the test site.

Hydrogeology

Regional groundwater flow is directed from east to west, towards the river Dosse, which acts as a drainage and is situated approximately 800 m apart from the injection wells.

In order to determine the local groundwater flow direction and flow velocity at the site, six groundwater wells were installed 60–160 m away from the injection wells (see also Peter et al. 2011), in addition to the monitoring wells depicted in Fig. 1. Groundwater levels measured in March and June 2011 at 25 monitoring wells

Fig. 2 EC-log, geologic profile and HPT-log located 2 m east of injection well Inj1

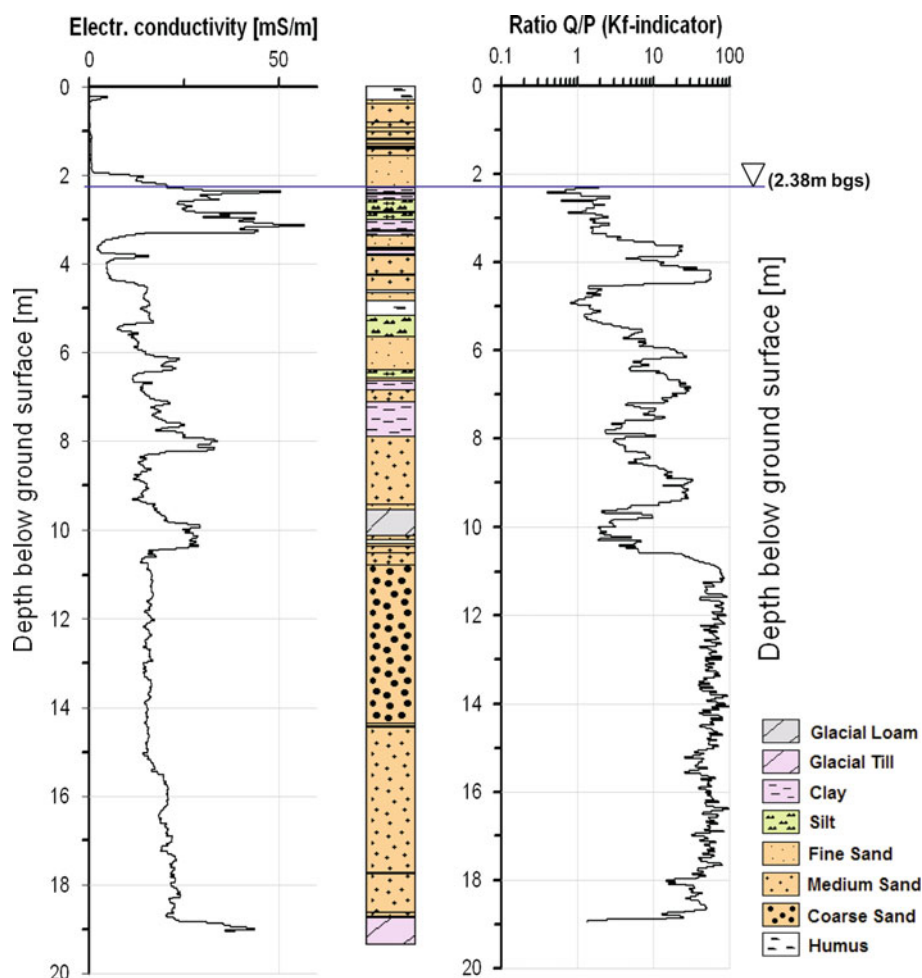
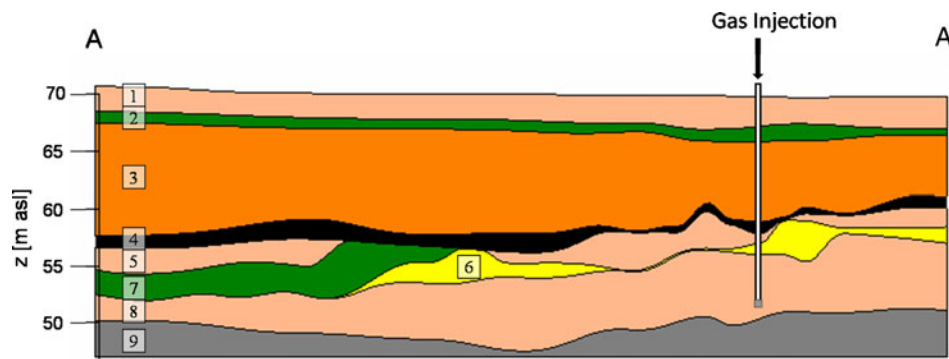


Fig. 3 Geologic profile from A to A' (see Fig. 1) with position of injection lance 1. Layer numbers refer to Table 1



revealed relatively small hydraulic gradients of about 1.4 ‰ in the eastern part of the test site down to monitoring well GWM1H, whereas gradients increase west of GWM1H to approximately 6.8 ‰. The groundwater flow direction derived from the groundwater levels confirms the general flow direction as being from east to west, however due to very small head differences within the injection area, no reliable conclusion could be made concerning the local flow direction at the injection lances.

Thus, a salt tracer test using electrical resistivity measurements (e.g. Hoffmann and Dietrich 2004) was performed in November 2010 to investigate the local flow regime in the vicinity of the CO₂ injection wells. In the present study, NaCl was added to drinking water to obtain a concentration of 10 g/L, to achieve a clear difference between electric conductivity values measured in the local groundwater (about 600 μS/cm) and in the injected saline water (about 17 mS/cm). The saline tracer was injected

Table 1 Schematic geologic profile at the test site

Average layer depth (m bgl)	Layer no.	Lithological description	Hydrogeologic classification
0–2	1	Sands (primarily medium sand)	Unsaturated zone
2–3.5	2	Silt	Unsaturated/saturated zone
3.5–11	3	Inter-bedded sand, silt, clay and humus layers	Aquifer 1
11–11.5	4	Glacial loam (discontinuous)	Aquiclude 1
11.5–13.5	5	Medium sand	Aquifer 2
13.5–15	6	Coarse sand (eastern area)	Aquifer 2
13.5–16	7	Silt (western area)	Local Aquiclude
15/16–19.5	8	Medium sand, some fine sand	Aquifer 2 (injection horizon)
>19.5	9	Glacial till	Aquiclude 2

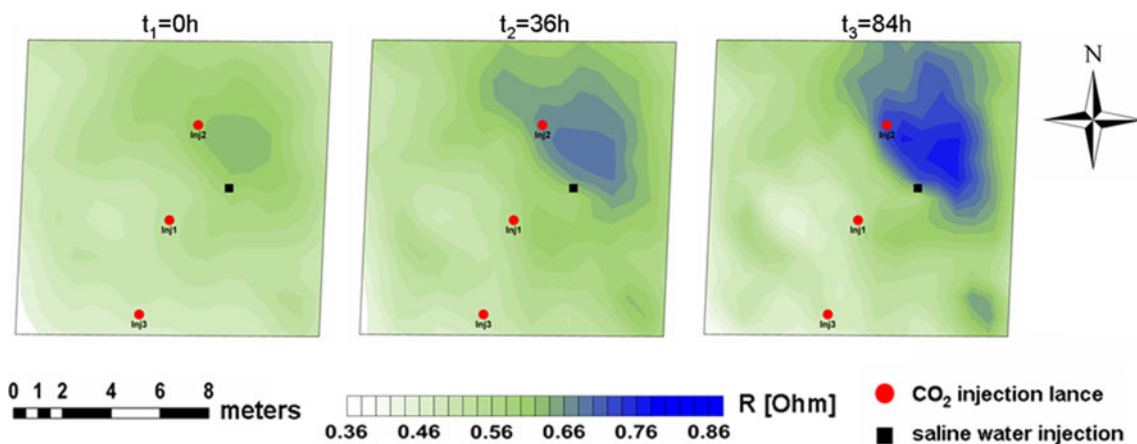


Fig. 4 Normalized equipotential lines of salt tracer injection at different times. *Left* before saline water injection; *middle* 36 h after saline water injection commenced; *right* 84 h after saline water injection commenced

with a constant flow of 0.4 L/min over a period of 84 h, in a depth of 13.2 m below ground level into aquifer 2.

The movement of the tracer was observed by charging the injected plume and by carrying out repeated measurements of electrical resistivity at various time steps, using electrodes installed at the surface. The resulting shift of normalized equipotential lines indicates a north–northwesterly groundwater flow direction in the vicinity of the central and northern injection wells (Fig. 4). Estimates of the local groundwater flow velocity based on tracer test data as well as on hydraulic gradients together with hydraulic conductivity values obtained from sieve analysis and slug-test data revealed groundwater flow velocities of <0.1 m/day up to 1 m/day.

Monitoring network

In order to enable spatially dense monitoring of the geochemically altered groundwater to be performed, 34 groundwater monitoring wells were installed, most of them being down-gradient from the injection lances (see Fig. 1).

Four different types of monitoring wells were installed between September 2010 and April 2011: (1) 12 two-inch

groundwater monitoring wells using a conventional dry drilling method. The wells were generally screened over a 6 m interval, in which the upper end of the screen is located 2 m below the glacial loam, which acts as a confining top layer for aquifer 2. This gap between the top end of the screen and the glacial loam should ensure that no gaseous CO₂ that spreads below the glacial loam could escape through the filter screen into the atmosphere. (2) One four-inch groundwater monitoring well was drilled, also using dry drilling technology. The larger diameter allows for equipment with multi-parameter probes (see “Monitoring of CO₂ and geochemically altered groundwater”). The filter screen covers 3 m (15–18 m bgl) of the injection horizon. (3) Seven one-inch groundwater monitoring wells were installed using SonicDrill technology, thus no annular space filling is required, as the wells were directly inserted into the collapsing borehole. However, bentonite sealing was installed at the depth of the glacial loam to prevent CO₂ ascent along the well casing. One-metre filter screens were installed at 12.5–13.5, 14.5–15.5 and 17.5–18.5 m depths, so that depth-oriented groundwater sampling using an inflatable packer system could be achieved. (4) Pneumatic driven low flow mini pumps were

installed directly into the sediment using Direct Push-technology. At 10 locations, three pumps were installed at each point at depths of 12, 15 and 18 m bgl, and at another four locations (Z1–Z4) a single pump was installed at a depth of approximately 1 m below the glacial loam.

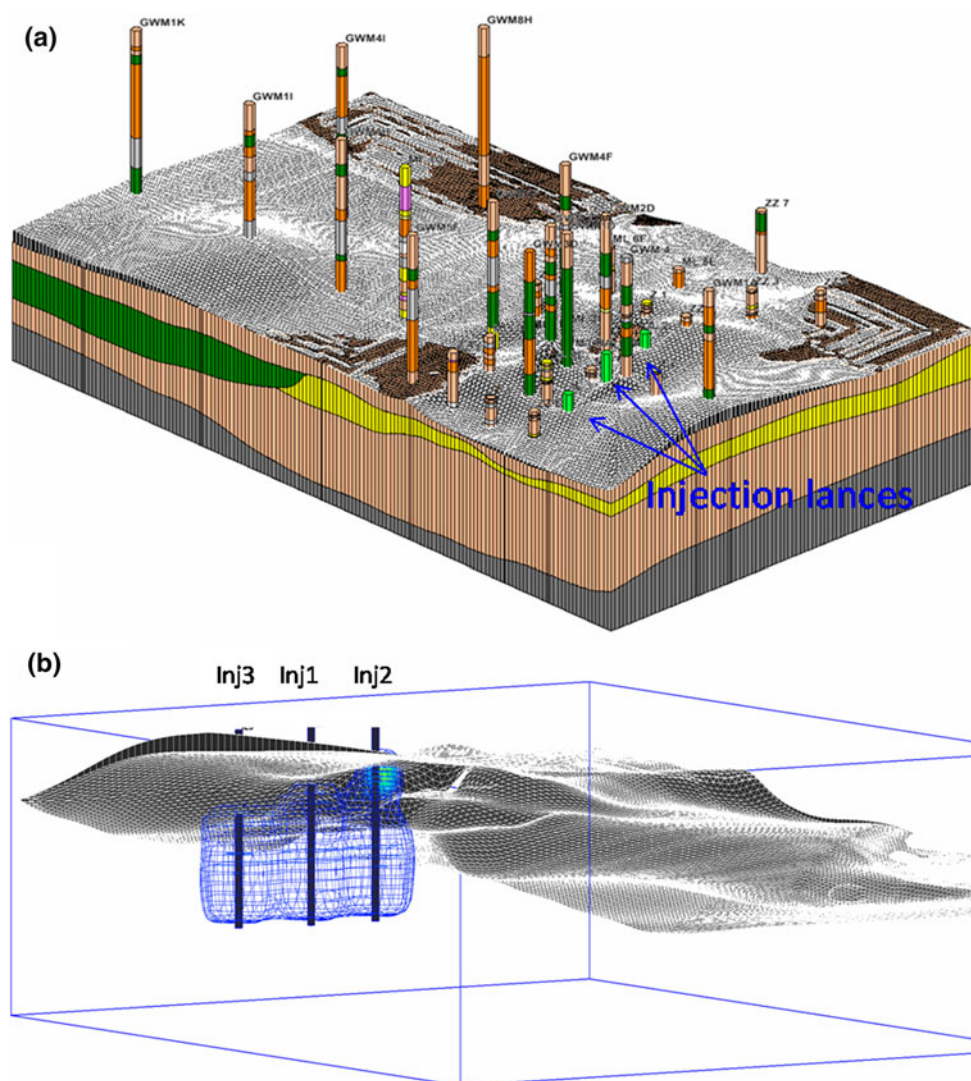
Injection test design and operation

Based on results from multiphase modelling, optimal operating conditions for the CO₂-injection test were established, e.g. injection rate, injection pressure, injection time, and injection regime. The most important operational constraint was that injected CO₂ should remain within the aquifer and any breakthrough to the unsaturated zone or atmosphere should be avoided, as the focus of the present study is upon the impact of CO₂ and application of monitoring methods on groundwater. Furthermore, it was aimed to produce a coherent plume of dissolved CO₂ in the

groundwater, in order to enhance the chances of detecting CO₂ and/or altered groundwater down-gradients of the injection wells.

To design an optimal injection regime, first 2D and then 3D multiphase simulations were performed using TOUGH2 and the ECO2-module (for details see Pruess et al. 1999 and Geistlinger et al. 2009). Based on the geological structure model (see “Test site”), a 3D numerical model of aquifer 2 (consisting of layer numbers 4–9, according to Fig. 3 and Table 1) was set up, consisting of 37,125 cells (=55 × 45 × 15) with a grid spacing of 1 m (see Fig. 5a). Key hydraulic parameters for a multiphase-model are horizontal and vertical permeability, as well as capillary pressure for each sediment type. The permeability values were taken from sieve analysis and HPT logs (see “Test site”). For each geological layer, the permeability was calculated as a mean value over different located values, e.g. the value for lower medium sand was obtained by averaging 15 different values. For constitutional relationships, i.e. the

Fig. 5 **a** Geological structure model showing the model boundaries of the simulated aquifer 2, the locations of the borehole profiles and injection lances (light green). Viewing direction is from southeast. **b** 3D simulated gas distribution (blue isolines correspond to 0.5 % gas saturation), accumulating beneath the glacial loam 10 days after stopping the gas injection. Viewing direction is from northeast



permeability-saturation relationship and the capillary-pressure relationship, a van Genuchten model was used (van Genuchten 1980). The corresponding van Genuchten parameters α and m were determined using the ROSETTA-database (Simunek and van Genuchten 1999) and the SOILPROP-database (Mishra and Parker 1989; Stump et al. 2009) and are listed in Table 2.

Optimal simulation results for obtaining a closed coherent dissolved CO₂-plume were achieved using a low injection rate of 10 L CO₂/min at an injection gallery of 3 lances with an inter-well spacing of 5 m and a continuous injection regime over 10 days.

In Fig. 5b, the simulated CO₂ gas distribution after 20 days (i.e. 10 days after gas injection had stopped) is depicted for this injection scenario. The gas saturation attains its maximum values of about 5 % at the centre line. The blue isolines correspond to 0.5 % gas saturation. Both the maximum and minimum values are realistic values at field scale. The overlapping of the three gas plumes suggests that a closed, coherent dissolved CO₂-plume will be produced in the field. This plume was also calculated by TOUGH2 and is presented in Lamert et al. (2012). As can be seen from Fig. 5b, the covering glacial loam layer plays a crucial role in preventing breakthrough to the upper aquifer and into the atmosphere.

Based on the aforementioned simulation results, three injection lances were installed at distances of 5 m perpendicular to groundwater flow using SonicDrill technology, 5 months before the injection test started. To avoid gas losses through tube fittings, a continuous multichannel tubing system (CMT Solinst, Georgetown, Canada) with an injection screen of 20 cm at a depth of 18 m bgl was used. At the depth of the glacial loam, that acts as an aquiclude between aquifer 1 and 2, bentonite packers were installed to prevent CO₂ breakthrough along the tubing. To test the tightness of the bentonite sealing, optical O₂ sensors (PreSens, Regensburg, Germany) were installed above and below the glacial loam on the outer part of the tubing. Gas injection tests with pressurized air carried out 3 weeks before CO₂ injection proved the tightness of the seal, as no oxygen was detected above the glacial loam layer.

Between 29 March 2011 and 9 April 2011, 787 kg of CO₂ and 0.466 kg of SF₆ (as a tracer) in total were injected, with low injection pressure approximately equal to the hydrostatic pressure at the three injection lances. This corresponds to injection rates of 10 L CO₂/min and 1.67 mL SF₆/min, respectively, at each lance. As CO₂ was detected in the soil gas in well ZZ5 two days after the injection begun, the injection rate was reduced at injection lance Inj2 from 10 to 7.5 L/min and again after eight days to 5 L/min, to avoid losses of CO₂ into the atmosphere. As a counterpart, the injection rate at Inj3 was increased after 9 days from 10 to 13.5 L CO₂/min.

Monitoring of CO₂ and geochemically altered groundwater

Different monitoring methods have been applied to monitor the injected CO₂ and the resulting alteration of groundwater, which also enables recommendations to be derived for monitoring shallow aquifers that might be subject to CO₂ intrusions.

Groundwater sampling and analyses

Thirteen groundwater sampling campaigns were carried out in total—three before, three during and seven after the injection experiment. In total, 669 groundwater samples were taken between November 2010 and October 2011.

Groundwater sampling together with recording of on-site parameters (pH, electrical conductivity, redox potential, oxygen and temperature) was performed according to German quality standards (DVWK 1992, 1997). Groundwater samples were filtered using 0.45 µm cellulose acetate single-use filter units and samples for cation analyses were acidified on-site using concentrated HNO₃. Furthermore, alkalinity was determined on-site by titration to quantify carbonate and bicarbonate content of the water samples.

Groundwater samples were analysed for TIC/TOC, major cations, anions, ammonium, trace elements, BTEX, chlorinated carbons (PCE, TCE, DCE, VC), ethane, ethene

Table 2 Hydraulic parameters of geological layers in aquifer 2

Layer No. and description	Porosity (–)	Permeability (m ²)	van-Genuchten α (m ⁻¹)	van-Genuchten m (–)
(4) Glacial loam	0.37	3.1×10^{-15}	7.1×10^{-4}	0.20
(5) Upper medium sand	0.33	2.0×10^{-11}	4.4×10^{-4}	0.39
(6) Coarse sand	0.34	4.2×10^{-11}	7.6×10^{-4}	0.40
(7) Silt	0.37	1.0×10^{-13}	2.7×10^{-4}	0.41
(8) Lower medium sand	0.30	2.6×10^{-11}	2.7×10^{-4}	0.58
(9) Glacial till	0.37	5.1×10^{-16}	7.1×10^{-4}	0.20

Layer numbers correspond to layers in Table 1 and Fig. 3

and methane at the Institute for Geosciences of the University of Kiel and for SF₆ at a commercial laboratory. TIC/TOC, BTEX and chlorinated carbon samples were generally analysed within 24–48 h after arrival in Kiel. Samples for trace element analysis were acidified after arrival in the lab with concentrated sub-boiled nitric acid and analysed in the ICP-MS laboratory of the Institute for Geosciences at the University of Kiel, according to Garbe-Schönberg (1993).

The three sampling campaigns prior to the injection test show a rather large spatial variability for most parameters measured at the site (see Table 3): pH, electrical conductivity and redox potential varied within 6.2–7.2, 420–1,060 μS/cm and 80–457 mV, respectively.

The alteration of groundwater composition due to CO₂ injection is depicted exemplarily for one monitoring well (GWM2D), located at 5 m down-gradient of an injection well (see Fig. 6). The injection of CO₂ leads to an increase in TIC (Fig. 6a), which results in a pH decrease (down to 5.4), due to dissolution of CO₂ in water, the formation of carbonic acid and its partial dissociation. Concomitantly, the electrical conductivity increases from approximately 550 μS/cm to more than 700 μS/cm, which is as a result of cation release, occurring due to pH-dependent cation exchange and mineral dissolution processes. As can be seen in Fig 6c, the concentrations of major cations Ca, K, and Mg increase by 24–38 % compared to background values. Sodium, however, decreases by 24 % compared to pre-injection concentrations, indicating either a fixing of sodium due to cation exchange processes or as a result of tailing of the salt tracer test from November 2010. Other trace elements (such as aluminium, silicium, manganese

and, to a lesser extent, iron) show significant increases with increasing TIC, revealing relative increases at GWM2D compared to background values of 184, 126, 116 and 17 %, respectively (Fig. 6d). Concentrations of heavy metals like copper, nickel, zinc, barium, cadmium and lead also increase distinctively; however, drinking water levels have not been exceeded due to CO₂ induced concentration increases (with the exception of nickel in two samples). More details on the behaviour of trace metals will be published separately. In general, all trace metals (as well as major cations and anions) attain background values after the CO₂ plume has passed, as can be seen in Fig. 6.

The relative change in groundwater composition at two additional monitoring wells (GWM1D–GWM3D, all located 5 m down-gradient of the injection wells) is shown in a Piper diagram in Fig. 7. The results of two sampling campaigns are depicted in the Piper diagram: a sampling campaign prior to CO₂ injection and the sampling campaign 160 days after injection started, at which the mentioned monitoring wells showed the largest alteration of groundwater composition due to CO₂ injection. The injection of CO₂ led to an increased share of bicarbonate, while the share and absolute concentrations (compare Fig. 6b) of other major anions (sulphate and chloride) decreased. Accordingly, the share of divalent cations (mainly calcium and to a lesser extent magnesium) increases, whereas the share of monovalent cations decreases.

Geophysical monitoring

Geoelectrical surveys have been applied for monitoring CO₂ in geological storage formations (e.g. at the CO₂

Table 3 Background concentration statistics of groundwater samples from three sampling campaigns before the injection test: mean, standard deviation, minimum and maximum values and number of samples (*n*)

	pH	Electrical conductivity (μS/cm)	O ₂ (mg/L)	Redox potential (mV)	Alkalinity (mg/L)	TOC (mg C/L)	TIC (mg C/L)			
Mean	6.7	631	0.6	276	185.9	2.8	45.1			
SD	0.2	150	1.3	86	59.7	1.0	12.0			
Min	6.2	420	0	80	81.7	1.3	19.4			
Max	7.2	1060	8.7	457	417.9	6.9	69.7			
<i>n</i>	101	99	101	82	86	67	67			
	Cl ⁻ (mg/L)	NO ₃ ⁻ (mg/L)	SO ₄ ²⁻ (mg/L)	K (mg/L)	Na (mg/L)	Mg (mg/L)	Ca (mg/L)	Fe (mg/L)	Mn (mg/L)	Si (mg/L)
Mean	20.1	13.7	141.6	2.7	24.2	7.0	107.3	0.18	0.18	4.7
SD	11.0	11.4	38.7	1.1	10.0	1.4	36.5	0.45	0.16	0.9
Min	6.6	0.6	75.8	1.3	12.3	4.3	59.9	0	0	2.7
Max	75.0	62.3	285.0	5.7	74.1	11.0	229.1	2.55	0.60	7.1
<i>n</i>	104	104	104	104	104	104	104	104	104	91

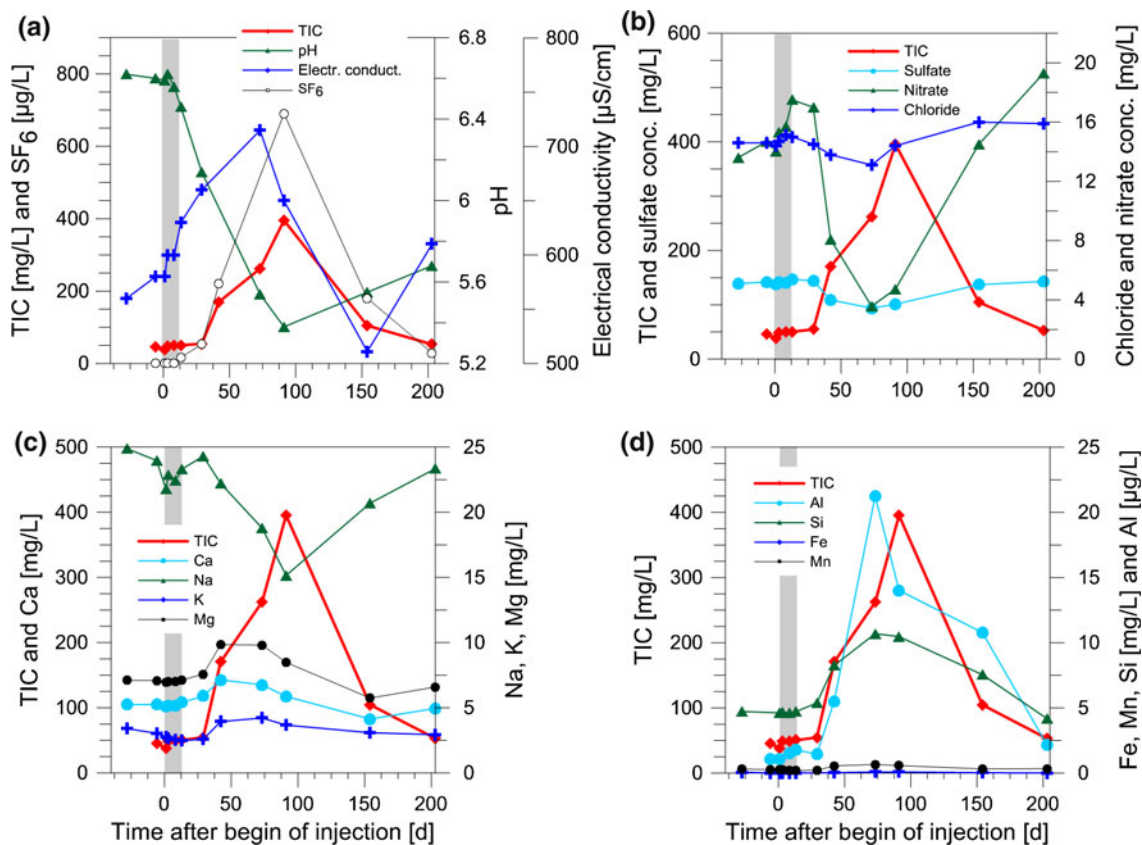


Fig. 6 Concentration time series at GWM 2D, which is approximately 5 m downstream from injection lance Inj2, for total inorganic carbon (TIC) and **a** pH, electrical conductivity and tracer SF₆,

b sulphate, nitrate and chloride, **c** calcium, sodium, potassium, magnesium and **d** aluminium, silica, iron and manganese. The grey bar indicates the duration of the injection period

storage test site Ketzin/Germany, described by Kiessling et al. (2010) and for the characterization of natural geological CO₂ leakage sites (Schütze et al. 2012).

However, the authors are not aware of other studies using geoelectrical measurements for monitoring gaseous CO₂ and/or altered groundwater caused by a CO₂ intrusion into near subsurface structures.

Gaseous CO₂ injection into a groundwater system causes an increased gas phase in the pore space and accordingly increased electrical resistivity. However, the subsequent dissolution and dissociation processes lead to an increase in electrical conductivity, thus a decrease in electrical resistivity.

At the test site, three injection lances and 33 monitoring wells were equipped with electrodes for geoelectrical monitoring of CO₂ injection. Ring shape electrodes fixed at pre-defined depths at the outer surface of the HDPE/MDPE well material allow for time efficient, spatially and temporally high resolution monitoring using both borehole and cross-borehole measurements. Geoelectrical monitoring results showed significant changes of electrical resistivity caused by injected CO₂ (Lamert et al. 2012). This data is clearly related to measured field parameters (pH, electrical

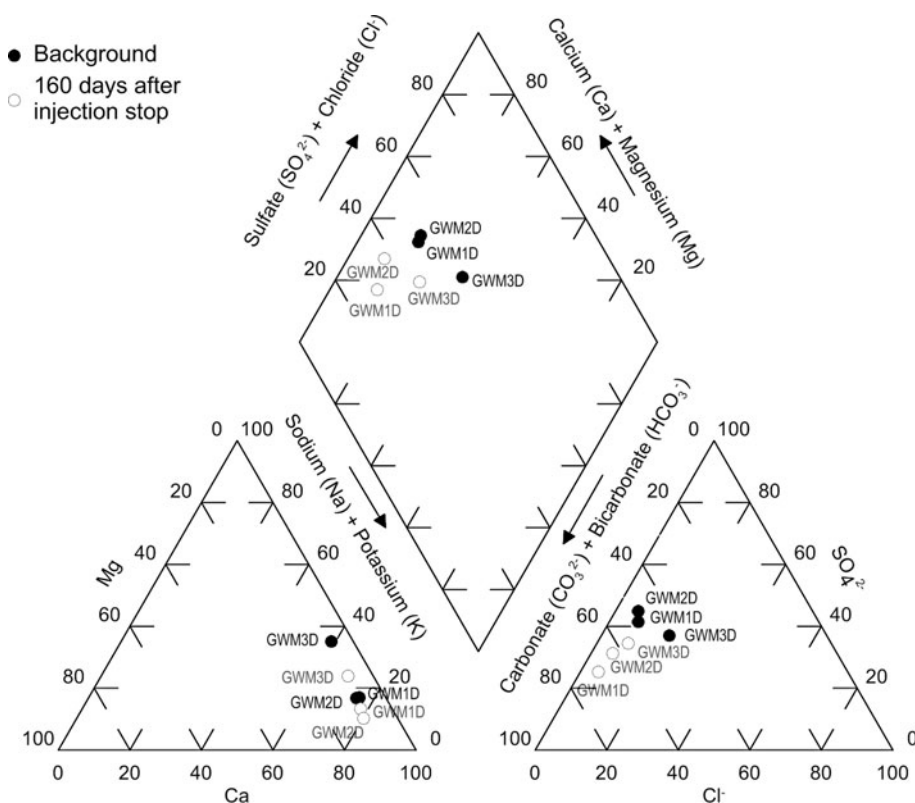
conductivity), water chemical parameters (TIC) and stable isotope data. Basic principles of geoelectrical monitoring of near subsurface CO₂ intrusions and the results of geoelectrical surveys that were used to monitor the CO₂ injection test are provided by Lamert et al. (2012).

Isotope monitoring

¹³C/¹²C isotope analyses of CO₂ were performed at the site in order to test the hypothesis that isotope signatures can be used to detect and/or identify potential leakages of CO₂ from deep storage sites.

Potential CO₂ leakage from deep geological formations affects the carbonate system of overlaying aquifers, thus the challenge is to distinguish naturally occurring CO₂ from potential CO₂ leakages, thereby enabling early warning and proper risk assessment to be undertaken. The intention of this study was to develop a monitoring concept based on stable isotope composition of CO₂, thereby allowing the identification of CO₂ sources. CO₂ produced by burning fossil fuels is expected to have an isotope composition of the carbon source (oil, coal, gas), which is generally isotopically depleted in δ¹³C (<−25 ‰)

Fig. 7 Piper diagram for groundwater samples from three monitoring wells (GWM1D, 2D, 3D) for two sampling campaigns, prior to and after the injection test



compared to CO₂ in natural aquifer systems (about δ¹³C -20 to +10 ‰) (Tissot and Welte 1984). The natural isotope composition of CO₂ in groundwater is governed by the isotopic composition of CO₂ in the atmosphere, the composition of carbonate minerals and, to some extent, by microbial recycled plant material. Due to different isotopic compositions of leaking CO₂ from fossil fuel combustion and of CO₂ in aquifers, the isotope ratio might be used as an indicator for leaks. The injected CO₂ was isotopically light, thus representing a typical combustion product, to simulate a CO₂ plume from a hypothetically leaking deep storage site.

The isotopic signature of the CO₂ in the groundwater was monitored for about 1 year before the injection test, in order to assess significant seasonal variations in the aquifer. When the injection test started, samples were taken in the course of the sampling campaigns to determine the fate of the injected CO₂. To perform this sampling, 100 ml serum bottles were filled with groundwater and sealed immediately with gas-tight butyl stoppers. 15 g NaCl was used to reduce microbial activity. The bottles were stored at 4°C and the isotope ratio of CO₂ was measured after acidification with 1 ml 25 % HCl, in order to avoid isotope fractionation of CO₂ in the carbonate system. CO₂ headspace was determined using the GC-IRMS device in the isotope lab of the Department Isotope Biogeochemistry of the Helmholtz Centre for Environmental Research, Leipzig

(settings described in Fischer et al. 2004). Groundwater at the field test site has an average isotopic signature of δ¹³C -21.9 ± 1.5 ‰, whereas the isotopic signature of the injected carbon dioxide has a significantly lighter composition of δ¹³C -30.5 ± 0.4 ‰. The difference of about 9 ‰ was large enough to detect the injected CO₂ and to distinguish it from naturally occurring CO₂. The δ¹³C values of CO₂ at the observation well ML2C-3 are listed in Table 4. As soon as eight days after the start of the injection test, the CO₂ plume could be detected at this observation well and it took about 6 months until attenuation of the CO₂ plume was achieved.

In addition, the CO₂ isotope signature of the soil gas was monitored at the experimental field site. Self-constructed

Table 4 δ¹³C values of CO₂ in the groundwater and pH at monitoring well ML2C-3

Date of sampling	Days after start of injection	δ ¹³ C (‰)	pH
02.04.2011	4	-20.92	6.38
06.04.2011	8	-29.87	5.45
12.04.2011	14	-30.44	5.18
28.04.2011	30	-31.50	5.53
11.05.2011	43	-31.50	5.39
28.06.2011	91	-30.19	5.91
30.08.2011	154	-22.07	6.15
19.10.2011	204	-23.04	6.24

sampling lances, as described by McCarthy and Reimer (1986), were used. A stainless steel tube containing a thin capillary tube inside (total volume 2.2 ml) was pushed one metre into the ground, and then subsequently soil gas samples were taken with a gas-tight syringe and transferred into evacuated glass vials. The background signature of the soil gas was $-19.5 \pm 2.1 \text{ ‰}$ and no seasonal variations were observed. Due to the presence of glacial loam at ca. 10 m depth, a migration of injected CO_2 towards the surface was evidently inhibited. Monitoring of the 53 sampling points confirmed this assumption and no changes in the isotopic ratio of the soil gas were observed. During the injection test, a minor CO_2 leakage occurred at one of the injection lances, which could be detected immediately in the soil gas samples from around this area. This observation showed that the sampling procedure is also useful for the detection of leakages in the very shallow subsurface.

Multiparameter probes

In four monitoring wells, the multi-parameter probe (MPP) *CDTplus* (UIT GmbH Dresden, Germany) was used to continuously measure basic groundwater parameters, i.e. pressure, pH, electrical conductivity (EC) and temperature. In one of the wells, an additional CO_2 probe was installed. The purpose of the probes, besides continuous measurement and thus exact determination of first and peak arrivals of CO_2 and/or chemically altered groundwater, was to test their practicability for long-term monitoring in groundwater systems that are potentially subject to CO_2 intrusions. Another advantage of measuring on-site parameters and CO_2 in situ at the monitoring well is the prevention of CO_2 losses due to degassing during groundwater pumping to the surface.

Three probes have been installed in two-inch groundwater monitoring wells in the down-gradient of the CO_2 injection lances (GWM2D, GWM3D and GWM4F: see Fig. 1) in the lower aquifer 2 at a depth of about 17 m bsl, where changes in pH, EC and TIC were expected. One probe that is supplemented with a sensor for CO_2 measurements has been installed in GWM1D. The CO_2 sensor utilized here detects dissolved CO_2 concentration in the groundwater, following the Severinghaus method (Severinghaus and Bradley 1958). The electrode combines an Ag/AgCl reference electrode for pH and a glass membrane electrode, which has a polymer membrane attached to it that is only permeable to CO_2 . The CO_2 partial pressure in the groundwater equilibrates through the membrane and is measured in terms of the resulting pH of the inner bicarbonate solution. This relationship is used to recalculate the dissolved CO_2 concentration in the groundwater. In combination with the pH value, the carbonate speciation can be estimated as well. Although CO_2 probes have been used to

continuously measure CO_2 in soil gas or air (e.g. Jones et al. 2009), to the authors knowledge, CO_2 concentrations have not been measured continuously in situ in groundwater before.

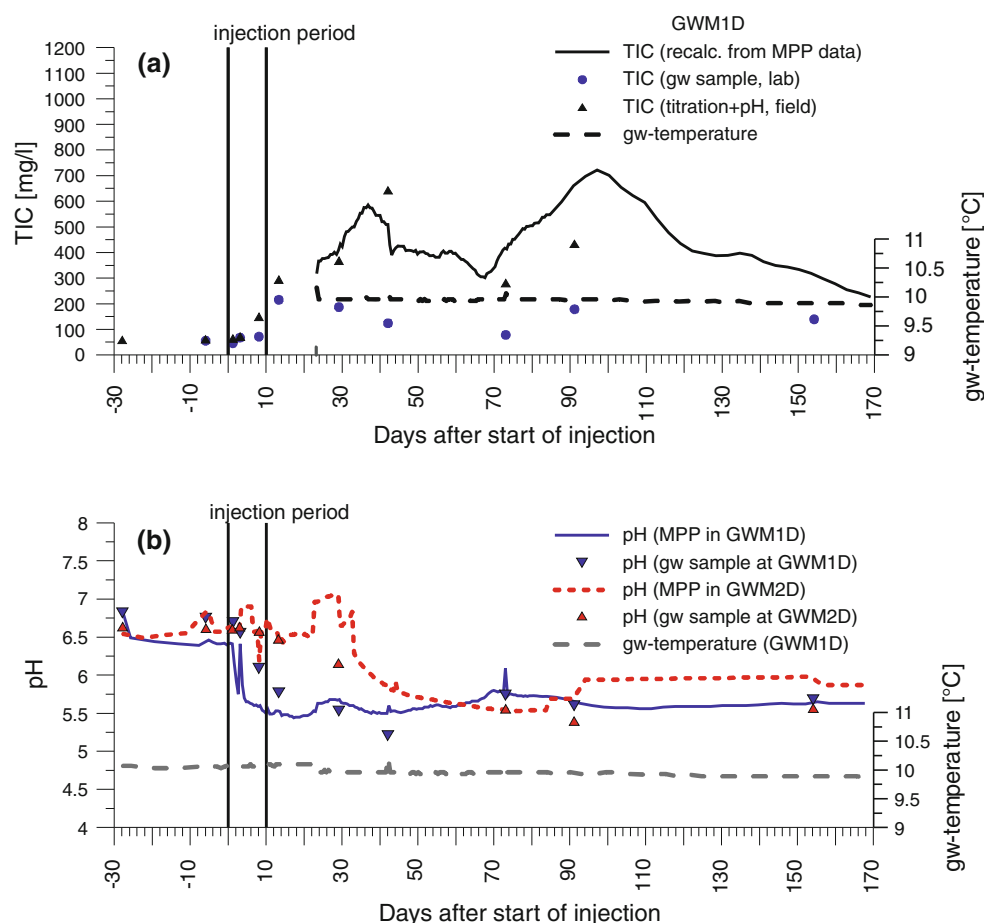
The monitoring phase started about 1 month in advance of the CO_2 injection test to record background and time-dependent parameter variations. Recent publications on numerical and field studies (Wang and Jaffe 2004; Zheng et al. 2009; Apps et al. 2010; Fahrner et al. 2012) as well as reactive transport simulations within this project (Hornbruch et al., in preparation) suggest a decrease in pH to levels in the range of 5.4–6 and an increase of EC in the range of hundreds of $\mu\text{S}/\text{cm}$, under similar field conditions. These values mainly depend on the amount of buffering minerals like calcite or iron hydroxides, gaseous CO_2 saturation and depth.

Figure 8 shows the time series of pH, EC and TIC (calculated from measured dissolved CO_2 concentrations) over the entire test period at GWM1D from the MPP compared to standard groundwater samples. There are some differences compared to the results of the groundwater samples: the significantly lower values of TIC in groundwater samples compared to MPP data is probably caused by degassing of CO_2 during sampling and potentially by subsequent losses during transport and lab analyses (Fig. 8a). The latter effects lowering the TIC concentrations were avoided by determination of alkalinity by field titration. The alkalinity and measured pH of the groundwater served as a basis for calculating TIC and, as can be seen in Fig. 8a, these values are in significantly better accordance with MPP data—in particular for high concentrations. This indicates that TIC concentrations obtained by titration and pH measurements in the field were more reliable in contrast to TIC measurements performed in the lab.

Figure 8b shows the temporal course of pH at GWM1D and GWM2D obtained by MPP measurements and from in situ determination of pH during groundwater sampling campaigns. Although both wells are 5 m apart from an injection well, GWM 1D shows a significantly faster response to CO_2 injection: within 5 days after starting the injection, the pH measured at GWM1D drops to 5.5; whereas in GWM2D, it took about three to four weeks longer to arrive at a similar pH value. Differences between MPP measurements and pH values taken during groundwater sampling probably arise due to different sampling volumes: unlike the probe that exclusively measured water in the well, the pH measured during sampling represents a mixed sample recorded after approximately 1 h of pumping, which results in a spatial average around the well.

The EC values (data not shown) reveal an increase of only 100 $\mu\text{S}/\text{cm}$ during the injection period of 10 days to a maximum of ca. 550 $\mu\text{S}/\text{cm}$ after 98 days. This is due to

Fig. 8 Comparison of **a** TIC and **b** pH values measured by multi-parameter probes (MPP) and obtained from groundwater sampling. TIC from MPP is calculated from sensor measuring dissolved CO₂



low content of buffering minerals, as sediment analyses showed (Peter et al. 2011).

The use of MPP was helpful for continuously monitoring CO₂ induced geochemical impacts over a long time period. However due to the relative high frequency of sampling campaigns at the test site and the associated insertion and removal of probes to obtain groundwater samples from the monitoring wells, the probes seem to be more susceptible to failure.

Passive samplers

Passive samplers, that allow for cost-effective, temporally integrated monitoring of relevant environmental parameters, have been used for various applications in the past (Namiesnik et al. 2005). While most of the passive samplers used so far sampled organic compounds (e.g. Verreydt et al. 2010), passive samplers for heavy metals have been applied in the past primarily as an extraction method for improved lab analyses (e.g. Brumbaugh et al. 2002). In the present study, passive samplers were applied for sampling of cations and heavy metals, using a system as described in de Jonge and Rothenberg (2005) and Roze-meijer et al. (2010). Two different adsorber resins were

used to sample for cations and specifically for heavy metals, respectively—one is a cation exchange adsorber material and the other a chelat-complexing type of resin (SorbiCell™, Denmark). Each adsorber resin is located within a cartridge that is open at both sites, to allow water to flow through. Together with the resin, a tracer salt is placed at the outlet of the cartridge, whose disappearance enables a volume estimate of the water volume that flowed through the system. Results of the passive samplers exposed in the field and of lab experiments on sorption behaviour of different adsorber resins will be published in a future paper.

Discussion

In the following section, the design and implementation of the injection test is discussed and experiences, recommendations and limitations are given concerning both the technical design of the test and the monitoring methods.

Concerning the design and installation of a test site for a gas injection experiment at a hitherto non-investigated field site, a hierarchical approach using first large-scale methods (i.e. geophysical methods), and then subsequently smaller

scale methods (i.e. Direct Push-methods using various in situ measurement techniques) was proven to be suitable. This iterative and adaptive procedure (including field site investigations, data analyses and multiphase modelling to establish dimensions of the injection test and monitoring network) continued up until the injection period was stopped, with additional monitoring wells having been drilled based on updated field observations and model simulations.

Regarding the technical realization of the injection wells, it has been proven advantageous to install the injection lances firstly using minimally invasive Direct Push-technologies. Thus, no annular space filling is required, which could provide potential preferential pathways for upward gas migration. Impermeable layers were tightened in the annular space using bentonite seals. Secondly, it was advantageous to install the injection lances at least several weeks in advance of the injection test, so that the sediment and sealing could reconsolidate, closing or minimizing preferential pathways along the outside of the injection wells. Injection tests using compressed air together with oxygen sensors installed on the outer walls of the wells at different depths have been shown to be valuable for proving sediment consolidation and seal tightness.

To further improve experimental process understanding, the installation of pH sensors and pressure sensors on the outer walls of the injection wells would also have been useful, as it was not desirable to perform groundwater sampling in the direct vicinity (<2.5 m) of the injection wells to avoid potential preferential pathways for upward gas migration. Thus, pH and pressure sensors here would have allowed for direct measurement of pH effects and potential pressure head changes, occurring due to CO₂ injection, as the latter were not observed in the monitoring wells 5 m apart from the injection wells.

Concerning monitoring methods, the various monitoring well types performed differently: comprehensive blank sampling of tap water and mineral water showed that the pneumatic driven mini pumps (imw, Tübingen, Germany), installed directly into the sediment, led to increased concentrations for some trace metals (zinc, copper, lead and cadmium), as did the inflatable packer system used to sample the 1"-monitoring wells. Only the submersible pump MP1 (Grundfos, Erkrath, Germany) used in the 2" and 4" wells yielded reliable blank concentrations for all measured trace metals. These results will be presented in detail in an additional paper on trace metal mobilization due to CO₂ injection (Peter et al., currently in preparation).

Furthermore, the injection experiment confirmed the susceptibility of TIC measurements in the groundwater, especially at high TIC concentrations. Measurements using the directly in the monitoring well-installed CO₂ probe yielded highest concentrations of TIC, as expected. At

wells in close vicinity to the injection lances, groundwater sampling resulted in CO₂ degassing, so that TIC concentrations obtained by titration of alkalinity in the field already revealed decreased concentrations, compared to concentrations measured using the CO₂ sensor in the well. Results of TIC measurements from lab analyses yielded the lowest concentration values, due to further losses occurring due to transportation and samples being warmed to room temperature.

All methods tested to detect either CO₂/TIC in groundwater or the geochemical alteration of groundwater due to CO₂ intrusions were applied at a small-scale, densely equipped test site, which does not reflect a realistic monitoring network at a real CCS site. However, some conclusions concerning the applicability of these methods at large-scale CCS sites can be drawn from this injection experiment. As other authors (e.g. Chalatumyk and Gunter 2005) have shown, monitoring strategies for CCS sites comprise different methods for all potentially affected compartments (i.e. from the reservoir formation up to the atmosphere), each covering a different scale. In order to cope with the large scales necessary to monitor a CCS site, hierarchical monitoring strategies are appropriate. Cortis et al. (2008) suggested a two-step approach for (1) detecting and locating CO₂ seepage(s) using large-scale monitoring on a fixed grid and (2) for pinpointing and quantifying the seepage using smaller-scale methods on a flexible dynamic monitoring grid. Although Cortis et al. (2008) developed their concept for monitoring the unsaturated zone and atmosphere, this concept can be extended to all compartments included in environmental CCS monitoring. Methods suitable for a large-scale monitoring scheme on a fixed grid should either comprise methods covering large scales (e.g. eddy covariance towers, airborne monitoring) or they should effectively monitor vulnerable areas on a smaller scale, like faults or abandoned boreholes. Thus, groundwater monitoring methods become suitable either for small-scale monitoring of 'a priori' selected vulnerable areas on a permanent fixed monitoring grid (case 1) or for pinpointing leakages on a dynamic monitoring grid (case 2). With regard to effective and economical groundwater monitoring methods, either multi-parameter probes installed in monitoring wells measuring pH and/or CO₂ or geoelectrical monitoring at boreholes (see also Lamert et al. 2012) seem to be suitable methods. Furthermore, groundwater sampling and analyses for basic parameters such as TIC, pH, anions and cations seem appropriate for targeting and identifying leakages into aquifers and additional analyses for isotope signatures, in order to identify CO₂ sources.

Finally, an important lesson learned during this research project was that early and transparent communication of planned research activities with local authorities, regulators

and especially with the local public is a crucial prerequisite for successful and undisturbed operation of even small-scale pilot projects.

Summary

A 10-day CO₂ injection experiment into a shallow aquifer was performed to investigate geochemical impact on groundwater and to test different monitoring methods. Careful ‘a priori’ site characterization and test design via multiphase simulations was necessary to obtain an optimally equipped test site, optimized injection rates and optimal distances between injection wells. Monitoring included groundwater sampling and subsequent standard analyses, as well as trace element and isotope analyses; geoelectrical borehole monitoring and the use of passive samplers and multi-parameter probes both installed in the wells.

CO₂ injection led to an increase in total inorganic carbon (TIC), mainly consisting of bicarbonate, and to a decrease of pH down to 5.1. Geochemical reactions comprised of a release of cations and trace elements, whereas anions were observed to decrease. Geoelectrical borehole monitoring was able to detect groundwater alteration (see also Lamert et al. 2012) and ¹³C/¹²C isotope analyses revealed a clear deviation from background values of up to 10.5 ‰. Multi-parameter probes that continuously measured CO₂, pH and electrical conductivity revealed that TIC analyses in the lab seem to be less reliable than values obtained by the multi-parameter probe in the wells or by field titration and pH measurements.

As the intension of this paper is to provide an overview of the injection test itself and the monitoring methods applied, detailed results concerning the individual methods will be published in additional papers.

Acknowledgments This project was funded by the German Ministry of Education and Research within the Priority Program *Geotechnologies*, Funding number 03G0670A-C. We thank all technicians and students supporting the field activities. Furthermore we thank the municipality of Wittstock and the Brandenburgische Boden GmbH for supporting the project.

References

- Apps J, Zheng L, Zhang Y, Xu T, Birkholzer JT (2010) Evaluation of groundwater chemistry changes in response to CO₂ leakage from deep geological storage. *Transp Porous Media* 82(1):215–246. doi:10.1007/s11242-009-9509-8
- Brumbaugh WG, Petty JD, Huckins JN, Manahan SE (2002) Stabilized liquid membrane device (SLMD) for the passive, integrative sampling of labile metals in water. *Water Air Soil Pollut* 133:109–119
- Chalatumyk R, Gunter WD (2005) Geological storage of CO₂: time frames, monitoring and verification. In: Wilson E, Monea M (eds) Seventh international conference on greenhouse gas technologies (GHGT-7). Vancouver, Canada, pp 623–632
- Cortis A, Oldenburg CM, Benson SM (2008) The role of optimality in characterizing CO₂ seepage from geologic carbon sequestration sites. *Int J Greenhouse Gas Control* 2(4):640–652
- De Jonge H, Rothenberg G (2005) New device and method for flux-proportional sampling of mobile solutes in soil and groundwater. *Environ Sci Technol* 39:274–282. doi:10.1021/es049698x
- Dietrich P, Leven C (2006) Direct push-technologies. In: Kirsch R (ed) *Groundwater geophysics*. Springer, Berlin, pp 321–340
- Dietrich P, Butler JJ, Faiss K (2008) A rapid method for hydraulic profiling in unconsolidated formations. *Ground Water* 46(2):323–328
- DVWK (1992) Entnahme und Untersuchungsumfang von Grundwasserproben. Merkblatt zur Wasserwirtschaft DVWK 128
- DVWK (1997) Tiefenorientierte Probenahme aus Grundwassermessstellen. Merkblätter zur Wasserwirtschaft DVWK 245
- Fahrner S, Schäfer D, Dahmke A (2012) A monitoring strategy to detect CO₂ intrusion in deeper freshwater aquifers. *Int J Greenhouse Gas Control* (in press)
- Fischer A, Vieth A, Knöller K, Wachter T, Dahmke A, Richnow H-H (2004) Charakterisierung des mikrobiellen Schadstoffabbaus mithilfe von isotopenchemischen Methoden. *Grundwasser* 3:159–172
- Garbe-Schönberg D (1993) Simultaneous determination of thirty-seven trace elements in twenty-eight international rock standards by ICP-MS. *Geostand Newslett* 17(1):81–97
- Geistlinger H, Lazik D, Vogel H-J (2009) Pore scale and continuum modeling of gas flow pattern obtained by high-resolutions-optical bench-scale experiments. *Water Resour Res* 45:W04423. doi:10.1029/2007WR006548
- Hoffmann R, Dietrich P (2004) Geoelektrische Messungen zur Bestimmung von Grundwasserfließrichtungen und -geschwindigkeiten. *Grundwasser* 3:194–203
- Jones DG, Barlow T, Beaubien SE, Ciotoli G, Lister TR, Lombardi S, May F, Müller I, Pearce JM, Shaw RA (2009) New and established techniques for surface gas monitoring at onshore CO₂ storage sites. *Energy Procedia* 1(1):2127–2134
- Kharaka YK, Thordsen JJ, Kakouros E, Ambats G, Herkelrath WN, Beers SR, Birkholzer JT, Apps JA, Spycher NF, Zheng L, Trautz RC, Rauch HW, Gullickson K (2010) Changes in the Chemistry of Shallow Groundwater Related to the 2008 Injection of CO₂ at the ZERT Field Site, Bozeman, Montana. *Environ Earth Sci* 60(2):273–284. doi:10.1007/s12665-009-0401-1
- Kiessling D, Schmidt-Hattenberger C, Schuett H, Schilling F, Krueger K, Schoebel B, Danckwardt E, Kummerow J (2010) Geoelectrical methods for monitoring geological CO₂ storage: first results from cross-hole and surface-downhole measurements from the CO₂SINK test site at Ketzin (Germany). *Int J Greenhouse Gas Control* 4:816–826. doi:10.1016/j.ijggc.2010.05.001
- Lamert H, Geistlinger H, Werban U, Schütze C, Peter A, Hornbruch G, Pohlert M, Kalia S, Beyer M, Schulz A, Großmann J, Dahmke A, Dietrich P (2012) Feasibility of geoelectrical monitoring and multi-phase modeling for process understanding of gaseous CO₂ injection into a shallow aquifer. *Environ Earth Sci*. doi:10.1007/s12665-012-1669-0 (this issue)
- Lewicki JL, Birkholzer J, Tsang C-F (2007) Natural and industrial analogues for leakage of CO₂ from storage reservoirs: identification of features, events, and processes and lessons learned. *Environ Geol* 52 (3):457–467. doi:10.1007/s00254-006-0479-7
- Little MG, Jackson RB (2010) Potential impacts of leakage from deep CO₂ sequestration on overlying freshwater aquifers. *Environ Sci Technol* 44(23):9225–9232

- Lu J, Partin JW, Hovorka SD, Wong C (2010) Potential risks to freshwater resources as a result of leakage from CO₂ geological storage: a batch-reaction experiment. *Environ Earth Sci* 60: 335–348. doi:[10.1007/s12665-009-0382-0](https://doi.org/10.1007/s12665-009-0382-0)
- McCarthy JJ, Reimer G (1986) Advances in soil gas geochemical exploration for natural resources: some current examples and practices. *J Geophys Res* 91(B12):12327–12338
- Mishra S, Parker JC (1989) A user's guide to SOILPROP. Environmental Systems and Technology, Blacksburg
- Namiesnik J, Zabiegala B, Kot-Wasik A, Partyka M, Wasik A (2005) Passive sampling and/or extraction techniques in environmental analysis: a review. *Anal Bioanal Chem* 381:279–301
- Peter A, Hornbruch G, Dahmke A (2011) CO₂ leakage test in a shallow aquifer for investigating the geochemical impact of CO₂ on groundwater and for developing monitoring methods and concepts. *Energy Procedia* 4:4148–4153. doi:[10.1016/j.egypro.2011.02.359](https://doi.org/10.1016/j.egypro.2011.02.359)
- Pruess K, Oldenburg CM, Moridis G (1999) TOUGH2 user's guide. Version 2.0. Lawrence Berkeley National Lab, Berkeley
- Rozemeijer J, Van der Velde Y, De Jonge H, Van Geer F, Broers HP, Bierkens M (2010) Application and evaluation of a new passive sampler for measuring average solute concentrations in a catchment scale water quality monitoring study. *Environ Sci Technol* 44:1353–1359. doi:[10.1021/es903068h](https://doi.org/10.1021/es903068h)
- Schulmeister MK, Butler JJ, Healey JM, Zheng L, Wysocki DA, McCall GW (2003) Direct-push electrical conductivity logging for high-resolution hydrostratigraphic characterization. *Ground Water Monitor Remediat* 23(3):52–62
- Schütze C, Sauer U, Beyer K, Lamert H, Bräuer K, Strauch G, Flechsig C, Kämpf H, Dietrich P (2012) Natural analogues—a potential approach developing reliable monitoring methods to understand subsurface CO₂ migration processes. *Environ Earth Sci*. doi:[10.1007/s12665-012-1701-4](https://doi.org/10.1007/s12665-012-1701-4) (this issue)
- Severinghaus JW, Bradley AF (1958) Electrodes for blood pO₂ and pCO₂ determination. *J Appl Physiol* 13(3):515–520
- Simunek J, van Genuchten MT (1999) HYDRUS 2D software, version 2.0. International Groundwater Modeling Center, Colorado
- Spangler LH, Dobeck LM, Nehrir A, Humphries S, Barr J, Keith C, Dhaw J, Rouse J, Cunningham A, Benson S, Oldenburg C, Lewicki J, Wells A, Diehl R, Strazisar B, Fessenden J, Rahn T, Amonette J, Barr J, Pickles W, Jacobson J, Silver E, Male E, Rauch H, Gullickson K, Trautz RC, Kharaka Y, Birkholzer JT, Wielopolski L (2010) A shallow subsurface controlled release facility in Bozeman, Montana, USA, for testing near surface CO₂ detection techniques and transport models. *Environ Earth Sci* 60(2):227–239. doi:[10.1007/s12665-009-0400-2](https://doi.org/10.1007/s12665-009-0400-2)
- Stumpp C, Engelhardt S, Hofmann M, Huwe B (2009) Evaluation of pedotransfer functions for estimating soil hydraulic properties of prevalent soils in a catchment of the Bavarian Alps. *Eur J Forest Res* 128:609–620. doi:[10.1007/s10342-008-0241-7](https://doi.org/10.1007/s10342-008-0241-7)
- Tissot BP, Welte DH (1984) Petroleum formation and occurrence, 2nd edn. Springer, Berlin
- Van Genuchten MT (1980) A closed-form equation for predicting the hydraulic conductivity in unsaturated soils. *Soil Sci Soc Am J* 44:892–898
- Verreydt G, Bronders J, Van Keer I, Diels L, Vanderauwera P (2010) Passive samplers for monitoring VOCs in groundwater and the prospects related to mass flux measurements. *Ground Water Monitor Remediat* 30(2):114–126. doi:[10.1111/j1745-6592.2010.001281.x](https://doi.org/10.1111/j1745-6592.2010.001281.x)
- Wang S, Jaffe PR (2004) Dissolution of a mineral phase in potable aquifers due to CO₂ releases from deep formations; effect of dissolution kinetics. *Energy Convers Manage* 45(18–19):2833–2848. doi:[10.1016/j.enconman.2004.01.002](https://doi.org/10.1016/j.enconman.2004.01.002)
- Wilkin RT, Digiulio DC (2010) Geochemical impacts to groundwater from geologic carbon sequestration: controls on pH and inorganic carbon concentrations from reaction path and kinetic modeling. *Environ Sci Technol* 44(12):4821–4827. doi:[10.1021/es100559j](https://doi.org/10.1021/es100559j)
- Zheng L, Apps JA, Zhang Y, XU T, Birkholzer JT (2009) On Mobilization of Lead and Arsenic in Groundwater in Response to CO₂ Leakage from Deep Geological Storage. *Chem Geol* 268:281–297
- Zheng L, Apps JA, Spycher N, Birkholzer JT, Kharaka Y, Thordsen JJ, Beers SR, Herkelrath WN, Kakouros E, Trautz RC (2012) Geochemical modeling of changes in shallow groundwater chemistry observed during the MSU-ZERT CO₂ injection experiment. *Int J Greenhouse Gas Control*. <http://dx.doi.org/10.1016/j.ijggc.2011.10.003>

Appendix B

Monitoring of a simulated CO₂ leakage in a shallow aquifer using stable carbon isotopes

Schulz, Alexandra; Vogt, Carsten; Lamert, Hendrik; Peter, Anita; Heinrich, Ben; Dahmke, Andreas; Richnow, Hans-Hermann

Environmental Science and Technology, 2012, 46 (20); pp 11243-11250.

Monitoring of a Simulated CO₂ Leakage in a Shallow Aquifer Using Stable Carbon Isotopes

Alexandra Schulz,^{*,†} Carsten Vogt,[†] Hendrik Lamert,[‡] Anita Peter,[§] Ben Heinrich,[⊥] Andreas Dahmke,[§] and Hans-Hermann Richnow[†]

[†]UFZ - Helmholtz Centre for Environmental Research, Department of Isotope Biogeochemistry, Permoserstraße 15, 04318 Leipzig, Germany

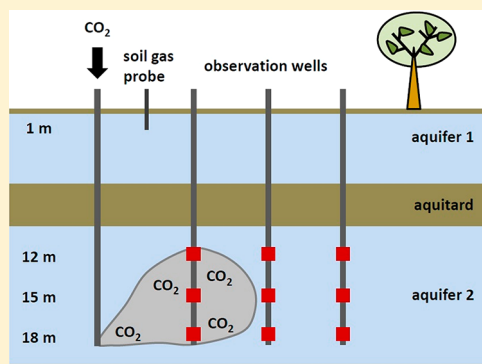
[‡]UFZ - Helmholtz Centre for Environmental Research, Department of Monitoring and Exploration Technologies, Permoserstraße 15, 04318 Leipzig, Germany

[§]Institute for Geosciences, Christian-Albrechts-University Kiel, Ludewig-Meyn-Straße 10, 24118 Kiel, Germany

[⊥]GICON - Tiergartenstraße 48, 01219 Dresden, Germany

S Supporting Information

ABSTRACT: Artificial carbon dioxide leakage into a shallow aquifer was monitored using stable carbon isotope measurements at a field site near the town of Wittstock, Brandenburg, Germany. Approximately 400 000 L of CO₂ were injected into a shallow aquifer at 18 m depth over 10 days. The ¹³C/¹²C ratios of the CO₂ were measured in both groundwater and soil gas samples to monitor the distribution of the injected CO₂ plume and to evaluate the feasibility and reliability of this approach to detect potential CO₂ leakage, for example from carbon capture and storage (CCS) sites. The isotopic composition of the injected CO₂ ($\delta^{13}\text{C} -30.5\text{‰}$) was differentiable from the background CO₂ ($\delta^{13}\text{C} -21.9\text{‰}$) and the artificial CO₂ plume was monitored over a period spanning more than 204 days. The results demonstrate that this stable isotope monitoring approach can be used to identify CO₂ sources and detect potential CO₂ migration from CCS sites into overlying shallow aquifers or even into the upper subsurface. A significant difference between the isotope ratios of the natural background and the injected CO₂ is required for this monitoring approach to be effective.



INTRODUCTION

The development of the carbon capture and storage (CCS) technology, wherein carbon dioxide (CO₂) is sequestered indefinitely in underground storage areas, has progressed rapidly in recent years. This technology is considered an option for the reduction of CO₂ emissions to the atmosphere.^{1,2} The potential for leakage of stored CO₂ through faults, boreholes, or permeable rock formations into shallow aquifers is one concern associated with CCS.^{3–5} Until now, no direct observations of leakage from a CO₂ storage site existed. Thus, only natural and/or industrial analogues were used to predict the effects of CO₂ leakage in shallow groundwater. A review by Lemieux⁶ pointed out the necessity of further field studies to establish data for the behavior of CO₂ in a shallow aquifer. Monitoring tools for detecting potential leakages of CO₂ from CCS sites in deep geological formations are needed for the development of early warning systems for assessing the tightness of cap rocks, and for a rigorous evaluation of risks associated with CCS technology.

Thus far, several methods have been developed for measuring CO₂ concentrations associated with underground leakage. In the near-surface environment for example, the

chamber method is used, which is based on measurements of CO₂ accumulations at the potential leakage site,⁷ whereas eddy-flux methods analyze net CO₂ leakage flux over a large area using a fast CO₂ analyzer.⁸ Parameters like pH and/or electrical conductivity allow for the monitoring of overall CO₂ flux in shallow aquifers, but source identification is not possible. On the one hand, the problem is insufficient spatial resolution for realistic monitoring tools; on the other hand, the discrimination between biogenic and fossil sources of CO₂ is an unresolved disadvantage for both techniques. Stable carbon isotope analysis has the potential to address both of these shortcomings.

CO₂ occurs naturally in both aquifers and in the shallow soil zone. The challenge for a CCS monitor seeking to provide early warning or conduct risk assessment is to distinguish naturally present CO₂ from potential underground CO₂ leakage. The geochemistry of a shallow aquifer will be affected by the upward migration of CO₂ from a storage site. Batch-reactor experi-

Received: July 4, 2012

Revised: September 11, 2012

Accepted: September 24, 2012

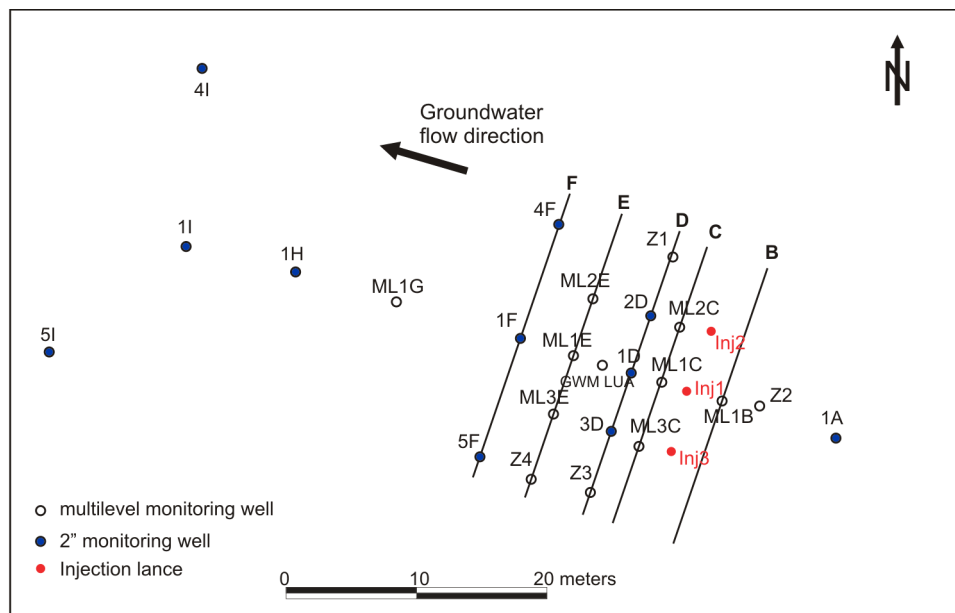


Figure 1. Map of Germany with the field site in the northeast (left), and detailed plan for the monitoring field of the CO₂ injection test site. The plan is showing the installed monitoring wells and the three CO₂ injection lances (red) (modified after (Peter et al., 2012)). The control levels (B–F) are explained in more detail in the text.

ments,⁹ computational simulations,^{10–13} and a small-scale field study at the zero emission research and technology (ZERT) site^{14,15} all suggest the mobilization of cations from the host rock, pH decrease, and electrical conductivity increase following an underground CO₂ release. These parameters have the potential to be used as indirect indicators of CO₂ intrusion.¹⁰ However, measurements of CO₂ concentration or indirect parameters can both be distorted by naturally occurring spatial and temporal variations in the CO₂ inventory of soil–aquifer systems. This impedes upon the ability to reliably identify CO₂ sources and suggests the necessity of isotope monitoring to allow the clear attribution of detected CO₂ to its source.

Several researchers have used and established a stable carbon isotope approach to determine changes in fluid isotope composition due to CO₂ injection¹⁶ or to quantify ionic trapping of injected CO₂ as HCO₃[−].¹⁷ Furthermore, the isotope signature of CO₂ was used for baseline monitoring before CO₂ injection to detect anomalous locations that could act as possible leakage pathways.¹⁸ Additionally, at the ZERT site a laser-based analyzer capable of measuring both CO₂ concentrations and isotope ratios was used to monitor a controlled subsurface CO₂ release event.¹⁹

In this study, the behavior of an artificially generated gaseous CO₂ plume, caused by a controlled and temporally limited CO₂ injection experiment, was monitored by stable carbon isotope analysis. The natural isotopic composition of CO₂ in groundwater is determined by the isotopic composition of CO₂ in the atmosphere, the composition of carbonate minerals, and by microbial recycled plant material. Conversely, the CO₂ to be stored in the underground sites is produced by the combustion of fossil fuels and has the isotope composition of the carbon source (i.e., oil, coal, or gas). This source is generally more isotopically depleted in $\delta^{13}\text{C}$ (<−25 ‰) than CO₂ found in aquifer systems ($\delta^{13}\text{C}$ −20 to +10 ‰).²⁰ Naturally CO₂-rich springs, related to volcanic activities or admixture with mantle-derived CO₂, generally have isotope ratios of between −11.5 and 0.5 ‰.^{21–23} A study of CO₂-rich waters in general showed

an average value of −2.8 ‰.²⁴ These results show that, even at field sites with naturally increased groundwater-CO₂ concentrations, interference from the background isotope signatures with the injected CO₂ isotope signatures cannot be expected. Therefore, the different isotope ratios of carbon dioxide in shallow confined aquifers can aid in discriminating between carbon sources.

A CO₂ leakage scenario was simulated at a field site in Germany by injecting carbon dioxide into a shallow aquifer.^{25,26} To test whether the CO₂ plume of a leaking CCS site could be assessed, spatial and temporal development of the plume was monitored in several ways: the isotope composition of CO₂ in soil gas and groundwater samples, geochemical parameters (pH, total inorganic carbon - TIC, electric fluid conductivity), and geoelectrics for the groundwater samples. CO₂ (397 938 L, 787 kg) were injected 18 m below ground level (bgl) into a shallow aquifer over a period of ten days. Groundwater sampling and soil gas measurements were performed to determine whether the released CO₂ migrated from the aquifer to the upper soil horizon and whether it was possible to detect migrating CO₂ within a reasonable time frame. The overall goal was to determine whether stable isotope measurement of CO₂ is a reliable monitoring tool for detecting potential leakage events from CCS sites. A further aim was to test and evaluate the application of the soil gas sampling system as a routine monitoring method.

INJECTION TEST AND SAMPLING METHODS

Field Site. The injection experiment was performed at a former military airfield about 100 km north of Berlin in the state of Brandenburg, Germany (Figure 1). The subsurface is composed of Quaternary sediments, specifically of fine to coarse sands, silt, clay, and glacial loam of the Saale and Vistula ice age. Two aquifers are present up to the investigation depth of about 20 m below ground level (bgl), both of which were relevant for the injection test. The upper confined aquifer (aquifer 1) is characterized by heterogeneously distributed

interbedded sand and silt layers and has an average thickness of about 11 m. Glacial loam with a highly variable thickness averaging 0.5 m separates the upper aquifer from the lower aquifer (aquifer 2). Aquifer 2 ranges from 11.5–19.5 m bgl and is the main groundwater aquifer. It consists of a carbonate-free, relatively homogeneous medium-to-coarse sand formation, with hydraulic conductivities in the range of $4.5\text{--}6.8 \times 10^{-4} \text{ m s}^{-1}$.²⁵ The lower part of aquifer 2 (16–19.5 m bgl) was chosen as the injection horizon. Glacial till underlies aquifer 2 and acts as an aquitard. In some profiles of the northwestern, northeastern, and southern area, no glacial loam was found, thus hydraulic contact between aquifers 1 and 2 can be assumed. The regional groundwater flow direction is westward with a northwest tendency. The groundwater flow velocity varies between $<0.1 \text{ m d}^{-1}$ up to 1 m d^{-1} (for a more detailed description of the field site and the geochemical parameters refer to refs 25 and 26).

Injection Test. The CO_2 injection was performed in aquifer 2, which was chosen due to its relatively homogeneous composition. The isotope ratio of the injected CO_2 was $-30.5 \pm 0.4 \text{ ‰}$ (Westfalen AG), to mimic a CO_2 source generated by fossil fuel combustion. The injection lances were screened over 0.2 m at 18 m to ensure a depth-defined CO_2 injection. Three injection lances with a lateral spacing of 5 m were installed perpendicularly to the regional groundwater flow direction (Figure 1). The injection rate averaged 10 L of $\text{CO}_2 \text{ min}^{-1}$ at normal temperature and low injection pressure (approximately equal to hydrostatic pressure) at each injection lance. In total 397,938 L (1 bar, 0 °C) of CO_2 were injected over ten days. In addition, SF_6 gas (70.24 L) was used as a conservative tracer and was mixed with the CO_2 . The injection test took place over a ten-day period in March and April of 2011. The settings were chosen according to multiphase simulations,²⁷ which predicted complete dissolution of the injected CO_2 in the groundwater, whereas the plume ascended to the confining upper boundary of the aquifer. Thirty-four observation wells of differing diameters were installed. To assess potential CO_2 leakage at the monitoring wells themselves, CO_2 surface gas flow measurements were performed at the surface using a LICOR CO_2 surface flow measurement system. For more detailed information about the design of the injection test and the monitoring network refer to ref 26.

Soil Gas Sampling in the Unsaturated Zone. Soil gas samples were taken using self-constructed sampling lances, which were first described by McCarthy and Reimer.²⁸ The 1.45 m sampling devices (refer to the Supporting Information for a detailed description) were constructed of stainless steel with an outer diameter of 14.3 mm and an inner diameter of 5.0 mm. The lances were pushed manually with a percussion hammer approximately 1.10 m into the ground to ensure a constant sampling depth. This depth was chosen to minimize the influence of the upper soil horizon due to soil respiration in the root zone and exchange with the atmosphere. The soil gas samples were taken with a 5 mL gastight glass syringe and transferred into evacuated glass vials, which were sealed gastight with butyl rubber stoppers and aluminum crimp seals. The samples were kept cool and stored at about 4 °C and measured within four days of sampling using a gas chromatograph – isotope ratio mass spectrometer (GC-IRMS).

Groundwater Sampling. Groundwater samples were taken during 13 sampling campaigns, with three campaigns taking place prior to injection, three during, and seven taking

place after the injection experiment. Groundwater sampling was performed according to German quality standards (DIN 38402 A13, DVWK information sheet 245 and DVGW W112/2011). Site parameters such as pH, temperature, oxygen concentration, electrical conductivity and redox potential were also recorded at each sampling campaign using a universal pocket meter (Multi 350i, WTW). The groundwater samples for the analyses of stable carbon isotopes of CO_2 were transferred into sterilized 200 mL glass bottles amended with 15 g NaCl to suppress microbiological activity. The bottles were closed gastight with butyl rubber stoppers and aluminum crimp seals and were stored at 4 °C. Samples were measured within four days of sampling using a GC-IRMS. Alkalinity was also analyzed on-site using potentiometric titration with 0.1 M HCl to quantify the carbonate and bicarbonate content of the water samples. The Institute for Geoscience at the University of Kiel analyzed the water samples for TIC/TOC, major cations, anions, trace elements, BTEX, and chlorinated hydrocarbons. The gas-chromatographic analyses for SF_6 were carried out at a commercial laboratory (ERGO Umweltinstitut GmbH).

Measurement Settings for Stable Carbon Isotope Analyses of CO_2 . The $^{13}\text{C}/^{12}\text{C}$ ratios of gaseous CO_2 in the headspace of the groundwater samples were measured after each sampling campaign. In addition, the $^{13}\text{C}/^{12}\text{C}$ ratios of the dissolved inorganic carbon were measured after acidification with concentrated HCl to obtain a pH between one and two to ensure a complete transfer of the dissolved CO_2 into the gas phase and to avoid isotope fractionation effects related to the carbonate system. Analysis of the carbon isotope ratios of the CO_2 was performed with a GC-IRMS in which a gas chromatograph (6890 Series, Agilent Technology, USA) is coupled via a combustion device to an isotope ratio mass spectrometer (Finnigan MAT 253, Thermofinnigan Bremen). The headspace samples (50 to 100 μL) were injected into the GC using a gastight syringe (Hamilton, USA). The GC was equipped with a CP-Porabond Q column (50 m \times 0.32 mm \times 0.5 μm , Varian, USA) and the samples were held at a constant temperature of 40 °C and a helium-flow rate of 2 mL min^{-1} . Samples were each measured three times and a statistical standard deviation of $\leq 0.5 \text{ ‰}$ was always achieved for the described settings. All measured $^{13}\text{C}/^{12}\text{C}$ ratios are reported in delta notation ($\delta^{13}\text{C}$) which is defined:

$$\delta^{13}\text{C} = (R_{\text{Sample}} - R_{\text{Standard}}/R_{\text{standard}}) \times 1000 \quad (\text{eq. 1})$$

where R_{standard} and R_{sample} are the isotope ratios in the standard and the sample, respectively. The values are reported relative to the international Vienna Pee Dee Belemnite (VPDB) standard.²⁹ A simple mixing model was used to verify that the decreased isotope ratios of groundwater samples resulted from the addition of isotopically light injected CO_2 . The following equation was used:

$$A^{13}\delta_{(\text{B})} + (1 - A)^{13}\delta_{(\text{I})} = {}^{13}\delta_{(\text{M})} \quad (\text{eq. 2})$$

where $^{13}\delta_{(\text{B})}$ is the isotope signature of the background, $^{13}\delta_{(\text{I})}$ is the isotope signature of the injected CO_2 , and $^{13}\delta_{(\text{M})}$ is the isotope signature after the injection, and A and $1 - A$ are the mixing ratios of the background isotope ratio and the isotope ratio of the injected CO_2 , respectively.³⁰

RESULTS

Stable Carbon Isotope Ratios of the Soil Gas. Monitoring of the background- CO_2 isotope ratio in the soil

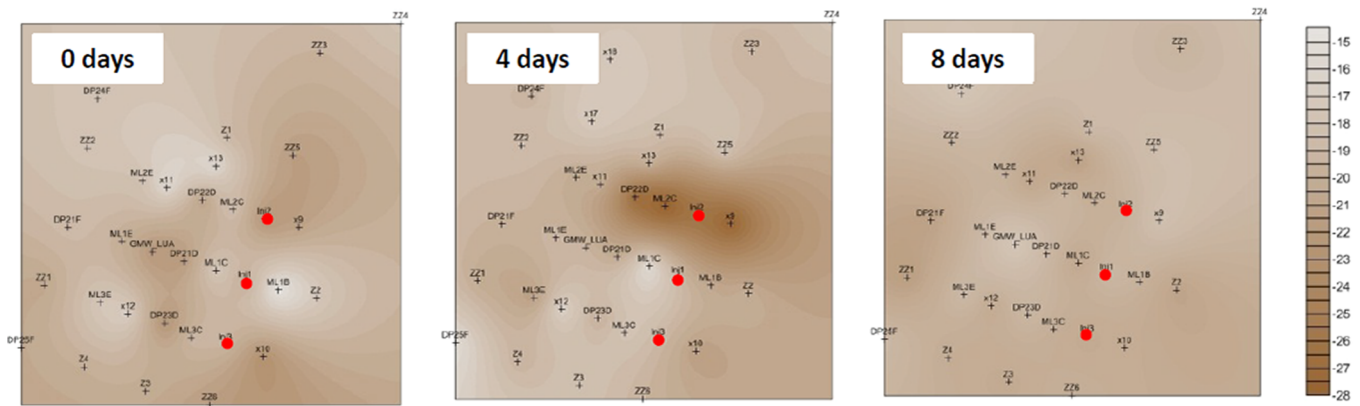


Figure 2. Contour maps showing the distribution of $\delta^{13}\text{C}$ values of CO_2 [‰] in soil gas before, during, and after (from left to the right) the injection of isotopically light CO_2 in March/April 2011. Relatively homogeneously distributed values were observed before and after the injection of CO_2 . During the injection, a slight leakage occurred at the northern injection lance Inj2, which was detected immediately in the soil gas samples taken in the close vicinity of the leak.

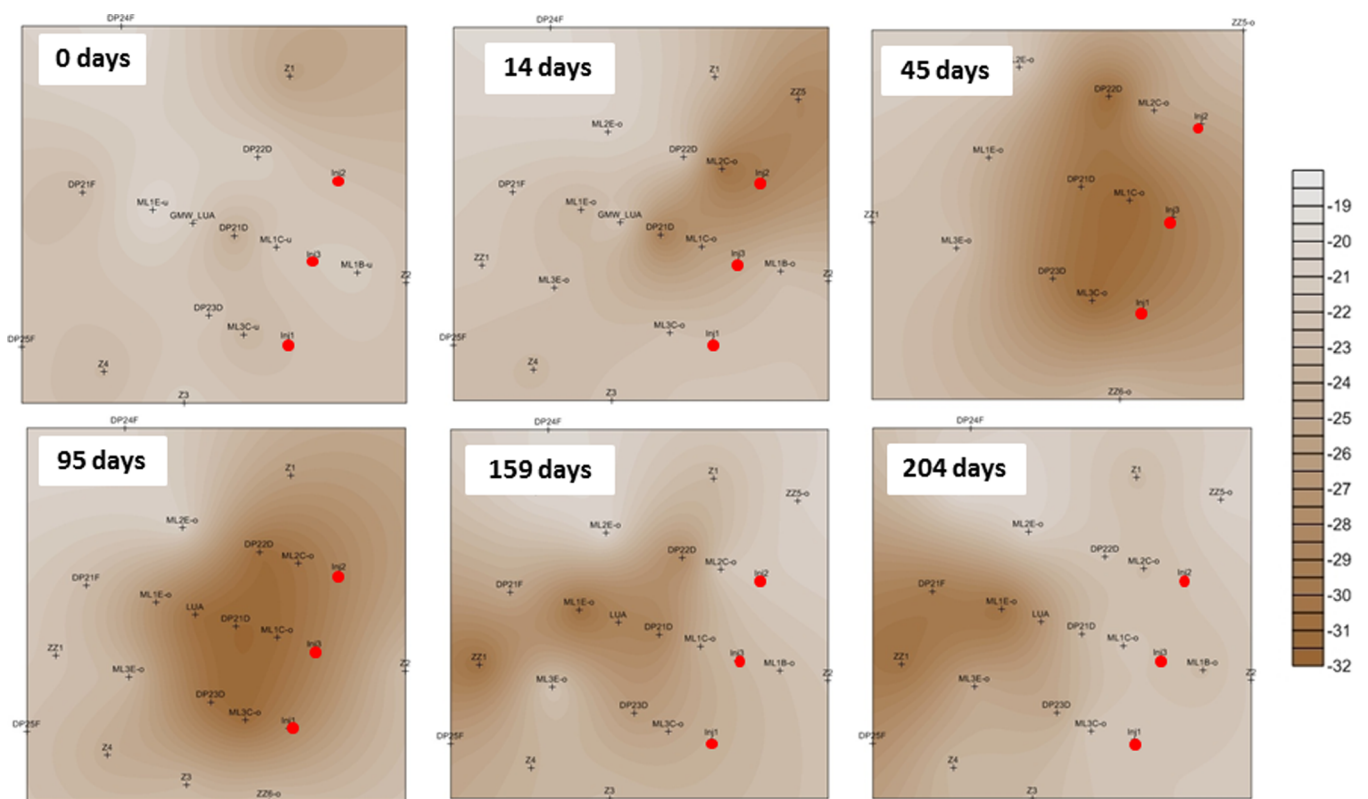


Figure 3. Distribution of $\delta^{13}\text{C}$ values of CO_2 [‰] in groundwater from the start of the CO_2 injection until the final sampling campaign at day 204. The numbers in boxes indicate the number of days after the beginning of the injection test. The red spots show the location of the CO_2 -injection lances.

gas began about nine months prior to the injection of isotopically light CO_2 into the aquifer, to assess potential seasonal variations (Table 1 of the Supporting Information). After three sampling campaigns (May 2010, November 2010, March 2011), an average isotope ratio of -19.5 ± 2.13 ‰ was measured and no significant seasonal variations were observed. Minor deviations of the CO_2 isotope ratio were observed at some sampling points (e.g., ML1B with -16.8 ‰ \pm 0.61 ‰ and $\times 12$ with -16.7 ‰ \pm 0.42 ‰), but these values were still well outside the range of the injected CO_2 (-30.5 ± 0.4 ‰) and thus could be easily distinguished as background CO_2 . The distribution of the $\delta^{13}\text{C}$ values of the CO_2 in the soil gas at 1.1

m depth displayed relative homogeneity over the entire field site (part A of Figure 2).

During the injection test, decreased isotope ratios of the CO_2 present in soil gas were detected at the northern injection lance Inj2. It is assumed that the injected CO_2 migrated back to the surface via preferential flow paths from underground. The input of injected CO_2 into the soil gas system was detected immediately at soil gas sampling points ML2C, GWM2D, and $\times 9$ in close proximity to the injection lance (part B of Figure 2). At these locations, the isotope ratios immediately decreased to -28.1 ‰ \pm 0.02 ‰, -27.0 ‰ \pm 0.13 ‰, and -27.7 ‰ \pm 0.22 ‰, respectively. Because of the construction

of the injection lances, it was not possible to use the LICOR surface flow measurement system to measure the CO₂ flow rate. Additionally, neither the GA94 gas analyzer nor the Testo 535 system was able to provide reliable data, as concentration could only be measured after dilution with atmospheric air. As a result, the soil gas isotope ratios were the sole indicators allowing detection of CO₂ leakage. The leakage of CO₂ was repaired and the CO₂ injection rate reduced to avoid further direct leakage of CO₂ at this sampling point. At the next sampling campaign, four days later, the isotope ratios had returned to background values (part C of Figure 2) indicating that the leaked CO₂ had infiltrated only the pore space of the soil and had equilibrated with the isotope composition of the surrounding air relatively quickly. During the remaining sampling campaigns, no changes in the $\delta^{13}\text{C}$ values of the soil gas CO₂ were measured and no enriched values below of -23.1‰ were detected.

Stable Carbon Isotope Ratios of the Groundwater.

Ten groundwater sampling campaigns were performed after the initiation of CO₂ injection (Table 2 of the Supporting Information). The sampling of both groundwater and soil gas began about nine months before the injection test. Three sampling campaigns were performed to measure the background isotope ratio of the groundwater to assess seasonal variations. The average isotope ratio for the background across all three sampling campaigns was $-21.9 \pm 1.4\text{‰}$ (Figure 3) with no significant seasonal variations. The isotope ratio distribution displayed relative homogeneity over the entire monitoring field. The contour maps with the isotope ratios plotted show the section of the monitoring field featuring the observation wells that were influenced by the injected CO₂ (Figure 3). The other wells at greater distances are not shown as the isotope ratio remained constant over the entire monitoring period.

Beginning four days after CO₂ injection, depleted isotope ratios of about $-29.9\text{‰} \pm 0.32\text{‰}$ were measured at the multilevel well *ML2C*, located about 2.5 m from the northern injection lance *Inj2* in control plane C. At the next sampling, 10 days later, the isotopically light injected CO₂ had reached the middle well in control plane D (about five meters away from injection lance *Inj1*), which showed an isotope ratio of $-29.1\text{‰} \pm 0.20\text{‰}$. The migration of the injected CO₂ was west-oriented, in line with the direction of local groundwater flow. This migration continued and after 45 days isotope ratios had decreased to $-29.8\text{‰} \pm 0.29\text{‰}$ throughout control plane D. In the final sampling campaign, 204 days after injection, the injected CO₂ had reached control planes E and F, where isotope ratios of $-29.8\text{‰} \pm 0.11\text{‰}$ and $-29.6\text{‰} \pm 0.17\text{‰}$ respectively, were detected. In control plane F, only the western and southwestern observation wells (*GWM1F*, *GWMSF*, *ZZ1*) were affected by the injected CO₂. The northern wells (*ZZ2*, *GWM4F*) showed no change in isotope ratios. During this period, the δ -values in control planes C and D gradually increased to values observed before injection. In control plane C isotope ratios reached values of $-22.4 \pm 0.74\text{‰}$, a near-complete return to the measured background value prior to CO₂ injection ($-21.9 \pm 1.4\text{‰}$), and in control plane D isotope ratios had risen back to $-23.7 \pm 1.46\text{‰}$. Control planes A and B were never affected by the injected CO₂, as they are located upgradient of the injection lances with respect to groundwater flow. As the injected CO₂ migrated with the groundwater flow direction, these observation wells were not influenced by the injected CO₂.

Physicochemical Parameters of the Groundwater. In addition to isotope ratios, physicochemical parameters including pH, TIC, concentration of the SF₆ tracer, and electrical fluid conductivity of groundwater samples were measured (Figure 4) for comparison with detected isotope

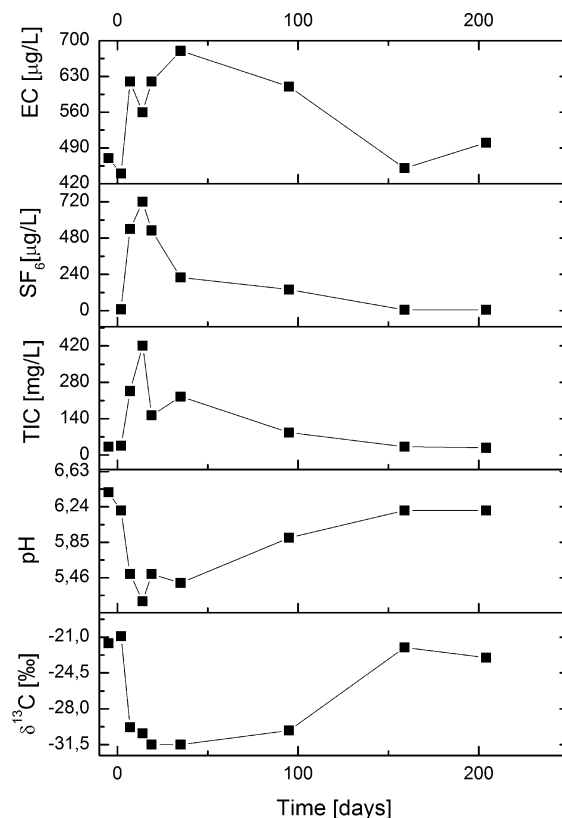


Figure 4. Various parameters for the shallowest sampling level (13 m) of the multilevel well *ML2C* in the northern part of the monitoring field. In addition to the parameters that were measured in the field (pH, electrical conductivity), the total inorganic carbon content, the concentration of the tracer SF₆, and the isotopic ratios are given for all sampling campaigns.

ratios. The physicochemical parameters displayed correlation with the measured isotope ratios. With depletion of isotope ratios, pH also decreases to minimal values of about 5.2. Electrical conductivity was significantly influenced by the injected CO₂, evidenced by an increase from 470 to 680 $\mu\text{S}/\text{cm}$ (Figure 4) was found when the injected CO₂ had reached the specific monitoring well. The TIC values also increased with decreasing isotope ratios (Figure 4) but, due to the degassing of the samples during sampling and transportation to the lab, these values are subject to greater variability (ref 26 for discussion of different TIC measurements). In one well, the CO₂ concentration was measured directly using a probe. The comparison of the TIC values obtained by titration directly in the field and the TIC values calculated using the CO₂ concentration and the pH showed a good correlation. Therefore, we assumed the measured TIC values to be a proxy for the CO₂ concentration. The distribution of the SF₆ concentrations correlated well with the distribution of the isotope ratios (Table 3 of the Supporting Information) and higher SF₆ concentrations being associated with more negative isotope ratios.

Additionally, the mixing model, which is based on the isotope ratios of the groundwater samples, showed that nearly all of the CO_2 detected in the groundwater samples of control planes C, D, and E was a result of added CO_2 from injections. The isotope ratios of $-30.8 \text{‰} \pm 0.17 \text{‰}$, $-30.6 \text{‰} \pm 0.04 \text{‰}$, and $-30.9 \text{‰} \pm 0.37 \text{‰}$ respectively correspond closely to the isotope ratio of the injected CO_2 ($-30.5 \pm 0.04 \text{‰}$). At none of the three control planes, a relevant indication for dilution of isotope ratios was observed. In control plane F, about 20 m in the main groundwater flow direction from the injection lances, a slight dilution in the amount of the arriving CO_2 was detected. The isotope ratios at the observation wells in control plane F ranged between $-25.9 \pm 0.16 \text{‰}$ and $-29.6 \text{‰} \pm 0.17 \text{‰}$, whereas at observation well ZZ1, located between 1F and 5F, no dilution was detected. These results show that the major part of the injected CO_2 moved consistently westward with the groundwater flow. According to the carbonate species distribution, at a pH of 5 only 5% of the CO_2 is presents as HCO_3^- , and the amount of CO_3^{2-} is negligible. It can therefore be assumed that the overwhelming majority of the CO_2 will be present as aqueous dissolved CO_2 and a fractionation between the different CO_2 species can be neglected.

DISCUSSION

The monitoring of carbon dioxide leakage in a shallow aquifer and in the upper soil zone using stable carbon isotopes can make an important contribution to the proper risk assessment

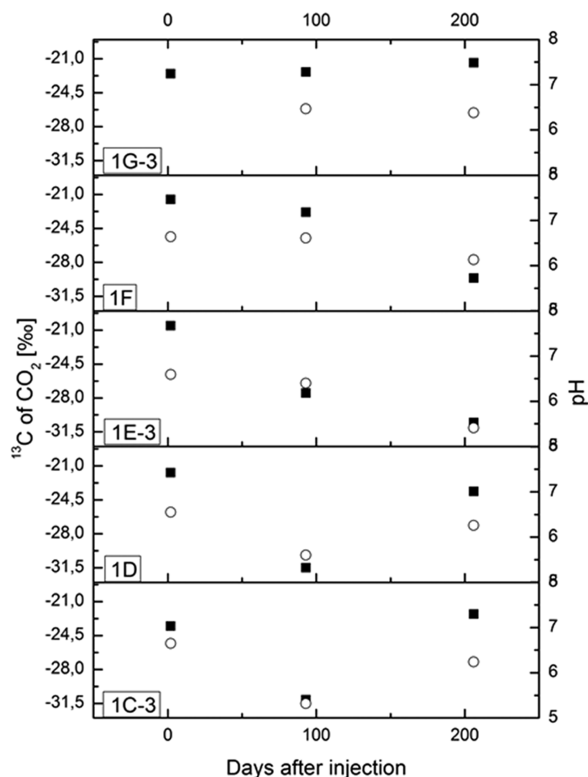


Figure 5. Variation of the isotope ratio (circles) of five specific wells along a cross-section in correlation with the variation of the pH (squares). Well ML1C-3 is the closest well to the injection lance; well ML1G-3 is about 25 m away (see figure 1). At first, the two closest wells showed indication of the injected CO_2 , whereas no change either in pH or isotope ratio was measured at the monitoring well farthest away from the injection well.

of carbon capture and storage technology. The measurement of the stable carbon isotope ratios of CO_2 in groundwater and soil gas allows distinction between the different sources of the CO_2 . The identification of the leakage source is of some importance, especially in cases where several CCS sites are in close proximity. In the case of leakage, aquifers are possible receptors of upwardly migrating CO_2 plumes. The CO_2 is expected to display conservative behavior in shallow aquifers lacking a carbonate mineral matrix, and our data suggest that the isotope fingerprint of CO_2 leakage events may be detectable over long time frames. Thus, confined shallow aquifers might be prime zones for monitoring CO_2 leakage with stable isotope techniques.

Factors Affecting the Isotope Ratios of Soil Gas. So far, relatively few data are available for carbon isotope ratios of soil gas (CO_2 that occupies the pore space in a the soil matrix)³¹ and most of the measurements have been performed for soil-respired CO_2 (the flux of CO_2 moving through the soil). This study concentrates on carbon isotope ratios of both soil gas and groundwater to monitor the behavior of an artificially created CO_2 plume. The CO_2 in soils is derived from three sources: respiration of plant roots, atmospheric CO_2 , and the decomposition of organic matter. The isotope ratios of background CO_2 in this study did not show significant seasonal variation related to periods of higher photosynthetic activity in the soil gas, as the sampling depth of 1.1 m was below the region of root respiration. We can therefore conclude that root respiration does not significantly influence the isotope ratios of CO_2 of deeper soil zones. At the field site, C_3 plants were dominant (e.g., *Achillea millefolium*, *Echium vulgare*) and according to Amundson³¹ the ^{13}C ratios of the flora will dominate the carbon isotope chemistry of the soil (average $\delta^{13}\text{C}$ values of C_3 plants = -27‰ ³²). As the background CO_2 within the soil gas is slightly depleted in ^{13}C ($-21.5 \pm \text{‰}$) compared to the atmosphere, it is assumed that a mixture of atmospheric gas exchange and the decomposition of organic material is responsible for the isotope ratios of the soil gas CO_2 .

Detection of CO_2 Leakage Using Soil Gas. On only one sampling campaign isotopically light CO_2 in soil gas was recorded, at three specific sampling points. We can thus conclude that the injected CO_2 remained below the aquitard (10 m bgl), which operated as a barrier between the two aquifers over the entire monitoring field. The isotopically light CO_2 that was detected in the soil gas at these three points is thought to have originated directly from a leak at one of the injection lances. The leak most likely occurred at the injection lance and then migrated into the pore space of the adjacent soil. In the initial phase of the experiment, decreased isotope ratios in the groundwater samples were not detected at these locations, so it can be assumed that the isotopically light CO_2 never reached the upper aquifer. The results of the soil gas monitoring convincingly demonstrate the ability to detect small CO_2 leaks in the vadose zone employing isotope analysis. Nevertheless, a high sampling frequency is necessary because the diffusion of soil gas and gaseous exchange with the atmosphere lead to a relatively fast dilution of the isotope signal.

Behavior of CO_2 in the Aquifer. In contrast to soil gas, the retention time of injected CO_2 in groundwater is much longer and the sampling frequency can therefore be reduced. As the westward migration of the injected CO_2 corresponded to the groundwater flow direction, it can be assumed that a substantial amount of the injected CO_2 was distributed via

dissolution and subsequent migration in the groundwater. Nevertheless, gas transport must also be taken into account, as geoelectrical monitoring showed clear evidence of upward migration and subsequent accumulation of the gas below the aquitard.²⁷ Several monitoring wells were equipped with multilevel packers, which allowed the vertical monitoring of the distribution of isotopically light CO₂ in groundwater (Figure 2 of the Supporting Information). The aquifer section into which the CO₂ was injected is composed of relatively homogeneous sand but with differences in grain size over the depth profile. Coarser grain sizes in the upper and lower sampling levels may account for the spatial distribution of groundwater containing dissolved isotopically light CO₂. Therefore, the migration of the CO₂ plume along flow paths with higher permeability is likely. In contrast, in areas composed of sediments of typically low hydraulic conductivity, a slower migration of the dissolved isotopically light CO₂ was found (geological profile in ref 27).

In general, the relatively long retention time of the CO₂ plume in control planes C and D fit the hypothesis for dissolution of CO₂ in groundwater and subsequent migration of the plume with the groundwater stream. In this case, the CO₂ plume moved with the groundwater flow and was only slowly diluted. The slow migration of the CO₂ plume corresponds well with the low groundwater flow velocity of 0.07 – 0.1 m d⁻¹.

Evaluation of the Stable Isotope Approach. According to the mass balance of the isotope ratios measured in groundwater, the monitoring method becomes more sensitive the larger the difference between the isotope ratio of the background and the injected CO₂ is. At a difference of only 5 ‰ (e.g., from background CO₂ at -25 ‰ and CO₂ from fossil fuel combustion at -30 ‰), about six times more isotopically light CO₂ would be necessary to decrease the isotope ratio of the groundwater by 1 ‰. The smaller the difference in isotope ratios, the more injected CO₂ is necessary to create an observable change; thus this monitoring method is only applicable in case of sufficiently large difference between isotope ratios. Additionally, the isotope ratio of the CO₂ to be stored underground must be known in advance to make this method applicable.

Another aspect that determines the applicability of this monitoring method is the absence of carbonates in the sediments. When carbonates are present in the groundwater, the pH would be buffered, at least in the early stages of a CO₂ leakage event, and a shift to a higher HCO₃⁻ concentration would be the result. Consequently, a higher amount of injected CO₂ would be necessary to determine a change in the isotope ratios. Further in case of carbonate rich soils an isotope exchange with the matrix has to be taken into account, which is not covered by this investigation.

In addition, this monitoring concept can only be considered reliable in cases where there is no significant exchange between the atmosphere and the aquifer; otherwise isotope fractionation would need to be considered. If a large degassing would occur while sampling, isotope fractionation would play a role but it was not the case for this study. The presence of an aquitard, especially for shallow aquifers, decreases exchange processes with the atmosphere and simplify the interpretation of isotope composition as well as the sensitivity of ¹³CO₂ monitoring. If no aquitard exists, the monitoring in deeper aquifers may avoid disturbances of the isotope signal in the groundwater by atmospheric influences. If the monitoring approach were based only on physicochemical parameters like pH, the identification

of the CO₂ source would not be possible indicating the possibility that a change in these parameters (e.g., due to the input of salt or organic material into the groundwater) could lead to a misinterpretation. Furthermore, spatial resolution should always be taken into account. Large-scale approaches based on a fixed grid would be necessary for rough detection of CO₂ seepage whereas small-scale approaches, like isotope monitoring, would be useful for pin-pointing and identifying the leakage source.³³

Implications. This study was performed on a small scale, thus a direct extrapolation and up scaling of these results to a real leakage scenario may be a challenge. Nevertheless, the observed results do clearly show that stable carbon isotope analysis is a reliable and fast-responding tool to detect CO₂ leakage from a storage site as measured in either groundwater or soil gas. This study thus may serve as proof-of-concept and establishes data that can provide a foundation for further research and eventual application.

■ ASSOCIATED CONTENT

📄 Supporting Information

Isotope ratios [‰] of soil gas for three sampling campaigns before and during the CO₂ injection; sampling campaigns, number of taken samples and the lowest measured isotope ratio of each campaign; isotope ratios and SF₆-concentration of groundwater samples for all sampling campaigns; schematic of a self-constructed soil gas sampling lance; profile of one monitoring well with different sampling depths and a correlation with the distribution of isotope ratios in the specific depth. This material is available free of charge via the Internet at <http://pubs.acs.org>.

■ AUTHOR INFORMATION

Corresponding Author

*E-mail: alexandra.schulz@ufz.de, tel: +49-341-235-1360, fax: +49-341-1443.

Notes

The authors declare no competing financial interest.

■ ACKNOWLEDGMENTS

This project was funded by the German Federal Ministry of Education and Research (Grant: 03G0670C) in the context of the project “CO₂ injection into a near surface aquitard for evaluating monitoring concepts and methods”. We thank I. Dumke from the BGR, Hannover for providing us with the prototype of the soil gas lances and we thank R. Schumann for the construction and maintenance of the adapted soil gas lances.

■ REFERENCES

- (1) Holloway, S. Storage of fossil fuel-derived carbon dioxide beneath the surface of the earth. *Annu. Rev. Energy Environ.* **2001**, *26*, 145–166.
- (2) Orr, F. M. Onshore geologic storage of CO₂. *Science* **2009**, *325* (5948), 1656–1658.
- (3) IPCC Special report on carbon dioxide capture and storage, Working group III of the Intergovernmental Panel on Climate Change; Cambridge, United Kingdom and New York, USA, 2005.
- (4) Little, M. G.; Jackson, R. B. Potential impacts of leakage from deep CO₂ geosequestration on overlying freshwater aquifers. *Environ. Sci. Technol.* **2010**, *44* (23), 9225–9232.
- (5) Oldenburg, C. M.; Unger, A. J. A. On leakage and seepage from geologic carbon sequestration sites. *Vadose Zone Journal* **2003**, *2* (3), 287–296.

- (6) Lemieux, J.-M. Review: The potential impact of underground geological storage of carbon dioxide in deep saline aquifers on shallow groundwater resources. *Hydrogeology Journal* **2011**, *19*, 757–778.
- (7) Lewicki, J. L.; Oldenburg, C. M.; Dobeck, L.; Spangler, L. Surface CO₂ leakage during two shallow subsurface CO₂ releases. *Geophys. Res. Lett.* **2007**, *34* (24), L24402.
- (8) Lewicki, J. L.; Hillel, G. E.; Fischer, M. L.; Pan, L.; Oldenburg, C. M.; Dobeck, L.; Spangler, L. Eddy covariance observations of surface leakage during shallow subsurface CO₂ releases. *J. Geophys. Res.* **2009**, *114* (D12), D12302.
- (9) Lu, J.; Partin, J.; Hovorka, S.; Wong, C. Potential risks to freshwater resources as a result of leakage from CO₂ geological storage: a batch-reaction experiment. *Environmental Earth Sciences* **2010**, *60* (2), 335–348.
- (10) Fahrner, S.; Schäfer, D.; Dahmke, A. A monitoring strategy to detect CO₂ intrusion in deeper freshwater aquifers. *International Journal of Greenhouse Gas Control* **2012**, *9* (0), 262–271.
- (11) Carroll, S.; Hao, Y.; Aines, R. Geochemical detection of carbon dioxide in dilute aquifers. *Geochemical Transactions* **2009**, *10* (1), 4.
- (12) Fahrner, S.; Schaefer, D.; Dahmke, A. Reactive transport modeling to assess geochemical monitoring for detection of CO₂ intrusion into shallow aquifers. *Energy Procedia* **2011**, *4* (0), 3155–3162.
- (13) Humez, P.; Audigane, P.; Lions, J.; Chiaberge, C.; Bellenfant, G. Modeling of CO₂ leakage up through an abandoned well from deep saline aquifer to shallow fresh groundwaters. *Transport in Porous Media* **2011**, *90* (1), 153–181.
- (14) Kharaka, Y. K.; Thordsen, J. J.; Kakouros, E.; Ambats, G.; Herkelrath, W. N.; Beers, S. R.; Birkholzer, J. T.; Apps, J. A.; Spycher, N. F.; Zheng, L.; Trautz, R. C.; Rauch, H. W.; Gullickson, K. S. Changes in the chemistry of shallow groundwater related to the 2008 injection of CO₂ at the ZERT field site, Bozeman, Montana. *Environmental Earth Sciences* **2010**, *60*, 273–284.
- (15) Spangler, L. H.; Dobeck, L. M.; Repasky, K. S.; Nehrir, A. R.; Humphries, S. D.; Barr, J. L.; Keith, C. J.; Shaw, J. A.; Rouse, J. H.; Cunningham, A. B.; Benson, S. M.; Oldenburg, C. M.; Lewicki, J. L.; Wells, A. W.; Diehl, J. R.; Strazisar, B. R.; Fessenden, J. E.; Rahn, T. A.; Amonette, J. E.; Barr, J. L.; Pickles, W. L.; Jacobson, J. D.; Silver, E. A.; Male, E. J.; Rauch, H. W.; Gullickson, K. S.; Trautz, R.; Kharaka, Y.; Birkholzer, J.; Wielopolski, L. A shallow subsurface controlled release facility in Bozeman, Montana, USA, for testing near surface CO₂ detection techniques and transport models. *Environmental Earth Sciences* **2010**, *60*, (2).
- (16) Emberley, S.; Hutcheon, I.; Shevalier, M.; Durocher, K.; Gunter, W. D.; Perkins, E. H. Geochemical monitoring of fluid-rock interaction and CO₂ storage at the Weyburn CO₂-injection enhanced oil recovery site, Saskatchewan, Canada. *Energy* **2004**, *29* (9–10), 1393–1401.
- (17) Raistrick, M.; Mayer, B.; Shevalier, M.; Perez, R. J.; Hutcheon, I.; Perkins, E.; Gunter, B. Using chemical and isotopic data to quantify ionic trapping of injected carbon dioxide in oil field brines. *Environ. Sci. Technol.* **2006**, *40* (21), 6744–6749.
- (18) Klusman, R. W. Detailed compositional analysis of gas seepage at the National Carbon Storage Test Site, Teapot Dome, Wyoming, USA. *Appl. Geochem.* **2006**, *21* (9), 1498–1521.
- (19) McAlexander, I.; Rau, G. H.; Liem, J.; Owano, T.; Fellers, R.; Baer, D.; Gupta, M. Deployment of a carbon isotope ratiometer for the monitoring of CO₂ sequestration leakage. *Anal. Chem.* **2011**, *83* (16), 6223–6229.
- (20) Clark, I.; Fritz, P. *Environmental Isotopes in hydrogeology*; Crc Press Inc: 1997.
- (21) Griesshaber, E.; O’Nions, R. K.; Oxburgh, E. R. Helium and carbon isotope systematics in crustal fluids from the Eifel, the Rhine Graben and Black Forest, F.R.G. *Chem. Geol.* **1992**, *99*, 213–235.
- (22) Yoshimura, K.; Liu, Z.; Cao, J.; Yuan, D.; Inokura, Y.; Noto, M. Deep source CO₂ in natural waters and its role in extensive tufa deposition in the Huanglong Ravines, Sichuan, China. *Chem. Geol.* **2004**, *205*, 141–153.
- (23) Du, J.; Cheng, W.; Zhang, Y.; Jie, C.; Guan, Z.; Liu, W.; Bai, L. Helium and carbon isotopic compositions of thermal springs in the earthquake zone of Sichuan, Southwestern China. *Journal of Asian Earth Sciences* **2006**, *26* (5), 533–539.
- (24) Redondo, R.; Yélamos, J. G. Determination of CO₂ origin (natural or industrial) in sparkling bottled waters by ¹³C/¹²C isotope ratio analysis. *Food Chem.* **2005**, *92*, 507–514.
- (25) Peter, A.; Hornbruch, G.; Dahmke, A. CO₂ leakage test in a shallow aquifer for investigating the geochemical impact of CO₂ on groundwater and for developing monitoring methods and concepts. *Energy Procedia* **2011**, *4*, 4148–4153.
- (26) Peter, A.; Lamert, H.; Beyer, M.; Hornbruch, G.; Heinrich, B.; Schulz, A.; Geistlinger, H.; Schreiber, B.; Dietrich, P.; Werban, U.; Vogt, C.; Richnow, H.-H.; Großmann, J.; Dahmke, A. Investigation of the geochemical impact of CO₂ on shallow groundwater: design and implementation of a CO₂ injection test in Northeast Germany. *Environmental Earth Sciences* **2012**, 1–15.
- (27) Lamert, H.; Geistlinger, H.; Werban, U.; Schütze, C.; Peter, A.; Hornbruch, G.; Schulz, A.; Pohlert, M.; Kalia, S.; Beyer, M.; Großmann, J.; Dahmke, A.; Dietrich, P. Feasibility of geoelectrical monitoring and multi-phase modeling for process understanding of gaseous CO₂ injection into a shallow aquifer. *Environmental Earth Sciences Special Issue* **2012**.
- (28) McCarthy, J. J.; Reimer, G. Advances in soil gas geochemical exploration for natural resources: some current examples and practices. *J. Geophys. Res.* **1986**, *91* (B12), 12327–12338.
- (29) Coplen, T. B. New guidelines for reporting stable hydrogen, carbon, and oxygen isotope-ratio data. *Geochim. Cosmochim. Acta* **1996**, *60* (17), 3359–3360.
- (30) Fischer, A.; Vieth, A.; Knöller, K.; Wachter, T.; Dahmke, A.; Richnow, H.-H. Charakterisierung des mikrobiellen Schadstoffabbaus mithilfe von isopenchemischen Methoden. *Grundwasser-Zeitschrift der Fachsektion Hydrogeologie* **2004**, *3*, 159–172.
- (31) Amundson, R.; Stern, L.; Baisden, T.; Wang, Y. The isotopic composition of soil and soil-respired CO₂. *Geoderma* **1998**, *82* (1–3), 83–114.
- (32) Deines, P., The isotopic composition of reduced organic carbon. In *Handbook of Environmental Isotope Geochemistry, 1. The Terrestrial Environment*, Fritz, P.; Fontes, J. C., Eds. Elsevier: Amsterdam, 1980; pp 329–406.
- (33) Cortis, A.; Oldenburg, C., M.; Benson, S. M. The role of optimality in characterizing CO₂ seepage from geological carbon sequestration sites. *International Journal of Greenhouse Gas Control* **2008**, *2*, 640–652.

SUPPORTING INFORMATION

Monitoring of a simulated CO₂ leakage in a shallow aquifer using stable carbon isotopes

Alexandra Schulz*¹, Carsten Vogt¹, Hendrik Lamert², Anita Peter³, Ben Heinrich⁴,
Andreas Dahmke², Hans-Hermann Richnow¹

¹ UFZ - Helmholtz Centre for Environmental Research, Department of Isotope Biogeochemistry, Permoserstraße 15, 04318 Leipzig, Germany, E-mail: alexandra.schulz@ufz.de. Tel: +49-341-235-1360. Fax: +49-341-1443

² UFZ - Helmholtz Centre for Environmental Research, Department of Monitoring and Exploration Technologies, Permoserstraße 15, 04318 Leipzig, Germany

³ Institute for Geosciences, Christian-Albrechts-University Kiel, Ludwig-Meyn-Straße 10, 24118 Kiel, Germany

⁴GICON – Tiergartenstr. 48, 01219 Dresden

*corresponding author

12. Appendix

SI-table 1 Isotope ratios [‰] of soil gas for three sampling campaigns before and during the CO₂ injection.

Sampling point	May 2010	January 2011	February 2011	April 2011	May 2011
1C	-19.8	-17.9	-17.4	-19.5	-19.5
2C	-19.5	-18.2	-19.9	-28.1	-22.1
3C	-19.3	-17.0	-19.8	-17.7	-22.9
1D	n.m.	-21.6	-19.6	-20.1	-21.8
2D	n.m.	-18.6	-20.9	-26.9	-19.9
3D	n.m.	-23.2	-22.4	-19.8	-20.6
1E	-18.4	-19.9	-18.9	-19.2	-20.0
2E	-18.9	-18.0	-19.6	-20.3	-20.3
3E	-22.2	-22.2	-18.9	-21.3	-21.3
1F	-17.1	-18.7	-21.2	-21.7	n.m.
4F	-20.7	-17.8	-17.7	-19.3	-19.3
5F	-19.4	-20.5	-19.0	-19.2	-19.2
1A	-20.8	-20.7	-18.7	n.m.	n.m.

n.m. not measured

SI-table 2 Sampling campaigns, number of samples and lowest measured $\delta^{13}\text{C}$ value of CO₂ in groundwater samples.

Campaign	Date	Lowest measured $\delta^{13}\text{C}$ value	Number of samples
-3	19.05.2010	-23.05 ± 0.06 ‰	5
-2	23.11.2010	-24.62 ± 0.22 ‰	21
-1	01. – 03.03.2011	-22.01 ± 0.14 ‰	43
0	23. – 25.03.2011	-24.74 ± 0.24 ‰	54
1	30. – 31.03.2011	-24.53 ± 0.47 ‰	39
2	01. – 02.04.2011	-31.42 ± 0.12 ‰	46
3	06. – 08.04.2011	-30.82 ± 0.17 ‰	46
4	11. – 13.04.2011	-31.63 ± 0.19 ‰	51
5	27. – 29.04.2011	-31.79 ± 0.02 ‰	60
6	10. – 12.05.2011	-31.87 ± 0.06 ‰	51
7	09. – 10.06.2011	-31.57 ± 0.02 ‰	40
8	28. – 30.06.2011	-31.54 ± 0.23 ‰	60
9	29. – 31.08.2011	-30.87 ± 0.37 ‰	59
10	17. – 20.10.2011	-30.82 ± 0.35 ‰	60

12. Appendix

SI-table 3 Isotope ratios and SF₆-concentration of groundwater samples over the entire monitoring campaign.

	18 m		15 m		12 m	
1/4/11						
	$\delta^{13}\text{C}/^{12}\text{C}$ [‰]	SF ₆ [mg/L]	$\delta^{13}\text{C}/^{12}\text{C}$ [‰]	SF ₆ [mg/L]	$\delta^{13}\text{C}/^{12}\text{C}$ [‰]	SF ₆ [mg/L]
1A	-23.85	5	-23.85	5	-23.85	5
1D	-24.48	64	-24.48	64	-24.48	64
2D	-20.90	5	-20.90	5	-20.90	5
3D	-21.83	5	-21.83	5	-21.83	5
LUA	-21.27	5	-21.27	5	-21.27	5
ML1B	-21.18	5	-23.54	5	-22.91	5
ML1C	n.s.	n.s.	-31.42	28	-24.44	5
ML2C		n.m.	-20.92	5	-20.92	35
ML3C	-23.40	5	-23.16	5	-21.32	5
ZZ5		n.m.	-29.61	45		n.m.
6/4/11						
1D	-26.76	150	-26.76	150	-26.76	150
2D	-22.45	5	-22.45	5	-22.45	5
3D	-23.00	5	-23.00	5	-23.00	5
LUA	-22.35	5	-22.35	5	-22.35	5
ML1B	-23.19	5	-22.39	5		n.m.
ML1C	n.s.	n.s.	-30.82	120	-24.40	5
ML2C	-21.68	5	-21.04	5	-29.87	540
ML3C	-23.03	5	-22.81	5	-22.15	5
ZZ3		n.m.	-20.81	5		n.m.
ZZ5	-25.05	140	-25.13	11	-25.19	120
ZZ6	n.s.	n.s.	-24.60	5	-24.60	5
11/4/11						
1D	-29.09	180	-29.09	180	-29.09	180
2D	-22.28	17	-22.28	17	-22.28	17
1F	-21.90	5	-21.90	5	-21.90	5
4F	-19.80	5	-19.80	5	-19.80	5
5F	-22.58	5	-22.58	5	-22.58	5
LUA	-21.90	5	-21.90	5	-21.90	5
ML1B	-21.87	5	-21.93	5	-22.68	5
ML1C	n.s.	n.s.	-31.63	120	-26.07	9.2

12. Appendix

ML1E	-20.23	5	-20.80	5	-23.67	5
ML2C	-31.64	530	-21.22	11	-30.44	720
ML2E	-20.44	5	-20.65	5	-20.71	5
ML3C	-22.78	5	-22.61	5	-22.37	5
ML3E	-22.10	5	-22.05	5	-22.44	5
ML8E	-20.08	5	-19.60	5	-19.75	5
ZZ3	-20.45	5	-20.66	5	-22.59	5
ZZ5	-27.21	390	-23.68	42	-28.53	580
ZZ6	n.s.	n.s.	-22.95	5	-22.99	5
10/5/11						
1D	-30.62	200	-30.62	200		n.m.
2D		n.m.		n.m.	-28.56	98
3D	-28.56	98	-28.56	98	-31.50	220
ML1C	n.s.	n.s.	-32.57	270	-29.22	410
ML2C	-31.60	630	-22.41	5	-31.87	370
ML3C	-30.78	85	-23.97	390	-23.18	5
ML1E	-21.80	5	-22.52	5	-25.47	5
ML3E	-22.93	5	-21.82	5	-21.25	5
ML8E	-20.20	5		n.m.	-20.96	5
ML6F	-20.93	5	-22.13	5	-20.53	5
ML1G	-21.47	5	-23.28	5	n.s.	n.s.
ZZ1	-22.21	5	-22.21	5	-22.21	5
ZZ2	-19.53	5	-20.64	5	-30.62	200
ZZ3	-22.12	5	-20.76	5		n.m.
ZZ5	-21.07	5	-20.80	5	-22.91	5
ZZ6	-23.61	5	-24.16	5	-23.66	5
28/6/11						
1A	-22.62	5.00	-22.62	5.00	-22.62	5.00
1D	-31.48	290.00	-31.48	290.00	-31.48	290.00
2D	-30.95	690.00	-30.95	690.00	-30.95	690.00
3D	-30.60	120.00	-30.60	120.00	-30.60	120.00
1F	-22.82	5	-22.82	5	-22.82	5
4F	-20.32	5.00	-20.32	5.00	-20.32	5.00
5F	-22.54	5.00	-22.54	5.00	-22.54	5.00
1H	-19.90	5.00	-19.90	5.00	-19.90	5.00
LUA	-30.82	270.00	-30.82	270.00	-30.82	270.00

12. Appendix

ML1B	-22.00	5.00	-22.39	5.00	-22.13	5.00
ML1C	n.s.	n.s.	-28.22	480.00	-31.11	670.00
ML2C	-21.36	5.00	-31.49	300.00	-30.19	140.00
ML3C	-26.91	130	-24.31	5.00	-31.01	980
ML1E	-21.34	5.00	-31.42	180	-27.48	74.00
ML2E	-21.70	5.00	-21.88	5.00	-20.82	5
ML3E	-22.70	5.00	-31.55	450	-23.32	5.00
ML8E	-19.00	5.00	-19.19	5.00	-19.39	5.00
ML6F	-19.89	5.00	n.s.	n.s.	n.s.	n.s.
ZZ1	-22.27	5.00	-22.27	5.00	-22.27	5.00
ZZ2	-21.05	5.00	-20.75	5.00		n.m.
ZZ3	-20.59	5.00	-20.52	5.00	-22.29	5.00
ZZ5	-21.67	5.00	-21.40	5.00	-20.96	5.00
ZZ6	-22.84	5	-23.08	5.00	-22.80	5.00
30/8/11						
1D	-28.74	350.00	-28.74	350.00	-28.74	350.00
2D	-28.21	180.00	-28.21	180.00	-28.21	180.00
3D	-26.50	100.00	-26.50	100.00	-26.50	100.00
1F	-25.28	57.00	-25.28	57.00	-25.28	57.00
4F	-20.37	5.00	-20.37	5.00	-20.37	5.00
5F	-25.92	49.00	-25.92	49.00	-25.92	49.00
LUA	-28.61	190.00	-28.61	190.00	-28.61	190.00
Z2	-22.39	5.00	-22.39	5.00	-22.39	5.00
ML1B	-22.83	5.00	-23.15	5.00	-23.03	5.00
ML1C	n.s.	n.s.	-25.48	110.00	-24.59	80.00
ML2C	-21.40	5.00	-25.61	110.00	-22.07	5.00
ML3C	-23.19	13.00	-23.62	5.00	-25.33	360.00
ML1E	-21.60	5.00	-28.53	230.00	-30.89	760.00
ML2E	-22.99	5.00	-21.08	5.00	-20.55	5.00
ML3E	-22.15	5.00	-30.28	800.00	-22.31	5.00
ZZ6	-22.36	5.00	-23.32	5.00	-22.32	5.00
19/10/11						
1D	-23.61	68.00	-23.61	68.00	-23.61	68.00
2D	-22.33	29.00	-22.33	29.00	-22.33	29.00
3D	-25.17	37.00	-25.17	37.00	-25.17	37.00
1F	-29.61	230.00	-29.61	230.00	-29.61	230.00

12. Appendix

4F	-21.34	5.00	-21.34	5.00	-21.34	5.00
5F	-27.62	95.00	-27.62	95.00	-27.62	95.00
1H	-19.73	5.00	-19.73	5.00	-19.73	5.00
LUA	-27.11	200.00	-27.11	200.00	-27.11	200.00
ML1B	-23.42	5.00	-23.11	5.00	-23.19	5.00
ML1C	n.s.	n.s.	-29.47	280.00	-22.30	7.40
ML2C	-21.40	5.00	-21.50	5.00	-23.13	5.00
ML3C	-23.04	5.50	-23.06	5.00	-22.11	8.30
ML1E	-25.91	58.00	-30.82	160.00	-30.55	650.00
ML2E	-30.82	44.00	-23.03	20.00	-21.07	5.00
ML3E	-30.82	44.00	-29.77	160.00	-25.15	35.00
ML1G	-19.77	5.00	-21.89	5.00	-21.40	5.00
ML6F	-19.73	5.00	-20.05	5.00	-19.93	5.00
ML8E	-19.96	5.00	-19.30	5.00	-20.09	5.00
ZZ1	-30.50	520.00	-30.50	520.00	-30.50	520.00
ZZ2	-20.14	5.00	-20.10	5.00	-20.14	5.00
ZZ3	-20.89	5.00	-20.31	5.00	-22.17	5.00
ZZ5	-20.85	5.00	-20.50	5.00	-20.68	5.00
ZZ6	-23.13	5.00	-24.36	5.00	-22.93	5.00

Detailed information about the construction of the monitoring wells

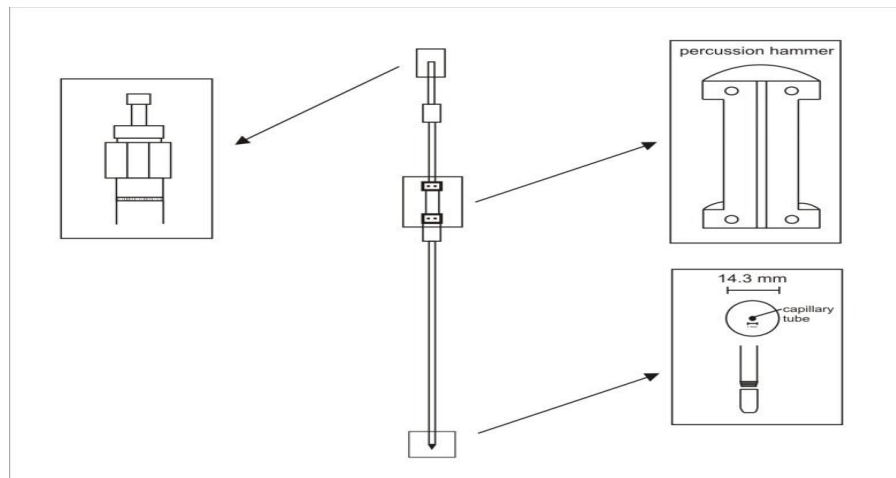
- 12 2" wells screened at 12-18 m bgl
- seven 1" wells screened at 12.5-13.5, 14.5-15.5 and 17.5-18.5 m bgl that were separately sampled using a packer system
- 11 multi-level wells with different diameters and sampling points at 12, 15 and 18 m bgl
- four sampling points at 12 m bgl
- one 4" well

Description of the soil gas probes

A thin capillary tube with an inner diameter of 0.99 mm (outer diameter 3.8 mm) is placed in the middle of the lance. A small diameter was chosen in order to keep the death volume (1.1 mL) as small as possible. On top of the lance a Swagelok[®] valve with a gas tight septum was used as sampling port.

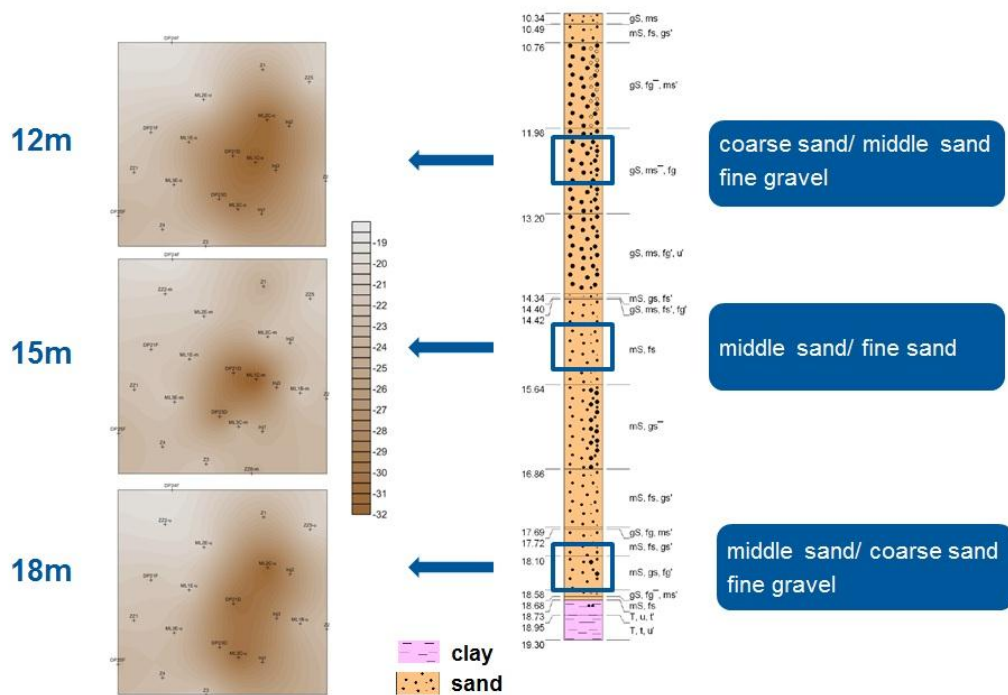
12. Appendix

Before the lance was pushed into the ground, a metal rivet was placed on the lower end of the lance to avoid a clogging of the capillary tube with sediments. The lance was pushed for about one meter manually into the ground. Afterwards, the lance was pulled about two centimeters out of the ground again, so that the rivet was lost and the lower end of the lance was open for sampling. A 5 mL gas-tight glass syringe (Hamilton, USA) was used to remove about five times the dead volume of the sampler from the capillary tube. The lances were left in the ground for at least 30 minutes to allow an equilibration of the soil gas before the samples were taken.



SI-figure 1. Scheme of the self-constructed soil gas sampling lances. The Swagelok® valve on the top is used as the sampling port. The percussion hammer is used to push the lance into the ground and to pull it out after the sampling.

12. Appendix



SI-figure 2. Distribution of the isotope ratios correlated to the different depth of a profile of *MLC2*. It shows that the lithology has an influence on the distribution of the isotope ratios as coarse to middle sand has a higher pore space and therefore the isotopically light CO_2 that is dissolved in the groundwater can migrate into a larger spatial area.

Appendix C

Feasibility of geoelectrical monitoring and multiphase modeling for process understanding of gaseous CO₂ injection into a shallow aquifer

Lamert, Hendrik; Geistlinger, Heinrich; Werban, Ulrike; Schütze, Claudia, Peter, Anita; Hornbruch, Götz; **Schulz, Alexandra**; Pohlert, Marco; Kalia, S.; Großmann, Jochen; Dahmke, Andreas, Dietrich, Peter

Environmental Earth Sciences, 2012, 67, pp 447-462

Feasibility of geoelectrical monitoring and multiphase modeling for process understanding of gaseous CO₂ injection into a shallow aquifer

Hendrik Lamert · H. Geistlinger · U. Werban · C. Schütze · A. Peter · G. Hornbruch · A. Schulz · M. Pohlert · S. Kalia · M. Beyer · J. Großmann · A. Dahmke · P. Dietrich

Received: 16 December 2011 / Accepted: 1 April 2012 / Published online: 26 April 2012
© Springer-Verlag 2012

Abstract Potential pathways in the subsurface may allow upwardly migrating gaseous CO₂ from deep geological storage formations to be released into near surface aquifers. Consequently, the availability of adequate methods for monitoring potential CO₂ releases in both deep geological formations and the shallow subsurface is a prerequisite for the deployment of Carbon Capture and Storage technology. Geoelectrical surveys are carried out for monitoring a small-scale and temporally limited CO₂ injection experiment in a pristine shallow aquifer system. Additionally, the feasibility of multiphase modeling was tested in order to describe both complex non-linear multiphase flow

processes and the electrical behavior of partially saturated heterogeneous porous media. The suitability of geoelectrical methods for monitoring injected CO₂ and geochemically altered groundwater was proven. At the test site, geoelectrical measurements reveal significant variations in electrical conductivity in the order of 15–30 %. However, site-specific conditions (e.g., geological settings, groundwater composition) significantly influence variations in subsurface electrical conductivity and consequently, the feasibility of geoelectrical monitoring. The monitoring results provided initial information concerning gaseous CO₂ migration and accumulation processes. Geoelectrical monitoring, in combination with multiphase modeling, was identified as a useful tool for understanding gas phase migration and mass transfer processes that occur due to CO₂ intrusions in shallow aquifer systems.

H. Lamert (✉) · U. Werban · C. Schütze · P. Dietrich
Department Monitoring and Exploration Technologies,
Helmholtz Centre for Environmental Research, Permoser Str. 15,
04318 Leipzig, Germany
e-mail: hendrik.lamert@ufz.de

H. Geistlinger · M. Pohlert · S. Kalia
Department of Soil Physics, Helmholtz Centre for
Environmental Research, Theodor Lieser Str. 4, 06120 Halle,
Germany

A. Peter · G. Hornbruch · A. Dahmke
Institute for Geosciences, University of Kiel,
Ludewig-Meyn-Str. 10, 24118 Kiel, Germany

A. Schulz
Department of Isotope Biogeochemistry, Helmholtz Centre for
Environmental Research, Permoser Str. 15, 04318 Leipzig,
Germany

M. Beyer · J. Großmann
GICON GmbH, Tiergartenstr. 48, 01219 Dresden, Germany

P. Dietrich
Centre for Applied Geoscience, University of Tübingen,
Hölderlinstraße 12, 72074 Tübingen, Germany

Keywords Carbon sequestration · CO₂ leakage · Geoelectrical monitoring · Multiphase modeling

Introduction

An approach currently being developed with the aim of reducing CO₂ emissions into the atmosphere is CCS technology (Carbon Capture and Storage). The main concern associated with CCS is that CO₂ from storage reservoir formations (such as deep saline aquifers or depleted oil and gas fields) may leak due to permeable cover sediments or natural and artificial pathways, such as faults or well structures. These potential pathways may allow upwardly migrating gaseous CO₂ to be released into near surface aquifers or even into the atmosphere (surface leakage), which would reduce the efficiency of CCS. Moreover, a potential leakage of CO₂ from storage sites could have

detrimental effects on the surrounding environment and even upon human health (Oldenburg and Unger 2003; Holloway et al. 2007; Lewicki et al. 2007).

Computational simulations (Carroll et al. 2009; Fahrner et al. 2011; Humez et al. 2011), batch-reactor experiments (Lu et al. 2010) and a small-scale field study at the ZERT site (Kharaka et al. 2010) describe significant changes of aquifer geochemistry (e.g., mobilization of cations from the host rock, pH decrease, electrical conductivity increase) in the groundwater system after CO₂ intrusion. Consequently, in the context of sound risk assessment, the availability of adequate methods for the detection and monitoring of potential CO₂ release is a prerequisite for the deployment of CCS technology, in both deep geological formations and the shallow subsurface (Wilson et al. 2007).

To monitor injected CO₂ in deep geological formations, geophysical methods are currently applied (Torp and Gale 2004). Geoelectrical methods are a promising tool for monitoring subsurface processes, which induce temporal or spatial variations of electrical conductivity. Some case studies have already been performed using geoelectrical methods for monitoring the CO₂ storage test site Ketzin/Germany (Kiessling et al. 2010) and for the characterization of natural geological CO₂ leakage sites (Schütze et al. 2012).

In our case study, a controlled CO₂ injection experiment was performed by injecting gaseous CO₂ into a pristine shallow aquifer, with the aim of further improving the understanding of CO₂ behavior in shallow groundwater systems (see Peter et al. 2012). During a period of 10 days in 2011, 787 kg in total of gaseous CO₂ was injected into a near surface aquifer at a depth of 18 m below ground surface. One of the main objectives of this field study was to design and test different monitoring methods to detect potential CO₂ release in near subsurface groundwater systems. For this purpose, three CO₂ injection lances and 34 monitoring wells were installed and additionally equipped with electrodes to allow spatially and temporally high resolution monitoring of subsurface processes caused by CO₂ intrusion.

To perform a CO₂ gas injection experiment in partially saturated heterogeneous porous media, understanding and control of complex non-linear multiphase flow processes is essential. The general objective of the present paper is to improve the understanding of transport processes monitored during the performed CO₂ injection experiment with respect to analogue processes, which might occur during a CO₂ leakage from deep storage reservoirs. In this context, a more detailed focus of this work could be outlined as follows (1) to prove and describe the feasibility of geoelectrical methods for monitoring CO₂ intrusions into near subsurface structures and (2) to test the feasibility of the multiphase model TOUGH2 (Pruess et al. 1999), to describe the gas flow patterns and the electrical behavior of partially saturated heterogeneous porous media. Therefore,

the goal of the modeling study is to answer whether or not TOUGH2 is able to describe experimentally measured geoelectrical breakthrough curves and additionally, whether TOUGH2 can adequately describe the gas flow patterns or at least the average gas phase distribution within a heterogeneous aquifer.

Geoelectrical monitoring of subsurface processes

An overview of physical parameters affecting electrical conductivity

In this section, rock-physical basic principles for geoelectrical monitoring are presented with respect to CO₂ intrusion into a shallow aquifer system.

Due to the lower pressure regime present in shallow aquifers, potentially upward migrating supercritical CO₂ from deep geological formations changes into its gas phase. Gaseous CO₂ intrusion into shallow groundwater systems generally causes increased gas phase content in the soil pore space, which accordingly leads to decreased bulk electrical conductivity of the subsurface. However, a subsequent dissolution of CO₂ leads to a formation of carbonic acid, which generally leads to decreased pH values. This is followed by an increase of electrical fluid conductivity.

Following Rein et al. (2004), potential effects of factors inducing variations of electrical conductivity in the subsurface are discussed, i.e., gas and soil water content, concentration variation of ions in groundwater, and temperature.

An empirical, widely used equation for estimating the electrical conductivity of partly saturated rocks was developed by Archie (1942), which assumed that the electrical conductivity of the soil matrix is negligible:

$$\sigma_{ps} = \sigma_f \frac{1}{F} S_w^n \quad (1a)$$

where σ_{ps} denote electrical conductivity of partly saturated rocks (subsurface); σ_f electrical conductivity of fluid; F formation resistivity factor; S_w water saturation; n exponent of saturation (often assumed: $n = 2$, e.g., Archie 1942).

With [according to Dahnov (Schön 1996)]:

$$F = \frac{a}{\phi^m} \quad (1b)$$

where ϕ denote porosity; m exponent of cementation; a empirical coefficient, see also Schön (1996).

However, in the presence of an electrical conductive matrix (e.g., clay-rich sediments), the corresponding component of electrical conductivity is not negligible. A list of appropriate studies and models investigating matrix conductivity as a component of rock conductivity is provided

by Schön (1996). Taking the electrical conductivity of the matrix into account, a more general equation for σ_{ps} is:

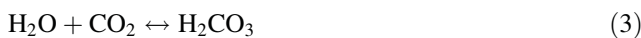
$$\sigma_{ps} = \sigma_f \frac{1}{F} S_w^n + \sigma_m \tag{2}$$

where σ_m denote electrical conductivity of the soil matrix.

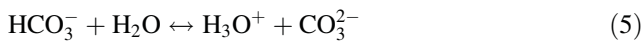
According to Eq. (2), parameters, which generally might be affected by a CO₂ intrusion are water saturation S_w and fluid conductivity σ_f .

Naturally, large variations of water saturation S_w are expected in the area of groundwater table fluctuations as well as in the upper part of the unsaturated zone (soil moisture content). However, gas intrusion into the saturated zone firstly induces decreasing water saturation in the pore space, which is in turn associated with an increase in electrical resistivity (reciprocal of conductivity) of the subsurface. According to Rein et al. (2004), a calculated variation in water saturation from 100 to 95 % results in a conductivity decrease of about 10 %, whilst a change in water saturation from 100 to 80 % leads to a conductivity decrease of about 36 %.

Fluid conductivity σ_f is primarily characterized by the geological background, which affects the composition of ions dissolved in groundwater. Basically, CO₂ intrusion in water (H₂O) leads to dissolution processes depending on pressure and temperature:



The subsequent dissociation of carbonic acid in water:



and the geochemical alteration of groundwater due to CO₂ intrusion, which strongly depends on mineral and groundwater composition, affect the electrical fluid conductivity (see also Kharaka et al. 2010; Lu et al. 2010; Fahrner et al. 2011).

Electrical conductivity of the fluid can be estimated by ionic mobility and ion concentrations (Keller and Frischknecht 1966):

$$\sigma_f = Fa \sum_{i=1}^{N_i} C_i^{eq} v_i \tag{6}$$

where Fa denotes Faraday Constant; C_i^{eq} equivalent concentration of ion i ; v_i the temperature depended mobility of ion i .

Equation (6) neglects the interaction of ions. This simplification does not account for the activity coefficient, which relates activities to molal concentrations (see Appelo and Postma 1993). This is justified for fluids containing low salt concentrations, which are associated with low ionic strengths.

Ionic fluid composition is changing due to CO₂ intrusion into an aquifer system. According to Eq. (6), changes of equivalent concentrations of present ions lead to variations in fluid conductivity. However, σ_f variations in response to a CO₂ intrusion depend on various factors, i.e., variations in depth, groundwater dynamic, initial groundwater composition, mineralogy of the host rock, and CO₂ intrusion rate (Fahrner et al. 2011). Fahrner et al. (2011) calculated the geochemical impact of CO₂ intrusion upon the electrical conductivity of groundwater by using different scenarios including varying conditions. For a shallow freshwater aquifer with calcite present, Fahrner et al. (2011) calculated a significant increase of fluid conductivity in the order of 1 mS/cm. The presence or lack of calcite was identified as a major geochemical factor inducing electrical conductivity variations of groundwater in the case of CO₂ intrusion, as the solubility of carbonates increases with increasing content of dissolved CO₂. For an equivalent scenario in the absence of calcite, the increase of fluid conductivity was less pronounced due to the low dissociation rate of dissolved carbonic acid.

Detailed information on CO₂ dissociation processes and the carbonate-equilibrium-system are given, e.g., in Appelo and Postma (1993).

The electrical conductivity of a fluid can generally be estimated using Eq. (6). However, dynamic geochemical processes (e.g., cation exchange processes) associated with site-specific conditions (e.g., presence or absence of buffering materials) must be taken into account when assess variations in fluid conductivity caused by CO₂ intrusion.

Due to deep geological storage of CO₂ and the associated potential upward migration of gaseous CO₂, temperature variations may also influence σ_f (Fig. 1). Variations of electrical conductivity caused by temperature changes can be approximated according to empirical equations presented by Arps (1953):

$$\sigma_f(T_1) = \sigma_f(T_0) \frac{T_1 + 21.5}{T_0 + 21.5} \tag{7}$$

where T_0, T_1 denote fluid temperature at time t_0 and t_1 ; $\sigma_f(T_0), \sigma_f(T_1)$ denote electrical conductivity of the fluid at temperature T_0, T_1 in (°C).

And by Dachnov (Schön 1996):

$$\sigma_f(T_1) = \sigma_f(T_0) \frac{1 + \alpha_T(T_1 - 18)}{1 + \alpha_T(T_0 - 18)} \tag{8}$$

where α_T denotes temperature coefficient, for temperatures about 18 °C is $\alpha_T \approx 0.025 \text{ } ^\circ\text{C}^{-1}$.

For example, temperature changes of 5 °C result in a relative electrical resistivity variation of approx. 16 % (Fig. 1).

The three parameters described above—variations in water saturation, changing ion content in groundwater, and temperature variations—significantly influence the electrical conductivity of variable saturated porous media.

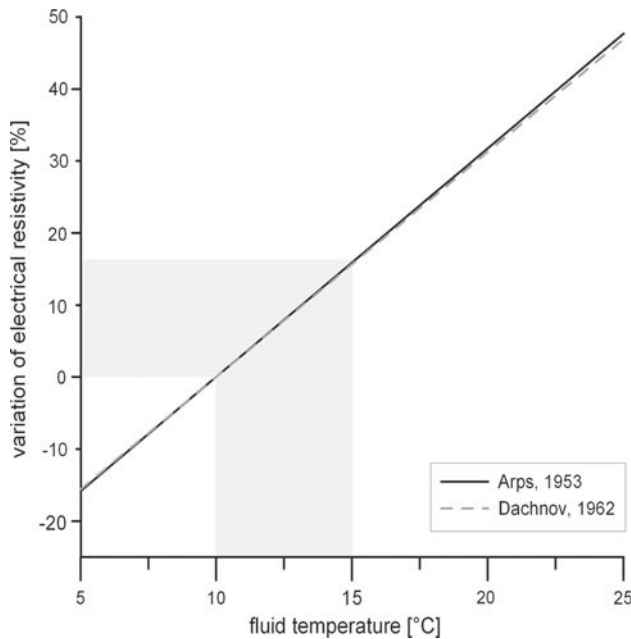


Fig. 1 Relative variation of electrical fluid resistivity due to temperature variation. Approximation according to Arps (1953) and Dachnov (Schön 1996), reference temperature: 10 °C

However, the impact strength of each parameter depends on numerous conditions (e.g., geological settings, depth, and groundwater composition) and is thus highly site-specific (see also Kolditz et al. 2012).

An overview of geoelectrical time-lapse monitoring of subsurface processes

Geoelectrical methods allow time efficient as well as temporal and spatially high resolution monitoring of hydrodynamic subsurface processes. Generally, surveys using electrodes installed in boreholes at selected depths of interest (e.g., tracer injection horizon) are more suitable than using electrodes installed at the ground surface level. This is due to the fact that the latter are usually more influenced by external perturbations, i.e., changes in air temperature or soil moisture (e.g., Binley et al. 2002; Rein et al. 2004). The sensitivity distribution of a four-electrode array (two current and two potential electrodes) configuration primarily denotes regions, which are sensitive to the measurement. Typical behavior reveals that the highest sensitivities occur in the vicinity of the electrodes (e.g., Knödel et al. 2007). Electrodes located at wells in the injection horizon are placed nearby or within the altered groundwater, which commonly results in better spatial and temporal resolution.

Geoelectrical measurements allow conclusions about varying electrical parameters and thus, help the assessment of hydrodynamic subsurface processes.

For monitoring variations of electrical parameters in the subsurface, two approaches can be used. Firstly, determining variations of absolute values:

$$\Delta\sigma_{ps} = \sigma_{ps}^{t,1} - \sigma_{ps}^{t,0} \quad (9)$$

where $\Delta(\sigma_{ps})$ denotes the variation of electrical conductivity of partly saturated rock at time step $t = 0$ and $t = 1$.

According to Eqs. (1a, 1b) and (2), electrical variations of partly saturated rocks are induced by variations of fluid conductivity and water saturation:

$$\Delta(\sigma_{ps}) = (\sigma_f^{t,1}(S_w^n)^{t,1} - \sigma_f^{t,0}(S_w^n)^{t,0})F^{-1} \quad (10a)$$

$$= \Delta(\sigma_f S_w^n)F^{-1} \quad (10b)$$

Using absolute values for monitoring variations of electrical parameters, $\Delta(\sigma_{ps})$ also depends upon the formation resistivity factor F and accordingly on geological heterogeneities (see Eq. 10a, 10b). Generally, F might be assumed to be constant over time. However, due to mineral dissolution and chemical precipitation, F may be variable (e.g., Huq et al. 2012). For the assumption that F is constant over time, no alteration processes of the sediment structure occur. Consequently, for conditions with constant F and constant $\Delta\sigma_f$, parameters ΔS_w^n and $\Delta\sigma_{ps}$ are linearly related (Eq. 10a, 10b).

The second approach for monitoring variations of electrical parameters determines relative values, e.g., determination of ratios that correspond variations relative to $\sigma_{ps}^{t,0}$:

$$\sigma_{ps}^{t,1} / \sigma_{ps}^{t,0} = \frac{\sigma_f^{t,1} F^{-1} (S_w^n)^{t,1} + \sigma_m}{\sigma_f^{t,0} F^{-1} (S_w^n)^{t,0} + \sigma_m} \quad (11a)$$

This approach seems more complex. When matrix conductivity is negligible ($\sigma_m \ll \sigma_f^{t,z} F^{-1} (S_w^n)^{t,z}$), Eq. (11a) can be simplified (assuming that F is constant over time):

$$\sigma_{ps}^{t,1} / \sigma_{ps}^{t,0} \approx \frac{\sigma_f^{t,1} (S_w^n)^{t,1}}{\sigma_f^{t,0} (S_w^n)^{t,0}} \quad (11b)$$

This assumption depends strongly on site-specific geological and mineralogical conditions (e.g., presence of clay-rich sediments) and must consequently be assessed for each field site. However, according to Eq. (11b) using relative values, determined variations do not depend on F .

The approach using absolute variation (Eq. 10a, 10b) could generally be used for homogeneous geological conditions. In geological conditions with negligible matrix conductivity a more appropriate approach is the second one [Eq. (11a, 11b); Dietrich 1999]. Consequently, the choice of which approach should be taken is site-dependent.

CO₂ injection scenario: test site and test setup

In order to prove the feasibility of geoelectrical measurements for monitoring CO₂ intrusion scenarios in shallow aquifer systems, a field study was carried out at a former military airfield near the town of Wittstock. The test site is located approx. 100 km north of Berlin, in the state of Brandenburg (Germany). At the test site, a plane fallow land, the geological conditions are primarily characterized by glacial or glacial-fluvial unconsolidated Quaternary sediments. Based on a detailed field site investigation, information on stratigraphic composition was collected using Direct Push soundings (e.g., Dietrich and Leven 2006; Leven et al. 2011; Vienken et al. 2012), as well as drilling samples (see also Peter et al. 2011, 2012).

The stratification of the uppermost aquifer (aquifer 1) consists of interbedded strata composed of sands, silts, clays and humus with total thickness of about 11 m. Glacial loam is underlying aquifer 1. According to drilling results, the depth and thickness (in average 0.5 m) of the loam is highly variable. At the test site, aquifer 2 extends approx. 11.5–19.5 m below ground level (bgl). Due to its large extent in depth and relatively homogeneous composition, the sandy sediments of this aquifer were chosen as an appropriate injection horizon for the gaseous CO₂ (Fig. 2). Glacial till is underlying aquifer 2 and forms the base of the CO₂ injection horizon.

Collected data resulted in a detailed geological structure model of the test site. The geological structure model for the injection horizon is described in detail by Peter et al. (2012). It consists of six different layers from top to

bottom: (1) glacial loam, (2) upper medium sand layer, (3) coarse sand layer in the eastern part, (4) silt layer in the Western part, (5) lower medium sand layer, and (6) continuous boulder clay layer.

Regional groundwater flow direction is roughly directed from east to west. The average pore water velocity (subsequently referred to as ‘groundwater flow velocity’) varies within the range <0.1 up to 1 m day⁻¹.

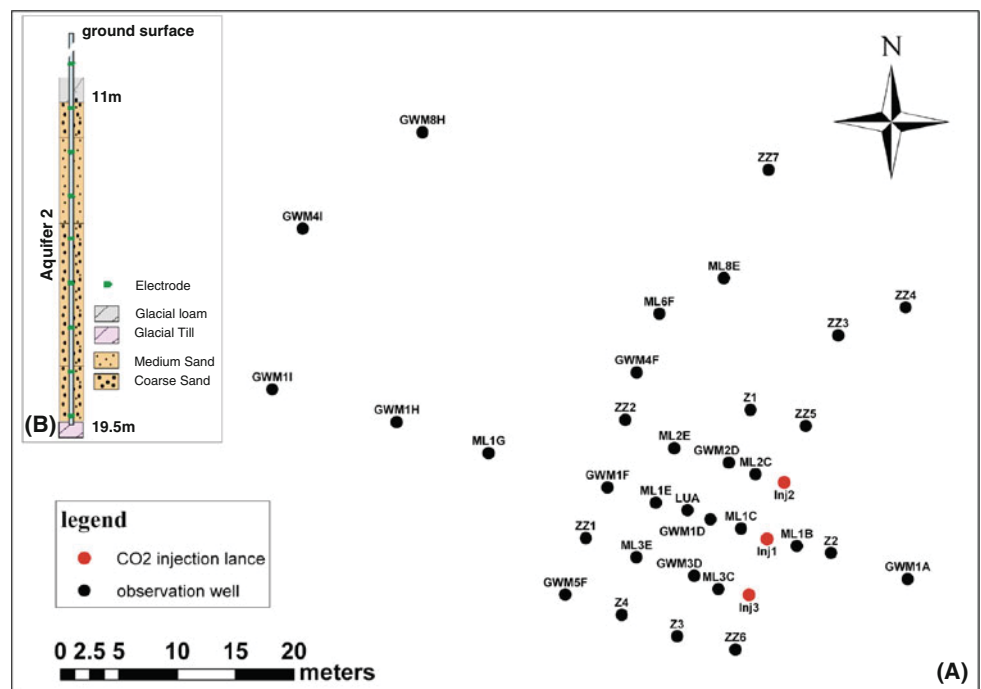
In order to perform the field test, three CO₂ injection lances and 34 monitoring wells in total were installed at the test site, oriented perpendicular to regional groundwater flow direction (Fig. 2). One of the main operational constraints was to produce a coherent plume of dissolved CO₂ in groundwater. Injection lances (1.1” continuous 3-channel tubing) were installed using minimally invasive Direct Push technologies and are screened over 0.2 m at a depth of 18 m to realize a depth-defined CO₂ injection. Injection lances were installed several weeks in advance of the injection period with the aim that the sediment may reconsolidate again, thereby minimizing potential preferential pathways along the well.

The design and implementation of the injection experiment is described in detail by Peter et al. (2012).

Between 29.03.2011 and 08.04.2011, 787 kg CO₂ in total was injected with a low injection pressure (approximately equal to the hydrostatic pressure) simultaneously at the three injection lances into aquifer 2. This corresponds to injection rates of 10 L CO₂/min (at standard pressure and temperature) at each injection well.

Altogether, four different types of monitoring wells were installed to implement an extensive monitoring set-up

Fig. 2 **a** Test site Wittstock. Regional groundwater flow is directed from GWM1A to GWM1I, roughly from east to west. **b** Schematic geological profile and schematic illustration of a well equipped with electrodes



for the CO₂ injection experiment (see Peter et al. 2012). They allow for groundwater sampling before, during and after the CO₂ injection scenario. Additionally, injection lances and 33 monitoring wells are equipped with a total of 300 ring-shaped copper electrodes for implementing geoelectrical surveys. The electrodes fixed at the outer surface of the HDPE/MDPE well material are installed in pre-defined depths between 8.0 m and 18.5 m bgl, thus allowing for an electrical resistivity monitoring covering the entire thickness of aquifer 2 (Fig. 2b).

In this manner, borehole and cross-borehole measurements are realized. Generally, the spacing of the electrodes was selected to be 1 and 1.5 m, respectively. Monitoring wells GWM1D, GWM2D and GWM3D are equipped with additional electrodes to realize an electrode spacing of 0.75 m. These electrodes allow a more detailed detection of potentially accumulating gaseous CO₂ beneath the glacial loam.

Geoelectrical monitoring of the performed CO₂ injection scenario

In the presented field study, variations in apparent electrical resistivity of the subsurface are monitored by using multichannel resistivity equipment and were converted into apparent electrical conductivity values (σ_a). Extensive geoelectrical monitoring was performed by repeating a pre-defined measuring cycle with all installed electrodes.

Monitoring was performed by using different 4-point arrays (Wenner, Schlumberger, gradient, and dipole–dipole). A temporal resolution of the electrical resistivity data of 120 min was realized. Geoelectrical monitoring began approximately 1 day before the CO₂ injection scenario was started, in order to obtain baseline values. Monitoring during and after the CO₂ injection period was carried out during an initial campaign, followed by additional ‘shorter time frame’ field campaigns (Table 1), which became necessary due to the low regional groundwater flow velocity of approximately 0.05 m/day.

In this manner, approximately 350 monitoring cycles (including about 4,200 measurements each) were performed.

Electrodes fixed at pre-defined depths at discrete wells allowed high resolution geoelectrical monitoring of the

CO₂ injection scenario to take place. Measurements at various time intervals are normalized to corresponding values of mean baseline measurements [see Eq. (11a, 11b)]. This approach was used due to the fact that matrix conductivity is negligible in the identified sandy CO₂ injection horizon at the test site. Assuming the formation resistivity factor F is constant over time, the geoelectrical observed variations are caused by variations of σ_f and S_w^n [see Eq. (11b)]. Temperature in aquifer 2 was measured using multi-parameter probes. Temperature variations were determined to be in the order of 0.1 °C and have been neglected for geoelectrical monitoring (see also Peter et al. 2012; Fig. 1).

The first interpretation step carried out during process monitoring was to use breakthrough curves from borehole measurements to analyze variations of σ_a at a total of 36 wells. Breakthrough curves of borehole measurements (single spacing at discrete wells) are used since variations of σ_a can be quickly determined in high resolution over the entire test site (see also Fig. 2). Highest variations in σ_a were observed in the area between the three injection lances down to well ML1G. Based on extensive geoelectrical monitoring, single spacing borehole measurements at three wells ML1C (1.1" diameter well), GWM1D (2" diameter well), and ML1E (1.1" diameter well) were exemplarily selected and will be presented in this paper. The effects of the radius of monitoring wells with respect to the geoelectrical measurements are negligible. The breakthrough curves from the configuration arrays used (Wenner, Schlumberger, gradient, dipole–dipole) show similar behavior and provided comparable results. However, Wenner array results are presented because the noise of the Wenner data is generally minor lower.

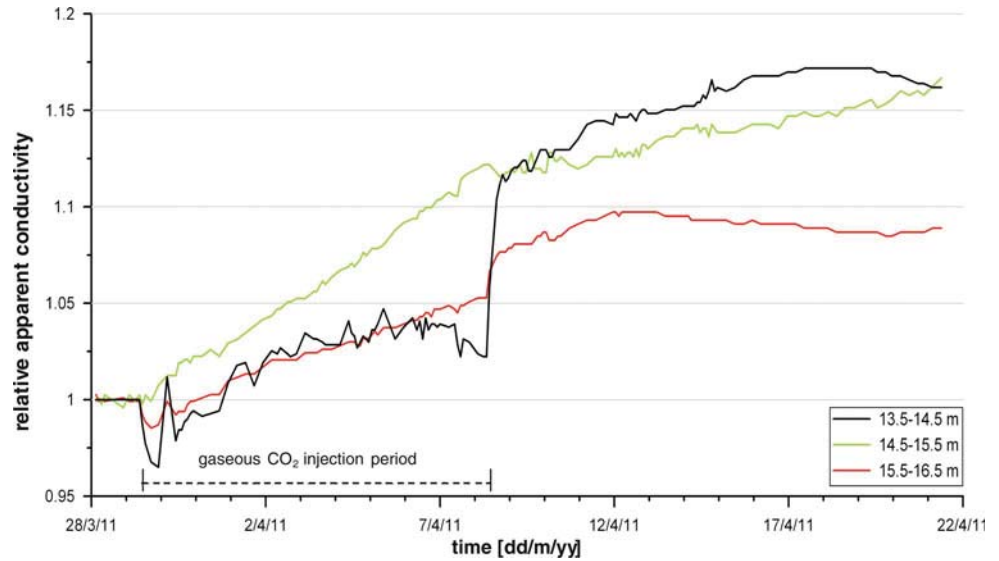
The selected wells are located along the regional groundwater flow path 2.5, 5 and 10 m distance apart from the central CO₂ injection lance Inj1, respectively (Fig. 2).

Immediately after gaseous CO₂ injection started, significant variations in σ_a at well ML1C (located 2.5 m away from injection lance 1) were detected (Fig. 3). Using a single electrode spacing of 1.0 m, the most likely explanation for the initial decrease of σ_a is increased gas saturation in the pore space (see also Sect. 2.1). This effect is subsequently followed by an increase of σ_a up to approx. 17 %, which might be caused by dissolution and dissociation processes of CO₂ in the groundwater, as well as subsequent geochemical processes, e.g., cation exchange processes. A significant ‘step-like increase’ in σ_a was detected on 8th April, when gaseous CO₂ injection was stopped. This effect was most pronounced at potential electrodes installed at depths of 13.5 and 14.5 m (black curve in Fig. 3). Furthermore, the “step-like” increase of σ_a was detected by each of the aforementioned

Table 1 Performed geoelectrical monitoring campaigns

Monitoring campaign	Time period
1	28.03.2011–21.04.2011
2	26.04.2011–29.04.2011
3	09.05.2011–12.05.2011
4	08.06.2011–10.06.2011
5	27.06.2011–29.06.2011

Fig. 3 Temporal variation of apparent conductivity (σ_a) relative to baseline measurements at well ML1C (1.1" diameter well) during Monitoring Campaign 1; electrode configuration: Wenner (AMNB). Depths (meter below ground level) of potential electrodes M–N are given in the legend. The *bottom* of glacial loam layer is located 12.0 m bgl



configuration arrays used during a period of approx. 5 h, representing measurements recorded over three successive time intervals.

The initial σ_a decrease after CO₂ injection began and the significant step-like increase in σ_a (in the order of 10 % for the uppermost Wenner array) after injection stopped, showing the gas phase dynamics caused by gaseous CO₂ injection. These effects indicate rapid gas ascent towards the glacial loam layer, representing an impermeable geological layer overlying the injection horizon.

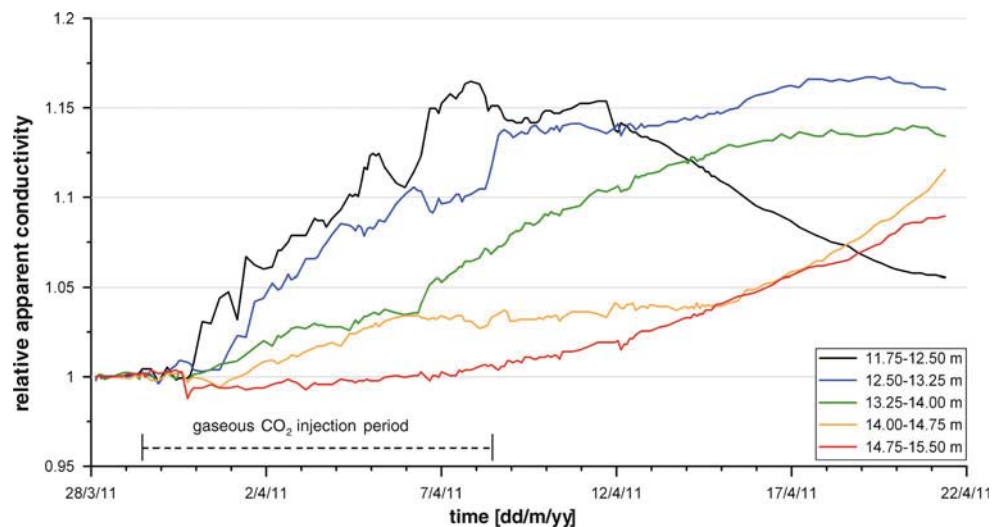
Monitoring well GWM1D is located at a distance of 5 m from the central injection lance towards regional groundwater flow direction (Fig. 2). First and most significant variations in σ_a were measured at electrodes located directly below glacial loam (black and blue curve in Fig. 4). The most likely explanation for this is the occurrence of upwardly migrated and subsequently accumulated gaseous CO₂ below the impermeable loam layer, which

lead to the formation of a gaseous CO₂ pool. Using a single electrode spacing of 0.75 m at the potential electrodes located in depths of 12.50 and 13.25 m, electrical conductivity variations of approx. 17 % were measured during Monitoring Campaign 1 (Fig. 4).

Monitoring well ML1E is located 10 m away from the central CO₂ injection lance towards the main groundwater flow direction (Fig. 2). Until Monitoring Campaign 3, geoelectrical measurements yielded no significant variations in σ_a . However, during the fourth campaign σ_a variations of approx. 12 % and during the fifth campaign σ_a variations up to 32 % were measured (Fig. 5).

Field parameters of groundwater samples are used to validate geoelectrical breakthrough curves. Values for pH and EC (σ_f) of groundwater samples taken from 15 m depth are illustrated in Fig. 5. At well ML1E (depths: 15 m bgl), pH values decreased from 6.4 to 5.2 and σ_f of groundwater samples increased from about 500 to 800 $\mu\text{S}/\text{cm}$.

Fig. 4 Temporal variation of apparent conductivity (σ_a) relative to baseline measurements at well GWM1D (2" diameter well) during Monitoring Campaign 1; electrode configuration: Wenner (AMNB). Depths (meter below ground level) of potential electrodes M–N are given in the legend. The *bottom* of glacial loam layer is located approx. 11 m bgl



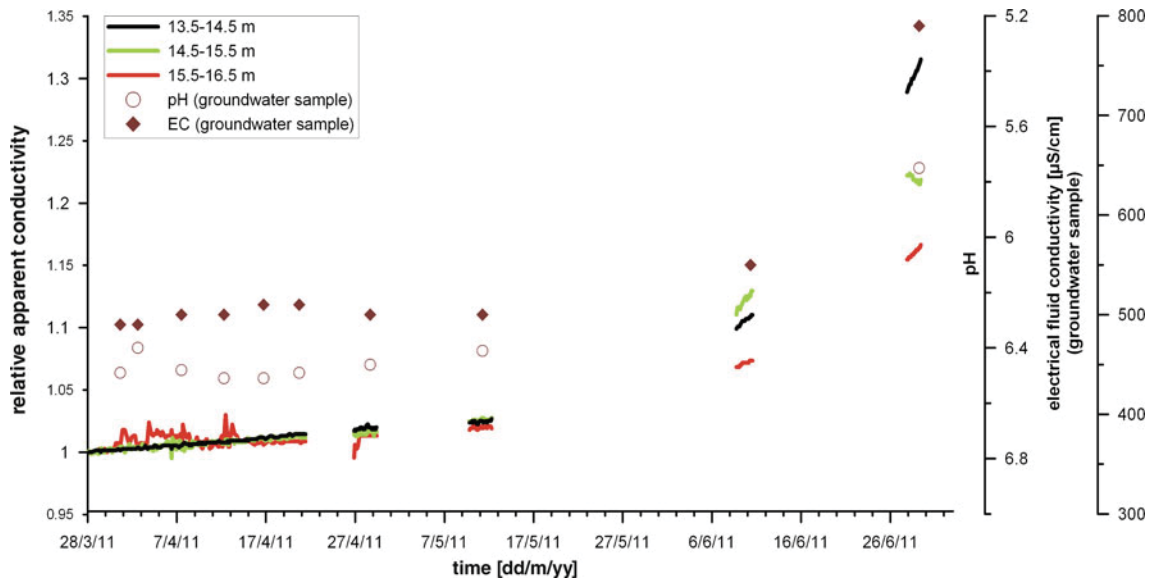


Fig. 5 Field parameters of groundwater samples (symbols) and temporal variation of apparent conductivity (σ_a) relative to baseline measurements (solid lines) at well ML1E (1.1" diameter well);

In addition to geoelectrical monitoring results (σ_a), field parameters of water samples also indicate significant alteration in groundwater chemistry caused by the injected CO_2 . Geoelectrical monitoring results and field parameters are clearly related (Fig. 5).

Geoelectrical measurements at monitoring wells ML1C, GWM1D and ML1E showed significant variations of σ_a . The geoelectrical results of ML1C clearly demonstrate the interaction of both contrary processes affecting subsurface electrical conductivity: increased gas saturation in the pore space and a higher ion concentration. Furthermore, geoelectrical monitoring results of ML1C and GWM1D indicate a rapid upward migration of gaseous CO_2 associated with accumulation processes below the glacial loam layer. Possible upward migration paths are discrete gas channels within the sediment and potential pathways at the outside of installed wells. However, only using geoelectrical monitoring results for comprehensive understanding of gas phase migration processes is difficult. Therefore, a complementary multiphase modeling was performed.

Multiphase modeling with TOUGH2

Mathematical and numerical basis

The TOUGH2 program was chosen for multiphase modeling, since it can sufficiently describe the spatial and temporal gas saturation of our bench-scale experiments (Geistlinger et al. 2009). The agreement between theoretical and experimental results was excellent. Our conclusion

electrode configuration: Wenner (AMNB). Depths (meter below ground level) of potential electrodes M–N are given in the legend. The bottom of glacial loam layer is located 12.1 m bgl

was that the average gas flow behavior is adequately described by the TOUGH2 program. Furthermore, TOUGH2 is capable of taking realistic stochastic permeability fields into account, which can be implemented relatively easily by the permeability modifier concept. In real field scenarios, stochastic permeability fields will have a significant impact on the gas flow process.

One focus of this modeling study is to investigate if the continuum model TOUGH2 (Pruess 2005; Geistlinger et al. 2009) can adequately describe the gas flow pattern or at least the average gas phase distribution within a heterogeneous aquifer. A second focus of the modeling study is to answer whether or not the widely accepted multiphase model TOUGH2 is able to describe experimental breakthrough curves (BTCs).

Most of the field studies in literature on CCS are based on continuum models (see references in Hesse et al. 2008; Pruess 2008; Cinar et al. 2009). These models assume that the complex multiphase flow processes can be averaged over a representative elementary volume (REV) and that the essential features of the flow process can be described on a REV scale. There is an ongoing controversy in literature, if continuum models are able to adequately describe the complex flow patterns observed in heterogeneous porous media, especially the channelized stochastic flow pattern. From both bench-scale and field-scale experiments, there is overwhelming evidence that the injected gas flows through single stochastic gas channels. Based on Selker's stochastic hypothesis (Selker et al. 2007), a gas channel is caused by a Brownian-motion process during gas injection. Therefore, pore-scale heterogeneity will determine the

shape of individual stochastic gas channels. Since continuum models average over pore-scale heterogeneity, they are in principle unable to describe the channelized flow patterns (see for details Geistlinger et al. 2009).

On the other hand, there are many studies on air sparging, which are based on continuum modeling (see references in McCray 2000; Thomson and Johnson 2000). To date, it is not clear under which conditions a continuum model can describe the essential features of complex gas flow patterns. TOUGH2 is an established multiphase program tested for different benchmark problems and is often used in CCS field studies (Pruess 2008; Class 2009). It is important to develop a “real world”-continuum model, since geological heterogeneity is a key driver on all scales (pore scale, bench scale, and field scale) for stochastic gas flow patterns. Therefore, conditioned parameter fields are used to map the real geological and hydraulic properties of the test site to a numerical model.

Firstly, in order to be consistent, a short overview of the TOUGH2 mathematical model and its numerical basis is presented. The volumetric fluxes of the two phases or fluids, water q_w and gas q_g , are given by generalized Darcy laws:

$$q_w = -\frac{kk_{rw}}{\mu_w} \nabla(P_w - \rho_w gz) \tag{12a}$$

$$q_g = -\frac{kk_{rg}}{\mu_g} \nabla(P_g - \rho_g gz) \tag{12b}$$

where w and g stands for water and gas, k absolute permeability, k_r relative permeability, P pressure, μ viscosity, ρ density, g earth’s gravity acceleration.

The concept of relative permeability is based on the assumption that all immiscible phases can flow simultaneously through the REV of the porous medium. The flow equations of phase i in a multiphase flow system, which are solved by TOUGH2 numerically, are obtained by substituting the volumetric flux into the continuity equation:

$$\frac{\partial(\rho_w S_w \phi)}{\partial t} + \nabla \left(-\rho_w \frac{k \cdot k_{rw}}{\mu_w} \nabla(P_w - \rho_w gz) \right) = I_w \tag{13a}$$

$$\frac{\partial(\rho_g S_g \phi)}{\partial t} + \nabla \left(-\rho_g \frac{k \cdot k_{rg}}{\mu_g} \nabla(P_g - \rho_g gz) \right) = I_g \tag{13b}$$

where S denotes the phase saturation, ϕ porosity, I injection rate.

The difference between water phase pressure and gas phase pressure is called capillary pressure p_c . In order to solve the system of partial differential equations, the constitutive relationships between gas saturation, permeability and the capillary pressure are needed. For this purpose, the van Genuchten–Mualem (e.g., van Genuchten 1980) model was used, which is described by the following equations:

$$k_{rw}(S_g) = (S_g)^{0.5} \left[1 - \left(1 - S_g^{1/m} \right)^m \right] \tag{14a}$$

$$p_c(S_g) = \rho_w g h(S_g) = \frac{\rho_w g}{\alpha} \left(S_g^{-1/m} - 1 \right)^{1/n} \tag{14b}$$

where α denotes inverse capillary head, $m = 1 - 1/n$, n van Genuchten parameter.

For numerical simulations, we used the equation-of-state (EOS) module ECO2N. The ECO2N-module can describe the physico-chemical processes of a single CO₂-rich phase, in our case the gaseous CO₂ phase. The more recent EOS-module ECO2M (Pruess 2011) is able to describe a single (aqueous or CO₂-rich) phase, as well as two- and three-phase mixtures of aqueous, liquid CO₂ and gaseous CO₂ phases. Since we are only interested in the flow behavior of an injected CO₂ gas phase within a shallow aquifer and its dissolution into the groundwater both modules describing the same processes. These EOS-modules were designed for applications related to geologic sequestration of CO₂ in saline aquifers. The used module includes a comprehensive description of the thermodynamics and thermo-physical properties of H₂O–NaCl–CO₂ mixtures. Flow processes can be modeled isothermally or non-isothermally, and phase conditions represented may include a single (aqueous or CO₂-rich) phase, as well as two-phase mixtures. Hence, the following physico-chemical processes are described by TOUGH2–ECO2N: (1) gas injection, which leads both, to gas flow and water flow, as well as (2) CO₂ dissolution into the groundwater and its transport processes. In this context, it is important to note that for gas dissolution, local partitioning equilibrium condition is assumed.

Creating heterogeneous parameter fields

Both heterogeneous permeability and capillary pressure fields may have a strong impact on gaseous and dissolved CO₂-distribution, and therefore on the time course of the different BTCs at different locations. Based on extensive field site investigation at the test site (Sect. 2.3; Peter et al. 2012), the geological structure model of the CO₂ injection horizon consists of six different layers (Table 2). For each geological layer, the heterogeneous permeability field was derived using a conditioned Gaussian field with an exponential covariance function and a correlation length of 5 m. For conditioning the sequential Gaussian simulation was used (Deutsch and Journal 1998). The capillary pressure field was obtained by Leverett scaling (Leverett 1940).

Key hydraulic parameters for a multiphase model are horizontal and vertical permeability and the capillary pressure for each sediment type. The permeability values are taken from sieve analysis, slug tests and HPT (hydraulic profiling tool) logs (Dietrich et al. 2008).

Table 2 Hydraulic parameters of different geological layers at the test site (see also Peter et al. 2012)

Layer	Porosity (–)	Permeability (m ²)	van Genuchten α (m ⁻¹)	van Genuchten m (–)
(1) Glacial loam	0.37	3.1×10^{-15}	7.1×10^{-4}	0.20
(2) Upper medium sand	0.33	$2.0 \pm 0.6 \times 10^{-11}$	4.4×10^{-4}	0.39
(3) Coarse sand	0.34	$4.2 \pm 0.6 \times 10^{-11}$	7.6×10^{-4}	0.40
(4) Silt	0.37	1.0×10^{-13}	2.7×10^{-4}	0.41
(5) Lower medium sand	0.30	$2.6 \pm 1.3 \times 10^{-11}$	2.7×10^{-4}	0.58
(6) Boulder clay	0.37	5.1×10^{-16}	7.1×10^{-4}	0.20

Permeability was calculated according to Hazen (e.g., Knödel et al. 2007), based on a total number of 42 sieve analyses. Comparison with relative permeability obtained by HPT logs was used to perform a consistency check. For each geological layer, permeability was calculated as a mean value over different located values. The variance was used to generate the conditioned stochastic permeability field. The corresponding van Genuchten parameters α and m for each layer were determined using the ROSETTA database (Schaap 2002) and the SOILPROP database (Stumpp et al. 2009). All parameters are listed in Table 2. Porosity was determined by directly measuring the bulk and rock volume.

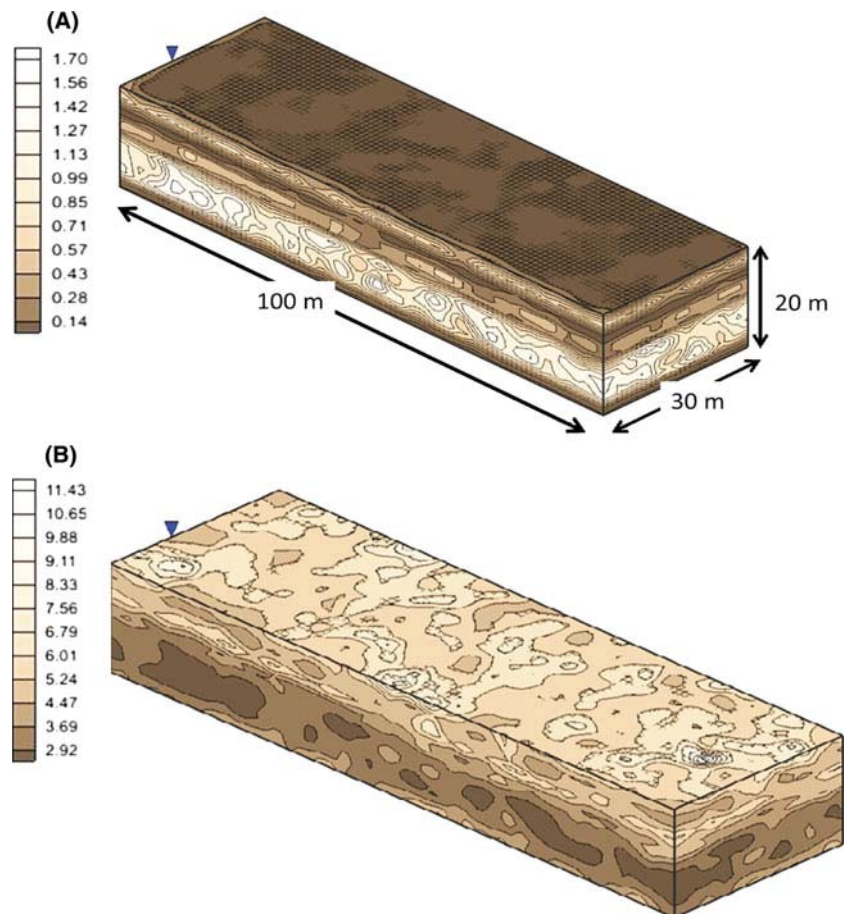
The 3D-numerical grid consists of 60,000 cells (=100 × 30 × 20) with a grid spacing of 1 m. The conditioned heterogeneous permeability and capillary pressure fields are shown in Fig. 6.

From local measurements of the hydraulic potential, a local groundwater velocity of 0.4 m/d was estimated.

CO₂ injection scenario: distribution of gaseous CO₂ and dissolved CO₂

The calibration of geoelectrical breakthrough curves was achieved during various trial-and-error attempts. Since the central injection lance and the monitoring wells

Fig. 6 a Heterogeneous permeability for the test site: values of the *color scale* are given in 10⁻¹⁰ m², **b** Simulated capillary pressure distribution: values of *color scale* are given in kPa



ML1C–GWM1D are located nearly along a flow path, a 2D-cross-section of the 3D-model was considered, i.e., a $100\text{ m} \times 1\text{ m} \times 20\text{ m}$ model cut along the center line. There are two main differences between 2D and 3D that can influence the spatial gas flow pattern: (1) the injection rate and (2) the anisotropy caused by the heterogeneous permeability field.

To take into account a realistic 2D-injection rate, we conducted a dimensional transformation. For the same injection rate of 10 L/min as was used for the 3D-model, gas saturation and radius of influence are overstated by a geometry factor of about $\pi R^2/2R\Delta x$ (=volume of paraboloid/volume of 2D-slice). Consequently, the 2D-injection rate was scaled, i.e., a rate of 2 L/min instead of 10 L/min was applied.

In order to check our scaled injection rate and the influence of the anisotropy, we also ran the 3D-model for special test cases. We found that the 2D-simulation yields almost the same BTC-curves as the 3D-model. A more elaborated 3D-theory is currently under preparation.

In Fig. 7, an aquifer cross-section of $20\text{ m} \times 20\text{ m}$ is shown. The upper row of Fig. 7 shows the distribution of

gaseous CO_2 and the lower row shows dissolved CO_2 at 5, 10 and 20 days after CO_2 injection started for the aquifer section Inj1-ML1C-GWM1D (Fig. 2). The red square in S_g (10 days)-image indicates the CO_2 injection point (18 m bgl). Black squares indicate positions of installed electrodes at wells ML1C and GWM1D, from left to right.

CO₂ injection scenario: simulating breakthrough curves

Experimental data showing breakthrough curves of geo-electrical monitoring results (σ_a), simulated BTCs are calculated for corresponding positions (nodes) at wells ML1C and GWM1D and show values for σ_{ps} . Using geo-electrical monitoring data, a higher spatial resolution could be achieved. However, it can be assumed that in first approximation the presented geo-electrical BTCs show the typical behavior of accordant local varying subsurface conductivity σ_{ps} . Since the focus of the modeling study was to investigate if the continuum model TOUGH2 is able in principle to describe experimental breakthrough curves, we assume that $\sigma_a \approx \sigma_{ps}$ in order to compare the experimental BTCs with the simulated data. A more detailed analysis of

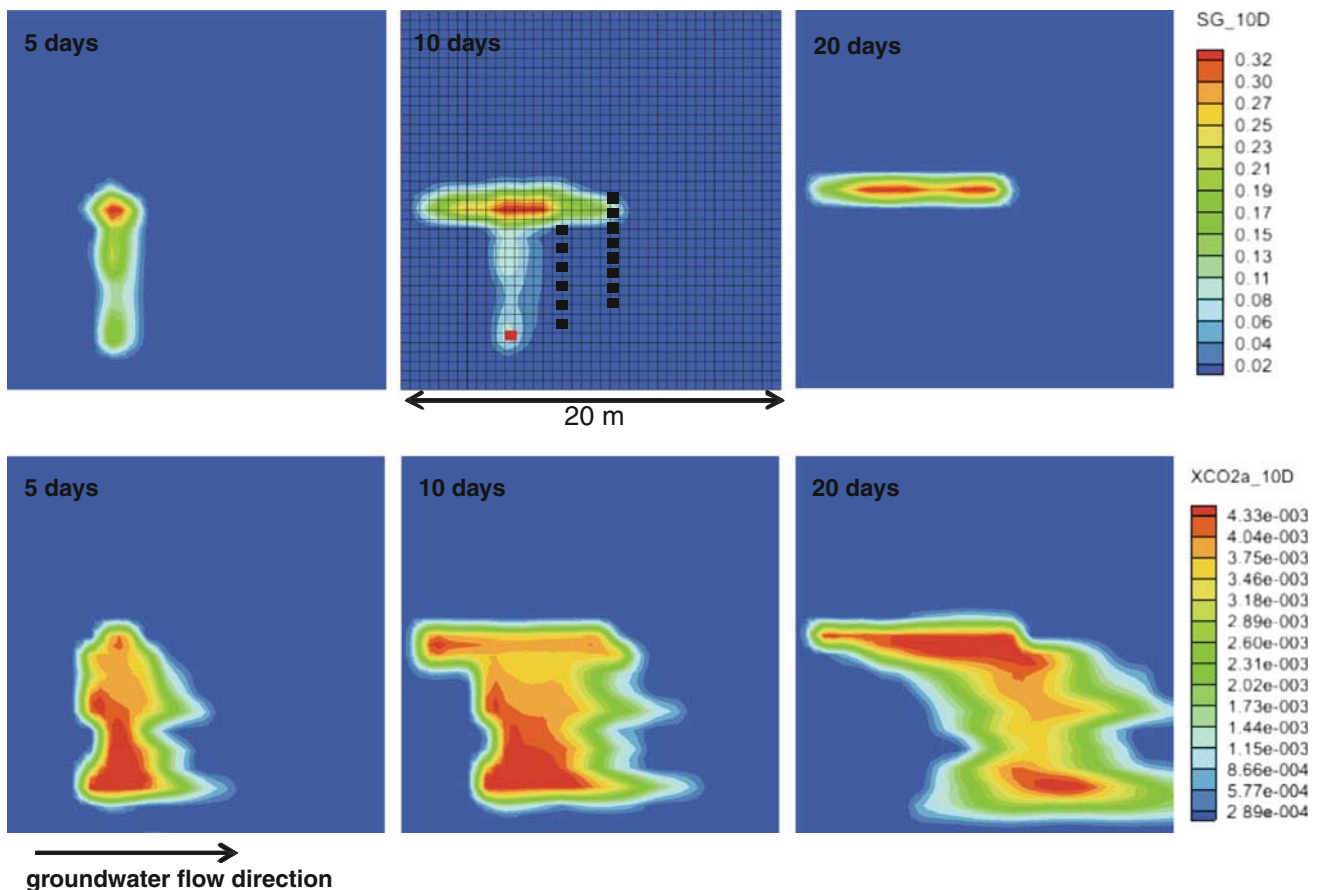


Fig. 7 Upper row saturation gaseous CO₂ (%); lower row dissolved CO₂ as mol-fraction X_{CO₂} (mol/mol), both at t = 5, 10, and 20 days after CO₂ injection started; red square in S_g (10 days)-image indicates

the CO₂ injection point (18 m bgl), black squares indicate positions of installed electrodes at wells ML1C and GWM1D from left to right

geolectrical data could be carried out but goes beyond the scope of this paper.

The electrical conductivity of a partially saturated porous medium is a complex non-linear function of gas saturation and is given by Eq. (11b). However, this is just a rough estimation, since the dynamic distribution of the gas phase plays a key role for connectivity of different sections of the pore space. During injection, channelized coherent gas flow is established in the vicinity of the injection wells and the adjacent water phase is also moved by friction forces. This will have a significant effect on σ_{ps} . However, the gas plume may move upwards even after gas injection is stopped, driven by buoyancy forces—as long as the gas channels do not collapse. Hence, for static residual gas saturation, a smaller impact on the electrical conductivity is expected due to lower gas saturation and lower static water phase.

Wenner arrays, e.g., at ML1C 13.5–14.5 m (black curve in Fig. 3) detected this change in the gas phase dynamics as a ‘step-like increase’ of σ_a . However, only the upper Wenner electrodes significantly detected the gas phase dynamic processes (Fig. 3). The most likely explanation for this is the development of a gas pool underneath the glacial loam layer, which either encloses the upper electrodes or is in the vicinity of them (Fig. 7, upper row: gas saturation at 10 days). Since geolectrical measurements provide information over a certain matrix volume, the gas saturation or number of gas channels in this volume had to be high enough so that the saturation effects become significant enough to enable detection.

Usually, isotropic paraboloids are assumed when designing gas injection tests (see e.g., Peter et al. 2012). One important question is whether or not applied multiphase models can adequately describe such ‘step-like’ behavior. Based on Faraday’s law and the fact that dissolved CO_2 species are the main ions in the water phase, a reasonable linear proportionality of σ_f on the CO_2 -mol fraction X_{CO_2} , i.e., $\sigma_f(\text{CO}_2) \propto X_{\text{CO}_2}$ was assumed. For calculating the relative electrical conductivity of the fluid, the following empirical function was used (compare with Eq. 11b):

$$\sigma_{f,\text{rel}} = \frac{\sigma_f^{f,1}}{\sigma_f^{f,0}} = \frac{X_{\text{CO}_2}^0 + X_{\text{CO}_2}}{X_{\text{CO}_2}^0 + \Delta f(X_{\text{CO}_2})} \quad (15)$$

where $\Delta f = (1 - a)X_{\text{CO}_2}$ is a correction term. The constants a and $X_{\text{CO}_2}^0$ are unknown parameters and have to be determined by the experimental BTCs. One could choose the Δf -term zero and use $X_{\text{CO}_2}^0$ as the only unknown fitting parameter. However, this would only describe relative conductivity change and not yield the correct time scale (=time at which the maximum conductivity is reached). To

describe the experimental time scale, the second fitting parameter a is required.

The focus of this paper is to investigate if multiphase modeling is able to help us understand and explain the key characteristics of geolectrical BTCs. We found that the parameter set, for $a = 0.15$ and $X_{\text{CO}_2}^0 = 1 \times 10^{-4}$, respectively, can explain the characteristic change of σ_a and the breakthrough time. In a future paper, we will present a more elaborated 3D-theory including a best fit algorithm for each BTC. It is obvious that different parameter sets for different curves make sense, since the dissolved CO_2 of different BTCs has traveled through different aquifer sections.

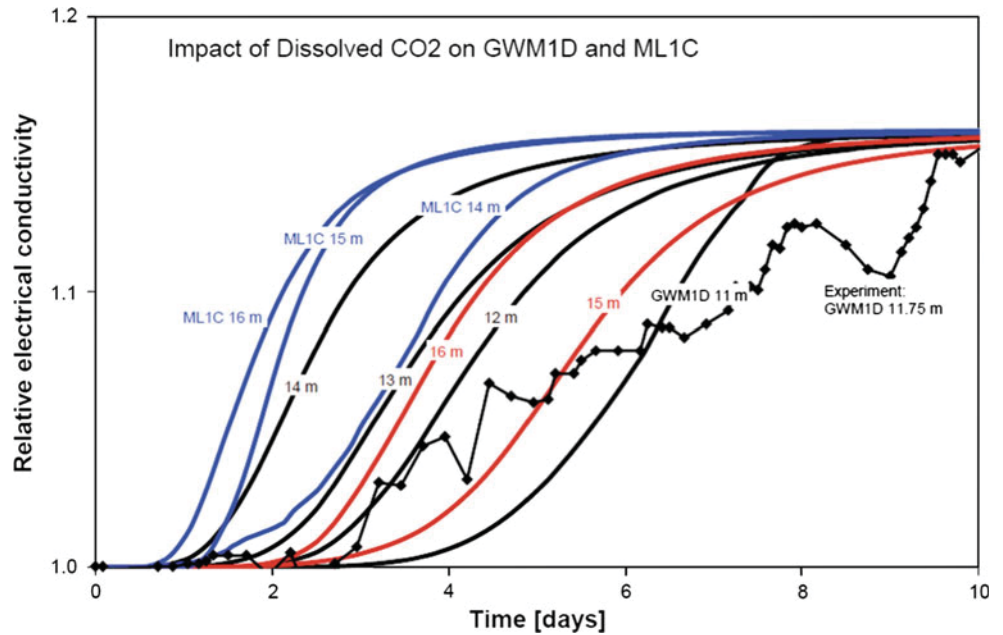
Based on Eqs. (11b, 15) and assuming that $S_g = 0$, the BTCs of relative σ_{ps} at different depths for GWM1D and ML1C are calculated (Fig. 8). According to Fig. 7, most of the Wenner arrays (=BTC-sampling points) do not “experience” gaseous CO_2 , i.e., the change of the fluid conductivity $\sigma_f(\text{CO}_2)$ is the only impact on σ_{ps} .

When interpreting Fig. 8 as well as comparing Fig. 8 with Fig. 4 (experimental BTCs), it can be seen that both show a relative change of electrical conductivity in the order of 10 to 15 %. This characteristic shows that the assumption $\sigma_a \approx \sigma_{ps}$ is justified for the purpose of the modeling study. However, when comparing experimental and simulated BTCs, this simplification must be taken into account.

The comparison between the uppermost experimental curve of GWM1D and the theoretical curves at 11 and 12 m show reasonable agreement. The slope of the experimental curve is less compared to the slope of the theoretical curve. One evident reason is the heterogeneous permeability field that has, in reality, a broader distribution and a lower mean value than the theoretical one. This would lead to smaller pore water velocities and a broader spectrum of arrival times and slopes of the BTCs. Small-scale heterogeneity could lead to more pronounced fingering of the dissolved CO_2 -front and hence to a weaker concentration gradient. As previously mentioned, the correlation length of clusters with similar permeability values is 5 m. Compared to model dimension, this correlation length yields relatively large permeability clusters. A more elaborate study should consider stochastic permeability fields with different and smaller correlation lengths.

Another reason for the different arrival times of the experimental and theoretical BTCs is the strong influence of the heterogeneous gas flow pattern during gas injection. To understand this influence, firstly the time development of the gas plume has to be discussed (Fig. 7, upper row). Considering the shape of the gas plume after 10 days injection, the gaseous CO_2 has accumulated below the glacial loam and the front of the gas plume has moved

Fig. 8 Relative conductivity (σ_{ps}) for monitoring wells GWM1D (black and red curves) and ML1C (blue curves) at different depths. For monitoring well GWM1D the experimental curve (σ_a) is shown for depth of approx. 11.75 m (black curve with squares)



about 5 m in 10 days. This represents the mean gas phase velocity, which is nearly independent of the groundwater velocity, since the same extension of the gas plume is also established against groundwater flow direction.

Based on this simulated gas distribution, measurements using the upper electrodes of monitoring wells ML1C and GWM1D can be said to be influenced by the gas phase. This is in fact the case for ML1C-BTCs, since the upper experimental BTC shows the indicative step-like behavior (black curve in Fig. 3). Using the upper electrodes of GWM1D, this step-like behavior was not detected. However, early arrival of the uppermost BTC at well GWM1D (black curve in Fig. 4) is a strong indicator that the gas phase velocity adds to groundwater and for upward migration of gaseous CO₂ in the vicinity of the injection wells up to the overlying glacial loam layer. The arrival times at all deeper BTCs are more time-delayed. In addition to gaseous CO₂ distribution, the dissolved CO₂-distribution (Fig. 7, lower row) also has a strong impact upon BTCs. As can be seen from the heterogeneous distribution, the theoretical BTC of well GWM1D at a depth of about 14 m has the shortest arrival time (Fig. 8). The theoretical BTCs in the middle of the investigated depths (13, 14 m) exhibit an earlier arrival time compared to the BTC below the glacial loam (Fig. 8). This strongly contradicts the experimental arrival times (Fig. 4), i.e., the arrival times increase from top to bottom. For two depths, 11 m (black curves) and 13 m (green curves), this comparison between experimental and theoretical curves is also shown in Fig. 9. The theoretical curve at depth 13 m arrives earlier than that of the curve at a depth of 11 m and vice versa for the experimental curves. The same inverse behavior can be

recognized for the BTCs of monitoring well ML1C (Fig. 3, blue curves in Fig. 8). Consequently, the multiphase model is unable to explain the time evolution of the dissolved CO₂. The reason for this discrepancy is the local equilibrium approach (LEA) for mass transfer processes. However, most of the multiphase models that are currently used in literature (see references in Class, 2011) in order to carry out prognoses or risk analysis for CCS technology are based on LEA. Good agreement between experimental BTCs and the gas phase distribution shows that the multiphase model correctly simulates the time evolution of the gas phase. If the buoyancy-driven gas phase velocity within the single stochastic gas channels is too fast, no partitioning equilibrium can be established along the pathway from the injection point to the gas pool. Only if the mass transfer

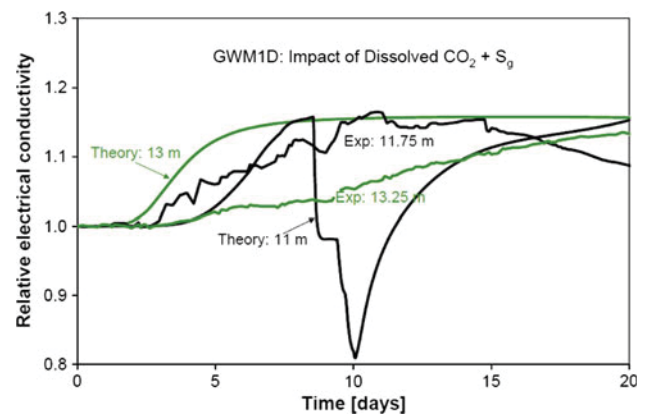


Fig. 9 Comparison of experimental (σ_a) and theoretical conductivity (σ_{ps}) relative to baseline measurements at well GWM1D for two different depths: 11 m (black curves) and 13 m (green curves)

process is *kinetically limited*, the experimental BTCs can be understood.

Now, returning to the important question of whether or not the multiphase model is able to adequately describe the experimentally observed ‘step-like behavior’. The only theoretical BTC, which “experiences” the gaseous phase is the BTC of well GWM1D, representing a depth of 11 m. Calculating this BTC ($S_g \neq 0$, $n = 2$) according to Eq. (11b), it exhibits a ‘step-like behavior’ due to temporal variation of the gas saturation (Fig. 9).

Such behavior is a rather sensitive indicator of the temporal evolution of the gas saturation. The most likely explanation for the two-step BTC is due to two subsequent saturation fronts with $S_{g1} < S_{g2}$, which move through the sampling point of BTC-11 m and are caused by the heterogeneous flow field. Comparing the theoretical curve at 11 m with the upper experimental curve (potential electrodes located at depths of 11.75 and 12.50 m) such a step-like behavior is not observed. The most likely explanation is due to the channelized flow behavior. Gas flows through discrete gas channels, whereas the continuum model TOUGH2 “smeared” the gas channels over a certain averaged volume, e.g., cell volume of 1 m^3 . Hence, the model experiences a gas channel as averaged gas saturation over the cell volume. If this gas channel is too small compared to significant sensitivity volume of the Wenner array, then the gas flow behavior, i.e., the gas channel, will be not detected. Possible pathways for observed rapid gas migration are stochastic gas channels and potential preferential pathways at the outside of installed wells.

Summary and concluding remarks

It was shown that geoelectrical monitoring in combination with multiphase modeling is a useful tool for understanding gas phase migration processes and mass transfer processes. A multiphase model has to be based on a real heterogeneous geological structure model. Parameter fields have to be conditioned on experimental data sets, in order to map the *real* aquifer to the *model* aquifer.

For the first time, we found that the ‘step-like behavior’ of electrical conductivity for both experimental and theoretical BTCs is a rather sensitive indicator for temporal variations of the gas phase. Due to the gaseous CO_2 injection into the injection horizon at depth of 18 m bgl, gaseous CO_2 flows relatively fast (see also Oldenburg and Lewicki 2006) through discrete gas channels upwards to the glacial loam layer and a gas pool is formed. Along the temporally gas channels, no local equilibrium can be reached between gaseous CO_2 and dissolved CO_2 . Therefore, a multiphase model that is based on LEA (local equilibrium approach) overestimates dissolved CO_2 (lower

row in Fig. 7). Since most of the multiphase models that are currently used in CCS technology for prognoses and risk analysis are based on LEA, we urgently recommend checking the theoretical results by performing in situ measurements of both, gas phase distribution and dissolved CO_2 distribution. Further main conclusions include:

- Geoelectrical measurements provided significant variations of σ_a in the order of 15 to 30 %. Hence, this field study has shown the feasibility of geoelectrical measurements for monitoring CO_2 intrusions into shallow aquifers. However, at the presented wells, electrodes were placed at a maximum distance of 1 m apart from each other within the injection horizon. The experimental monitoring setup used permits the detection of small-scale variations in both σ_a (geoelectrical breakthrough curves) and σ_f (groundwater sampling). In order to apply this monitoring strategy at real CCS sites, this approach has to be adapted for significantly larger areas, i.e., several km^2 (see also Singh et al. 2012).
- In this field study, it has been proven that it is highly beneficial to install electrodes for geoelectrical borehole monitoring below an impermeable geological layer, allowing detection of rapid variations in σ_a due to upwardly migrated gaseous CO_2 . Additionally, interpretation of geoelectrical breakthrough curves allows rapid initial process understanding. Consequently, this approach is a promising tool for borehole monitoring at CCS sites.
- The injection horizon used is only affected by the injected CO_2 . Other sources, which might have an impact upon electrical conductivity (e.g., input of fertilizers, saline water intrusion) are negligible at the test site. Such external factors may lead to ambiguity in terms of geoelectrical monitoring and must be considered when monitoring CCS sites. Field parameters of groundwater samples should be used to obtain additional information showing that potentially observed variation in σ_a are caused by leaked CO_2 or not.
- The application and feasibility of geoelectrical monitoring of CO_2 intrusions strongly depends upon site-specific conditions with respect to dynamic (geochemical) processes, as well as the measuring setup used. Consequently for each field site, a specific characterization of relevant parameters must be implemented (see also Kolditz et al. 2012). Generally, hydraulic and electrical properties are not constant in space due to heterogeneous structures in the subsurface. Hence, the inference from measured geoelectrical data to variation in σ_f is ambiguous. Geoelectrical monitoring is applicable for detecting the zone of varying electrical conductivity, but for quantitative conclusions,

additional information is required (e.g., from groundwater sampling).

Acknowledgments We would like to thank the town of Wittstock and the Brandenburgische Boden GmbH for supporting this project. This study was funded by the German Ministry of Education and Research (BMBF) within the Priority Program *Geotechnologies*, funding numbers 03G0670A-C.

References

- Appelo CAJ, Postma D (1993) Geochemistry, groundwater and pollution. A.A. Balkema, Rotterdam, p 536
- Archie GE (1942) The electrical resistivity log as an aid in determining some reservoir characteristics. *Pet. Trans.* 146:54–62
- Arps JJ (1953) The effect of temperature on the density and electrical resistivity of sodium chloride solutions. *Trans Am Inst Min Metall Eng* 198:327–330
- Binley A, Winship P, West LJ, Pokar M, Middleton R (2002) Seasonal variation of moisture content in unsaturated sandstone inferred from borehole radar and resistivity profiles. *J Hydrol* 267(3–4):160–172. doi:10.1016/S0022-1694(02)00147-6
- Carroll S, Hao Y, Aines R (2009) Geochemical detection of carbon dioxide in dilute aquifers. *Geochem Trans* 10. <http://www.geochemicaltransactions.com/content/10/1/4>
- Cinar Y, Riaz A, Tchelepi HA (2009) Experimental study of CO₂ injection into saline formations. *SPE J* (SPE 110628), pp 1–7
- Class H (2009) Intercomparison of codes and models: how can we improve reliability and understanding of model predictions for CO₂ storage? Workshop on Modeling and risk assessment of geological storage of CO₂ August 3–7, 2009. Longyearbyen, Svalbar. <http://www.org.uib.no/cipr/Workshop/2009/CO2/presentations.htm>
- Deutsch CV, Journal AG (1998) *GSLIB: Geostatistical software library and user's guide*, 2nd edn. Oxford university press, Oxford
- Dietrich P (1999) Konzeption und Auswertung gleichstromgeoelektrischer Tracerversuche unter Verwendung von Sensitivitätskoeffizienten, vol 50. *Tübinger geowissenschaftliche Arbeiten: Reihe C, Hydro-, Ingenieur- und Umweltgeologie*. Inst. und Museum für Geologie und Paläontologie, Tübingen
- Dietrich P, Leven C (2006) Direct push-technologies. In: Kirsch R (ed) *Groundwater geophysics*. Springer, Berlin, pp 321–340
- Dietrich P, Butler JJ, Faiß K (2008) A rapid method for hydraulic profiling in unconsolidated formations. *Ground Water* 46(2):323–328
- Fahrner S, Schaefer D, Dahmke A (2011) Reactive transport modeling to assess geochemical monitoring for detection of CO₂ intrusion into shallow aquifers. *Energy Procedia* 4:3155–3162. doi:10.1016/j.egypro.2011.02.230
- Geistlinger H, Lazik D, Vogel H-J (2009) Pore scale and continuum modeling of gas flow pattern obtained by high-resolutions optical bench-scale experiments. *Water Resour Res* 45:W04423. doi:10.1029/2007WR006548
- Hesse MA, Orr FM, Tchelepi HA (2008) Gravity currents with residual trapping. *J Fluid Mech* 611:35–60
- Holloway S, Pearce JM, Hards VL, Ohsumi T, Gale J (2007) Natural emissions of CO₂ from the geosphere and their bearing on the geological storage of carbon dioxide. *Energy* 32(7):1194–1201
- Humez P, Audigane P, Lions J, Chiaberge C, Bellenfant G (2011) Modeling of CO₂ leakage up through an abandoned well from deep saline aquifer to shallow fresh ground waters. *Transp Porous Media* 90(1):153–181. doi:10.1007/s11242-011-9801-2
- Huq F, Blum Ph, Marks M, Nowak M, Haderlein SB, Grathwohl P (2012) Chemical changes in fluid composition due to CO₂ injection in the Altmark Gas Field: preliminary results from batch experiments. *Environ Earth Sci* (submitted, this issue)
- Keller GV, Frischknecht FC (1966) *Electrical methods in geophysical prospecting*. Pergamon Press, New York, p 519
- Kharaka YK, Thordsen JJ, Kakouros E, Ambats G, Herkelrath WN, Beers SR, Birkholzer JT, Apps JA, Spycher NF, Zheng L, Trautz RC, Rauch HW, Gullickson KS (2010) Changes in the chemistry of shallow groundwater related to the 2008 injection of CO₂ at the ZERT field site, Bozeman, Montana. *Environ. Earth Sci.* 60:273–284. doi:10.1007/s12665-009-0401-1
- Kiessling D, Schmidt-Hattenberger C, Schuett H, Schilling F, Krueger K, Schoebel B, Danckwardt E, Kummerow J (2010) Geoelectrical methods for monitoring geological CO₂ storage: first results from cross-hole and surface–downhole measurements from the CO₂SINK test site at Ketzin (Germany). *Int J Greenh Gas Control* 4(5):816–826. doi:10.1016/j.ijggc.2010.05.001
- Knödel K, Lange G, Voigt H-J (2007) *Environmental geology. Handbook of field methods and case studies*. Springer-Verlag, Berlin, p 1357
- Kolditz O, Bauer S, Beyer C et al (2012) A systematic benchmarking approach for geologic CO₂ injection and storage. *Environ Earth Sci.* doi:10.1007/s12665-012-1656-5
- Leven C, Weiß H, Vienken T, Dietrich P (2011) Direct-Push-Technologien—Effiziente Untersuchungsmethoden für die Untergrunderkundung. *Grundwasser—Zeitschrift der Fachsektion Hydrogeologie*. doi:10.1007/s00767-011-0175-8
- Leverett MC (1940) Capillary behavior in porous solids. *AIME* 142:152–169 (paper number 941152-G)
- Lewicki JL, Birkholzer J, Tsang CF (2007) Natural and industrial analogues for leakage of CO₂ from storage reservoirs: identification of features, events, and processes and lessons learned. *Environ Geol* 52(3):457–467
- Lu J, Partin J, Hovorka S, Wong C (2010) Potential risks to freshwater resources as a result of leakage from CO₂ geological storage: a batch-reaction experiment. *Environ Earth Sci* 60(2):335–348. doi:10.1007/s12665-009-0382-0
- McCray JE (2000) Mathematical modeling of air sparging for subsurface remediation: state of the art. *J Hazard Mater* 72:237–263
- Oldenburg CM, Lewicki JL (2006) On leakage and seepage of CO₂ from geologic storage sites into surface water. *Environ Geol* 50(5):691–705. doi:10.1007/s00254-006-0242-0
- Oldenburg CM, Unger AJA (2003) On leakage and seepage from geologic carbon sequestration sites: unsaturated zone attenuation. *Vadose Zone J* 2(3):287–296
- Peter A, Hornbruch G, Dahmke A (2011) CO₂ leakage test in a shallow aquifer for investigating the geochemical impact of CO₂ on groundwater and for developing monitoring methods and concepts. *Energy Procedia* 4:4148–4153
- Peter A, Lamert H, Beyer M, Hornbruch G, Heinrich B, Schulz A, Geistlinger H, Schreiber P, Dietrich P, Werban U, Vogt C, Richnow HH, Großmann J, Dahmke A (2012) Investigation of the geochemical impact of CO₂ on shallow groundwater: design and implementation of a CO₂ injection test in Northeast Germany. *Environ Earth Sci* (submitted, this issue)
- Pruess K (2005) *ECO2N: a TOUGH2 fluid property module for mixtures of water, NaCl, and CO₂*. Lawrence Berkeley National Laboratory, CA. Earth Sciences Div., Berkeley
- Pruess K (2008) On CO₂ fluid flow and heat transfer behavior in the subsurface, following leakage from a geologic storage reservoir. *Environ Geol* 54(8):1677–1686. doi:10.1007/s00254-007-0945-x
- Pruess K (2011) *ECO2M: a TOUGH2 fluid property module for mixtures of water, NaCl, and CO₂, including super- and sub-critical conditions, and phase change between liquid and gaseous*

- CO₂. Report LBNL-4590E, Lawrence Berkeley National Laboratory, Berkeley, Calif
- Pruess K, Oldenburg C, Moridis G (1999) TOUGH2 user's guide, version 2.0, Report LBNL-43134, Lawrence Berkeley National Laboratory, Berkeley, Calif
- Rein A, Hoffmann R, Dietrich P (2004) Influence of natural time-dependent variations of electrical conductivity on DC resistivity measurements. *J Hydrol* 285(1–4):215–232. doi:10.1016/j.jhydrol.2003.08.015
- Schaap H (2002) Rosetta database, University of Arizona, 2002. <http://www.cals.arizona.edu/research/rosetta/index.html>
- Schön JH (1996) Physical properties of rocks: fundamentals and principles of petrophysics. Pergamon Press, New York, p 583
- Schütze C, Sauer U, Beyer K, Lamert H, Strauch G, Braeuer K, Flechsig C, Kaempf H, Dietrich P (2012) Natural analogues: a potential approach for developing reliable monitoring methods to understand subsurface CO₂ migration processes. *Environ Earth Sci* (submitted, this issue)
- Selker J, Niemet M, McDuffie N, Gorelick S, Parlange J-Y (2007) The local geometry of gas injection into saturated homogeneous porous media. *Transp Porous Media* 68(1):107–127. doi:10.1007/s11242-006-0005-0
- Singh AK, Pilz P, Zimmer M, Kalbacher T, Goerke U-J, Kolditz O (2012) Numerical simulation and geophysical monitoring of tracer transport in the Altmark gas field. *Environ Earth Sci* (submitted, this issue)
- Stumpp C, Engelhardt S, Hofmann M, Huwe B (2009) Evaluation of pedotransfer functions for estimating soil hydraulic properties of prevalent soils in a catchment of the Bavarian Alps. *Eur J For Res* 128:609–620. doi:10.1007/s10342-008-0241-7
- Thomson NR, Johnson RL (2000) Air distribution during in situ air sparging: an overview of mathematical modeling. *J Hazard Mater* 72:265–282
- Torp TA, Gale J (2004) Demonstrating storage of CO₂ in geological reservoirs: the Sleipner and SACS projects. *Energy* 29(9–10):1361–1369. doi:10.1016/j.energy.2004.03.104
- van Genuchten MT (1980) A closed-form equation for predicting the hydraulic conductivity of unsaturated soils. *Soil Sci Soc Am J* 44:892–898
- Vienken T, Leven C, Dietrich P (2012) Use of CPT and other direct push methods for (hydro-) stratigraphic aquifer characterization—a field study. *Can Geotech J* 49:197–206. doi:10.1139/T11-094
- Wilson EJ, Friedmann SJ, Pollak MF (2007) Research for deployment: incorporating risk, regulation, and liability for carbon capture and sequestration. *Environ Sci Technol* 41(17):5945–5952

12. Appendix

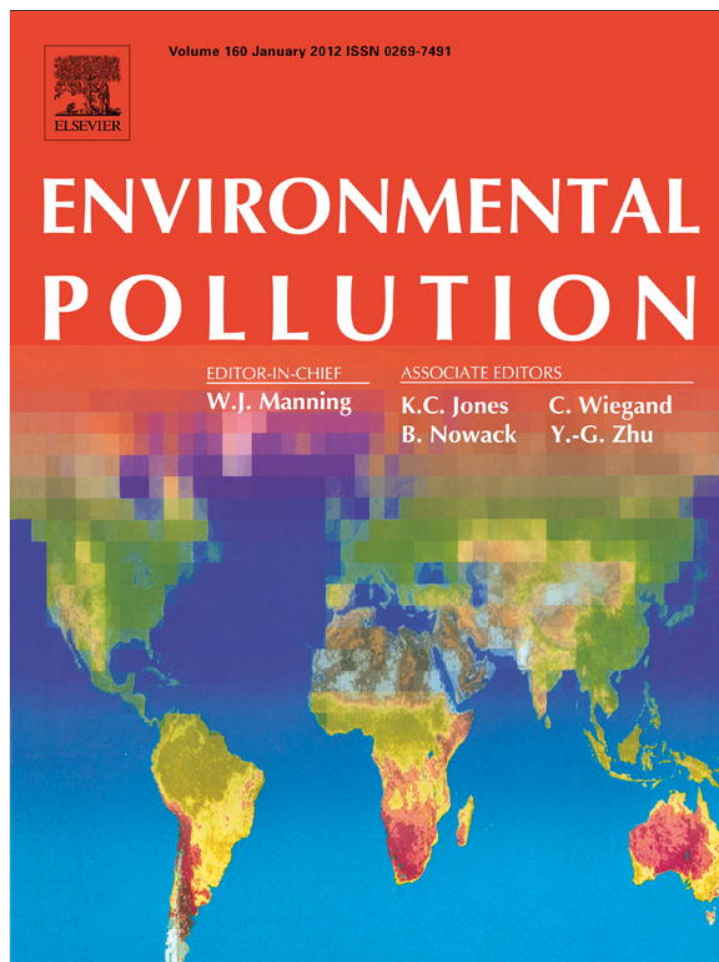
Appendix D

Effects of high CO₂ concentrations on ecophysiologicaly different microorganisms

Schulz, Alexandra; Vogt, Carsten; Richnow, Hans-Hermann

Environmental Pollution, 2012, 169, pp 27-34.

Provided for non-commercial research and education use.
Not for reproduction, distribution or commercial use.



(This is a sample cover image for this issue. The actual cover is not yet available at this time.)

This article appeared in a journal published by Elsevier. The attached copy is furnished to the author for internal non-commercial research and education use, including for instruction at the authors institution and sharing with colleagues.

Other uses, including reproduction and distribution, or selling or licensing copies, or posting to personal, institutional or third party websites are prohibited.

In most cases authors are permitted to post their version of the article (e.g. in Word or Tex form) to their personal website or institutional repository. Authors requiring further information regarding Elsevier's archiving and manuscript policies are encouraged to visit:

<http://www.elsevier.com/copyright>



Contents lists available at SciVerse ScienceDirect

Environmental Pollution

journal homepage: www.elsevier.com/locate/envpolEffects of high CO₂ concentrations on ecophysiologicaly different microorganisms

Alexandra Schulz, Carsten Vogt*, Hans-Hermann Richnow

Department of Isotope Biogeochemistry, UFZ – Helmholtz Centre for Environmental Research, Permoserstraße 15, 04318 Leipzig, Germany

ARTICLE INFO

Article history:

Received 10 February 2012

Received in revised form

7 May 2012

Accepted 11 May 2012

Keywords:

CO₂ toxicity

Soil microorganisms

High-pressure CO₂

Carbon capture and storage

CCS

ABSTRACT

We investigated the effect of increasing CO₂ concentrations on the growth and viability of ecophysiologicaly different microorganisms to obtain information for a leakage scenario of CO₂ into shallow aquifers related to the capture and storage of CO₂ in deep geological sections. CO₂ concentrations in the gas phase varied between atmospheric conditions and 80% CO₂ for the aerobic strains *Pseudomonas putida* F1 and *Bacillus subtilis* 168 and up to 100% CO₂ for the anaerobic strains *Thauera aromatica* K172 and *Desulfovibrio vulgaris* Hildenborough. Increased CO₂ concentrations caused prolonged lag-phases, and reduced growth rates and cell yields; the extent of this effect was proportional to the CO₂ concentration. Additional experiments with increasing CO₂ concentrations and increasing pressure (1–5000 kPa) simulated situations occurring in deep CO₂ storage sites. Living cell numbers decreased significantly within 24 h at pressures ≥ 1000 kPa, demonstrating a severe lethal effect for the combination of high pressure and CO₂.

© 2012 Elsevier Ltd. All rights reserved.

1. Introduction

In recent decades, the concentration of carbon dioxide (CO₂) in the atmosphere has increased significantly as a result of anthropogenic emission. One option for the reduction of the CO₂ emission is Carbon Capture and Storage (CCS), the capture of CO₂ from large emission sources and storage in deep geological structures, e.g. saline Permian sandstone aquifers such as Rotliegend strata (IPCC, 2005). Leakage of CO₂ from an underground storage site into a near surface aquifer is one concern associated with the CCS technology. The complete tightness of a CO₂ reservoir in geological strata has been questioned (Wu et al., 2010) and semi-analytical models have shown that if cracks and crevices are present in cap rock formations of the storage site, a leakage of free phase CO₂ can be a significant pathway for losing sequestered CO₂ (Saripalli and McGrail, 2002). The upwardly migrating CO₂ can reach shallow aquifers located over deep CO₂ storage sites, and chemical, geological and/or microbiological changes may be induced in the soil environment as well as in the shallow groundwater, which can be a source of drinking water (Wu et al., 2010). A pH decrease, mineral dissolution and a change in the growth of characteristic microorganisms are some of the potential risks of a leakage scenario. Proper risk assessment for proposed CO₂ storage sites should include simulated leakage scenarios and exploration of the

impacts of increasing CO₂ concentrations on indigenous microorganisms. Several studies have previously examined changes in microbial communities induced by long-term exposure to CO₂ (Blagodatskaya et al., 2010; Freeman et al., 2004; Oppermann et al., 2010). These ecosystems had the chance to adapt to these conditions and therefore the effects of a possible leakage into aquifer environments are difficult to predict. Consequently, a study on the reaction of soil microorganisms towards a sudden increase of the CO₂ concentration is necessary. Furthermore, to the best of our knowledge, a detailed study on the change of the growth characteristics of microbial soil organisms due to elevated CO₂ concentrations has not been performed. In the present study, the effects of different CO₂ concentrations on the growth and viability of aerobic and anaerobic microorganisms were investigated. Microbial strains (*Pseudomonas putida*, *Bacillus subtilis*, *Desulfovibrio vulgaris*, and *Thauera aromatica*), routinely detected in terrestrial or freshwater systems, were used to investigate the consequences of a CO₂ leakage from a deep geological storage site. These strains were used as model organisms to study the principal effects of high CO₂ concentrations on ecophysiologicaly different microbes. Here, we address questions associated with how the growth and survival rates of aerobic and anaerobic microorganisms change in response to rapidly elevated CO₂ concentrations. Furthermore, variable stress responses of microorganisms of various ecotypes (aerobes, nitrate reducer, sulphate reducer) towards increased CO₂ concentrations are discussed. In addition, as a worst case scenario for CO₂ leakage, we examined the influence of high CO₂ partial pressures on the viability of typical microorganisms for the different ecotypes. All

* Corresponding author.

E-mail address: carsten.vogt@ufz.de (C. Vogt).

experiments are performed with pure cultures under favourable growth (temperature, medium, carbon source) conditions to study the specific influence of CO₂ and to exclude disturbing side effects.

2. Material and methods

2.1. Microorganisms and culture media

Bacillus subtilis sbsp. *subtilis* strain 168, *Pseudomonas putida* strain F1, *Desulfovibrio vulgaris* strain Hildenborough and *Thauera aromatica* strain K172 were obtained from the German Collection of Microorganisms and Cell Cultures (DSMZ; Braunschweig, Germany). The microorganisms were originally isolated from soil (*D. vulgaris*, *P. putida*) or sewage sludge (*T. aromatica*). *B. subtilis* is a typical non-pathogenic soil bacterium. The organisms were chosen as they were of terrestrial origin and genome-sequenced, which is a prerequisite for further experiments regarding the molecular basis of CO₂ toxicity. *B. subtilis* and *P. putida* were cultivated in a modified, phosphate-buffered Brunner mineral medium (2.44 g/L Na₂HPO₄; 1.52 g/L KH₂PO₄; 0.50 g/L (NH₄)₂SO₄; 0.20 g/L MgSO₄ × 7H₂O; 0.05 g/L CaCl₂ × 2H₂O; 1 mL/L trace element solution 10; 5 mL/L vitamin solution) with glucose [5 mM] or acetate [5 mM] as substrates. Cultures were grown at 30 °C and pH 7 in an orbital shaker at 150 rpm. *D. vulgaris* was cultured under anoxic conditions in the same Brunner mineral medium (see above) at pH 7 and 37 °C. After autoclaving at 121 °C for 20 min, the medium was purged with nitrogen to remove oxygen. Na₂SO₄ [20 mM] was provided as the terminal electron acceptor, the medium was amended with 1 mL/L selenite-tungsten solution (0.5 g/L NaOH, 3 mg/L Na₂SeO₃ × 5H₂O; 4 mg/L Na₂WO₄ × 2H₂O), and lactate [10 mM] was the sole carbon and energy source. *T. aromatica* was cultured in a modified anoxic Brunner mineral medium at pH 8 and 25 °C; the medium was prepared anoxically as described above. KNO₃ [8 mM] and 1 mL/L of a selenite-tungsten solution (see medium for *D. vulgaris*) were amended, and acetate [5 mM] was provided as the sole carbon and energy source. Generally, additional solutions were added from sterile oxalic (for *P. putida*, *B. subtilis*) or anoxic (for *T. aromatica*, *D. vulgaris*) stock solutions using sterile plastic syringes, which were nitrogen-flushed in case of anoxic media. Pre-cultures for growth experiments were grown in 118 mL glass bottles, sealed gas-tight with butyl rubber stoppers. 20% of CO₂ was already added into the pre-cultures of *D. vulgaris* to achieve the best growth conditions, which caused an initial pH drop to about 6.8. For maintenance, all strains were re-inoculated into fresh medium once per week. The pH of subsamples (800 µl volume) was determined by using a pH meter 765 Calimatic (Knick). Subsamples (e.g. for HPLC or, pH measurements) were always taken with nitrogen-flushed syringes to avoid any addition of oxygen into the culture flasks. All chemicals were of reagent-grade quality and obtained from Merck and Sigma–Aldrich.

2.2. Growth experiments under different CO₂ concentrations at ambient pressure

The growth experiments were conducted in 30 mL glass tubes. Each tube was filled with 4.5 mL of Brunner mineral medium modified for each strain (see 2.1) and closed with gas-tight butyl rubber stoppers. The medium was purged with gas mixtures of N₂ and CO₂ with compositions between approximately 0 (refers to no amendment of CO₂) to approximately 100% CO₂ by using a mass flow controller (EL-FLOW, Bronkhorst High-Tech, Germany). Each glass vial was purged with the appropriate gas mixture for 15 min to receive a full saturation of the atmosphere and the medium. For the aerobic experiments using *B. subtilis* and *P. putida*, 20% O₂ was added by removing the adequate headspace volume with a gas-tight syringe and replacing it with the appropriate volume of pure O₂. The O₂ concentrations were monitored using O₂ sensors (sensor type PSt3, detection limit 0.03%, PreSens, Germany). The CO₂ concentration was increased up to 100% in the headspace for experiments with the anaerobic organisms *D. vulgaris* and *T. aromatica*. After autoclaving, the medium was inoculated with 0.5 mL of a freshly grown culture to achieve an initial OD₆₆₀ of at least 0.015 (0.04 ± 0.006 for *P. putida*, 0.027 ± 0.008 for *B. subtilis*, 0.018 ± 0.007 for *D. vulgaris* and 0.016 ± 0.003 for *T. aromatica*). The microorganisms were subsequently grown at the previously described growth temperatures (25 °C for *T. aromatica*, 30 °C for *B. subtilis* and *P. putida*, 37 °C for *D. vulgaris*) on an orbital shaker at 150 rpm. As the focus of this study was to investigate the effects caused by elevated CO₂ concentrations, we used the appropriate growth temperature for each organism to exclude disturbing side effects. The optical density was measured every 2 h at a wavelength of 660 nm with a UV/VIS spectrophotometer (Pharmacia LKB Novaspec II) for up to 90 h. The glass vials were placed directly into the spectrophotometer to ensure constant measurements during the course of the experiments. The growth rate μ was calculated as follows:

$$\mu = \frac{2.303(\log OD_2 - \log OD_1)}{(t_2 - t_1)} \quad 1$$

where OD values are chosen such that OD₁ is two times OD₂ with the corresponding time points *t* (see Table 1) (Widdel, 2010). Lag-phases were approximated by visual inspection of the growth curves and defined as the phase after inoculation where the OD stayed stable over time. At the end of the experiments, the viable cell numbers were determined in three replicates, each of them composed of 10 parallels, using

Table 1
The relative inhibitory effect (RI) of CO₂ and the growth rate μ for CO₂ concentrations from 0 to 100% for the investigated microorganisms. The standard deviation was calculated on the basis of at least three biological replicates.

CO ₂ [%]	Aerobic			CO ₂ [%]			Anaerobic					
	<i>P. putida</i>			<i>B. subtilis</i>			<i>D. vulgaris</i> (sulphate-reducing)			<i>T. aromatica</i> (nitrate-reducing)		
	pH	RI [%]	μ [h ⁻¹]	pH	RI [%]	μ [h ⁻¹]	pH	RI [%]	μ [h ⁻¹]	pH	RI [%]	μ [h ⁻¹]
0	7.18	0	0.52 ± 0.16	7.1	0	0.48 ± 0.16	6.96	0	0.11 ± 0.03	8.00	0	0.06 ± 0.01
50	6.58	54.8 ± 21.6	0.32 ± 0.14	6.56	25.4 ± 21.0	0.44 ± 0.09	6.65	7.3 ± 2.5	0.09 ± 0.01	6.96	11.8 ± 2 ^a	0.05 ± 0.01
60	6.52	79.5 ± 8.7	0.13 ± 0.03	6.53	n.m.	0.35 ± 0.12	6.60	40.9 ± 9	0.05 ± 0.01	6.91	40.7 ± 4.6 ^a	0.04 ± 0.02
70	6.51	84.0 ± 8.1	0.10 ± 0.03	6.49	n.m.	0.31 ± 0.09	6.41	57.1 ± 2 ^a	0.05 ± 0.004	6.84	51.2 ± 5.7	0.03 ± 0.002
80	6.48	86.4 ± 3.8	0.07 ± 0.01	6.37	75.1 ± 3.3	0.25 ± 0.09	6.35	77.6 ± 5.5	0.03 ± 0.01	6.79	83.7 ± 11.9	0.02 ± 0.01

n.m., not measured
^a The standard deviation was calculated based on three replicates as no repetition experiments were performed.

the Most Probable Number method (MPN) (Sutton, 2010). 96-well microtiter plates (Nunc, Denmark) with a volume of 300 μl per well were filled with 200 μl of Brunner medium modified for each strain and inoculated with 100 μl dilutions from 10^{-4} – 10^{-10} . The cell numbers and the 95% confidence limit on the log of the MPN were computed using a computer program designed by Robert Blodgett based on the normal approximation previously described (Garthright and Blodgett, 1996; Haldane, 1939). The relative inhibitory effect (RI) of CO_2 was calculated according to Enfors and Molin (Enfors and Molin, 1981) as follows:

$$\text{RI} = [(r_c - r_{\text{CO}_2}) / r_c] \times 100 \quad (2)$$

where r_c and r_{CO_2} are the growth rates for the control and the specific CO_2 concentrations respectively. In order to exclude an influence of substrate limitation on cell growth, HPLC measurements were performed with glucose and acetate for *P. putida*, *B. subtilis* and *T. aromatica* every 2 h for the duration of the experiments. HPLC analyses were performed on a Shimadzu 10A HPLC equipped with an RID detector and a VA 300/7.8 Nucleogel ION 300 OA column (Macherey & Nagel, Germany) using an eluent of 0.005 N H_2SO_4 at a flow rate of 0.6 mL/min.

2.3. Viability experiments under CO_2 stress at high pressure

For the high-pressure experiments, two self-made pressure vessels of stainless steel with a volume of 0.56 L, on which a maximum pressure of 7500 kPa can be applied, were used (Fig. 1). The maximum temperature used for the experiments was 38 °C. The pressure vessels were placed in a water bath with a compact low temperature thermostat (RM6 Lauda, Germany), allowing temperature adjustment for the different growth conditions. Seven glass vials with a volume of 30 mL were filled with 10 mL of inoculum from a freshly grown culture, closed with silicon stoppers and aluminium grip seals, and placed in one vessel. Two needles were placed into the stopper of each glass vial to allow for pressure equilibration between the media in the glass vials and the pressure vessel. The vessel was closed gas tight with a torque wrench by applying a force of first 25 Nm and then 50 Nm. The vessels containing anaerobic strains were purged with CO_2 for 5 min. A pressure of 500, 1000, 2000, 3000, 4000 and 5000 kPa was applied to each vessel using pressure-reducing valves. The O_2 content was controlled before and after the experiment using optical O_2 sensors (sensor type PSt3, PreSens, Germany). The pressure was maintained for 24 h and released as slowly as possible. The pressure release rate was around 2 bar per minute (manually controlled and based on the results of preliminary tests). MPN assays were performed after each run on three parallels of each pressure vessel, as described above. In addition to the pressure experiments with CO_2 , the same pressure experiments were performed with pure nitrogen and pressures of up to 7500 kPa, to distinguish between pressure-induced effects on the microorganisms or effects caused by both pressure and increasing CO_2 concentrations.

3. Results

3.1. Influence of pH on growth and viability

Culture experiments in the presence of higher CO_2 concentrations were conducted in a phosphate-buffered medium by constant

pH to investigate direct effects of CO_2 on microbial growth. The addition of gaseous CO_2 to the phosphate-buffered mineral medium still resulted in a decrease of the pH from an initial value of 7.0 to a minimum pH of 6.3 for *P. putida*, 6.3 for *B. subtilis*, 6.2 for *T. aromatica* and 6.4 for *D. vulgaris*, respectively (Table 1). Thus, to investigate the inhibitory effect of the low pH alone on microbial growth, experiments with all four strains were conducted using mineral medium in which the pH was adjusted to 6 by the addition of HCl (0.5 M). In these preliminary experiments, the cultures were not amended with additional CO_2 . *P. putida*, *B. subtilis* and *D. vulgaris* showed slightly decreased growth rates and, with the exception of *D. vulgaris*, slightly diminished growth yields at the lower pH (Fig. 2). *T. aromatica* grew poorly when the pH was decreased from 7 to 6 (SI-Fig. 1). Therefore, the buffer concentration of the mineral medium was adjusted and the initial pH was increased from 7 to 8. After addition of CO_2 , the pH decreased from 8 to 7. The growth rate at pH 7 was only slightly reduced compared to the growth rate at pH 8 (Fig. 2). In summary, all tested microorganisms grew fairly well in the pH ranges used later in the CO_2 stress experiments. Hence, experimentally observed effects could be attributed to elevated CO_2 concentrations. When adjusting lower pH values (to a minimum of 4), the growth of all tested strains was significantly inhibited (SI-Fig. 1).

3.2. Cell growth and viability under different CO_2 concentrations at ambient pressure

Three obvious changes were observed when high CO_2 concentrations were applied to the strains. First, the lag-phase was significantly prolonged for all four strains. In particular, the lag phase for *P. putida* increased from one to 8 h, and from two to 7 h for *B. subtilis* (Fig. 3). For the sulphate-reducing *D. vulgaris*, the prolongation of the lag-phase was even more pronounced and increased from nine to 23 h (Fig. 3). For *T. aromatica* lag-phases at ambient conditions varied between four and 6 h but after addition of 100% CO_2 lag-phase and exponential growth phase could not be distinguished anymore as the growth rate decreased dramatically (Fig. 3). The second observation was a notable decrease in the growth rate (μ) with increasing CO_2 concentrations. Finally, it was observed that the growth yields, in the presence of CO_2 concentrations higher than 60%, decreased for all four strains (Fig. 3). A comparison of the MPN values (in the presence of 80% CO_2) with the non-amended CO_2 controls at the end of each experiment

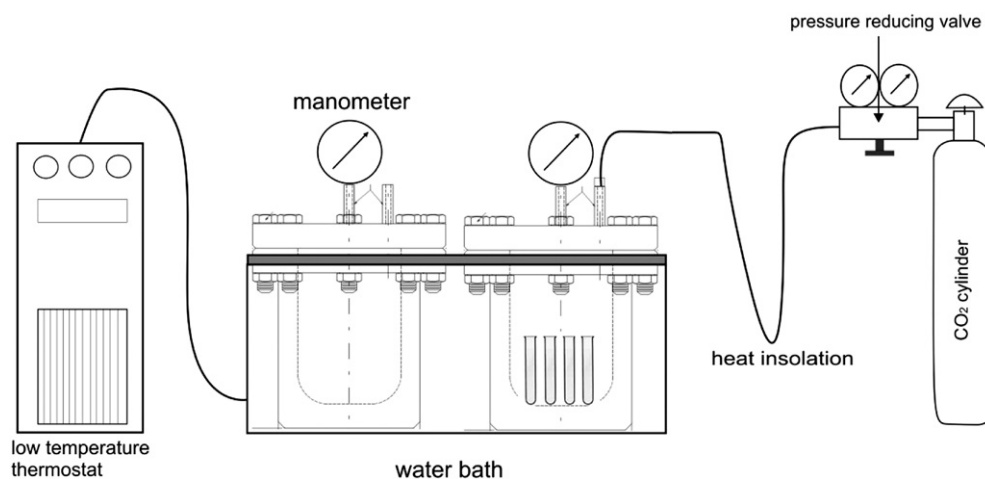


Fig. 1. Experimental set up for growth experiments with CO_2 at high pressure. The two stainless steel pressure vessels were placed in a water bath and connected to a thermostat. The pressure was applied by using CO_2 cylinders and a pressure-reducing valve permitting pressure up to 7500 kPa.

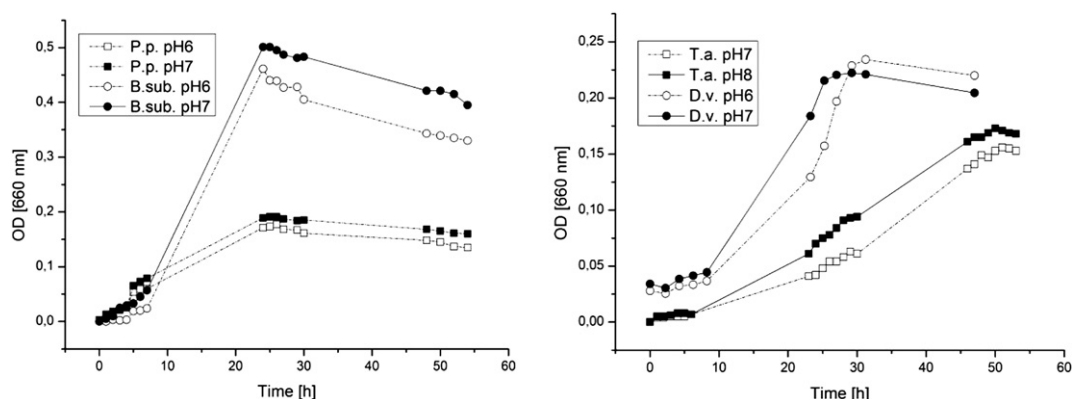


Fig. 2. Comparison of growth at different pH values for *P. putida* and *B. subtilis* (left) and for *D. vulgaris* and *T. aromatica* (right). The pH in the medium was reduced by the addition of HCl (0.5 M).

showed a reduction in MPN counts by $22.7 \pm 0.2\%$ for *P. putida* and by $51.6 \pm 5.5\%$ for *B. subtilis*. MPN counts for *D. vulgaris* and *T. aromatica* decreased by 86.6 ± 4.9 and $84.9 \pm 11.3\%$, respectively. The calculation of the relative inhibitory effect of CO₂ (RI) also showed a different response of the four strains to increasing CO₂ concentrations (Table 1). The Gram-negative *P. putida*, growing aerobically with acetate, was most affected by CO₂, as the RI was significantly higher at 50–80% CO₂ than the RI of the other tested strains, being already severely growth inhibited by 60% CO₂ (Table 1, SI-Fig. 4). The RI's of the Gram-negative *D. vulgaris* and *T. aromatica* and the Gram-positive *B. subtilis* increased similarly and gradually between 50 and 100% CO₂ (Table 1, SI-Fig. 4). The final degree of growth inhibition was comparable for *D. vulgaris*, *T. aromatica* and *P. putida* and amounted of RI values of around 80%. Since the aerobic *B. subtilis* could be treated by maximally 80% CO₂, the final RI was under 50%. To investigate if different substrates affect cellular growth at different CO₂ concentrations, glucose was used in place of acetate for *P. putida* cultures. In contrast to the monosaccharide glucose, acetate is a weak acid which protonates at lower pH; the undissociated acid can freely diffuse through the cell membrane and release protons into the cytoplasm, leading to several toxic effects e.g., (Roe et al., 2002). On the other hand, acetate is a metabolite emerging in almost every habitat, making acetate to an ideal substrate for model investigations. *P. putida* showed slightly higher growth rates and corresponding lower RI values at 80% CO₂ when grown with glucose as the sole energy source; the differences between the two substrates were not significant at 50% CO₂ (Table 1, SI-Fig. 4). Glucose-grown cultures had higher final OD₆₆₀ values, due to the higher amount of energy available from this substrate in the given concentrations (Fig. 3). Substrate consumption by *P. putida* was significantly reduced at CO₂ concentrations of 80%, compared to no CO₂ addition, and acetate uptake effectively stopped at the highest CO₂ levels (SI-Fig. 3). Another aspect to be considered was, whether O₂ limitation leads to a reduction of growth for the aerobic strains. The O₂ concentration was measured in the gas and liquid phase for aerobic cultures, using O₂ sensors. Oxygen consumption during the growth experiments was significantly higher for *B. subtilis* compared with *P. putida* (SI-Fig. 2). The O₂ concentration for *P. putida* (growing on acetate) for 0% CO₂ decreased from an initial concentration of 0.46 mM in the liquid phase down to 0.29 mM, compared to a decrease from 0.41 mM down to 0.19 mM in the presence of 80% CO₂. A reduction of the oxygen concentration from initially 0.5 mM down to 0.01 mM was observed in the liquid phase of *B. subtilis* (growing on glucose) when no additional CO₂ was added, whereas an oxygen decrease of 0.43 mM–0.07 mM was observed when 80% CO₂ was provided.

3.3. Cell viability under CO₂ stress at high pressure

Freshly grown cells were incubated at elevated pressures in self-constructed stainless steel vessels (Fig. 1) and the pressure was increased up to 5000 kPa for CO₂ and up to 7500 kPa for the control experiments using pure nitrogen. These control experiments were performed to distinguish between the effect of the elevated pressure itself, and the combination of high CO₂ concentrations and pressure. The results of these experiments are shown in Fig. 4. When cells were incubated for 24 h in the presence of pure nitrogen at pressures up to 5000 kPa, a reduction in MPNs of 59%, 12% and 33% was observed for *P. putida*, *B. subtilis* and *T. aromatica*, respectively compared to the 0 kPa control experiments. Pressures up to 7500 kPa caused a MPN reduction of 57% for *P. putida* and of 25% for *B. subtilis*, compared to the 0 kPa experiments. The strictly anaerobic *D. vulgaris* was less affected by pressure, and an MPN reduction of only 8% at 7500 kPa was observed, whereas MPNs were reduced by 55% for the facultative anaerobic *T. aromatica*. In contrast, when pressure (100–5000 kPa) was combined with increased CO₂ concentrations, the MPNs decreased by about 99% for *P. putida* and for *B. subtilis* and by 100% for *T. aromatica* and *D. vulgaris*. Thus, while no living cells were observed for the anaerobic strains after the pressure experiment with CO₂, viable cells were recovered for the aerobic strains. Here, *P. putida* seems to be more resistant to the CO₂ – pressure treatment compared to *B. subtilis*: at a pressure of 1000 kPa, the MPN value was reduced by 97.6% for *B. subtilis*, in contrast to a reduction of only 25.3% for *P. putida*. The low percentage of *B. subtilis* cells might have survived by endospores. Also the pH decreased significantly with increasing pressure compared to the control experiments with nitrogen (SI-Table 1). For 5000 kPa the pH was reduced to about 5.63 for *P. putida*, 5.56 for *B. subtilis*, 5.90 for *D. vulgaris* and 5.33 for *T. aromatica*.

4. Discussion

The potential risk of CO₂ leakage from a geological sequestration site or from CO₂-driven geothermic probes into the groundwater, and the impacts on the ecological system, might be very diverse and the response of various bacterial communities will differ strongly. Several studies have addressed the effect of pressurized CO₂ on spoilage bacteria in the food and medical industry, where bacteria have the potential to lead to food spoilage and patient infection (Dillow et al., 1999; Enomoto et al., 1997; Farber, 1991). However, little is known about the influence of CO₂ on environmentally relevant microorganisms in shallow aquifers overlying geological CO₂ sequestration sites. In this study, we address this scenario by determining the effects of different CO₂ concentrations

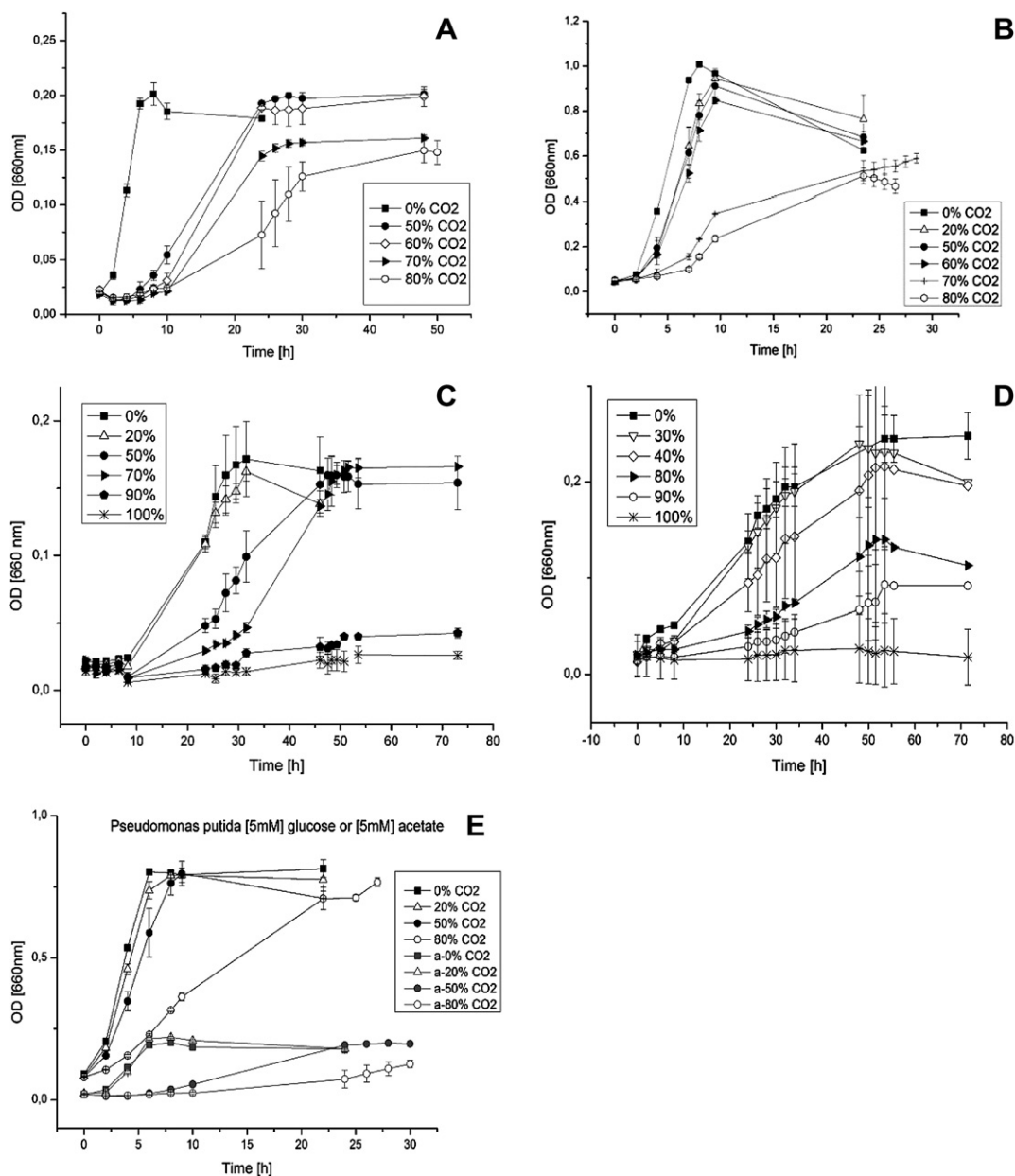


Fig. 3. Growth (OD_{660 nm}) at different CO₂ concentrations between 0 and 80% (for aerobic strains *P. putida* – (A), *B. subtilis* – (B)) and 100% (for anaerobic strains *D. vulgaris* – (C) and *T. aromatica* – (D)). The time is plotted against the optical density, measured at a wavelength of 660 nm. For *P. putida*, growth with acetate (5 mM) or glucose (5 mM) at different CO₂ concentrations is plotted (E).

on two aerobic and two anaerobic model organisms (*P. putida*, *B. subtilis*, *T. aromatica*, *D. vulgaris*), all of which are typically present in shallow aquifers.

CO₂ that infiltrates a freshwater aquifer under oxidizing conditions and under atmospheric pressure will have an immediate impact on water chemistry, leading to a reduction in pH and an increase in the concentration of total dissolved solids. The respective ratios of different CO₂ chemical species (CO₂, HCO₃⁻, H₂CO₃, CO₃²⁻) will vary as a function of the aqueous pH and the geochemical composition of the aquifer matrix. Generally, a pH decrease will lead to an increase in the relative portion of CO₂, while the portion of HCO₃⁻ will decrease. At pH values below eight, as investigated in this study, the concentration of carbonate ions can be neglected (Yagi and Yoshida, 1977). Although an increase in carbonic acid may be buffered by carbonate dissolution, a decrease of aqueous pH will be the result of CO₂ addition, in any case; likely

changing the composition of the microbial community and exerting selective pressure for microbial cells able to adapt to the more acidic conditions. For example, the four model organisms used in our study grew only poorly at pH values of 5 or lower (SI-Fig. 1). Therefore, the leakage of CO₂ into an unbuffered aquifer would influence the composition of the microbial community much more than leakage into an aquifer with a high buffering capacity and a pH decrease down to 5 or even lower would be very likely for unbuffered groundwater.

On the other hand, considering Permian sandstones as possible storage sites for CO₂ in Germany, the carbonate rocks of the overlying basal Zechstein should be taken into account (e.g. the lower Werra Carbonate Subformation Thuringian Basin). Aquifers composed of a carbonate rock matrix will have a natural buffering capacity for the leaking CO₂, and therefore the key microbial changes will be dominated by the increased CO₂ partial pressure

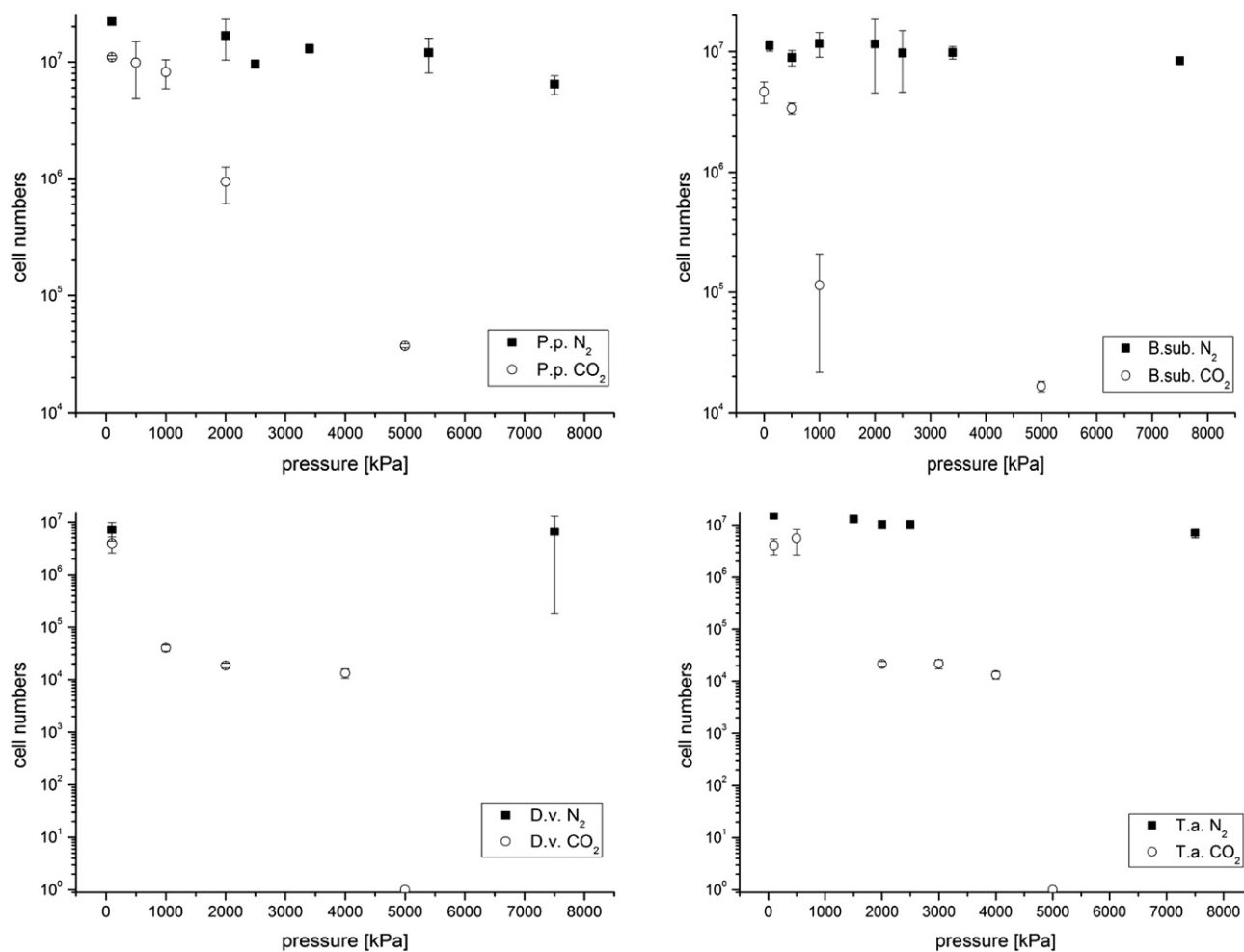


Fig. 4. MPNs of the tested strains after incubation at high pressure and elevated CO₂ concentrations. To examine a negative effect of the pressure itself on the viability of the cells, control experiments were performed with pure nitrogen and no CO₂ amendments. For the anaerobic strains *T. aromatica* and *D. vulgaris*, all cells were killed at a pressure of 5000 kPa (no growth corresponds to the value one for the log scale) and elevated CO₂ concentrations. A significant number of *P. putida* and *B. subtilis* cells still survived at 5000 kPa pressure.

and not by the pH alteration. Hence, the goal of the present study was to investigate the direct metabolic effects of increased CO₂ concentrations and pressures. Therefore, we have adjusted the pH of our culture medium by using a phosphate buffer generally to values allowing the test organisms to grow unaffected by extreme pH values. Toxic effects due to the protonation of the weak acid acetate (Roe et al., 2002) were therefore considered to be negligible. A slightly lower RI for glucose-grown *P. putida* cells compared to acetate-grown cells at 80% CO₂ (Table 1, SI-Fig. 4) indicates however that the substrate acetate may have caused additional growth inhibition at high CO₂ concentrations in this strain.

Generally, we cannot rule out that the cell internal pH in all investigated strains decreased as a function of the external CO₂ concentration due to dissociation of diffusively transported CO₂ inside of the cell, eventually damaging the cell's metabolism by inhibiting or inactivating key metabolic enzymes (Bertoloni et al., 2006). Before the experiments with increased CO₂ concentrations were performed, we investigated if the used strains can grow under the absence of externally provided CO₂, since previous studies have shown that some organisms need CO₂ for growth due to essential heterotrophic CO₂ fixation reactions (Feisthauer et al., 2008; Valley and Rettger, 1927; Walker, 1932; Wood et al., 1941). In our experiments, all strains were able to grow without an external CO₂

supply; probably, the inoculum contained low but sufficient CO₂ concentrations for an immediate restart of growth.

At ambient pressure, the growth of all strains was severely constrained by rising CO₂ concentrations. However, based on the RI values, *P. putida* was shown to be significantly more vulnerable to CO₂ as the other tested strains (Table 1, new SI-Fig. 4). A general conclusion if aerobic or anaerobic strains are more sensitive to CO₂ based on the RI values is not possible, but our results point to a strain-specific response to CO₂, independent of the cell structure and general metabolism (Table 1, SI-Fig. 4). Slightly differential responses to increased CO₂ concentrations among the four model strains may partially be explained by the different incubation temperatures, as the solubility of CO₂ increases with lower temperatures (1.5 g/L H₂O at 24.8 °C and only 1.2 g/L H₂O at 34.6 °C (Morrison and Billett, 1952)). Douglas King and Nagel (1967) proposed the displacement of O₂ by CO₂ as a reason for the reduced growth rate of microorganisms but this could not be confirmed, as the O₂ concentration never became a rate limiting factor in our experiments. However, other researchers have shown that the impact of elevated CO₂ concentrations is more severe under O₂-limited conditions (Molin, 1983), which could lead to a shift towards communities dominated by microaerophilic or anaerobic organisms implying that aerobic organisms of O₂ depleted aquifers are even more affected by a CO₂ leakage.

Most authors explain the effect of CO₂ as an alteration of cell membrane properties (Sears and Eisenberg, 1961). The effect of phospholipid solubilisation by liquid CO₂ should be more pronounced in the membrane of Gram-negative microorganisms due to the presence of two membranes. Furthermore, Gram-positive microorganisms have a thick layer of peptidoglycan, that may slow the diffusion of CO₂ into the cell (Oulé et al., 2010). Therefore, several studies proposed a higher resistivity of Gram-positive microorganisms towards CO₂ stress (Oulé et al., 2010; Stier et al., 1981). Correspondingly, we observed a better growth of the Gram-positive aerobic model strain *B. subtilis* in our experiments at ambient CO₂ pressure, compared to the Gram-negative aerobic *P. putida* (Table 1). On the other hand, the anaerobic Gram-negative model strains *T. aromatica* and *D. vulgaris* responded to CO₂ in a similar manner as *B. subtilis*, suggesting that CO₂ resistivity cannot be solely controlled by the type of cell wall. Furthermore, *B. subtilis* was more sensitive against CO₂ stress in a pressure range between 100 and 5400 kPa. Further suggestions for the mode of physiological effects of CO₂ are a penetration of CO₂ into the membrane and cytoplasm, resulting in a decrease of the intracellular pH due to dissociation of CO₂ (Ballestra et al., 1996) (Bertoloni et al., 2006), a direct influence on physicochemical properties of enzymes e.g. carboxylases/decarboxylases (Spilimbergo and Bertucco, 2003) and an alteration of the cell membrane, including effects on nutrient uptake and absorption properties (Jones and Greenfield, 1982). We will investigate the putative cellular effects of CO₂ on our model organisms in future studies on a proteomic level to receive information about the influence of increased CO₂ concentrations on the activation or repression of specific proteins because a preliminary study with *Pseudomonas fluorescens* as model strain suggested that, based on results of respiration tests, adaptive enzyme synthesis does not occur in response to higher CO₂ concentrations (Gill and Tan, 1979). Previous experiments with samples from freshwater aquifers showed also an increase of alkali and alkaline metal (Li, Rb, Sr, Mg, Ca/Mn, Fe, Co, Ni, Zn – increase after 2 weeks of exposure to CO₂) concentrations (Little and Jackson, 2010). As the concentration of the metals increased significantly immediately after an exposure of the freshwater of an aquifer to CO₂ under oxidized conditions and atmospheric pressure, the influence of increased metal concentrations in combination with high CO₂ concentrations on the growth behaviour of microorganisms should be investigated in future studies as well.

Besides the pH effect, the effect of pressure itself was tested and the results demonstrated that pressure can reduce the viability of the tested strains, but the effects are in the order of one magnitude at maximum and not strain specific. Only the combination of pressure and increased CO₂ leads to a dramatic reduction in cellular growth and detected MPN counts. Therefore, especially for deeper aquifers and for areas with higher lithostatic pressure gradients, CO₂ leakage can be more severe when both, high pressure and increased CO₂ concentrations are present. Extrapolating these observations, the average lithostatic and hydrostatic pressure (i.e. an increase of 350 kPa for every 10 m increase in depth, if the groundwater table equates the ground level and the average matrix density is 2.5 times the density of the water) at a depth of 50 m would significantly inhibit microbial activity in the presence of high CO₂ concentrations.

In summary, it can be concluded that the effect of CO₂ is not dependent upon the electron acceptor present in the system, as aerobic, nitrate- and sulphate-reducing organisms showed similar reactions to the CO₂ stress. Leakages may enhance CO₂ concentrations in aquifers to levels where toxic effects can be expected and elevated CO₂ concentrations in combination with pressures ≥ 1000 kPa already lead to a dramatic decrease in cell viability. Long-term studies are necessary to make clear statements about the

microbial responses and the adaptation abilities to increased CO₂ concentrations in shallow aquifers. This study provides principal information on the influence of suddenly increasing CO₂ concentrations on the viability of microorganisms present in shallow aquifers. This information can be used for a proper risk assessment, which is necessary to evaluate the Carbon Capture and Storage technology.

Acknowledgements

This project was funded by the German Federal Ministry of Education and Research (Grant: 03G0670C) under the context of the project “CO₂ injection into a near surface aquitard for evaluating monitoring concepts and methods”. We thank R. Schumann for construction and maintenance of the high pressure reactors, Denise Przybylski for the HPLC measurements, Roshani Sitaula for help in the laboratory and Jana Rakoczy, Angela Woods and Brandon Morris for English correction.

Appendix A. Supplementary material

Supplementary data associated with this article can be found, in the online version, at doi:10.1016/j.envpol.2012.05.010.

References

- Ballestra, P., Silva, A.A.D., Cuq, J.L., 1996. Inactivation of *Escherichia coli* by carbon dioxide under pressure. *Journal of Food Science* 61, 829–836.
- Bertoloni, G., Bertucco, A., De Cian, V., Parton, T., 2006. A study on the inactivation of micro-organisms and enzymes by high pressure CO₂. *Biotechnology and Bioengineering* 95, 155–160.
- Blagodatskaya, E., Blagodatsky, S., Dorodnikov, M., Kuzyakov, Y., 2010. Elevated atmospheric CO₂ increases microbial growth rates in soil: results of three CO₂ enrichment experiments. *Global Change Biology* 16, 836–848.
- Dillow, A.K., Dehghani, F., Hrkach, J.S., Foster, N.R., Langer, R., 1999. Bacterial inactivation by using near- and supercritical carbon dioxide. *Proceedings of the National Academy of Sciences of the United States of America* 96, 10344–10348.
- Douglas King Jr, A., Nagel, Charles, W., 1967. Growth inhibition of a *Pseudomonas* by carbon dioxide. *Journal of Food Science* 32, 575–579.
- Enfors, S.-O., Molin, G., 1981. The influence of temperature on the growth inhibitory effect of carbon dioxide on *Pseudomonas fragi* and *Bacillus cereus*. *Canadian Journal of Microbiology* 27, 15–19.
- Enomoto, A., Nakamura, K., Nagai, K., Hashimoto, T., Hakoda, M., 1997. Inactivation of food microorganisms by high-pressure carbon dioxide treatment with or without explosive decompression. *Bioscience, Biotechnology and Biochemistry* 61, 1133–1137.
- Farber, J.M., 1991. Microbiological aspects of modified - atmosphere packaging – a review. *Journal of Food Protection* 54, 58–70.
- Feisthauer, S., Wick, L.Y., Kästner, M., Kaschabek, S.R., Schlömann, M., Richnow, H.H., 2008. Differences of heterotrophic ¹³C₂ assimilation by *Pseudomonas knackmussii* strain B13 and *Rhodococcus opacus* 1CP and potential impact on biomarker stable isotope probing. *Environmental Microbiology* 10, 1641–1651.
- Freeman, C., Kim, S.-Y., Lee, S.-H., Kang, H., 2004. Effects of elevated atmospheric CO₂ concentrations on soil microorganisms. *The Journal of Microbiology* 42, 267–277.
- Garthright, W.E., Blodgett, R.J., 1996. Confidence intervals for microbial density using serial dilutions with MPN estimates. *Biometrical Journal* 38, 489–505.
- Gill, C.O., Tan, K.H., 1979. Effect of carbon dioxide on growth of *Pseudomonas fluorescens*. *Applied and Environmental Microbiology* 38, 237–240.
- Haldane, J.B.S., 1939. Sampling errors in the determination of bacterial or virus density by the dilution method. *Journal of Hygiene* 39, 289–293.
- IPCC, 2005. IPCC Special Report on Carbon Dioxide Capture and Storage. In: Working Group III of the Intergovernmental Panel on Climate Change, Cambridge, United Kingdom and New York, NY, USA.
- Jones, R.P., Greenfield, P.F., 1982. Effect of CO₂ on yeast growth and fermentation. *Enzyme and Microbial Technology* 4, 210–222.
- Little, M.G., Jackson, R.B., 2010. Potential impacts of leakage from deep CO₂ geo-sequestration on overlying freshwater aquifers. *Environmental Science and Technology* 44, 9225–9232.
- Molin, G., 1983. Combined carbon dioxide inhibition and oxygen limitation of the growth of *Pseudomonas fragi* 72 in batch and continuous culture. *Journal of General Microbiology* 129, 2885–2891.
- Morrison, T.J., Billett, F., 1952. 730. The salting-out of non-electrolytes. Part II. The effect of variation in non-electrolyte. *Journal of the Chemical Society (Resumed)*, 3819–3822.
- Oppermann, B.I., Michaelis, W., Blumenberg, M., Frerichs, J., Schulz, H.M., Schippers, A., Beaubien, S.E., Krüger, M., 2010. Soil microbial community changes as a result of long-term exposure to a natural CO₂ vent. *Geochimica et Cosmochimica Acta* 74, 2697–2716.

- Oulé, M.K., Dickman, M., Arul, J., 2010. Microbicidal effect of pressurized CO₂ and the influence of sensitizing additives. *European Journal of Scientific Research* 41, 570–582.
- Roe, A.J., O'Byrne, C., McLaggan, D., Booth, I.R., 2002. Inhibition of *Escherichia coli* growth by acetic acid: a problem with methionine biosynthesis and homocysteine toxicity. *Microbiology* 148, 2215–2222.
- Saripalli, P., McGrail, P., 2002. Semi-analytical approaches to modeling deep well injection of CO₂ for geological sequestration. *Energy Conversion & Management* 43, 185–198.
- Sears, D.F., Eisenberg, R.M., 1961. A model representing a physiological role of CO₂ at the cell membrane. *Journal of General Physiology* 44, 869–887.
- Spilimbergo, S., Bertucco, A., 2003. Non-thermal bacterial inactivation with dense CO₂. *Biotechnology and Bioengineering* 84, 627–638.
- Stier, R.F., Bell, L., Ito, K.A., Shafer, B.D., Brown, L.A., Seeger, M.L., Allen, B.H., Porcuna, M.N., Lerke, P.A., 1981. Effect of modified atmosphere on *C. botulinum* toxigenesis and the spoilage microflora of salmon fillets. *Journal of Food Science* 46, 1639–1642.
- Sutton, S., 2010. The most probable number method and its uses in enumeration, qualification, and validation. *Journal of Validation Technology* 16, 35–38.
- Valley, G., Rettger, L.F., 1927. The influence of carbon dioxide on bacteria. *Journal of Bacteriology* 14, 101–137.
- Walker, H.H., 1932. Carbon dioxide as a factor affecting lag in bacterial growth. *Science* 76, 602–604.
- Widdel, F., 2010. *Theory and Measurement of Bacterial Growth*. University Bremen, pp. 11.
- Wood, H.G., Werkman, C.H., Hemingway, A., Nier, A.O., 1941. Heavy carbon as a tracer in heterotrophic carbon dioxide assimilation. *Journal of Biological Chemistry* 139, 365–376.
- Wu, B., Shao, H., Hu, Z.W., Tang, Y.J., Jun, Y.-S., 2010. Viability and metal reduction of *Shewanella oneidensis* MR-1 under CO₂ stress: implications for ecological effects of CO₂ leakage from geologic CO₂ sequestration. *Environmental Science and Technology* 44, 9213–9218.
- Yagi, H., Yoshida, F., 1977. Desorption of carbon dioxide from fermentation broth. *Biotechnology and Bioengineering* 19, 801–819.

SUPPORTING INFORMATION

Effects of High CO₂ Concentrations on Typical Aquifer Microorganisms

Alexandra Schulz¹, Carsten Vogt¹ and Hans-Hermann Richnow¹

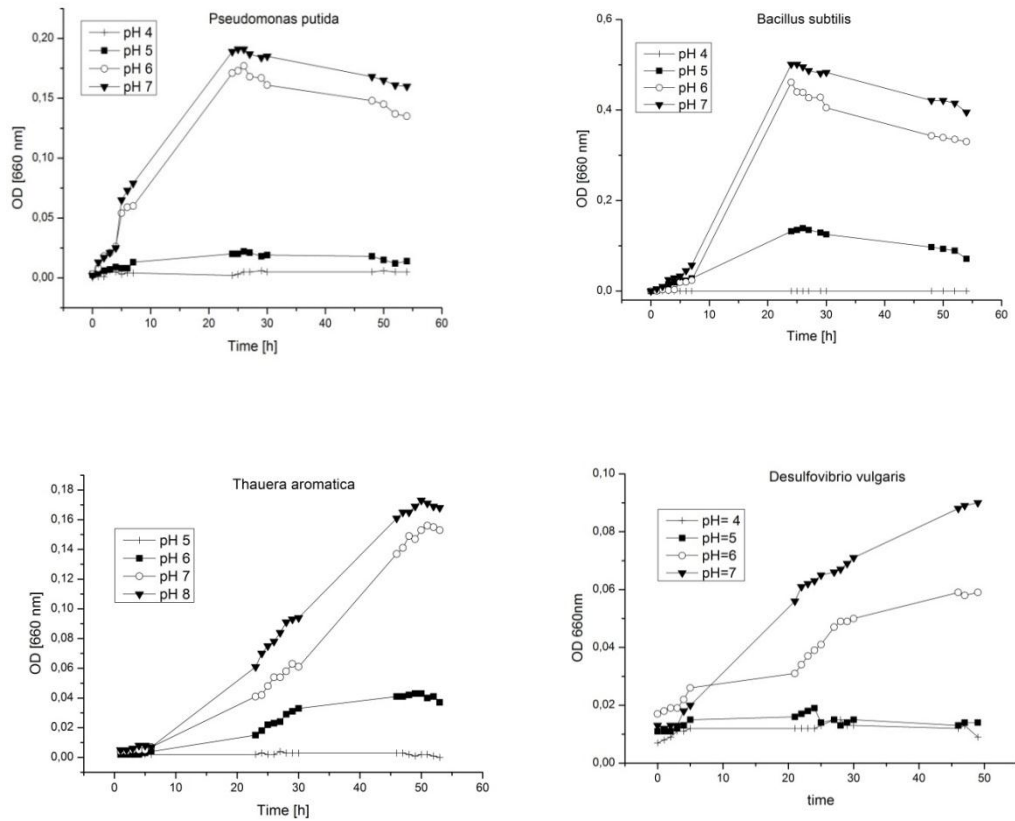
¹Department of Isotope Biogeochemistry, UFZ - Helmholtz Centre for Environmental Research,
Leipzig, Germany

***Corresponding author**

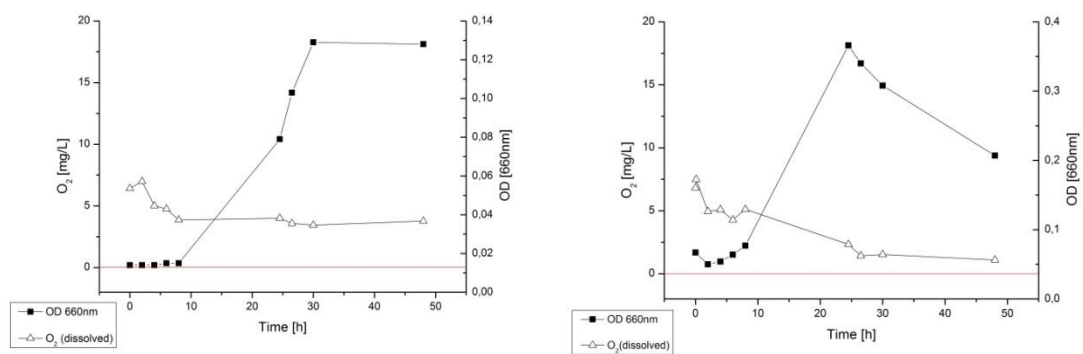
Mailing address: Helmholtz Centre for Environmental Research, Dept. Isotope
Biogeochemistry, Permoserstr. 15, 04318 Leipzig, Germany

E-mail: carsten.vogt@ufz.de, Tel: +49-341-235-1357, Fax: +49-341-1443

12. Appendix

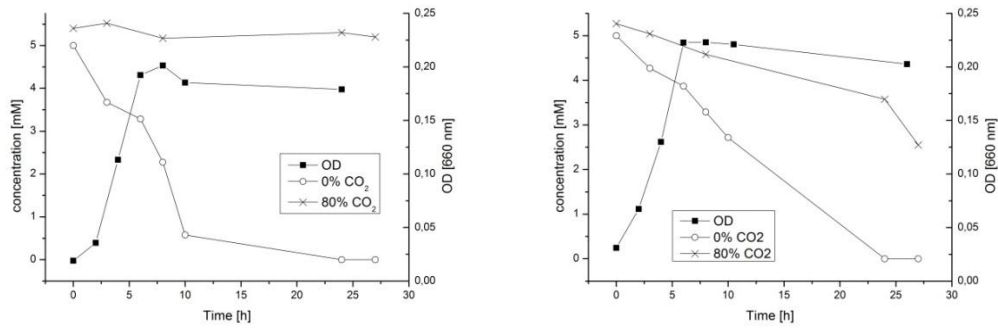


SI-Figure 1. Growth at different pH values. The strains can compensate for a reduced pH of about one unit, but lower pH values inhibited cell growth in all four strains.

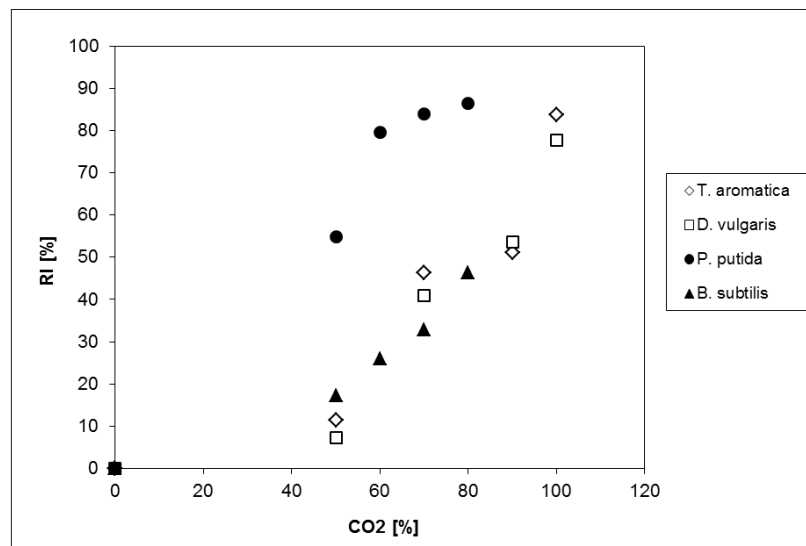


SI-Figure 2. Dissolved oxygen concentration in mg/L for the two aerobic strains *Pseudomonas putida* (left) and *Bacillus subtilis* (right). The measurements were taken during growth experiments in the presence of 80% CO₂.

12. Appendix



SI-Figure 3. Acetate (left) and glucose (right) consumption at various concentration of CO₂ by *P. putida* during the experiment. The OD₆₆₀ of a culture growing on 0% CO₂ shows that the added amount of substrate is not a rate-limiting factor for growth.



SI-Figure 4. Relative inhibitory effect (RI) is plotted against the CO₂ concentration for the four different model organisms. The figure shows that *B. subtilis* is less sensitive towards increasing CO₂ concentrations compared to the highly sensitive *P. putida*.

12. Appendix

SI-Table 1. Comparison of the pH values for the pressure experiments with CO₂ and N₂

	<i>P. putida</i>		<i>B. subtilis</i>		<i>D. vulgaris</i>		<i>T. aromatica</i>	
Pressure [kPa]	CO ₂	N ₂	CO ₂	N ₂	CO ₂	N ₂	CO ₂	N ₂
100	6.35	6.88	6.23	6.82	6.40	6.91	6.90	8.0
500	6.15	6.85	6.13	6.79	6.29	6.90	6.41	8.01
1000	6.08	6.79	6.06	6.77	6.24	6.86	6.35	8.0
2000	6.03	6.79	6.00	6.76	6.19	6.85	6.31	7.98
5000	5.63	6.73	5.56	6.70	5.90	6.86	5.33	7.97

SI-Table 2. Different solubility of CO₂ at atmospheric pressure and different temperatures

	25°C <i>T. aromatica</i>	30°C <i>B.subtilis, P.putida</i>	37°C <i>D. vulgaris</i>
CO ₂ [%]			
10	0.150	0.131	0.109
20	0.299	0.262	0.219
30	0.449	0.393	0.329
40	0.598	0.524	0.438
50	0.748	0.655	0.548
60	0.898	0.786	0.657
70	1.047	0.917	0.767
80	1.197	1.047	0.876
90	1.346	1.179	0.986
100	1.496	1.280	1.095